



HAL
open science

Design of optimal experiment for estimation of Hydro-thermal properties of porous media. Application in baking process

Puvikkarasan Jayapragasam

► **To cite this version:**

Puvikkarasan Jayapragasam. Design of optimal experiment for estimation of Hydro-thermal properties of porous media. Application in baking process. Chemical and Process Engineering. Université de Bretagne Sud, 2021. English. NNT : 2021LORIS586 . tel-03409357

HAL Id: tel-03409357

<https://theses.hal.science/tel-03409357>

Submitted on 29 Oct 2021

HAL is a multi-disciplinary open access archive for the deposit and dissemination of scientific research documents, whether they are published or not. The documents may come from teaching and research institutions in France or abroad, or from public or private research centers.

L'archive ouverte pluridisciplinaire **HAL**, est destinée au dépôt et à la diffusion de documents scientifiques de niveau recherche, publiés ou non, émanant des établissements d'enseignement et de recherche français ou étrangers, des laboratoires publics ou privés.

THÈSE DE DOCTORAT DE

L'UNIVERSITE DE BRETAGNE SUD

ECOLE DOCTORALE N° 602

Sciences pour l'Ingénieur

Spécialité : Energetics-Thermics-Combustion

Par

Puvikkarasan Jayapragasam

Conception d'une expérience optimale pour l'estimation des propriétés hydro-thermiques des milieux poreux. Application dans le processus de cuisson.

Thèse présentée et soutenue à Lorient, le 12 Janvier 2021

Unité de recherche : IRDL, PTR4 Procédés Thermiques

Thèse N° : 586

Rapporteurs avant soutenance :

M. Emmanuel Purlis Scientific Researcher, Consejo Nacional de Investigaciones Cientificas y Técnicas, Argentina
M. Benjamin Remy Professor, LEMTA Université de Lorraine

Composition du Jury :

Président :	M. Marcel Lacroix	Professor, University of Sherbrooke, Canada
Examineurs :	M. Patrick Glouannec	Professor, IRDL, Université de Bretagne Sud
	M. Emmanuel Purlis	Scientific Researcher, CONICET, Argentina
	M. Benjamin Remy	Professor, LEMTA Université de Lorraine
	Mme. Patricia Arlabosse	Professor, IMT Mines Albi-Carmaux
	Mme. Vanessa Jury	Maître de conférence, GEPEA, Université de Nantes
Dir. de thèse :	M. Tahar Loulou	Professor, IRDL, Université de Bretagne Sud
Co-dir. de thèse :	M. Pascal Le Bideau	Maître de conférence, IRDL, Université de Bretagne Sud

Acknowledgments

I would like to express my deepest gratitude to Professor Tahar Loulou for his continuous support and encouragements during my thesis. Over last three years, I have learned many important aspects of research and scientific approaches from him. Every and every step of achievement is possible because of his special care on me. He has helped me to have a comfortable time in France. I would also like to thank Dr Pascal Le Bideau for sharing his experience and insight on the computational and experimental part of the work. His time, patience and encouragement are greatly appreciated.

I want to express special thanks to Dr Bertrand Garnier and Dr Allanic Nadine who helped in monitoring annual progress of the thesis. I will never forget my lab members for funding my trip to Metti 7 school which has really helped in shaping up my knowledge on inverse problems and optimizations. Finally, I would like to thank Professor Emmanuel Purlis and Professor Benjamin Remy for showing their support to improve the quality and technical writing of this work.

Contents

Contents

List of Tables

List of Figures

Introduction	1
1 Heat and mass transfer during food baking	3
1.1 Physical phenomena	3
1.1.1 Major phenomena	4
1.1.2 Commonly used ratios	4
1.2 Modeling approaches	5
1.2.1 Transport mechanisms	6
1.2.2 Models from literature	8
1.3 Required physical properties	10
1.4 Inverse procedure for properties determination	14
1.4.1 Note about function estimation	15
List of symbols	16
Bibliography	18
2 Cake baking: Experimental and modeling developments	20
2.1 Experimental considerations	20
2.1.1 Moisture content measuring techniques	21
2.1.2 Preparation of dough	22
2.1.3 Experimental set-up	23
2.1.4 Typical baking test	25
2.1.5 Incoming heat flux	26
2.1.6 Measurement of thermophysical properties	27
2.2 Development of heat and mass transport models	31
2.2.1 Diffusive model	33
2.2.2 TMPN model: Multiphase model with non-equilibrium approach	37
2.2.3 TMPE model: Multiphase model with equilibrium approach	40
2.3 Model validation with known properties	43
2.3.1 Diffusive model	43
2.3.2 TMPN model	46
2.3.3 TMPE model	46

2.4	Conclusive remarks	50
	List of symbols	50
	Bibliography	53
3	Selection of the appropriate model for physical properties estimation	56
3.1	Inverse procedure and considerations	56
3.1.1	Sensitivity or Jacobian matrix	58
3.1.2	Objective function	63
3.1.3	Parameterization of a function	64
3.2	Sensitivity analysis	67
3.3	Correlation analysis	71
3.4	Design of experiments	78
3.4.1	D-Optimality	79
3.4.2	E-Optimality	82
3.5	Numerical Analysis	82
3.5.1	TM Model	83
3.5.2	TMPN Model	84
3.5.3	TMPE Model	85
3.6	Conclusive remarks	87
	List of symbols	88
	Bibliography	90
4	Estimation of physical properties from experimentation	94
4.1	Introduction	94
4.2	Parameter estimation	95
4.2.1	TM Model	95
4.2.2	TMPN Model	97
4.2.3	TMPE Model	99
4.2.4	Extension of inverse solution	101
4.2.5	Literature	104
4.3	Function estimation	106
4.3.1	Mathematical Modeling	107
4.3.2	Sensitivity analysis	109
4.3.3	Analysis on inverse solution	112
4.3.4	Functionality	116
4.3.5	Literature	121
4.4	Note about one way coupling	122
4.5	Conclusive remarks	124
	List of symbols	125
	Bibliography	128
	Conclusion	130

A	Heat-flux estimation	132
A.1	Governing equations	132
A.1.1	Variational problem	132
A.1.2	Adjoint problem	134
A.2	Inverse problem procedure	135
A.3	Conjugate gradient algorithm	136
A.4	Inverse solutions	136
	Bibliography	136
B	Steps of Non-dimensionalization	138
B.1	Diffusive model	138
B.2	TMPN model	139
B.3	TMPE model	141
B.4	TMPE model for function estimation	143

List of Tables

2.1	Composition for 100 gm of Francine mix	23
2.2	Sensor locations from surface of heating coil	24
2.3	Expressions for all non-dimensional parameters used in Diffusive, TMPN and TMPE models	44
2.4	Parameters used for simulations	45
3.1	Comparison of test cases	66
3.2	Correlation matrix for TM model based on temperature and moisture content . .	73
3.3	Correlation matrix for TM model based on temperature only	73
3.4	Correlation matrix for TM model based on moisture only	73
3.5	Correlation matrix for TMPN model based on temperature and moisture content (combined form)	75
3.6	Correlation matrix for TMPN model based on temperature only	75
3.7	Correlation matrix for TMPN model based on moisture content only	76
3.8	Correlation matrix for TMPE model based on temperature and moisture content	76
3.9	Correlation matrix for TMPE model based on temperature only	76
3.10	Correlation matrix for TMPE model based on moisture content only	77
3.11	Cases for determinant	79
3.12	Eigenvalues of determinant for TMPE model	82
3.13	Inverse solution with synthetic measurements for TM Model	83
3.14	The rms values between simulated and measured data for TM model	83
3.15	Inverse solution with synthetic measurements for TMPN Model for various objective functions	84
3.16	The rms values of measured and simulated data at sensor locations for different objective functions for TMPN model	85
3.17	Inverse solution with synthetic measurements for TMPE Model for various objective functions	86
3.18	The rms values of measured and simulated data at sensor locations for different objective functions for TMPE model	87
4.1	Imposed parameters	96
4.2	The rms values between simulated and measured data for TM model	97
4.3	Inverse solution for TM model with experimental measurements using S_{WLS} of $\phi = 0.4$	98
4.4	The rms values between simulated and measured data for TMPN model	98

4.5	Inverse solution for TMPN model with experimental measurements using S_{WLS} of $\phi = 0.6$	99
4.6	rms value between simulated and measured data for TMPE model	100
4.7	Inverse solution for TMPE model with experimental measurements using S_{WLS} of $\phi = 0.6$	100
4.8	The rms values between simulated and measured profiles for regulator temperature 170°C	102
4.9	Estimated parameters in dimensional form	105
4.10	Dimensionless variables and constants	110
4.11	Cases with T - temperature and U - moisture content	116
4.12	rms comparison	120

List of Figures

1.1	Physical phenomena	4
1.2	Pore structure	5
1.3	Evolution of thermal conductivity, heat capacity (a), density and diffusivity (b) as function of temperature for Purlis model	10
1.4	Evolution of thermal conductivity as function of liquid saturation with constant porosity	11
1.5	Evolution of viscosity and relaxation time as function of temperature	13
1.6	Spring and dash-pot arrangement for Maxwell, Kelvin model (a) and evolution of strain with time with applied stress for corresponding models (b)	14
1.7	Flow chart for conjugate gradient method	15
2.1	Various measuring techniques for water content	22
2.2	Schematic representation of experimental set-up	24
2.3	Experimental measurements of temperature (a) and mean moisture content (b) for dough	25
2.4	Mean mass loss rate	26
2.5	Temperature variation in cast iron floor (a) and estimated heat flux (b)	27
2.6	Comparison of water activity profile fitted by Ferro-Fontan at temperature 70°C with experimental measurements	28
2.7	Measurement of specific heat capacity during heating (H.P.) and cooling phase (C.P.)	29
2.8	Evolution of temperature during measurement - for representation purpose	30
2.9	Basic physics involved in contact baking	31
2.10	Step function for temperature (C_1) (a) and moisture content (C_2) (b) for Diffusive model	35
2.11	Simulated profiles of temperature (a) and moisture content (b) for Diffusive model	45
2.12	Evaporation rate for Diffusive model	46
2.13	Simulated profiles of temperature (a), relative gas pressure (b) and moisture content (c) for multiphase model with non-equilibrium approach	47
2.14	Evaporation rate for multiphase model with non-equilibrium approach	47
2.15	Simulated profiles of temperature (a), relative gas pressure (b) and moisture content (c) for multiphase model with equilibrium approach	48
2.16	Evaporation rate for multiphase model with equilibrium approach	49
3.1	Sensitivity and temperature profiles as function of time computed analytically.	61

3.2	Variation of rms and relative error ε values for parameters \mathbf{c} and \mathbf{k} as a function of sensor position x_s with $\mathbf{h} = 10^{-08}$	62
3.3	Variation of relative error ε and rms values for parameters \mathbf{c} and \mathbf{k} as a function step-size \mathbf{h} in range between 10^{-01} and 10^{-30} at $x_s = 0$	62
3.4	Behavior of basis functions in β -splines for order 4	65
3.5	Performance of β -spline for different cases	66
3.6	Scaled sensitivity profile for temperature at $X = 0$ (a), 0.25 (b), 0.50 (c), 0.75 (d), 1 (e) and mean moisture content (f) for TM model	68
3.7	Scaled sensitivity profile for temperature at $X = 0$ (a), 0.25 (b), 0.50 (c), 0.75 (d), 1 (e) and mean moisture content (f) for TMPN model	69
3.8	Scaled sensitivity profile for temperature at $X = 0$ (a), 0.25 (b), 0.50 (c), 0.75 (d), 1 (e) and mean moisture content (f) for TMPE model	70
3.9	Sensitivities of parameters with respect to total gas pressure at $X = 0$ for TMPN model (a) and TMPE model (b)	72
3.10	Correlation analysis for TM model	74
3.11	Correlation analysis for TMPN model	75
3.12	Correlation analysis for TMPE model	77
3.13	Determinant at various number of sensors in individual (a) and combined (b) form for TM model	80
3.14	Determinant at various number of sensors in individual (a) and combined (b) form for TMPN model	81
3.15	Determinant at various number of sensors in individual (a) and combined (b) form for TMPE model	81
3.16	Comparison of synthetic data with noise with simulated data of temperature (a) and mean moisture content (b) for TM model	84
3.17	Comparison of synthetic data with noise with simulated data for S_{WLS} with weight $\phi = 0.5$, of temperature (a) and mean moisture content (b) for TMPN model	85
3.18	Comparison of synthetic data with noise with simulated data for S_{SLS} of temperature (a) and mean moisture content (b) for TMPE model	86
4.1	Comparison of measurements and simulations of temperature (a) and mean moisture content (b) for TM model	97
4.2	Comparison of measurements and simulations of temperature (a) and mean moisture content (b) for TMPN model	98
4.3	Comparison of measurements and simulations of temperature (a) and mean moisture content (b) for TMPE model	100
4.4	Evolution of heat flux for temperature 170°C (a) and 200°C (b)	101
4.5	Experimental measurements and simulated results of TMPN and TMPE models for regulator temperature 170°C (where exp is experimental data and sim is simulated results)	103
4.6	Sensitivity coefficient	111
4.7	Comparison of measurements and simulations of temperature (a) and mean moisture content (b) for model without heat flux in objective function OLS	113

4.8	Comparison of measurements and simulations of temperature (a), mean moisture content (b) and heat flux(c) for model with heat flux in objective function OLS_q	114
4.9	Absolute difference between measurements and simulations of temperature (a) and mean moisture content (b) for model without heat flux (OLS) and with flux (OLS_q) in objective function	114
4.10	Comparison of thermophysical properties for model with (OLS_q) and without (OLS) heat flux in objective function	115
4.11	Comparison of measurements and simulations of temperature (a) and mean moisture content (b) for test case II	117
4.12	Comparison of measurements and simulations of temperature (a) and mean moisture content (b) for test case III	117
4.13	Comparison of measurements and simulations of temperature (a), mean moisture content (b) and heat flux(c) for case IV	118
4.14	Estimated thermophysical properties for case IV	119
4.15	Overview of estimated thermophysical properties for model with heat flux in objective function compared against literature data	122
4.16	Comparison of measurements and simulations of temperature (a), mean moisture content (b), local moisture content (c) and deformation in % (d) for model with one-way coupling	123
4.17	Evolution of nodes during deformation with respect to time (a) and comparison of moisture content for model with and without deformation (b)	124
A.1	Thermophysical properties of cast iron	133
A.2	Inverse solutions for estimation of initial condition (a) and heat flux evolution (b)	137

Introduction

Food engineering has always been a field of interest for scientific community and industries as it is part of human's daily activity. Bread and bakery products are one of the most staple foods with long history. In Europe, bakery industry dominates more than 60% in the food sector. Literature emphasizes mammoth amount of thermal energy is spent for baking operation. In the past few decades, studies were carried out to understand the phenomenon hidden behind the baking process and tried to reduce the heat input. Hitherto, "cook and look" strategy is used for baking operation despite long history.

Even though there are several stages in preparation of a bakery product, baking is more crucial and focused part. Baking is a complicated process which comprises of transport of heat, migration of liquid water, evaporation of liquid water, condensation of water vapor, sometimes generation and transportation of gases, some biochemical reactions like starch gelatinization and also structural deformation. All these phenomena are strongly interlinked with each other and become the deciding factor of bakery quality. A proper knowledge of these fundamental processes would help to improve their quality and consistency.

In early nineties, there were several attempts to precisely simulate the baking process and estimate some of their thermal properties. With step by step improvement, in recent times researches are able to simulate accurately with model that can focus even microscopic changes like local porosity evolution. These advancements have helped researchers in evaluating an optimal energy required to bake a bread with desirable physical attributes like texture, brownness, crust thickness, etc. These emphases strongly emphasize the necessity of knowledge on their physical and governing properties during baking process.

Now the focus has been shifted to other bakery products like sponge cakes, pizza, etc to minimize their energy consumption. This work focuses on contact baking of more moist dough on a hot pan which resembles cooking of crêpes, pan cakes, Indian style dough like rotli, naan, etc. The kind of baking involved here is completely different from bread baking in a convectional oven. Since the processing and environmental conditions are different, the thermophysical properties available from literature might not suit well and shall result in poor simulation results deviated from actual experimental measurements.

The main purpose of the work is to simultaneously estimate significant and influential thermophysical properties by non-dimensionalizing the governing equations. For better approximation of the parameters and functions, design of experiment is equipped to obtain optimal number and location of sensors. Complex step differentiation method is employed to compute the sensitivity coefficients of the parameters, first derivative of objective function, in place of conventional finite difference method. Initially, these properties are estimated as constant parameter. Due to their

constrains, the models failed to be accurate. Hence, most influential properties are identified as functions of state variables.

Specific objectives

The main intention of this work is to identify the thermophysical properties of one-sided contact baking process discussed later. The specific objectives of each chapters are:

Chapter 1: gives an insight on the fundamental science behind a baking process. And also provides further information about previously used models in literature and optimization methods for solving inverse problems.

Chapter 2: discusses the experimental set-up used for one-sided baking process and other measuring techniques that are used for computing unknown quantities like water activity. Later, it explains and validates the mathematical approaches that govern accurately the baking process.

Chapter 3: shows how effective and accurate is complex step differentiation (CSD) than finite difference method (FDM) in computing Jacobian or sensitivity coefficients with an example. Then, CSD is used in evaluating the sensitivities of parameters with respect to temperature and mean moisture content. In the last part of the chapter, numerical study are performed with synthetic measurement data for objective functions like ordinary, weighted and scaled least square functions in order to know feasibility of retrieving back the parameters accurately.

Chapter 4: provides the inverse solutions of the models discussed earlier using actual measurements. And also describes a sample inverse problem for function estimation using β -spline approach. The estimated functions are compared between the objective functions with and without heat flux measurements, for the best model selected based on previous solutions.

Chapter 1

Heat and mass transfer during food baking

Abstract

The overview of heat and mass transfer phenomena during baking of dough are showcased. Transport mechanisms that are derived from law of physics are detailed for better understanding. Various modeling approaches that were used for describing a baking process are presented with their strengths and drawbacks. The required physical properties are listed with their mathematical expressions as given in literature. In the end of this chapter, the procedure used for inverse problem is discussed.

1.1 Physical phenomena

Baking can be considered as an extended version of drying process in a porous media. Apart from structural change and chemical reactions, transformation of dough into crust-crumbs is largely due to evaporation of liquid (usually water) that happens during the baking process. Hence, two significant phenomena to be considered mandatory for simulating the baking process are heat and mass transport of fluids. Extended insight in baking mechanism leads to inclusion of evaporation-condensation effect caused by mass transport of water vapor (gaseous phase). This extension involves gaseous phase such as considering mass transport of trapped air during fermentation, water vapor and sometimes carbon dioxide (CO_2 , evolving due to baking agents like yeast). All these considered phenomena come under the umbrella of transport phenomena. The physics involved in the baking process demands inclusion of a new phenomenon that causes structural change (expansion/shrinkage). Structural change is a result of stress-strain variations arising due to generation and expansion of gases. The dough during baking is considered as viscoelastic material. For example, rubber has similar structural properties whose porosity (ratio of void volume to total volume) and total volume change during baking. The phenomenon of structural changes can be termed as deformation. The strong association of these various phenomena is presented in figure 1.1.

1.1.1 Major phenomena

Energy Energy transport during baking is considered as migration of heat from hot region to cold. Heat is transferred by conduction, convection and radiation. Presence of void volume paves the way for convective and radiative heat transfer during baking. Convection and radiation effects can be ignored as the pore structure of dough is smaller than mean free path of gases. Thus, heat energy is transported between various regions by conduction that is governed by Fourier law and advected by migration of fluids and deformation effect. Dufour effect is included in evaporation-condensation expression of liquid water and water vapor during the process.

Mass The migration of fluids within permeable dough is mainly governed by Darcy’s law, Fick’s law of molecular diffusion, Soret effect due to temperature gradient.

Deformation The deformation effect is occurs due to gases that are generated and released by baking agent and evaporation of water. Building up of gas pressure induces stress on the structure which leads to noticeable strain. The mathematical expressions for these individual phenomena are enlisted in upcoming section §1.2.

1.1.2 Commonly used ratios

Some of the commonly used ratios in pore structure are presented in the following section. Figure 1.2 gives an idea about the pore structure for a system of solid and two fluids.

Porosity Porosity (π) is an important aspect in porous media that is defined as ratio of void volume to total volume.

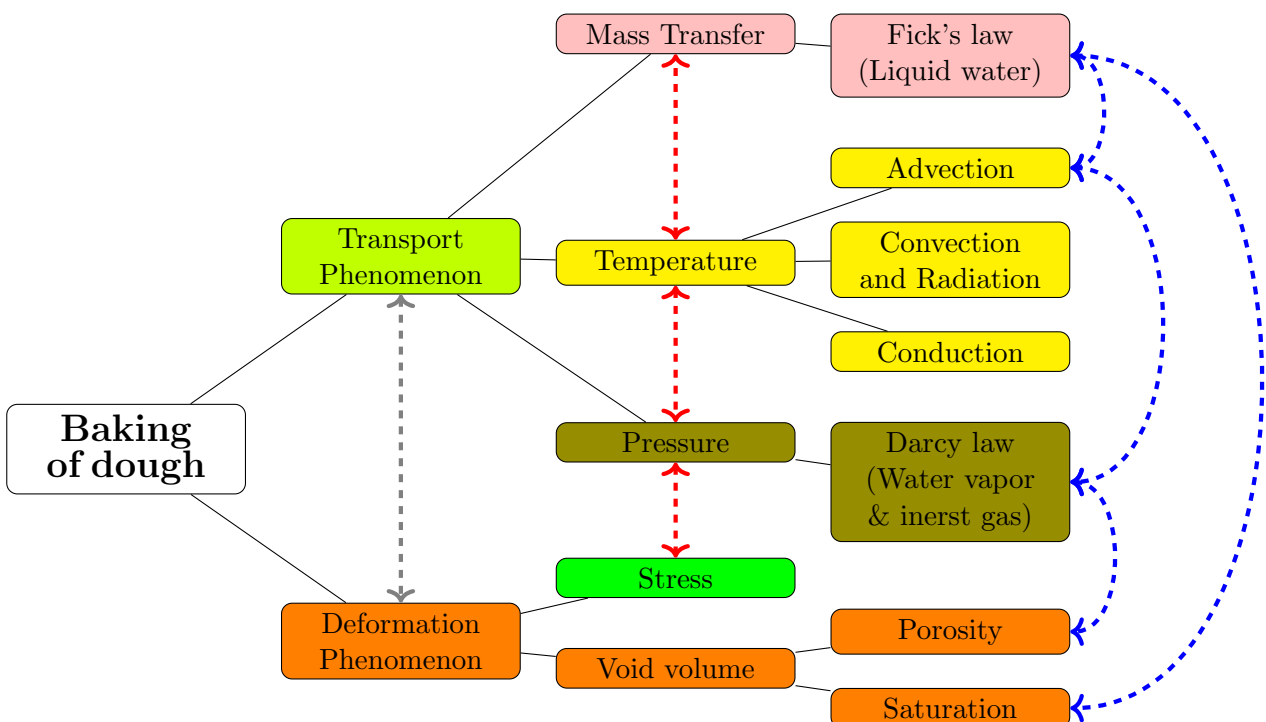


Figure 1.1: Physical phenomena

Tortuosity Tortuosity (ω) gives an idea how the porous structure is distributed inside. It is defined as the ratio of actual path covered by a fluid particle between two points inside to the shortest distance between them.

Saturation Saturation (S) comes into play when the porous medium is composed of more than one fluid and could be defined as fraction of volume occupied by a fluid in the void volume. Depending upon the fluids in the medium, saturation can be subdivided as gas saturation (S_g), liquid saturation (S_l) and sometimes liquid 2 saturation . For example, deep frying of meat in oil, the porous media which is meat has water, water vapor and oil (two immiscible fluids). It should be noted that the summation of all fluid saturations is always unity.

Water content Water content (U) is the amount of liquid water present inside the medium. It is ratio of liquid mass to solid mass and can be extended as ratio of liquid apparent density to solid apparent density.

$$U = \frac{\rho_l^a}{\rho_s^a} \quad (1.1)$$

Water activity (a_w) gives the relative humidity in the medium which is usually defined as ratio of actual vapor pressure present in the medium to equilibrium vapor pressure. There are several mathematical expressions for water activity which are given either as function of water content or as function of temperature and water content. With known water activity and saturated vapor pressure (from literature), the actual vapor pressure inside the medium could be found, assuming equilibrium condition.

$$a_w = \frac{P_v}{p_{v, \text{sat}}} \quad (1.2)$$

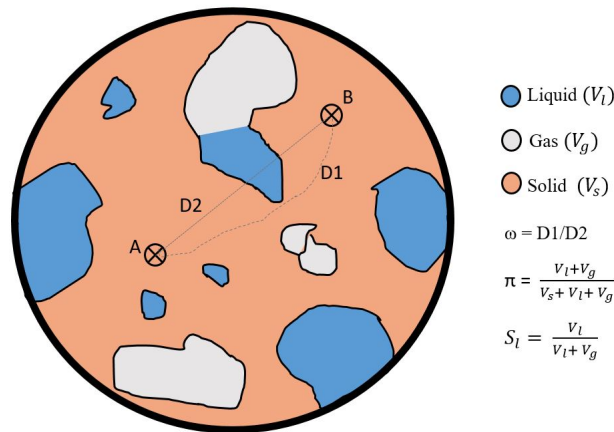


Figure 1.2: Pore structure

1.2 Modeling approaches

In literature, there are many mathematical formulations available that describe baking of dough. According to Datta [1], the mathematical approaches can be classified based on their origin and concept inspiration as given below.

Phenomenological approach This approach is formulated based on observations and empirical factors. Examples of such model are Luikov's model [2, 3], Zannoni model [4], Thorvaldsson model [5], etc. The advantage of this approach lies in its formulation simplicity, but it lacks in providing proper knowledge of some physical parameters as these are approximated by experimental measurements and therefore, vary from experiment to experiment (like thermo-gradient δ , diffusion coefficient ε , phase conversion factor ϵ that appear in Luikov's model). Analytical solutions for Luikov's model are readily available for certain configurations of boundary conditions [6, 7].

Mechanistic approach This approach is developed from the laws of conservation. Whitaker's model [8], Lostie model [9], De Vries model [10] are few to be labeled under this approach. The main advantages are simple and clear mathematical expressions. Since it is derived from physics, there is no ambiguity in the physical parameters.

Semi-empirical approach Although mechanistic model is simple in formulation, yet it sometimes leads to complications during computing. This is apparent when estimating liquid permeability and capillary pressure for calculating the mass flux of liquid water becomes tedious. This can be simplified by combining liquid water and water vapor as moisture content so as to reduce an elaborate diffusion term into an effective diffusion (D_{eff}). Many authors nowadays use semi-empirical approach as evident from Zhang model [11], Nicolas model [12], etc. Effective properties or simplified parameters are also obtained by making approximations from experimental measurements. The origin of semi-empirical approach is similar to mechanistic approach and is governed by laws of conservation.

1.2.1 Transport mechanisms

A material that deforms during heating process with a large portion of bound water is called hygroscopic material. Bakery products are categorized as hygroscopic material due to deformation of dough during baking. In these materials, mass transport mechanisms are mainly due to molecular diffusion, capillary diffusion (for liquid) and convection (Darcy flow). By assuming Stoke's flow for the momentum of gases in porous media, Whitaker has derived velocity term based on Darcy's law [13]. The number of governing equations to be solved are reduced as Whitaker's velocity term for gases gets incorporated in their respective mass conservation equations.

Molecular diffusion The gaseous components, vapor and air (CO_2), undergo binary diffusion which is governed by Fick's law. The mass flux is given by following equation

$$\mathbf{n}_g^F = -D_g \nabla \left(\frac{x}{X} \right) \quad (1.3)$$

where x is the concentration of a particular gas, X corresponds to total concentration of gaseous mixture, D_g is binary diffusivity of gases in porous medium.

Convection It represents the flow of gaseous phase under the influence of pressure by Darcy's law.

$$n_g^D = -\rho_x \frac{k_g}{\mu_g} \nabla P_g \quad (1.4)$$

where k_g is the gas permeability, μ_g is the viscosity of gas, P_g is the total gas pressure inside medium. In nutshell, mass flux for gaseous phase is given as

$$n_g = n_g^D + n_g^F \quad (1.5)$$

and is written as follows

$$n_g = -\rho_x \frac{k_g}{\mu_g} \nabla P_g - D_g \nabla \left(\frac{x}{X} \right) \quad (1.6)$$

Mass flux for moisture Since liquid water is strongly bonded with starch or dough, mass flux by Fick's law of diffusion cannot be implemented here. Instead, diffusion due to pressure difference is taken. The capillary pressure ($p_c = P - P_l$) is a function of liquid saturation (S_w) and temperature (T) [14].

$$n_l = -\rho_l \frac{k_l}{\mu_l} \nabla P_l \quad (1.7)$$

$$= -\rho_l \frac{k_l}{\mu_l} \nabla (P - p_c) \quad (1.8)$$

$$= -\rho_l \frac{k_l}{\mu_l} \nabla P - \underbrace{\rho_l \frac{k_l}{\mu_l} \frac{\partial p_c}{\partial S_l}}_{D_l^S} \nabla S_l - \underbrace{\rho_l \frac{k_l}{\mu_l} \frac{\partial p_c}{\partial T}}_{D_l^T} \nabla T \quad (1.9)$$

which can be written by introducing the coefficients D_l^S and D_l^T as :

$$n_l = -\rho_l \frac{k_l}{\mu_l} \nabla P - D_l^S \nabla S_l - D_l^T \nabla T \quad (1.10)$$

The coefficients in the above equations can be simplified. As liquid permeability k_w tends to zero, hence the term associated with ∇P can be neglected. By expressing liquid saturation S_w in form of moisture content, the above expression is simplified as

$$n_l = -D_{eff} (\nabla U + \delta_T \nabla T) \quad (1.11)$$

where U is moisture content (ratio of apparent liquid density to apparent solid density), δ_T is thermo-gradient coefficient which is responsible for Soret effect. Due to weak contribution of Soret effect (generally in range of 10^{-3}), the expression is further simplified as

$$n_l = -D_{eff} \nabla U \quad (1.12)$$

In some cases, diffusivity of liquid water is defined as product of hydraulic conductivity (K_l) and change of capillary pressure (p_c) with respect to moisture content [10].

$$D_{eff} = K_l \frac{\partial p_c}{\partial U} \quad (1.13)$$

Hydraulic conductivity is the property of porous system. It is the ability of the material to transmit fluid through its void volume by means of hydraulic pressure gradient. Hydraulic

conductivity can be defined from permeability, viscosity and density of the fluid.

Soret effect This effect is neglected in most of the modeling approaches due to its weak contribution. Moisture diffusion due to temperature gradient in Nicolas model [12] is derived from ideal gas law and does directly indicate the Soret effect of diffusion. But in Luikov's model, Soret effect is taken care by the term δ_T which is given by

$$\delta_T = \frac{(\partial U / \partial T)_U}{(\partial T / \partial U)_T} \quad (1.14)$$

Energy transport Energy here refers only to thermal energy gets migrated from hotter region to colder region by Fourier law of conduction, convective, radiative and advective modes. Diffusive transport by conduction is the predominant mode when Peclet number (Pe) that is the ratio of advective transport rate to diffusive transport rate, is very much smaller than 1 ($Pe \ll 1$). This is because of low permeability and diffusion of gases as these are responsible for convective transfer of heat in void volume. With this understanding, the major contribution of energy (heat) transfer is by conduction and can be represented by

$$\mathbf{n}_q = -\lambda_{eff} \nabla T \quad (1.15)$$

Contact resistance In this work, baking is performed by placing the dough over a hot plate (experimental set-up will be explained in chapter 2). When two dissimilar metals come in contact, the heat flux from one surface to another is constrained due to microscopic irregularities at the contact surface. This is called as thermal contact resistance. Since there is transformation of the product during the baking of dough into bakery product, thermal contact resistance varies as a function of time at the point of contact. The inverse of thermal contact resistance gives a parameter analogous to convective heat transfer coefficient ($W/(m^2.K)$). It is included in while estimating the heat flux leaving the surface of the hot plate. Since the system in equilibrium, it is assumed that the heat flux entering the dough is equivalent to that leaving the hot plate via the contact surface.

1.2.2 Models from literature

Luikov's model Luikov's equations are coupled heat and mass transfer equations, based on simple phenomenological approach. There are some uncertainties in the model for describing baking of dough. The main challenge with the model is its inability to formulate evaporation-condensation effect completely [15, 16] which is one of the significant processes during baking and explains migration of moisture content. Nonetheless, Rita et al. [17] used this model to predict phase conversion factor as a function for baking of potato and Ivanka et al. [3] used this to simulate baking of bread in microwave oven. However, the measured temperature profiles matched with simulated profiles. Also, the simulated moisture content almost matches with other literature and is a bit surprising. The governing equations for Luikov's model are stated as follows [18]

$$\frac{\partial T}{\partial t} = \nabla(a_T \nabla T) + \varepsilon \frac{r}{C} \frac{\partial U}{\partial t} \quad (1.16)$$

for temperature gradient

$$\frac{\partial \mathbf{u}}{\partial t} = \nabla \left(\alpha_{\mathbf{u}} (\nabla \mathbf{u} + \delta_{\mathbf{T}} \nabla T + \delta_{\mathbf{P}} \nabla P) \right) \quad (1.17)$$

for total moisture content

$$\frac{\partial P}{\partial t} = \nabla (\alpha_{\mathbf{P}} \nabla P) - \varepsilon \frac{\partial \mathbf{u}}{\partial t} \quad (1.18)$$

for total pressure in the medium.

The parameters appearing in equations (1.16) - (1.18) are defined as $\alpha_{\mathbf{T}}$ - thermal diffusivity, ε - phase conversion factor, r - latent heat of vaporization, $\alpha_{\mathbf{u}}$ - mass diffusivity, $\delta_{\mathbf{T}}$ - thermo-gradient, $\delta_{\mathbf{P}}$ - mass transfer coefficient and $\alpha_{\mathbf{P}}$ - diffusion coefficient for filtration motion. Most of these parameters are approximated for particular experimental setup. The biggest advantage of these coupled equations is availability of analytical solution for certain geometries, boundary conditions, etc. that enables the numerical stability and accuracy of forward problem while solving the inverse problem.

Purlis model Purlis and Salvadori [19, 20] developed a model for baking of bread using moving boundary problem (MBP) or Stefan problem. Authors have used coupled equations and effective thermophysical properties as functions of temperature to replicate evaporation-condensation effect and movement of dough boundary as crust transforms into crumb. This kind of modeling can be categorized under semi-empirical approach. The equations developed by authors are as follows:

$$\rho C_p \frac{\partial T}{\partial t} = \nabla (k \nabla T) \quad (1.19)$$

for temperature, and

$$\frac{\partial \mathbf{u}}{\partial t} = \nabla (D \nabla \mathbf{u}) \quad (1.20)$$

for mass balance.

The MBP formulation in this problem considers the jump in thermophysical properties ρC_p , k and D appearing in equations (1.19)-(1.20) that is caused by enthalpy change (see figure 1.3). Thus, product properties are approximated as a function of temperature with some discontinuities around evaporation temperature as can be seen in the previous figure. Deformation of dough during baking is also taken into account by one-way coupling. Deformation is measured experimentally and implemented in the model via moving mesh algorithm.

Lostie model Lostie et al. [9] formulated a mathematical model for baking of sponge cake and successfully estimated various unknown parameters from experimental measurements to complete the system. This model is based on mechanistic approach where the origin of governing equations is from laws of conservation. The deformation effect is taken into account by two-way coupling. This implies that the change in product volume is computed as a function of stress-strain variation inside the product which is dough and is considered as a viscous fluid. The energy balance incorporates enthalpy formulation and moisture content that is the total water content (liquid + vapor) inside the medium as

$$\rho_s \frac{\partial}{\partial t} \left((1 - \pi) h (X H_l + X_v H_v + X_a H_a + H_s) \right) = \nabla (\lambda \nabla T - H_l n_l - H_v n_v - H_a n_a - H_s n_s) \quad (1.21)$$

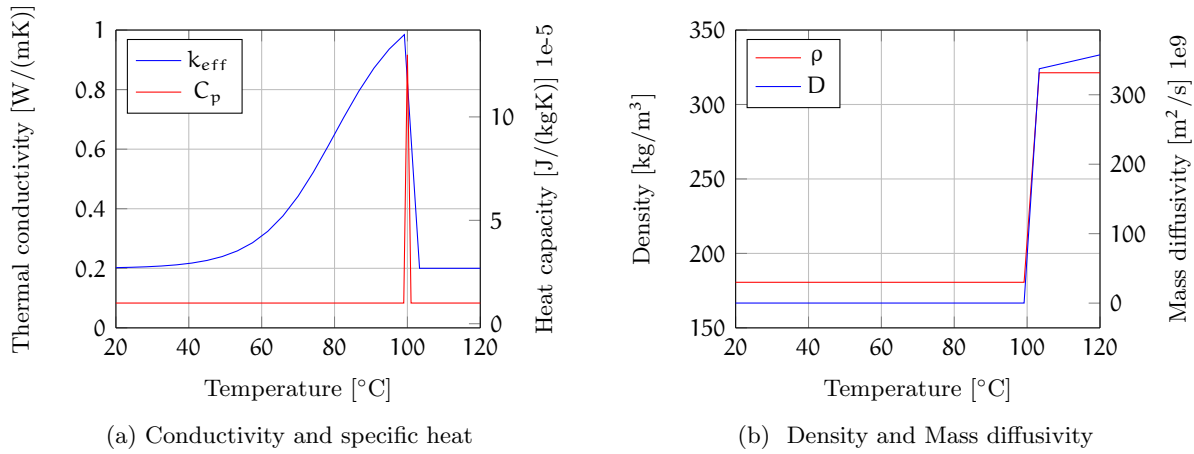


Figure 1.3: Evolution of thermal conductivity, heat capacity (a), density and diffusivity (b) as function of temperature for Purlis model

for energy balance

$$\rho_s \frac{\partial}{\partial t} \left((1 - \pi)h \right) = -\nabla n_s \quad (1.22)$$

for mass balance of solid dough

$$\rho_s \frac{\partial}{\partial t} \left((1 - \pi)h(X + X_v) \right) = -\nabla (n_w + n_v) \quad (1.23)$$

for mass balance of moisture content

$$\rho_s \frac{\partial}{\partial t} \left((1 - \pi)hX_a \right) = -\nabla n_a \quad (1.24)$$

for mass balance of air

$$\Delta P = \eta \nabla v \quad (1.25)$$

for deformation considering the case of viscous material.

The parameters are π - porosity, h - height of the product, ρ_s - solid density, X - moisture content, X_v - vapor content, X_a - air content, $H_{l,v,a,s}$ - H is enthalpy of liquid water, water vapor, air and solid respectively, $n_{l,v,a,s}$ - n is mass flux of liquid, vapor, air and solid correspondingly. The mass flux of gaseous phase is given by equation (1.6), for liquid by equation (1.12) and for solid by deformation velocity v 1.25. Further, some other models in literature namely Zhang and Datta, Nicolas et al. [11, 12] are similar to Lostie model but they have considered dough as viscoelastic material like rubber and not as viscous material. The change of pressure inside the medium is solely responsible for inducing the stress on the structure which results in volumetric strain given by equation 1.25.

1.3 Required physical properties and methods for determining them

There are numerous physical properties that are required to complete the formulation of these mathematical models and are listed here.

Thermal conductivity Thermal conductivity (λ_{eff}) is calculated as effective property and as a function of temperature and moisture content. There are different approaches for estimation

of effective thermal conductivity such as series, parallel and Maxwell's model [?, 21].

Series model In this model, the effective conductivity is computed as the inverse of sum of the thermal conductivity of the components placed in a series.

$$\lambda_{\text{eff}} = \frac{1}{\frac{\epsilon_s}{\lambda_s} + \frac{\epsilon_l}{\lambda_l} + \frac{\epsilon_g}{\lambda_g}} \quad (1.26)$$

Where ϵ_i is volume fraction of i^{th} component and i can be s - solid, l - liquid and g - gas. Volume fractions of liquid and gases are mostly functions of moisture content and hence the effective thermal conductivity is strongly influenced by moisture content and porosity.

Parallel model. Here, the effective conductivity is computed for the components that are placed in parallel mode.

$$\lambda_{\text{eff}} = \epsilon_s \lambda_s + \epsilon_l \lambda_l + \epsilon_g \lambda_g \quad (1.27)$$

Maxwell's model. This model is mathematically described as

$$\lambda_{\text{eff}} = \lambda_d \frac{2\lambda_d + \lambda_g - 2\epsilon_g(\lambda_d - \lambda_g)}{2\lambda_d + \lambda_g + \epsilon_g(\lambda_d - \lambda_g)} \quad (1.28)$$

For clarity, the variation of thermal conductivity as a function of liquid saturation for constant porosity is given in figure 1.4. These are generally used methods to calculate effective thermal conductivity in porous media and in multi-phase approach.

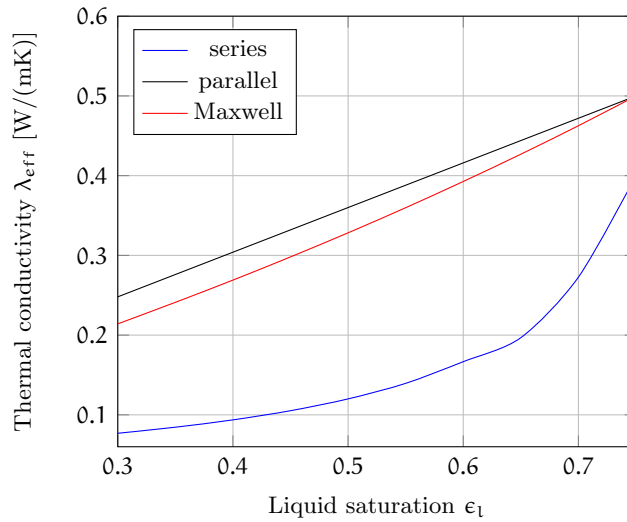


Figure 1.4: Evolution of thermal conductivity as function of liquid saturation with constant porosity

Diffusivity of liquid water: Diffusivity of liquid water (D_{eff}) is given as function of moisture content by Zhang and Datta [11]. Liquid water's diffusivity increases exponentially with the increase in concentration.

$$D_{\text{eff}} = 10^{-9} \times \exp\left(\pi[-2.5 + 2U]\right) \quad (1.29)$$

Binary diffusivity of gases The binary diffusion (D_g) between the gases (gaseous phase) inside the porous media is influenced by porosity (π) and tortuosity [1]. Hence, the standard expression for this diffusivity is not valid and needs to be modified prior to use.

$$D_g = \pi \frac{D_{vc}}{\omega} \quad (1.30)$$

Tortuosity (ω) is defined as ratio of actual path taken by fluid element between two points to shortest distance between them. It depends on porosity and liquid saturation and eventually the above equation can be rewritten as,

$$D_g = D_{vc} \left([1 - 1.11S_l] \pi \right)^{4/3} \quad (1.31)$$

Gas permeability Gas permeability (k_g) plays an important role in the transportation of gaseous phase through pores which is extracted based on Darcy's law. Since unreacted gases can move only in the volume unoccupied by liquid inside the total void volume also known as gas volume fraction (ratio of gas volume to total volume), gas permeability can be stated as a function of saturation [11].

$$k_g = 2.45(1 - 1.11S_l) \times 10^{-12} \quad (1.32)$$

As noticeable from expressions of k_g and D_g , tortuosity (ω) is expressed as $1 - 1.11S_l$, approximately.

Rheological properties Dough has been considered either as viscous or viscoelastic material. Based on this assumption, two models have been developed and are explained below. **Viscous model** Many authors have considered dough during baking as viscous fluid [9, 22]. This is advantageous over the visco-elastic model due to its simplicity and addition of just one equation to the balance equations that are considered for dough's deformation. Lostie et al. [9] approximated the dough's viscosity as a constant and obtained it by parameter estimation of the following stress-strain relation for fluids,

$$\frac{d\epsilon_i}{dt} = v_i = \frac{S_i}{\eta} \quad (1.33)$$

where ϵ_i is strain in i^{th} direction and its time derivative can be replaced by velocity component of solid in the corresponding direction, S_i is stress experienced which is usually equated to internal gas pressure and η is viscosity of the dough. Fan et al. [22] assumed dough as a bubble and their model gave viscosity as a function of temperature.

$$\eta = m_0 \exp \left[\frac{E_a}{R_g} \left(\frac{1}{T} - \frac{1}{T_0} \right) \right] \quad (1.34)$$

Where E_a is the activation energy, R_g is gas constant, m_0 is a constant and T_0 is reference temperature. **Viscoelastic model** Some authors consider dough as viscoelastic material similar to rubber. Such a material shows a behavioral combination of viscous fluid and that of elastic material, placed either in series (Maxwell) or in parallel (Kelvin-Voigt). The stress-strain relation

for a viscous fluid is similar to that of elastic material and is stated as,

$$S_i = \epsilon_i E \quad (1.35)$$

Where E is modulus of elasticity and a simple correlation between viscosity and elasticity is given by a factor called relaxation time (τ , ratio of viscosity η to modulus of elasticity E).

Zhang et al. used a variation of the viscosity given by Fan et al. [22] with relaxation time formulated as a function of temperature as,

$$\tau = 9 \left[\frac{2}{\pi} \arctan \left(\frac{T - 65}{2} \right) + 1 \right] + 2 \quad (1.36)$$

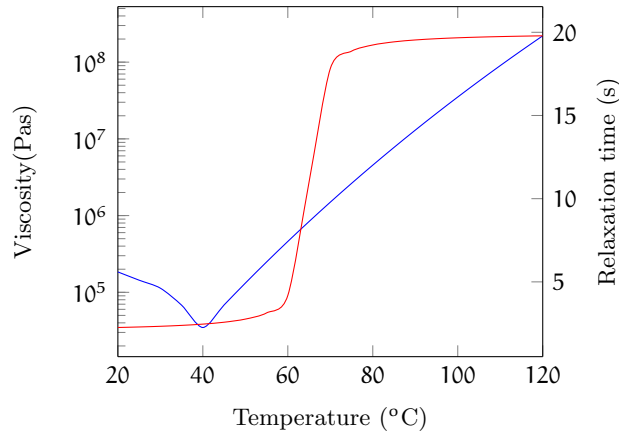


Figure 1.5: Evolution of viscosity (—) and relaxation time (—) as function of temperature [11, 22]

The variation of viscosity (η) and relaxation time (τ) as function of temperature can be seen in figure 1.5. Maxwell model has viscous and elastic members that are placed in series while Kelvin-Voigt model has them in parallel. The difference in these two models is reflected in the strain variations [23] as depicted in figure 1.6b. For constant stress, Maxwell model behaves like Bingham plastic (such as toothpaste) which starts to deform linearly after a certain stress value, whereas Kelvin-Voigt model shows non-linear increase right from the beginning. Mathematical expression for Maxwell model is as follows

$$\epsilon_i^t = \epsilon_i^E + \epsilon_i^\eta \quad (1.37)$$

Since the spring and dashpot are in series, then the derivative is obtained as

$$\frac{d\epsilon_i^t}{dt} = \frac{d\epsilon_i^E}{dt} + \frac{d\epsilon_i^\eta}{dt} = \frac{d}{dt} \left(\frac{S_i}{E} \right) + \frac{S_i}{\eta} \quad (1.38)$$

Which can be written in the following form

$$\eta \frac{d\epsilon_i^t}{dt} = \eta \frac{d}{dt} (S_i E) + S_i = \frac{d}{dt} \left(\frac{\eta^2 S_i}{2E} \right) + S_i$$

This can be further simplified as

$$\eta \frac{d\epsilon_i^t}{dt} = \frac{d}{dt} \left(\frac{\tau\eta S_i}{2} \right) + S_i \quad (1.39)$$

In Kelvin-Voigt model, spring and dashpot are in parallel and it is given by,

$$S_i^t = S_i^E + S_i^\eta \Leftrightarrow S_i^t = \epsilon_i E + \eta \frac{d\epsilon_i}{dt} \quad (1.40)$$

Usually in baking, the trend of deformation of bakery product replicates Kelvin-Voigt model. So, this model is considered for calculation of deformation. Upon knowing all the relevant parameters in equation (1.40), the deformation rate or solid velocity can be evaluated [24] with S_i as relative gas pressure inside the medium.

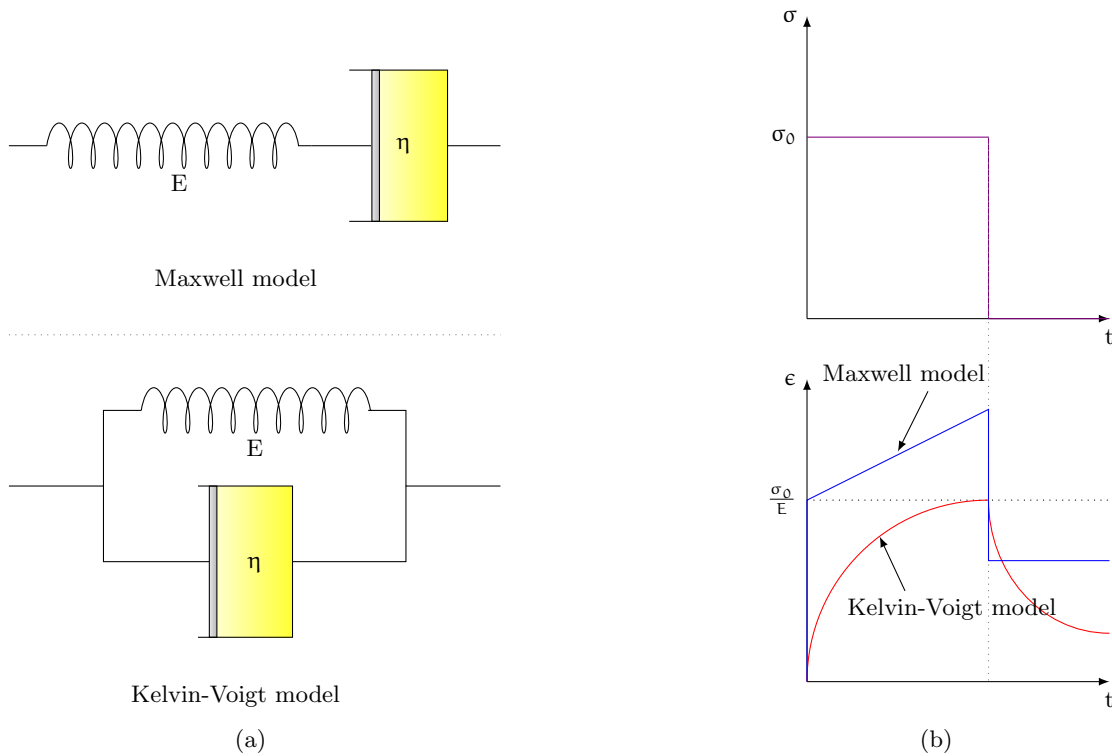


Figure 1.6: Spring and dash-pot arrangement for Maxwell, Kelvin model (a) and evolution of strain with time with applied stress for corresponding models (b)

1.4 Inverse procedure for properties determination

Inverse problem is an optimization based approach to search for a set of parameters or functions that minimizes or maximizes the cost or objective function at a certain condition. In this case, the objective function contains measurement and simulated data of temperature, moisture content, pressure and volume of the dough during baking. For the case of parameter or function estimation, the motive would be minimizing the euclidean distance between measurements and simulated data. There are two methods namely gradient-based and gradient-free methods for solving inverse problem. In gradient-based optimization, Conjugate Gradient Method (CGM), trust region method, Levenberg-Marquardt method are most commonly used tools. For computing the sensitivity or Jacobian matrix, which is an important component for solving gradient

based optimization, either complex step differentiation or finite difference central scheme is used and will be explained later.

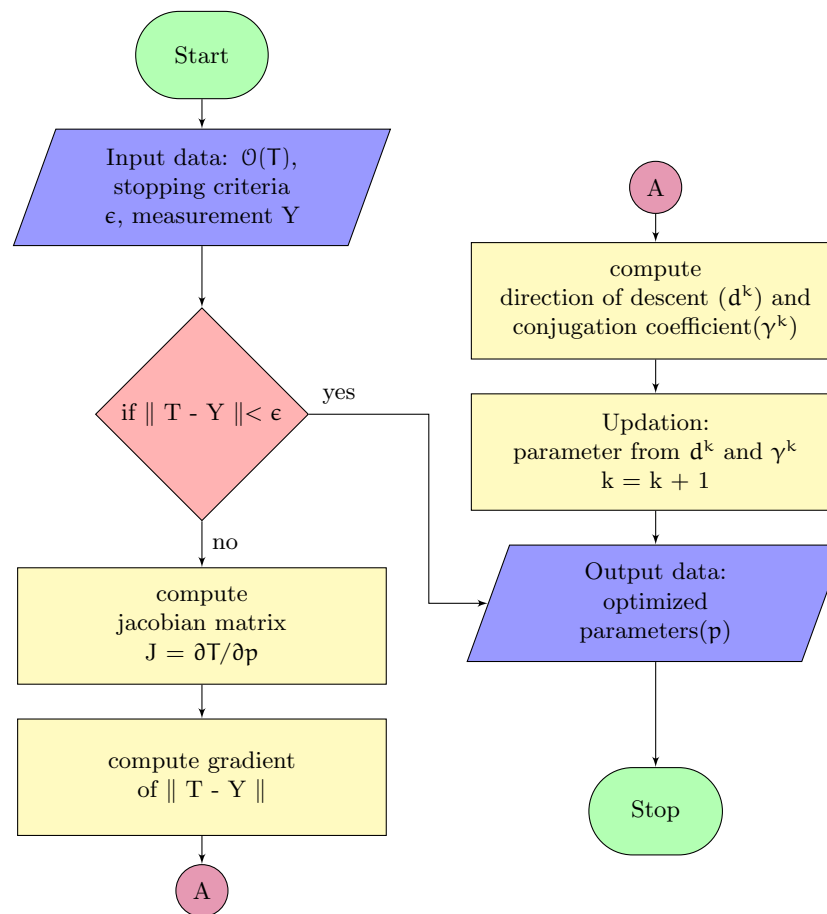


Figure 1.7: Flow chart for conjugate gradient method

1.4.1 Note about function estimation

Sometimes the evolution or behavior of a function is known through experimentation or from physics. For example, generally the mass diffusivity evolves exponentially with its component's concentration during diffusion. In such cases, the function can be expressed mathematically with some unknown coefficients and can be predicted by parameter estimation. But when the unknown variable is to be optimized as a function of state variables with no prior information, then the inverse problem leads to estimation of function. Function estimation procedure is different from parameter estimation as it deals with minimization of functional. The sensitivity or Jacobian matrix is replaced by variational problem as the variation of the undetermined function is not known beforehand. To ease the computation of functional gradient, Lagrange multipliers are included converting it into adjoint problem. This method of inverse problem is elaborated with examples in chapter 3 of book "Inverse Heat Transfer: Fundamentals and Applications", by M. Necati Özisik and Helico R. B. Orlande.

Parameterized form of function estimation

Any curve could be approximated by means of basis functions. By varying the coefficients of basis functions, a desired profile can be extracted using B-spline or β -spline. B-spline [25] is very

similar to polynomial interpolation such as Lagrange form and is formed by combining several piecewise polynomials. The basis function, $B_{i,k}(t)$, is defined as:

$$B_{i,k}(t) = \frac{t - t_i}{t_{i+k-1} - t_i} B_{i,k-1}(t) + \frac{t_{i+k} - t}{t_{i+k} - t_{i+1}} B_{i+1,k-1}(t) \quad \text{for } k > 1, i = 0, 1, \dots, n \quad (1.41)$$

Where k is the order of the polynomial and n is total number of polynomial pieces which is at least greater than $k - 1$. The points where pieces of polynomial meet are known as knots and are given in vector form called knot vector(t). The function passes through a set of points that determine the behavior of the curve and are called de Boor points or control. There are $n+1$ control points. The B-spline is defined as linear combination of control points and basis functions that is given by

$$f(x) = \sum_{i=1}^n p_i B_{i,k}(x), \quad n \geq k - 1 \quad (1.42)$$

By taking advantage of B-spline and implementing in inverse problem would reduced function estimation of $f(x)$ to parameter estimation of $P = [p_1, p_2, \dots, p_n]$.

List of symbols

Latin symbols

α_i	Diffusivity of i element [m^2/s]
S	Saturation [m^3/m^3]
U	Moisture content [$kg/kg \text{ dm}$]
α_w	Water activity
P	Pressure [Pa]
n_i	Mass flux of species i [kg/m^2s]
k_i	Permeability of species i [m^2]
D_g	Mass diffusivity of species i [m^2/s]
K_l	Hydraulic conductivity [m/s]
T	Temperature [K]
r	latent heat of vaporization [J/kg]
H_i	Enthalpy of element i [J]
v	Solid velocity [m/s]

E_a	Activation energy [J/mol]
E	Modulus of elasticity [Pa]
$B_{i,k}$	Basis function
p	Coefficient of basis function

Greek symbols

ρ	Density [kg/m ³]
π	Porosity
ϵ	Phase conversion factor
ϵ_i	Volume fraction of element i
ϵ_i^j	Strain due to component i at location j
λ	Thermal conductivity [W/(mK)]
ω	Tortuosity
η	Dynamic viscosity of solid [Pa.s]
μ	Dynamic viscosity of gas [Pa.s]
∇	gradient [1/m]
δ_T	thermogradient coefficient [1/K]
δ_p	Filtration transfer coefficient of vapor [1/Pa]
τ	Relaxation time [s]

Subscripts

c	capillary
eff	effective
s	solid
l	liquid
v	vapor
g	gas

Superscripts

S	saturation
T	temperature
F	Fick's diffusion
D	Darcy diffusion
α	apparent
sat	saturated

Bibliography

- [1] A.K. Datta. Porous media approaches to studying simultaneous heat and mass transfer in food processes i : Problem formulations. *Journal of Food Engineering*, 80:80–95, 2007.
- [2] Luikov A.V. Systems of differential equations of heat and mass transfer in capillary porous bodies(review). *Int. J. Heat Mass Transfer*, 18:1–14, 1975.
- [3] Ivanka Zheleva and Veselka Kamburova. *Modeling of Heating During Food Processing*, pages 79–99. Springer US, Boston, MA, 2009.
- [4] B. Zanoni, S. Pierucci, and C. Peri. Study of the bread baking process — ii. mathematical modelling. *Journal of Food Engineering*, 23(3):321 – 336, 1994.
- [5] Karin Thorvaldsson and Hans Janestad. A model for simultaneous heat, water and vapour diffusion. *Journal of Food Engineering*, 40(3):167 – 172, 1999.
- [6] Renata S.G. Conceição, Emanuel N. Macêdo, B.D. Pereira, Lucíia, and João N.N. Quaresma. Hybrid integral transform solution for the analysis of drying in spherical capillary-porous solids based on luikov equations with pressure gradient. *International Journal of Thermal Sciences*, 71:216 – 236, 2013.
- [7] Puvikkarasan Jayapragasam, Pascal Le Bideau, and Tahar Loulou. Luikov's analytical solution with complex eigenvalues in intensive drying. *Transport in Porous Media*, 130:923–946, 2019.
- [8] Stephen Whitaker. Simultaneous heat, mass and momentum transfer in porous media: A theory of drying. *Advances in Heat Transfer*, 13:119–203, 1977.
- [9] Mathieu Lostie, Roman Peczalski, Julien Andrieu, and Michel Laurent. Study of sponge cake batter baking process. ii. modeling and parameter estimation. *Journal of Food Engineering*, 55(4):349 – 357, 2002.

- [10] D. A. De Vries. Simultaneous transfer of heat and moisture in porous media. *Transactions, American Geophysical Union*, 39(5):909 – 916, 1958.
- [11] Zhang J. and Datta A.K. Mathematical modeling of bread baking process. *Journal of Food Engineering*, 75:78–89, 2006.
- [12] Nicolas V., Salagnac P., Glouannec P., Ploteau J.P., Jury V., and Boillereaux L. Modelling heat and mass transfer in deformable porous media : Application to bread baking. *Journal of Food Engineering*, 130:23–35, 2014.
- [13] Stephen Whitaker. Flow in porous media i: A theoretical derivation of darcy’s law. *Transport on Porous Media*, 1:3–25, 1986.
- [14] H. Ni, A. K. Datta, and K. E. Torrance. Moisture transport in intensive microwave heating of biomaterials: A multiphase porous media model. *International Journal of Heat and Mass Transfer*, 42(8):1501–1512, 1999.
- [15] Zhang J. and Datta A.K. Some considerations in modeling of moisture transport in heating of hygroscopic materials. *Drying Technology*, 22(8):1983–2008, 2004.
- [16] Chen X.D. and Putranto A. *Modeling Drying Processes: A Reaction Engineering Approach*. Cambridge University Press, 2013.
- [17] Rita M. Ablalone, Analia G. Gastón, and Miguel A.Lara. Effect of phase change criterion on the prediction of temperature evolution during food drying. *Mecánica Computacional*, XXIV:1135–1147, 2005.
- [18] Luikov A.V. *Heat and mass transfer in capillary porous bodies*. Pergamon Press, 1966.
- [19] Emmanuel Purlis and Viviana O. Salvadori. Bread baking as a moving boundary problem. part 2: Model validation and numerical simulation. *Journal of Food Engineering*, 91:434 – 442, 2009.
- [20] Emmanuel Purlis and Viviana O. Salvadori. A moving boundary problem in a food material undergoing volume change – simulation of bread baking. *Food Research International*, 43(4):949–958, 2010.
- [21] V. Jury, J. Monteau, J. Comiti, and A. Le-Bail. Determination and prediction of thermal conductivity of frozen part baked bread during thawing and baking. *Food Research International*, 40(7):874–882, 2007.
- [22] J. Fan, J.R. Mitchell, and J.M.V. Blanshard. A model for the oven rise of dough during baking. *Journal of Food Engineering*, 41(2):69 – 77, 1999.
- [23] Peter Moczo, Jozef Kristek, and Martin Gális. *Rheological models of a continuum*, page 18–57. Cambridge University Press, 2014.
- [24] Hadiyanto, A. Asselman, G. van Straten, R. M. Boom, D. C. Esveld, and A. J.B.van Boxtel. Quality prediction of bakery products in the initial phase of process design. *Innovative Food Science and Emerging Technologies*, 8(2):285–298, 2007.
- [25] Carl de Boor. *A Pratical Guide to Splines*. Springer, 2000.

Chapter 2

Cake baking: Experimental and modeling developments

Abstract

This chapter gives detailed insights on experimental set-up used in one-sided baking. Temperature and mean moisture content are measured for a baking condition. The heat flux at the interface of dough and cast-iron floor is estimated using inverse algorithm and an essential function. Water activity curve is approximated by Ferro-Fontan model. Different mathematical models with varying complexity are developed and validated with thermophysical properties that are obtained from literature.

2.1 Experimental considerations

The measurable thermodynamic variables during baking are temperature, mass of the product and pressure. Temperature variations in the medium can be measured using thermocouple or by non-contact type instruments like pyrometer or an infra-red device. One should remember that introduction of any foreign object into or over the substance under observation shall change its behavior during the process. Placement of thermocouple in parallel to heat transfer can ease the mass transfer but will increase heat conduction by thermocouple. This may lead to local ‘crust fingers’ around the sensor due to difference in their thermal conductivities. If thermocouple is aligned perpendicular to the direction of heat transfer, then the heat conduction is minimized but will hinder mechanical deformation. Crust finger formation can be reduced by using an optical fiber instrument for measuring temperature as its thermal conductivity is of the same order as that of dough. Since baking involves mass transfer phenomena, large number of sensors can lead to baffle effect on fluid migration which will eventually deteriorate the evaporation-condensation process. Hence, while designing the experiment for measurement, it must be assured that addition of sensor is not modifying the process at microscopic level. The second most significant measured quantity is moisture content. Moisture content is obtained from mass variation of the dough. Mass variation occurs due to loss of moisture and gives an overview of evaporation trend in a normalized form. Different measuring techniques to monitor moisture content locally or globally are presented elaborately in the following section § 2.1.1.

Due to complicated pore structure and opening of pores during the process, the measurements provided by pressure transducers are not exactly accurate. The pressure sensor may be positioned sometimes inside the pores or at times may come in contact with solid portion of the dough due to which additional pores may be created in the dough. For optimization problem in this work, the pressure information is neglected.

Initially, the prepared dough is in viscous liquid state. A support is required until dough's solidification or transformation to crumb. A hollow PTFE (polytetrafluoroethylene) mold is used as the support which also acts as an insulation for heat and mass transfer from lateral sides. In order to record temperature at stationary locations, thermocouples are inserted at pre-drilled locations across the PTFE mold. The mold provides provision to the dough, ensures firm positioning of sensors and also reduces the mathematical problem from two-dimensional to one-dimensional.

2.1.1 Moisture content measuring techniques

Water or moisture content in the dough during baking is one of the significant parameters that determines the physical, structural and sensory properties of bakery product. Hence, several attempts have been made to measure moisture content variation locally. Localized information about temperature and moisture content would provide supplementary insight about the mechanisms driving the baking process. Moreover, at least two local measurements will yield a clearer picture of moisture transportation. The measuring techniques can be broadly classified in two types: destructive method and non-destructive method.

Destructive method is an intermediate measuring technique for moisture content. As the name suggests, it disturbs and destructs the dough during baking. A small lump or portion of baking product is sliced out and weighed to obtain local average moisture content [1]. While performing this measurement, the product should be sufficiently long in the direction of the slicing axis. Heat and mass transfer should also be ensured to be taking place along the same direction and needs to be one dimensional. If the baking is two dimensional then equilibrium does not exist and measured local average values would not correspond to accurate measurements. The drawback of this measuring technique is the requirement of skilled labor for slicing out a portion without disturbing the complete process and weighing it before it cools. Measured values by this method prove the concept of rising moisture content within the crumb region due to evaporation-condensation mechanism during baking.

Non-destructive measurement methods are non-intrusive and provide continuous monitoring. This measurement can be sub-categorized as global measurement and local measurement. In global measurement, the moisture content is measured as an overall mean. This can be performed as intermittent or continuous weight measurements. For intermittent measurement, the baking sample needs to be weighed at desired time intervals. Continuous monitoring is not viable when baking in a convectional oven since weighing such a large setup will not be feasible. In such cases, intermediate measurement of moisture content is the best option.

Some other non-invasive, advanced and sophisticated measuring techniques are also available such as NIR (Near Infrared Reflectance) [2, 3], MRI (nuclear Magnetic Resonance Imaging) [4, 5], CT (Computer Tomography), etc. NIR works by principle of optics. Each molecule vibrates at a particular resonance frequency. When a light signal within that resonance frequency is passed, the molecule absorbs the energy from it and converts that energy into kinetic energy. In NIR, an

optic fiber is used to send and collect the signals transmitted back from a molecule at prescribed frequencies. Thorvaldsson [3] have shown excellently the dependency of moisture content with respect to structural change and temperature for the baked bread loaves. But still quantitative measurement of local moisture content for dough during baking process is not shown. It should be also noted that diameter of a probe is about 3 mm.

MIR is another special kind of non-invasive instrument to dynamically measure specific parameters like moisture content, lipid content (if any), void volume. For example, there are other surveying variables than water content and they are oil content and void volume during baking of biscuits available [5]. In MIR imaging, a strong magnetic field is generated that aligns the photons present within the sample along with the magnetic field. The variation in photon density is captured by sending additional energy usually in form of radio waves. This is the basic working principle of MRI scanner. Unlike NIR, MIR gives complete image of the sample at a instance with one non-contact image scanner. The quality of scanned image depends upon moisture content. Baking a dough beyond 20 minutes, excess heating causes the surface to evaporate more in crust region which can not be properly captured by scanner. This is due to loss of water content that reduces the amount of photons present in that particular region affecting the working principle of the instrument. To overcome such situation oil capsules whose melting point is above 120 °C is used on the surface without disturbing the deformation mechanism [4]. The demerits of these local measurements by non-invasive instruments are

1. Lack of proper image interpretation causes poor quantitative measurement during baking of dough.
2. Special experimental set-up is required for MIR imaging due to involvement of magnetic field.
3. Sometimes, the dimensions of the probe are bigger than the sample size (in case of NIR).
4. Separate experimental run is required for temperature measurement. It is imperative for MIR so as to avoid disturbance due to presence of sensor in imaging.

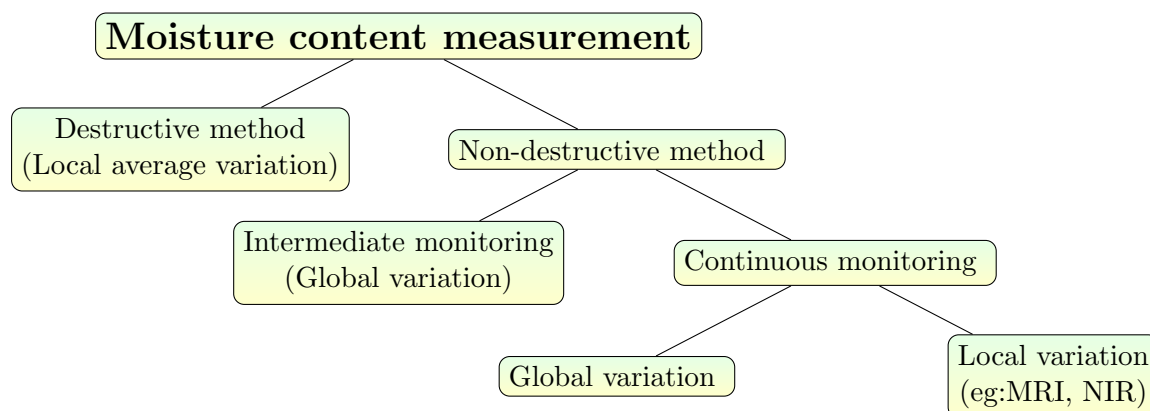


Figure 2.1: Various measuring techniques for water content

2.1.2 Preparation of dough

The ready-made mix Francine ® having right proportions of wheat flour, corn flour, egg white and salt is used for preparing the dough. The mass composition of various components in the

mix for 100 gm weight is presented in table 2.1. The mix is manually stirred with milk in a mass ratio of 33 % and 67% respectively, for a couple of minutes to form dough and is kept aside.

Compositions	mass (gm)
Fat	4.00
Carbohydrate	65.60
Fiber	3.70
Protein	14.00
Salt	1.20
Water	11.50

Table 2.1: Composition for 100 gm of Francine mix

2.1.3 Experimental set-up

Contact baking is similar to domestic cooking over an induction plate and is preferred mode of heating in this case study. In induction based domestic cooking, the coil underneath the ceramic top is supplied with high frequency alternating current, creating electromagnetic effect. This electromagnetic effect is used to generate heat energy when an iron plate (cooking vessel) is placed over the ceramic surface. A heating set-up similar to induction appliance is built with a hot coil that is heated electrically to a desired temperature (usually 200°C). Figure 2.2a shows the cross sectional view of the experimental set-up. A cast iron disk (alike cooking vessel) of diameter 23 cm and height 2cm is placed 2 cm above the coil. Heat transfers from hot coil to the bottom surface of cast iron disk via radiation mode. The entire cast iron disk gets heated up through conduction and also the object kept above it. The circumference of the heating coil and cast iron disk is insulated to ensure unidirectional heat transfer between them and also to reduce energy loss from lateral sides.

Since the cast iron disk does not sit on the coil, it is suspended with the support of suspension strings hanging down the weighting bridge. This construction provides a way for continuous monitoring of the mass variation in the product employing the weighing scale Radwag PS6000 R2. For measuring temperature inside the dough during baking, indigenous K-type thermocouples of diameter 0.125 mm are used. An optical pyrometer Optris CS LT measures the surface temperature. Temperature and mass measurements are acquired at frequency of 50 Hz (sampling interval of 0.02 s) by data acquisition system HBM QuantumX MX1609.

The outgoing heat flux from the surface of cast iron disk into baking product is estimated by a flux-meter. This flux meter is a cylindrical piece of diameter 3 cm that is drilled out from the center of cast iron floor. After gluing thermocouples (T1,T2 and T3) at distinct locations on the flux meter, it is hammered back to cast iron disk [6]. The purpose of flux-meter is to facilitate the heat-flux estimation by providing measurement of transient temperatures across the cast iron disk at different isotherm lines.

A polytetrafluoroethylene (PTFE) mold with 14×11.5×2 cm² hollow volume acts as support for dough and temperature sensors. Aluminum foil is spread across inner surface and at bottom of the mold before using it for baking. This assures uniform heating at the bottom and also easy removal of the baked product without any damage after the experiment. In the beginning,

thermostat for the heating coil is adjusted for a desired temperature and waited to attain thermal equilibrium. Once the temperatures of cast-iron is stabilized, the dough is poured inside the mold. Dough is baked for 20 minutes. The experimental duration of 20 minutes is an arbitrary choice.

Temperature variation inside the dough is measured at three different locations: one near bottom (T4) and two near center (T5,T6). The position of thermocouples inside the mold is fixed firmly with aid of the PTFE mold. Surface temperature is measured by optical pyrometer with emissivity of the dough being set to 0.9 [7]. Sensor locations for entire set-up are mentioned with relative to the surface of heating coil (reference point) in table 2.2.

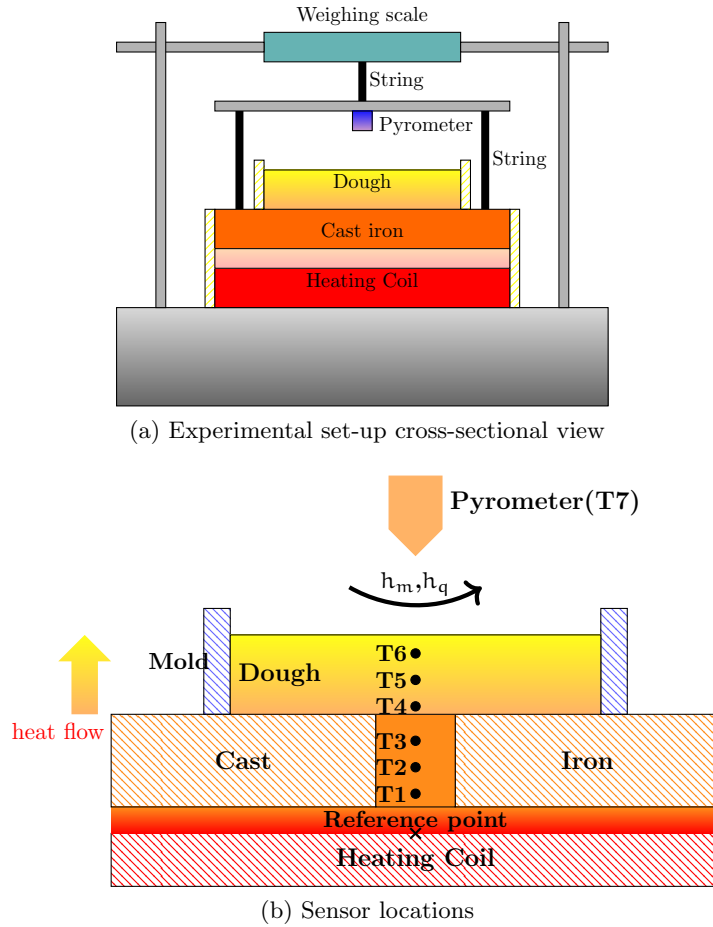


Figure 2.2: Schematic representation of experimental set-up

Thermocouple	distance (mm)	Thermocouple	distance (mm)
Cast iron		Dough	
T1	15	T4	31
T2	17.5	T5	34
T3	27	T6	37
T7 - Pyrometer			

Table 2.2: Sensor locations from surface of heating coil

2.1.4 Typical baking test

Baking experiment is carried out with thermostat set at 200°C and is repeated 4 times to statistically evaluate the measurement uncertainties and experimental bias. The temperature and moisture variations with respect to baking time are presented in figure 2.3. Moisture content is defined here as ratio of liquid mass to solid dry mass of dough. Solid or dry mass of the dough is measured by weighing the mass of the baked product after drying it in a climatic chamber at 0% relative humidity, 104°C for a day. Subtracting this solid mass from the total mass measured initially before baking, gives the liquid mass of the dough. It is assumed that the mass contribution from gases is negligible. The error in measurements is calculated statistically by standard student T distribution for the four trials [8].

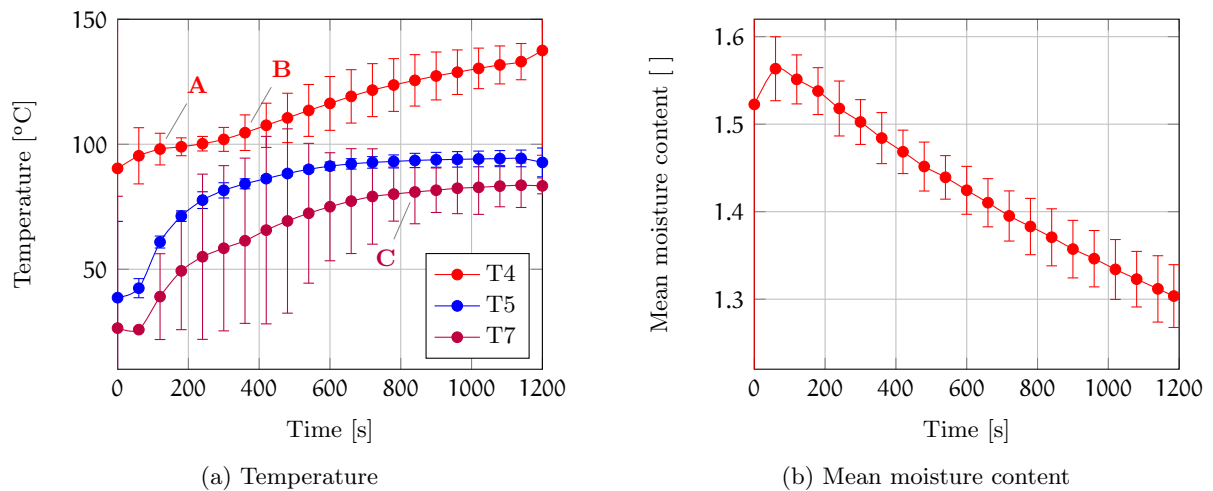


Figure 2.3: Experimental measurements of temperature (a) and mean moisture content (b) for dough

Understanding the experimental temperature and moisture content trends

Usually there are two intermediate stages for dough transformation during baking process. They are heating-up period and crust-crumb formation stage. Heating-up period is defined as when there is steep increase in temperature implying that dough takes sufficient heat before any transformation and then the temperature nearly plateaus during crumb formation. This plateau is due to absorption of latent heat by liquid water inside the dough. Crust formation takes place when the temperature begins to increase after the plateau period. Looking at the measured temperature profile (see figure 2.3a) from thermocouple T4, time period up to point A is the heating up stage, region between A and B is crumb-crust transformation zone and beyond point B is crust formation stage. Due to contact baking the heating up period is very short and last for only two minutes, while in oven baking it takes at least five minutes to reach this point [9, 10]. Going up from the base of the dough, temperature measured by thermocouples T5, T6 (not shown) and T7 shows similar behavior which is different from that of T4 as they show larger heating up period upto point C. The reason for such long heating period is due to crust formation at the bottom whose heat transferring capacity is lower than dough. Beyond point C, the plateau indicates crumb formation making the dough soft and moist. Mean moisture content measurement (see figure 2.3b) shows a linear mass loss throughout the baking period

depicting that overall evaporation rate is nearly constant. Figure 2.4 shows the derivative of mass loss with respect to time. Due to fluctuation in measurements, moving average with 50 elements gives a clear view of mass loss rate. The average trend shows maximum positive slope for first 200 s and a small negative slope beyond 200 s. This indicates a rapid mass loss for first few minutes and then the rate is slowed due to condensation and mechanical deformations.

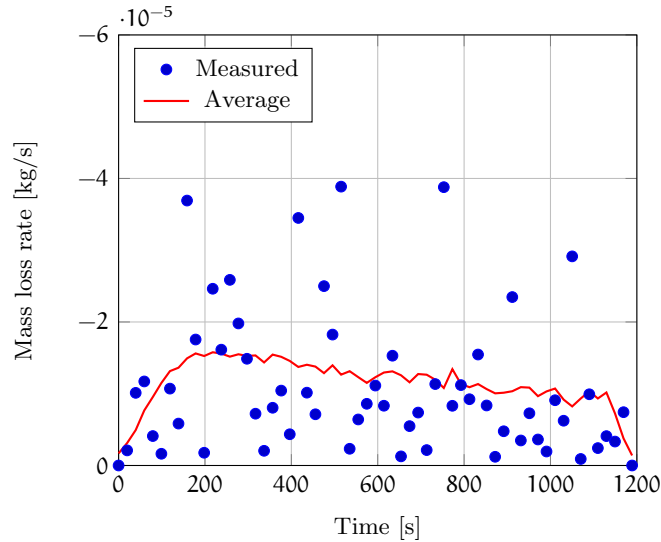


Figure 2.4: Mean mass loss rate

2.1.5 Incoming heat flux

Previously, Marc has performed heating of an elastic polymer of known physical properties on a hot plate using the experimental set-up explained above [11]. This work is significant as it experimentally proves that the heat flux leaving the hot plate is equivalent to that entering the polymer. The author has applied it to successfully estimate thermal contact resistance present at the interface. This instills the confidence for calculating the incoming heat flux using the information available from cast iron disk as the behavior of elastic polymer is similar to the dough with respect to heat transfer. Since baking is a complicated phenomenon and the true thermo-physical properties are not available, the estimation of boundary conditions using observations from dough while baking is a tedious task. Hence, the temperature variation recorded from cast-iron floor during baking process is used to compute the heat flux entering at the interface using inverse heat conduction problem.

Temperature variation in cast iron disk is presented in figure 2.5a. Cast iron disk is heated via radiation from the heating coil. Through heat conduction, the heat energy is carried from bottom to top surface of the disk. Since the lateral surfaces are insulated, the heat transfer is assumed to be unidirectional. Observing the temperature variation, maximum amount of heat is absorbed during first 3 - 4 minutes of baking as visible by sudden drop in temperature during that period. Beyond this time, the temperature is almost constantly increasing indicating the formation of crust. Heat flux as a function of time is estimated using calculus of variation approach that enables continuous estimation. The procedure for estimation is detailed in appendix A. Heat flux gained by the dough from cast iron also includes thermal contact resistance existing between them due to surface irregularities as given by figure 2.5b.

The heat flux received by dough is compared with other studies [9, 10]. In literature, for oven

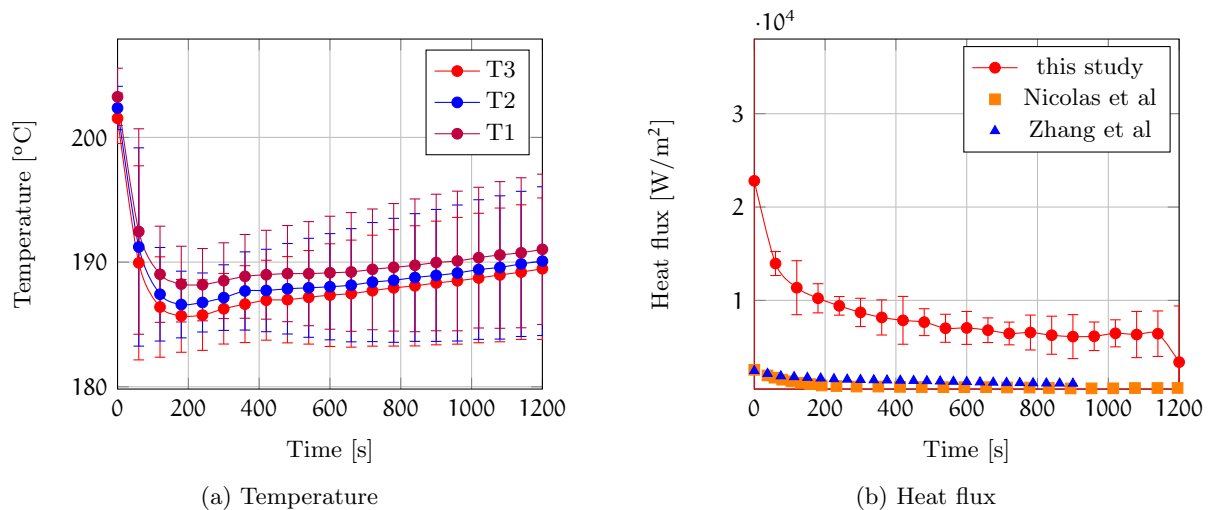


Figure 2.5: Temperature variation in cast iron floor (a) and estimated heat flux (b)

baking, the heat flux is in mainly due to convective heat transfer with a coefficient of $15 \text{ W/m}^2\text{K}$ and for air temperature of around $200 \text{ }^\circ\text{C}$. Heat flux in this study is an order greater than heat fluxes compared from literature at any instant of baking time (figure 2.5b). This comparison shows the difference arising due to the heat source being applied to the dough in direct contact baking and oven baking. The maximum heat flux exhibited by literature data is around 2.5 kW/m^2 and is even lower than the least value of heat flux (5 kW/m^2) for the current study.

2.1.6 Measurement of thermophysical properties

Water activity

Water activity (a_w) plays a pivotal role in major foodstuffs. It is defined as a ratio of equilibrium vapor pressure to saturated vapor pressure. Hence, with the knowledge of water activity and saturated vapor pressure from literature, it is possible to evaluate the equilibrium vapor pressure inside foodstuffs. This evaluated vapor pressure aids in the computation of evaporation front in the medium.

Several mathematical expressions are available in literature to evaluate water activity for bakery products. Some commonly used models are Oswin, GAB and Ferro-Fontan model. Rask et al. used Oswin model to express water activity of minced meat and dough as a function of temperature and moisture content [12]. But many authors used other models to evaluate the water activity only as a function of moisture content [13–15] to accurately simulate the baking process with respect to experimental measurements. This work also considers water activity as a function of moisture content only. The variation of moisture content corresponding to relative humidity at a desired temperature is observed. Hence, the measurements for industrial ready-mix dough are carried out at 70°C . Temperature higher than this is not used because then the dough will start baking. These measurements are used to approximate a set of coefficients in Ferro-Fontan model [16]. This model is capable of accurately representing the sorption isotherm for water activity in the range of 0.1 - 0.9 with only 2-4% of error in the moisture content [17] and is mathematically expressed as,

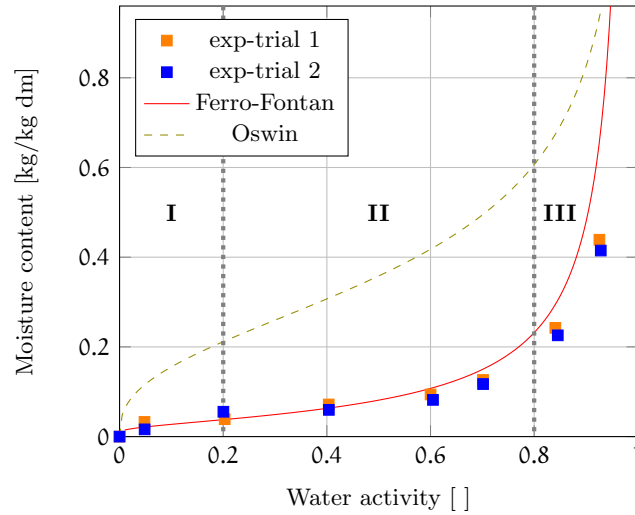


Figure 2.6: Comparison of water activity profile fitted by Ferro-Fontan at temperature 70°C with experimental measurements

$$\ln\left(\frac{\gamma}{a_w}\right) = \alpha U^{-r} \quad (2.1)$$

Where γ is net structure of sorbed water, r is an adjustable parameter representing net isotheric heat and α is a constant. These are estimated as $\gamma = 0.99$, $\alpha = 0.042$ and $r = 1.11$ for the dough in this case. Water activity is characterized by absorption isotherm curve that has three distinct regions [17]. From the experimental and approximated profiles as shown in figure 2.6, region I (when $a_w \leq 0.2$) represents water molecules bounded with solid matter and region II (when $0.2 < a_w \leq 0.8$) stands for less firmly bounded water molecules and region III (when $a_w > 0.8$) characterizes free water molecules. For analysis purpose, water activity expressed by Oswin model [9] is also plotted for bread. Comparing these two curves, it can be concluded that the dough (under consideration) exhibits wider range of free water molecules than bread. This might be due to high moisture content in the dough and difference in composition of ingredients. Moreover, broader free water molecules region also implies faster moisture content loss in that domain. Once the expressions for water activity and saturated vapor pressure are known, equilibrium vapor pressure can be computed.

Specific heat capacity

The specific heat capacity of the dough before and after baking is measured using microcalorimeter. The temperature of the sample inside the apparatus increases linearly when known power (W) is applied. Since, mass of the sample used is in milligrams, the lump mass is assumed to attain equilibrium instantly. During the experimentation, the power is applied such that the temperature of the sample increases linearly from room temperature to a maximum temperature of 96°C and is maintained for certain time (about 10 minutes). It is then cooled back linearly to room temperature. The dough is not to be heated upto the boiling point of water. The average temperature rate is set to 1.8°C/minute. This cycle of heating and cooling is represented by red and blue profiles, respectively in figure 2.7a.

Two sampling tests have been performed: one before baking (labeled as ‘before’) with mass (m) = 834 mg and another after baking (labeled as ‘after’) with mass (m) = 433 mg. The following

thermodynamic relation is used for specific heat capacity calculation,

$$Q = mC_p \frac{\Delta T}{\Delta t} \Rightarrow C_p = \frac{Q}{m \Delta T} \frac{\Delta t}{\Delta T}$$

As observed from figure 2.7b, the samples show similar specific heat capacity except for the test with unbaked dough during its heating phase (H.P. - before). The reason might be the partial baking of the dough lump while heating. It is a clear indication that the physical properties of dough vary during baking process. Since the temperature is raised linearly, it could be said that during heating phase the heat capacity is increasing linearly with temperature up to 65°C. After that a small dip in its values is noted. This temperature 65°C corresponds to time of 600s in plot 2.7b. Coagulation of egg between 60 - 65°C is the primary reason for such variation in heat capacity during heating process. But samples after baking show good consistency in their values for both heating and cooling phases. It can be said that the dough during baking exhibits specific heat capacity in the range of 2800 - 3400 [J/(kgK)].

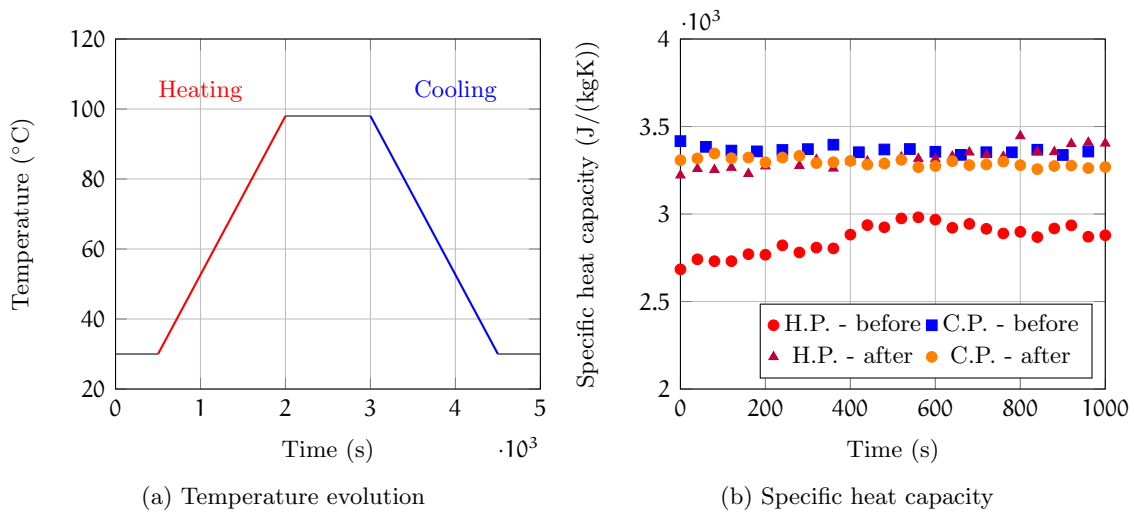


Figure 2.7: Measurement of specific heat capacity during heating (H.P.) and cooling phase (C.P.)

Thermal conductivity

Thermal conductivity measurements have been performed using hot wire and hot plane method. The working principle is similar in both the cases, but hot plane measuring instrument is able to measure both thermal conductivity and volumetric heat capacity.

Hot wire method: Transient hot wire method is one of the effective methods for measuring thermal conductivity of fluids. As the name suggests, a thin and long wire is used to generate heat while immersed inside the fluid whose conductivity is to be measured. The analytical expression for temperature variation with line heat source is,

$$T(r, t) = \frac{q}{4\pi\lambda l} \left[\ln \left(\frac{4\alpha t}{r^2} \right) - \gamma \right]$$

Where γ is Euler's constant, α - thermal diffusivity (m^2/s), λ - thermal conductivity ($W/(mK)$), r is distance (m) from heat source, q is applied power (W). But in test case, neither λ nor α

is known, so temperature difference between different times can reduce the above analytical expression to,

$$\Delta T = \underbrace{\frac{q}{4\pi l \lambda}}_{\text{slope}} \ln\left(\frac{t_2}{t_1}\right) \Rightarrow \lambda = \frac{q}{4\pi l} \frac{\ln(t_2 - t_1)}{\Delta T} \quad (2.2)$$

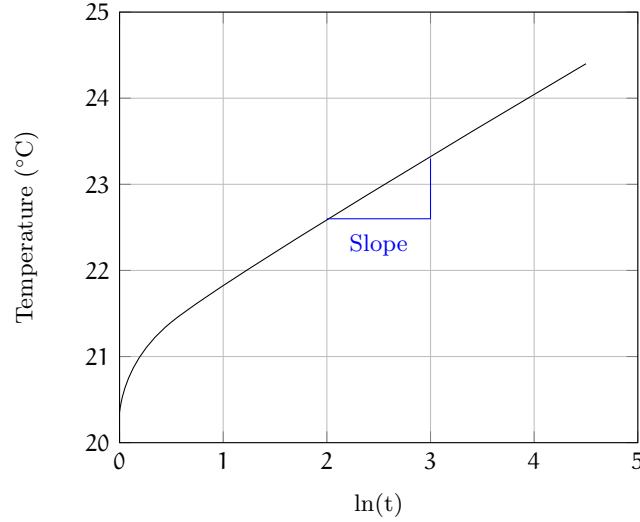


Figure 2.8: Evolution of temperature during measurement - for representation purpose

The final expression has eliminated thermal diffusivity α , distance of temperature measurement r (location of thermocouple from hot wire) and Euler's constant γ , and simplified the expression for evaluating thermal conductivity λ . The length of the wire used in this case is 0.093m and two thermocouples are employed for recording temperature variations. For repeatability, two measurements have been performed for different power with first case: current - 0.263 A, voltage - 2.5 V and second case: current - 0.15 A, voltage - 1.5 V. Knowing q , l , $\ln(t_2/t_1)$ and ΔT , equation (2.2) aids in computing thermal conductivity of the sample λ . Only dough sample before baking has been subjected to measurement as the baked dough shows some difficulty. The measurements have been carried out for about 200 seconds and showed maximum temperature difference of 0.7 K. The average estimated thermal conductivity for dough before baking is 0.3824 ± 0.0711 [W/(mK)].

Hot plane method In this measurement, hot wire (line heat source) is replaced with a hot disk (plane heat source). An electrically conducting material such as Nickel is etched in spiral form on a thin foil that acts as sensor. This hot disk is placed between the two halves of sample whose thermal properties are to be measured. As mentioned earlier, this method helps to measure both thermal conductivity and volumetric heat capacity (from thermal diffusivity). Alike the measurement of specific heat capacity, two tests are performed with dough before and after treating it in climatic chamber. The power generated by the coil for measurement is 50mW for 80 s and maximum temperature rise is 0.69K. For each test case, five trials are carried out with time interval of 48 minutes between all the trials. From several trial measurements, thermal conductivity and volumetric heat capacity measured for dough in initial state (for moisture content $U = 1.59$) are 0.4886 ± 0.0021 [W/(mK)] and 3.613 ± 0.0684 [MJ/(m³K)], respectively.

After initial stage measurements are performed, the dough is transferred into a glass beaker

and placed in climatic chamber until the surface temperature reaches 100°C taking about 60 minutes. As the local moisture content is not distributed equally, the sample is kept undisturbed for a couple of days to attain equilibrium. The average moisture content is noted to be $U = 1.21$ after climatic chamber treatment. The thermal conductivity and heat capacity are measured as 0.4363 ± 0.0152 [W/(mK)] and 2.499 ± 0.4714 [MJ/(m³K)] respectively.

2.2 Development of heat and mass transport models

Basic physics involved in contact baking process is illustrated in figure 2.9. Heat transfer between the heating coil and the cast iron floor has been explained in section § 2.1.5. Since the amount of heat flux supplied to dough from cast-iron floor is known by prior calculation, the focus in this section will be on dough baking process. From experimental temperature trends, it is visible that there are several transformations occurring in the dough. These transformations are facilitated by four major phenomena namely transport of heat, transport of fluids, evaporation - condensation effect and movement of evaporation front. Hence, any mathematical model should include these mentioned phenomena to accurately simulate the baking process.

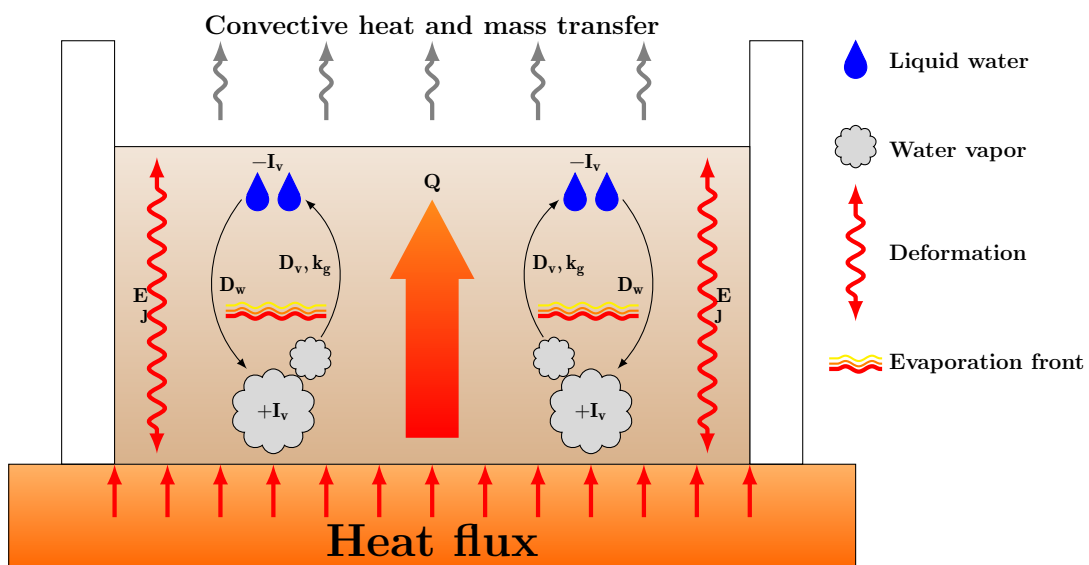


Figure 2.9: Basic physics involved in contact baking

During contact baking, there is immense transfer of heat to the dough in contrast to that during oven baking, shown by figure 2.5b. As the dough begins to heat up, evaporation of water also commences and leads to generation of water vapor. This causes increase in gas pressure at the bottom and development of pore connections. Soon a dry region is developed with interconnected pores, to pave the way for gas transport by diffusion and pressure gradient. An interface develops between the dry and wet region due to evaporation front. The moment when rising water vapor reaches colder region i.e. above the evaporation front, it releases the absorbed latent heat and condenses, raising the liquid content in the colder region. Counterpart to this is the diffusion of condensed and remaining liquid water from the colder region back to hotter region due to concentration gradient. Thus, evaporation-condensation effect is one of the major transporters of heat in baking apart from conduction [1, 18]. The evaporation and condensation effect can be briefly categorized into four stages that are given below:

1. Water in liquid form absorbs heat and evaporates until saturated moisture content is reached in the hotter region above, thus forming water vapor.
2. Water vapor migrates from hot to cold region through interconnected pores
3. Water vapor releases the latent heat and condenses in the cold region
4. Liquid water from cold region migrates back to hot region by diffusion process

The accumulation of liquid water at the center or in colder region is the main reason for softness of crumb, while evaporation of liquid water from dry regions forms crispy crust. Therefore, heat transport is strongly coupled with mass distribution of water (both in liquid and gaseous form). Along with transport phenomena, structural deformation is observed especially during the initial stage of baking period. It is formulated by an interlinked momentum equation that deploys the solid velocity for overall deformation from initial volume.

In this experimental study, a mold is used to support the dough having high moisture content during the initial stage of heating as discussed before. This support also provides insulation on lateral sides against heat and mass transfer and ensures unidirectional heat- and mass-flow. The flow of heat is from hot cast iron floor to dough and then to ambient air at room temperature. Water vapors are generated more in hotter areas and escape into ambience. Direction of water vapor is similar to that of heat transport, but liquid water also migrates backward upto the evaporation front due to concentration gradient. Again at evaporation front, the cycle of evaporation-condensation continues. As transfer is minimal in lateral direction, undertaking one dimensional formulation is sufficient in this study.

Requirement of non-dimensional numbers Thermophysical properties in dimensional form have large variations in their magnitude. For instance, volumetric heat capacity differs from thermal conductivity by roughly around 10^6 orders in magnitude. This discrepancy in magnitude order causes some hindrance in solving inverse problem. Non-dimensionalization of the governing equations not only helps in overcoming the issue stated above but also serves other facilities such as:

- Scales almost every parameter
- Helps to identify key parameters with their magnitude
- Classifies the flow characteristic inside the medium (for example: low mass diffusivity and large gas permeability values indicate that gas flow is majorly driven by Darcy's flow, which is true in porous medium)
- Assists optimization procedure as objective function having multiple components like temperature, moisture content, etc. can be expressed in similar dimensions

Thus, the models used here shall be non-dimensionalized with some unconventional parameters. Usually, experimental time is represented by Fourier number Fo which is defined as the ratio of experimental time to either thermal or mass diffusive time(i.e. mathematically expressed as $Fo = t \times \alpha_{q/m} / L^2$, where $\alpha_{q/m}$ - thermal or mass diffusivity, L is length and t is experimental time). If the focus is only on computational simulation for observing behavioral changes of state variables subject to certain environmental conditions, then a non-dimensional approach with

Fo number is preferred and can be used. But, solving inverse problem with properties being estimated as either constants or functions, Fo should not be preferred especially for the problem dealing with estimation of thermal diffusivity. It is because with every iteration of optimization, the computed Fo time also changes which could affect the numerical scheme solving the governing equation. This is the reason for implementing unfamiliar, non-dimensional numbers that are mostly scaled ratios. Appendix B contains the detailed process for non-dimensionalization of each model and definitions of these numbers.

2.2.1 Diffusive model

Diffusive model will only accounts liquid water along with heat transfer. Both liquid water and heat energy are considered to be transported by diffusion mechanism and hence the name diffusive model. It is the simplest one among all the models that are presented following sections.

Hypothesis The mathematical formulation for this model is based on the following assumptions:

1. Mass of water vapor is negligible
2. Liquid water is strongly bonded with solid. Hence, the transport of water is by diffusion only
3. Evaporation rate is formulated by explicit approach
4. Liquid water is not expelled from surface of the dough
5. Heat transfer by convection and radiation inside the porous structure is negligible
6. Thermophysical properties are constant

Balance equations

-Energy balance: The energy balance equation is formulated using Fourier's law of heat conduction.

$$\rho C_{p_{eff}} \frac{\partial T}{\partial t} = \frac{\partial}{\partial x} \left(k_{eff} \frac{\partial T}{\partial x} \right) - \lambda I_v \quad (2.3)$$

Here $C_{p_{eff}}$ and k_{eff} are effective heat capacity and thermal conductivity for the medium, respectively. Mass balance: Mass balance is expressed by mass diffusion equation using Fick's law. Moreover, mass balance is represented by balance of moisture content (U) which is ratio of apparent liquid density (ρ_l^a) to solid density (ρ_s^a).

For liquid water :

$$\frac{\partial(\pi S_l \rho_l)}{\partial t} = \frac{\partial}{\partial x} \left(D_l \frac{\partial(\pi S_l \rho_l)}{\partial x} \right) - I_v$$

As moisture content :

$$\rho_s^a \frac{\partial U}{\partial t} = \rho_s^a \frac{\partial}{\partial x} \left(D_l \frac{\partial U}{\partial x} \right) - I_v \quad \text{with } U = \frac{\pi S_l \rho_l}{\rho_s^a} \quad (2.4)$$

Necessity of explicit evaporation rate per unit volume Evaporation rate per unit volume is usually represented implicitly as the rate of change of liquid water or water vapor [19]. It is assumed that evaporation rate directly corresponds to rate of water loss as,

$$I_v = \epsilon \frac{\partial \rho_v}{\partial t} \quad (2.5)$$

Where ϵ is phase conservation factor. This expression of evaporation rate is localized for a particular domain and there is no bridge with other regions which leads to its underestimation. The explanation lies in mass conservation of liquid and vapor .

The mass conservation equations of mass flux for liquid water (\mathbf{n}_w) and vapor (\mathbf{n}_v) are,

$$\begin{aligned} \frac{\partial \rho_l}{\partial t} + \nabla \mathbf{n}_l &= -I_v \\ \frac{\partial \rho_v}{\partial t} + \nabla \mathbf{n}_v &= I_v \end{aligned}$$

Evaporation rate can be mathematically obtained by subtracting the above equations and it gives,

$$2I_v = \frac{\partial \rho_v}{\partial t} - \frac{\partial \rho_l}{\partial t} + \nabla \mathbf{n}_v - \nabla \mathbf{n}_l \quad (2.6)$$

This shows that the evaporation rate is not just the rate of change of water vapor with phase conversion factor as given by equation (2.5). It also informs why the evaporation rate given by Luikov does not encapsulate the complete evaporation process. Since in diffusive model water vapor is neglected, the former stated implicit evaporation rate can not be used. Rather, an instant and explicit evaporation formulation is used.

Evaporation rate per unit volume (I_v) is formulated on the assumption that evaporation starts when the temperature in a domain reaches 100°C and continues until the moisture content in that domain reaches a critical value beyond which bonded liquid water cannot evaporate. Hence, two step functions for toggling the evaporation are required, one for temperature and another for moisture content. The main source for evaporation is the incoming heat flux from previous domain and is given by Fourier law of conduction [20]. The mathematical expression for this explicit evaporation rate is,

$$I_v = C_1 C_2 \frac{Q}{\lambda} \quad (2.7)$$

Where C_1 is temperature step function, C_2 is moisture step function, Q is heat flux ($k \partial T / \partial x$) and λ is latent heat of vaporization. The step functions are given as,

$$C_1 = \begin{cases} 0 & : T < 100^\circ\text{C} \\ 1 & : T \geq 100^\circ\text{C} \end{cases}$$

$$C_2 = \begin{cases} 0 & : U < U_{cr} \\ 1 & : U \geq U_{cr} \end{cases}$$

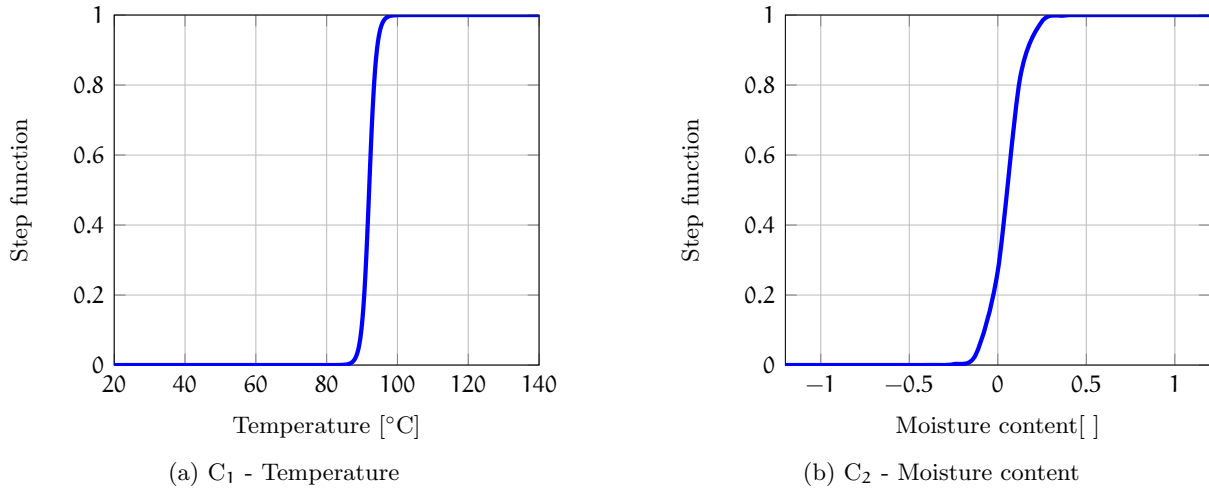


Figure 2.10: Step function for temperature (C_1) (a) and moisture content (C_2) (b) for Diffusive model

Boundary conditions The boundary conditions for energy include the heat flux applied at interface of dough and hot plate, and convective heat transfer at free surface of the dough with respect to ambient. As no liquid water is propelled out of dough during baking, the mass flux at either boundaries is zero and mass is conserved.

Energy balance (2.8)

$$-k_{\text{eff}} \nabla T(x, t) = \begin{cases} q(t) & : x = 0 \\ h_q(T(L, t) - T^\infty) & : x = L \end{cases}$$

Mass balance (2.9)

$$D_1 \nabla U(x, t) = 0 \quad : x = 0, L$$

Balance equations in non-dimensional form

The governing equations are non-dimensionalized as,

Energy balance:

$$\frac{\partial \theta}{\partial t^*} = (1 - C_1 C_2) (\nabla^* \alpha_q^* \nabla^* \theta) \quad (2.10)$$

Mass balance:

$$\frac{\partial U}{\partial t^*} = \nabla^* D_1^* \nabla^* U - R_1 I_v^* \quad (2.11)$$

Definitions of non-dimensional parameters and variables such as θ , U , α_q^* , D_w^* are detailed in table 4.10. Step functions are also expressed with non-dimensional temperature and moisture content. In order to have step functions with smooth transition from 0 to 1, following mathematical expressions of sigmoid are utilized,

$$C_1 = \frac{1}{1 + \exp(-365.15(\theta - 0.23))}$$

$$C_2 = \frac{1}{1 + \exp(-U + U_{cr})}$$

In these expressions, critical moisture content U_{cr} is taken to be 0.05. Boiling point of water in non-dimensional form is 0.23 corresponding to 100°C. Boundary conditions are altered by similar approach of non-dimensionlization.

Energy balance:

at $x^* = 0$:

$$\nabla^* \theta = k^* Q(t^*) \quad (2.12)$$

at $x^* = 1$:

$$\nabla^* \theta = k^* Bi_q (\theta - \theta^\infty) \quad (2.13)$$

Mass balance:

$$D_w^* \nabla^* U = 0 \quad \text{at } x^* = 0, 1 \quad (2.14)$$

Note on equilibrium approach vs non-equilibrium approach for computation of evaporation rate

Sensory properties of bakery products are mainly controlled by transport, chemical reactions and evaporation of liquid water or moisture content during baking. Evaporation-condensation effect is an important attribute during baking of dough. Hence, proper formulation of evaporation rate inside the product becomes significant for a mathematical model so that it can closely replicate the simulations to experimental measurements.

The main disadvantage of the above presented explicit evaporation rate is that it is activated only when the temperature is above boiling point of water which is not true in reality and also it does not account for vapor condensation. In the following models, diffusive model is improvised by considering gaseous phases (like water vapor, air) that are present inside the medium during baking. Inclusion of water vapor gives greater feasibility on calculation of evaporation rate either explicitly or implicitly.

In literature, there are different ways of describing evaporation rate but commonly used ones are equilibrium approach or non-equilibrium approach [21]. When a model is developed with the assumption that moisture content inside the medium attains equilibrium with vapor pressure instantly, then it is recognized as equilibrium approach. On other hand, a model based on non-equilibrium approach considers that there is time lag in attaining this equilibrium. Hitherto, there is no proper clarification about which approach is better, especially in application to food processing.

The shortcoming of equilibrium approach model is absence of experimental validation. The wet region has more free water molecules than gas bubbles which would attain equilibrium instantly. But a dry region has more gas bubbles than water bonded to solid matter and takes longer time to reach equilibrium [22]. This raises the question about validity of the basic assumption for the entire domain. Equilibrium approach largely depends on water activity and saturated

vapor pressure. The moisture isotherm curve used to calculate water activity is obtained experimentally at a particular temperature and relative humidity. Such experimentation is performed on a small lump of sample in a climatic chamber which would take some hours to reach equilibrium. Hence, the water activity approximation may not be a good relation to be used for a short baking process that involves large variation in heat energy. All these might result in some deviation of equilibrium approach from actual measurements. In support, literature shows that this model underestimates the product temperature in near core (crumb) regions [23] and sometimes overestimates the evaporation rate [22]. But the main advantage of this assumption is that the model becomes numerically simple since no separate solution for vapor conservation is required.

On the other hand, non-equilibrium approach covers some of the drawbacks of equilibrium approach. A proper mathematical formulation of evaporation rate using this approach is unavailable. Still, a linear difference of actual vapor pressure and equilibrium vapor pressure along with a constant is widely used now. The knowledge on this constant is limited and is deduced empirically. It should be noted that this empirical evaporation value is a function of both temperature and moisture content. Apart from this, the region near ambient surface where the pressure is atmospheric, would reach equilibrium instantly due to surface evaporation. In such a case, fine meshing should be implemented in boundary nodes while solving the governing equations to avoid deviations for the models with non-equilibrium assumption. It is mandatory to know if the element size used is smaller than the pore size. Else, that mesh element would not represent elementary volume and instead it would be pore volume which will violate the basic continuum approach. In cases with a sudden variation in surface vapor pressure, some numerical difficulty may be encountered.

Leaving aside the conflicts present in both approaches, they continue to account for proper transport of evaporation front and evaporation-condensation effect. Thus, upcoming sections will showcase the models using non-equilibrium and equilibrium approach.

2.2.2 TMPN model: Multiphase model with non-equilibrium approach

A multiphase model of solid, liquid and gaseous phases with non-equilibrium approach for evaporation rate computation is considered here. This model is tagged as **TMPN** model that represent **T**emperature, **M**oisture content and **P**ressure by **N**on-equilibrium approach. Unlike diffusive model presented before, this and upcoming models are mechanistic since fundamental equations governing them are derived from laws of conservation. The non-equilibrium approach of evaporation rate shall be explained in detail in forthcoming section.

Hypothesis: In order to simplify the process of mathematical formulation, following hypothesis is used to build this TMPN model:

1. Apart from solid and liquid phases, gaseous phase is also present
2. Gaseous phase obeys ideal gas law and Dalton's law of partial pressure
3. Evaporation rate per unit volume is formulated based on an explicit non-equilibrium thermodynamic approach

4. Convection of evaporated water vapor from the free surface to ambient occurs only in respective volume fraction of liquid water and vapor
5. Convection of gaseous phase inside the medium is expressed by Darcy's law
6. Convection of thermal energy by gaseous phase is in order of 10^{-5} and hence is neglected
7. Changes in solid phase are ignored, that is porosity is constant
8. No generation of gases like carbon-dioxide due to absence of baking agent

Balance equations

The mass conservation of fluids is as follows,

$$\frac{\partial \rho_l S_l \pi}{\partial t} + \nabla n_l = -I_v \quad (2.15)$$

$$\frac{\partial \rho_v S_g \pi}{\partial t} + \nabla n_v = I_v \quad (2.16)$$

$$\frac{\partial \rho_a S_g \pi}{\partial t} + \nabla n_a = 0 \quad (2.17)$$

Mass of a particular phase is represented by their volume fractions. The volume fraction for liquids and gases is given by πS_l and πS_g , respectively. There are only liquid and gaseous phase are present in void volume. Liquid saturation is denoted as S_l and specifies the amount of void volume occupied by liquid. It is defined as ratio of liquid volume to void volume (i.e. $S_l = v_l/(v_l + v_g)$). The summation of liquid and gas saturation is always unity, $S_l + S_g = 1$. Densities specified in equations (2.15 - 2.17) correspond to intrinsic one. For moisture content, equation (2.15) is altered as,

$$\rho_s^a \frac{\partial U}{\partial t} + \nabla n_l = -I_v \quad (2.18)$$

The mass flux of liquid water (n_l) for highly saturated porous media and with very low value of liquid permeability can be simplified by Fick's law of diffusion [9, 10].

$$n_l = -D_l \rho_s^a (\nabla U)$$

For gaseous phase, mass flux for water vapor (n_v) and air (n_a) is defined by binary diffusion (Fick's law) and pressure gradient (Darcy's flow) [24].

$$n_v = -\rho_v \frac{k_g}{\mu_g} \vec{\nabla} P_g - D_v \rho_g \nabla \left(\frac{\rho_v}{\rho_g} \right)$$

$$n_a = -\rho_a \frac{k_g}{\mu_g} \vec{\nabla} P_g - D_v \rho_g \nabla \left(\frac{\rho_a}{\rho_g} \right)$$

Energy conservation:

$$\rho C_{p\text{eff}} \frac{\partial T}{\partial t} = \frac{\partial}{\partial x} \left\{ k_{\text{eff}} \frac{\partial T}{\partial x} \right\} - \lambda I_v \quad (2.19)$$

Boundary conditions For liquid water and water vapor at free surface, the evaporated water present in their respective volume fractions diffuses to the ambient air via convection. Since at free surface, the total gas pressure is same as ambient pressure, the remaining gas pressure is computed as the difference of ambient pressure and vapor pressure at the surface. There is applied heat flux at the bottom and convective heat transfer at free surface.

Energy (2.20)

$$-k_{\text{eff}} \nabla T(x, t) = \begin{cases} q(t) & : x = 0 \\ h_q(T(L, t) - T^\infty) & : x = L \end{cases}$$

Moisture content (2.21)

$$n_l = \begin{cases} 0 & : x = 0 \\ h_m \pi S_l(\rho_v - \rho_v^\infty) & : x = L \end{cases}$$

Water vapor (2.22)

$$n_v = \begin{cases} 0 & : x = 0 \\ h_m \pi S_g(\rho_v - \rho_v^\infty) & : x = L \end{cases}$$

Air (2.23)

$$\begin{aligned} n_a &= 0 & : x = 0 \\ \rho_a &= (P_0 - P_v)/R_a T & : x = L \end{aligned}$$

Closure term - Evaporation rate In non-equilibrium approach, evaporation rate is given as linear difference between local and equilibrium vapor densities [25],

$$I_v = H(\rho_v^{\text{eq}} - \rho_v) \quad (2.24)$$

Where H is evaporation rate constant (1/s). Analyzing the above equation (as $I_v/H = \rho_v^{\text{eq}} - \rho_v$), when the constant tends to infinity then vapor in the medium and equilibrium vapor are equivalent (i.e. instant equilibrium is achieved). Whereas, for very small value of the constant there exists a large gap between equilibrium vapor and vapor present inside the medium. With the help of saturated vapor pressure P_{sat} and water activity a_w , equilibrium vapor density ρ_v^{eq} is calculated.

$$\rho_v^{\text{eq}} = a_w(T, U) \times P_{\text{sat}}(T)/(R_v T) \quad (2.25)$$

Balance equations in non-dimensional form

Mass conservation equations (2.15-2.17) are non-dimensionalized as,

$$\frac{\partial U}{\partial t^*} = \nabla^* (D_l^* \nabla^* U) - I_v^* \quad (2.26)$$

$$\frac{\partial V}{\partial t^*} = \nabla^* \left(\frac{V}{\pi S_g} a_p^* \nabla^* P_g^* + D_v^* G \nabla \left(\frac{V}{G} \right) \right) + I_v^* \quad (2.27)$$

$$\frac{\partial A}{\partial t^*} = \nabla^* \left(\frac{A}{\pi S_g} a_p^* \nabla^* P_g^* + D_v^* G \nabla \left(\frac{A}{G} \right) \right) \quad (2.28)$$

and energy conservation equation (2.19) as,

$$\frac{\partial \theta}{\partial t^*} = \nabla^* (a_q^* \nabla^* \theta) - R_1 I_v^* \quad (2.29)$$

Boundary conditions The boundary conditions for mass conservation of liquid water in non-dimensional form are,

$$n_l^* = \begin{cases} 0 & : x^* = 0 \\ Bi_m S_l / S_g (V - V^\infty) & : x^* = 1 \end{cases}$$

for water vapor,

$$n_v^* = \begin{cases} 0 & : x^* = 0 \\ Bi_m (V - V^\infty) & : x^* = 1 \end{cases}$$

and for air conservation,

$$n_a^* = 0 \quad : x^* = 0$$

$$A = \pi S_g \rho_{ref}^* \frac{1 - P_v^*}{\theta + 1} \quad : x^* = 1$$

The boundary conditions for energy balance are given by,

$$\nabla^* \theta = \begin{cases} k^* Q(t^*) & : x^* = 0 \\ k^* Bi_q (\theta - \theta^\infty) & : x^* = 1 \end{cases}$$

2.2.3 TMPE model: Multiphase model with equilibrium approach

TMPE here stands for **T**emperature, **M**oisture content and **P**ressure with **E**quilibrium approach. Due to implication of equilibrium assumption, the governing equations can be simplified and are clipped together. This eliminates the need for solving the mass conservation of vapor phase. In equation governing the moisture content, evaporation rate is replaced directly by water vapor equation and the total gas pressure is expressed from mass conservation of air.

Hypothesis: The assumptions enlisted in previous model are common for this model too, except points 3 and 4. Other hypothesis used in this model are:

1. There is equilibrium between vapor and liquid water (which is basic for this model)
2. The combined mass fluxes for liquid water and vapor at boundary nodes are replaced by convective mass loss of water vapor
3. Gases obey Dalton's law of partial pressure and ideal gas law

Balance equations

Moisture contents The moisture content equations as explained earlier, are simplified and combined with vapor conservation equations as,

$$\rho_s^a \frac{\partial U}{\partial t} + \frac{\pi S_g \rho_v}{\partial t} = \nabla (n_l + n_v)$$

with use of ideal gas law,

$$\rho_s^a \frac{\partial U}{\partial t} + \frac{\partial}{\partial t} \left(\frac{\pi S_g P_v}{R_v T} \right) = \nabla \left(\underbrace{\rho_s^a D_l \nabla U}_{\text{mass flux of liquid water}} + \underbrace{\rho_v \frac{k_g}{\mu_g} \nabla P_g + \rho_g D_v \nabla \left(\frac{\rho_v}{\rho_g} \right)}_{\text{mass flux of water vapor}} \right)$$

$$\Rightarrow \rho_s^a \frac{\partial U}{\partial t} + \frac{\pi P_v}{R_v T} \frac{\partial S_g}{\partial t} - \frac{P_v \pi S_g}{R_v T^2} \frac{\partial T}{\partial t} + \frac{\pi S_g}{R_v T} \frac{\partial P_v}{\partial t} = \nabla \left(\underbrace{\rho_s^a D_l \nabla U + \rho_v \frac{k_g}{\mu_g} \nabla P_g + \rho_g D_v \nabla \left(\frac{\rho_v}{\rho_g} \right)}_r \right) \quad (2.30)$$

Total pressure From air conservation, total gas pressure is derived using Dalton's law of partial pressure ($P_g = P_v + P_a$) with advantage of binary gas diffusion,

$$\frac{\partial (\pi S_g \rho_a)}{\partial t} = \nabla \left(\rho_a \frac{k_g}{\mu_g} \nabla P_g - \rho_g D_v \nabla \left(\frac{\rho_v}{\rho_g} \right) \right)$$

with use of ideal gas law,

$$\frac{\partial}{\partial t} \left(\frac{\pi S_g P_a}{R_a T} \right) = \nabla \left(\frac{P_a}{R_a T} \frac{k_g}{\mu_g} \nabla P_g - \rho_g D_v \nabla \left(\frac{(P_v/R_v T)}{\rho_g} \right) \right)$$

with use of Dalton's law,

$$\frac{\partial}{\partial t} \left(\frac{\pi S_g (P_g - P_v)}{R_a T} \right) = \nabla \left(\frac{(P_g - P_v)}{R_a T} \frac{k_g}{\mu_g} \nabla P_g - \rho_g D_v \nabla \left(\frac{P_v/R_v T}{\rho_g} \right) \right)$$

$$\frac{\partial}{\partial t} \left(\frac{\pi S_g P_g}{R_a T} \right) - \frac{\partial}{\partial t} \left(\frac{\pi S_g P_v}{R_a T} \right) - \frac{\pi S_g (P_g - P_v)}{R_a T^2} \frac{\partial T}{\partial t} + \frac{\pi (P_g - P_v)}{R_a T} \frac{\partial S_g}{\partial t} =$$

$$\begin{aligned}
&= \nabla \left(\frac{(P_g - P_v) k_g}{R_a T} \nabla P_g - (\rho_a + \rho_v) D_v \nabla \left(\frac{P_v / R_v T}{\rho_a + \rho_v} \right) \right) \\
&= \nabla \left(\frac{(P_g - P_v) k_g}{R_a T} \nabla P_g - (\rho_a + \rho_v) D_v \nabla \left(\frac{P_v / R_v T}{(P_g - P_v) / R_a T + P_v / R_v T} \right) \right) \\
&= \nabla \left(\frac{(P_g - P_v) k_g}{R_a T} \nabla P_g - \left(\frac{(P_g - P_v)}{R_a T} + \frac{P_v}{R_v T} \right) D_v \nabla \left(\frac{P_v / R_v T}{(P_g - P_v) / R_a T + P_v / R_v T} \right) \right) \\
&= \nabla \left(\frac{(P_g - P_v) k_g}{R_a T} \nabla P_g - \left(\frac{(P_g - P_v)}{R_a T} + \frac{P_v}{R_v T} \right) D_v \nabla \left(\frac{1}{((P_g - P_v) R_v) / (P_v R_a) + 1} \right) \right) \\
\Rightarrow &\frac{\partial}{\partial t} \left(\frac{\pi S_g P_g}{R_a T} \right) - \frac{\partial}{\partial t} \left(\frac{\pi S_g P_v}{R_a T} \right) - \frac{\pi S_g (P_g - P_v)}{R_a T^2} \frac{\partial T}{\partial t} + \frac{\pi (P_g - P_v)}{R_a T} \frac{\partial S_g}{\partial t} = \\
&= \nabla \left(\underbrace{\frac{(P_g - P_v) k_g}{R_a T} \nabla P_g - \left(\frac{(P_g - P_v)}{R_a T} + \frac{P_v}{R_v T} \right) D_v \nabla \left(\frac{1}{((P_g - P_v) R_v) / (P_v R_a) + 1} \right)}_{\Phi} \right) \tag{2.31}
\end{aligned}$$

Evaporation rate Evaporation rate is obtained directly from equation for water vapor conservation and isotherm curve for moisture content.

$$I_v = \frac{\partial}{\partial t} \left(\frac{\pi S_g P_v}{R_v T} \right) - \nabla \left(\rho_v \frac{k_g}{\mu_g} \nabla P_g \right) - \nabla \left(\rho_g D_v \nabla \left(\frac{\rho_v}{\rho_g} \right) \right) \quad \text{where } P_v = a_w \times P_v^{\text{sat}} \tag{2.32}$$

Boundary conditions The boundary conditions for balance equations are given as,

Mass transfer - moisture content (2.33)

$$\Gamma = \begin{cases} 0 & : x = 0 \\ h_m (\rho_v - \rho_v^\infty) & : x = L \end{cases}$$

Mass transfer - total gas (2.34)

$$\Phi = \begin{cases} 0 & : x = 0 \\ P_g = P_{\text{atm}} & : x = L \end{cases}$$

The governing equation and supporting initial and boundary conditions are exactly same as previous model and are repeated here.

Balance equations in non-dimensional form

The moisture content equation (2.30) is non-dimensionalized as,

$$\begin{aligned}
&\frac{\partial U}{\partial t^*} + \pi \frac{\rho_{\text{ref}} P_v^*}{R_v^* (\theta + 1)} \frac{\partial S_g}{\partial t^*} - \pi S_g \frac{\rho_{\text{ref}} P_v^*}{R_v^* (\theta + 1)^2} \frac{\partial \theta}{\partial t^*} + \pi S_g \frac{P_v^* \rho_{\text{ref}}}{R_v^* (\theta + 1)} \frac{\partial P_v^*}{\partial t^*} = \\
&= \nabla^* \left(\underbrace{D_w^* \nabla^* U + \frac{V}{\pi S_g} a_p^* \nabla^* P_g^* + G D_v^* \nabla^* \left(\frac{V}{G} \right)}_{\Gamma^*} \right) \tag{2.35}
\end{aligned}$$

The total gas pressure equation (2.31) as,

$$\begin{aligned} & \frac{\partial}{\partial t^*} \left(\frac{\pi S_g \rho_{\text{ref}} P_g^*}{\theta + 1} \right) - \frac{\partial}{\partial t^*} \left(\frac{\pi S_g \rho_{\text{ref}} P_v^*}{\theta + 1} \right) - \pi S_g \rho_{\text{ref}} \frac{(P_g^* - P_v^*)}{(\theta + 1)^2} \frac{\partial \theta}{\partial t^*} + \pi \rho_{\text{ref}} \frac{(P_g^* - P_v^*)}{\theta + 1} \frac{\partial S_g}{\partial t^*} = \\ & = \nabla^* \left(\underbrace{\rho_{\text{ref}} (P_g^* - P_v^*) a_p^* \nabla^* P_g^* - \frac{\rho_{\text{ref}}}{\theta + 1} \left(P_g^* - P_v^* + \frac{P_v^*}{R_v^*} \right) D_v^* \nabla^* \left(\frac{1}{1 + R_v^* ((P_g^* - P_v^*) / P_v^*)} \right)}_{\Phi^*} \right) \end{aligned} \quad (2.36)$$

The evaporation rate in non-dimensional form is presented as,

$$\Gamma_v^* = \frac{\partial}{\partial t^*} \left(\frac{\pi S_g \rho_{\text{ref}} P_v^*}{\theta + 1} \right) - \nabla^* \left(\frac{V}{\pi S_g} a_p^* \nabla^* P_g^* + G D_v^* \nabla^* \left(\frac{V}{G} \right) \right) \quad (2.37)$$

Boundary conditions are simplified as,

$$\Gamma^* = \begin{cases} 0 & : x^* = 0 \\ \text{Bi}_m (V - V^\infty) & : x^* = 1 \end{cases}$$

and for mass transfer of total gas:

$$\Phi^* = \begin{cases} 0 & : x^* = 0 \\ P_g^* = 1 & : x^* = 1 \end{cases}$$

2.3 Model validation with known properties

With the availability of mathematical formulations for models with different hypothesis, validation of them is carried out using available key parameters that are presented in table 2.4. These models are validated by comparing simulated trends with experimental ones. This can help to understand how well the model is formulated and if there are any conflicts in their simulation. It is one of the foremost steps for selecting proper mathematical model that will be used in future for solving the inverse problem. The key parameters listed in table are obtained from literature [9, 10, 13] as average or effective values since these variables are presented as functions.

2.3.1 Diffusive model

Simulated temperature and moisture content profiles are plotted for sensor positions at $x^* = [0, 0.25, 0.50, 0.75, 1]$ in figure 2.11. Temperature profiles seem to validate the heating process inside the medium. A stagnant temperature curve near 100°C and a slight increase in its value after baking time of 600 s for bottom sensor location is observed. This variation mimics the phase of dough's transformation as observed in measurements, even though there is some difference in magnitude. The maximum temperature reached at the end of baking is around 110°C whereas in reality it is about 130°C . For other sensor locations, a gradual increase in temperature is spotted.

On examining the local moisture content profiles, almost every region except the bottom area has moisture content value close to initial state. Strong evaporation is noticed mainly in the

Number	Description	Number	Description
$\theta = \frac{T - T_0}{T_0}$	Temperature	$\alpha_q^* = \frac{\alpha_q t_f}{L^2}$	Thermal diffusivity
$R_1 = \frac{\rho_s^a}{\rho_{eff}} \frac{\lambda}{C_{p_{eff}} T_0}$	ratio of densities and Jakob's number	$I_v^* = \frac{I_v t_f}{\rho_s^a}$	Evaporation rate
$Q = \frac{qL}{k_{ref} T_0}$	Heat flux	$k^* = \frac{k_{ref}}{k}$	Thermal conductivity
$Bi_q = \frac{h_q L}{k_{ref}}$	Biot number - thermal	$\theta^\infty = \frac{T^\infty - T_0}{T_0}$	Surrounding temperature
$U = \frac{\rho^a}{\rho_s^a}$	Moisture content on dry basis	$D_w^* = \frac{D_w t_f}{L^2}$	Mass diffusivity - liquid water
$\rho_{ref} = \frac{P_0}{R_a T_0 \rho_s^a}$	Reference density	$R_v^* = \frac{R_v}{R_a}$	ratio of specific gas constants
$P_v^* = \frac{P_v}{P_0}$	Vapor pressure	$V = \frac{\rho_v^a}{\rho_s^a}$	Vapor density
$\alpha_p^* = \frac{k_g t_f P_0}{\mu_g L^2}$	Darcy term	$P_g^* = \frac{P_g}{P_0}$	Total gas pressure
$D_v^* = \frac{D_v t_f}{L^2}$	Mass diffusivity - water vapor	$Bi_m = \frac{h_m t_f}{L}$	Biot number - mass
$V^\infty = \frac{\rho_v^\infty}{\rho_s^a}$	Ambient vapor density	$t^* = \frac{t}{t_f}$	time
$\nabla^* = \frac{\partial}{\partial(x/L)}$	Spatial gradient	$\Lambda = \frac{\rho_a^a}{\rho_s^a}$	Air density
$G = V + A$	Total gas density	$H^* = H \times t_f$	Evaporation rate constant

Table 2.3: Expressions for all non-dimensional parameters used in Diffusive, TMPN and TMPE models

Parameter	Value	Parameter	Value
Gussed parameters			
a_q^*	1.4	k^*	3.2
D_w^*	0.0093	D_v^*	23.125
Bi_q	0.080	a_p^*	1284
H^*	12000		
Other parameters			
Bi_m	$\frac{Bi_q}{(\rho C_p)_{air} Le^{2/3} (L^2/k_{ref} t_f)}$	a_w	$\frac{0.99}{\exp(0.042U^{-1.11})}$
R_1	$\frac{\lambda \rho_s^a k_{ref} t_f}{T_o k^* a_q^* L^2}$	S_l	$\frac{U \rho_s^a}{\pi \rho_l}$
λ [kJ/kg]	2500	π	0.76
k_{ref} [W/mK]	0.5	t_f [s]	1200
ρ_s^a [kg/m ³]	436	L [m]	0.008

Table 2.4: Parameters used for simulations

bottom region which leads to linear decrease of mean moisture content. These observations for simulated data match comparatively with literature on bread baking process [9, 10] and experimental measurements.

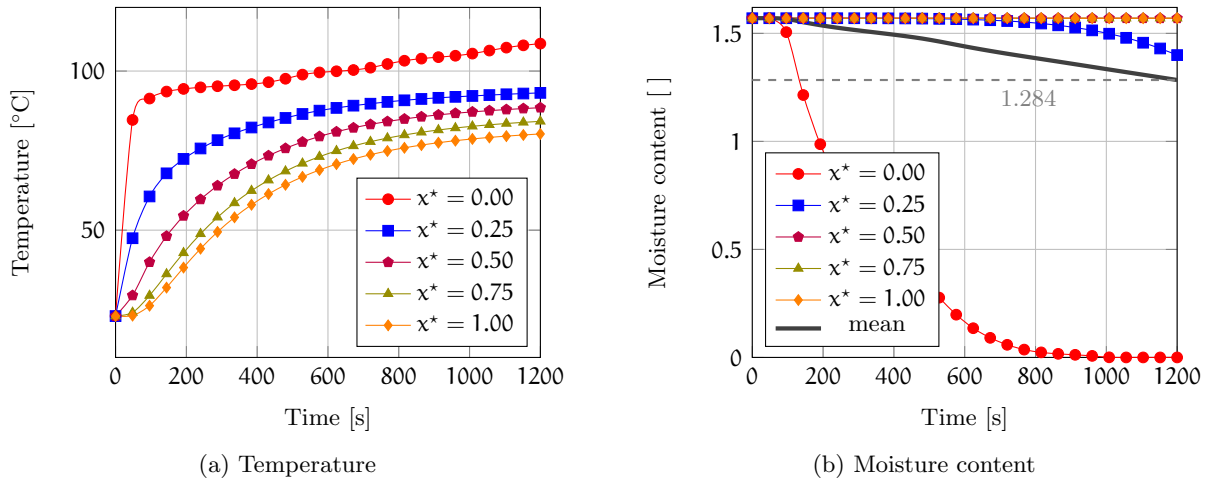


Figure 2.11: Simulated profiles of temperature (a) and moisture content (b) for Diffusive model

Evaporation rate

Evaporation rate as a function of baking time at various sensor locations is presented in figure 2.12. It is obvious that only the bottom region exhibits strong evaporation due to heat input. The evaporate rate is nearly zero for other region indicating that there is no presence of evaporation or condensation in these regions. It is mainly due to implementation of conditional functions

appearing in the explicit evaporation rate computation and the temperature in other region never exceed 100°C . Maximum evaporation is observed between 400 and 800s of baking time in this model. A small negative dip in this rate profile appears after baking time of 800s. It might be due to conditional function for moisture content that drops to zero when $U = -0.1$.

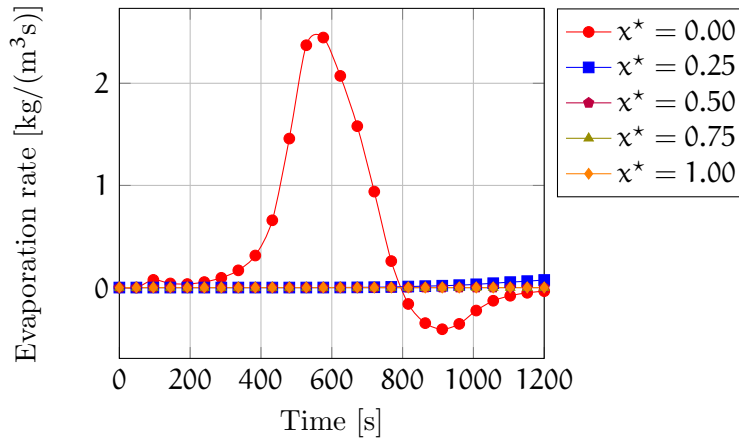


Figure 2.12: Evaporation rate for Diffusive model

2.3.2 TMPN model

With improvisation of mathematical formulation from diffusive model, TMPN model has three significant state variables: temperature, moisture content and gas pressure. These state variables are plotted against baking time in figure 2.13.

The trends of temperature (see figure 2.13a) are not close to measurement data presented earlier. For the heating period of first 100 s, a sharp temperature rise is noted that becomes less steep and linear going up to 600s of baking. Drop in temperature is spotted beyond this, amid the entire baking time that might be due to poor selection of evaporation rate and other parameters. Focusing on pressure evolution with baking time from figure 2.13b, there is a mild rise in gas pressure for first 400 s and after this time there exists a sudden jump in their magnitude. The reason for this is similar to that stated for temperature and causes aggressive rise in pressure during later stage of baking. Local moisture content profiles show evaporation is stronger at ambient surface than at bottom and is not true. Rise in the value of moisture content from initial condition near the core region indicates presence of condensation effect. This validates that this model includes evaporation-condensation effect.

Evaporation rate

Evaporation rate profiles from figure 2.14 clearly indicate condensation of vapor near the core region with negative evaporation rate. Evaporation rate at bottom is weaker than at free surface as reflected in moisture content profiles. Evaporation occurs mostly at the boundaries and condensation is noted in other regions.

2.3.3 TMPE model

The simulated results of TMPE model are showcased in figure 2.15 as temperature, moisture content and gas pressure variations. Temperature trends from figure 2.15a seem to fairly agree

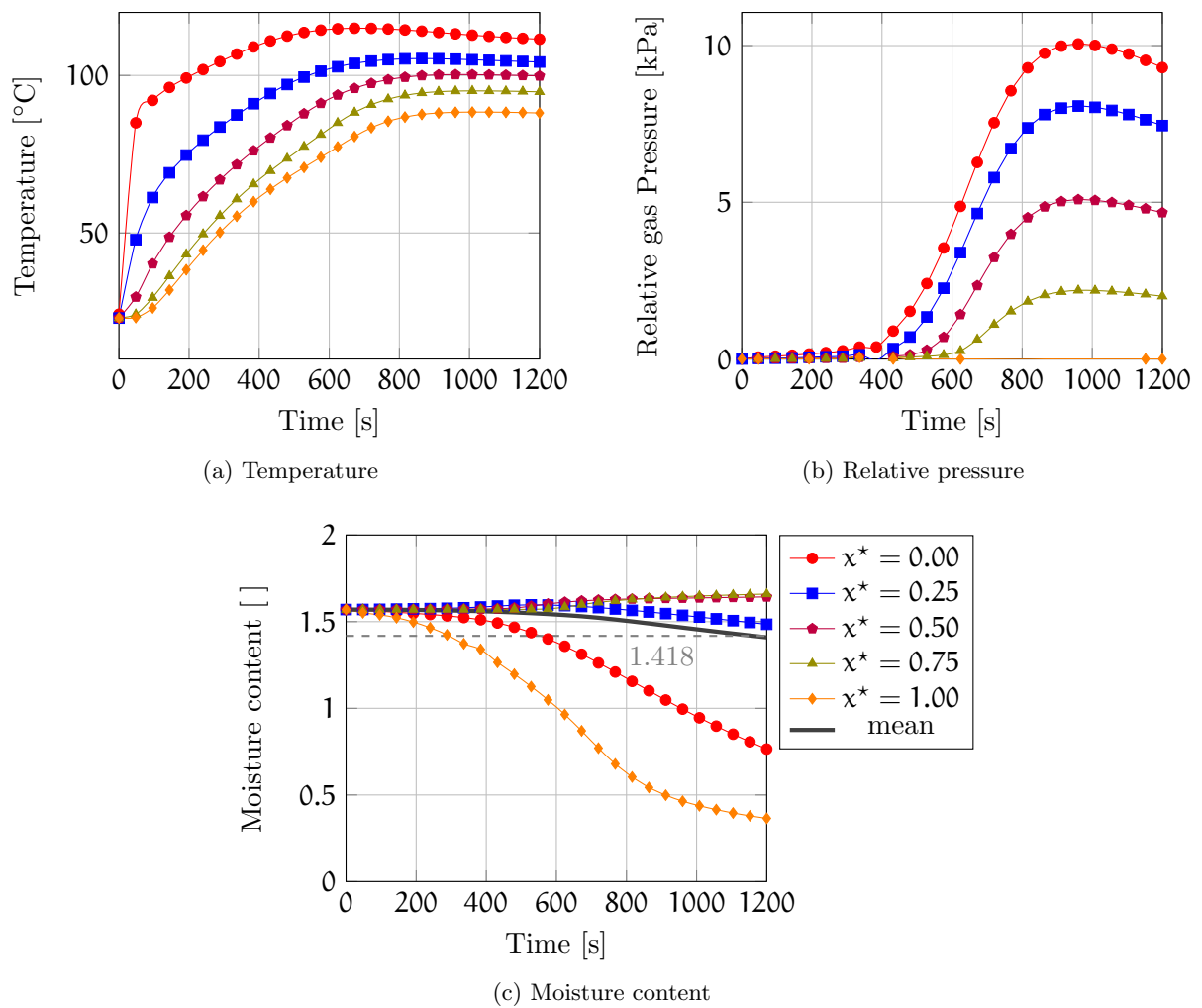


Figure 2.13: Simulated profiles of temperature (a), relative gas pressure (b) and moisture content (c) for multiphase model with non-equilibrium approach

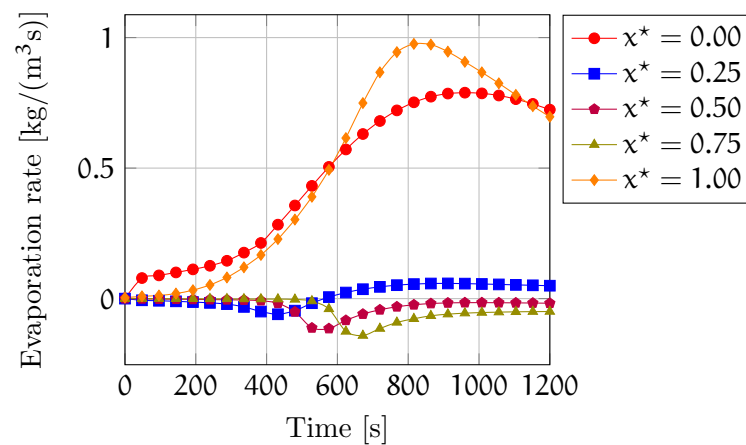


Figure 2.14: Evaporation rate for multiphase model with non-equilibrium approach

with trends of experimental measurements (from figure 2.3a). Temperature at bottom almost becomes stagnant once the boiling point of liquid water is reached. A minute stagnation of temperature is seen at 60°C at sensor location T₇. The relative gas pressure shown in figure 2.15b is drastically different from previous model (figure 2.13b). A linear increase in gas pressure is seen until mid of baking time. Significant pressure variations are noted only at sensor locations $x^* = 0$ and 0.25. Decrease in gas pressure amid the baking time at bottom is due to stagnant moisture content and temperature there.

From figure 2.15c, local moisture content variations can be understood. Only at boundaries, the moisture content has decreased and in other regions, it has increased from the initial value. Similar to previous model, this one also shows a strong moisture loss at ambient surface than at bottom. It may be either due to higher mass convection coefficient than the actual value or overestimated surface evaporation. Condensation factor is stronger than the previous TMPN model, as the maximum moisture content in core reaches a value of $U = 1.9$ at a certain baking time. This factor agrees with reality as the bakery products always have wet core and dry surface (except for biscuits).

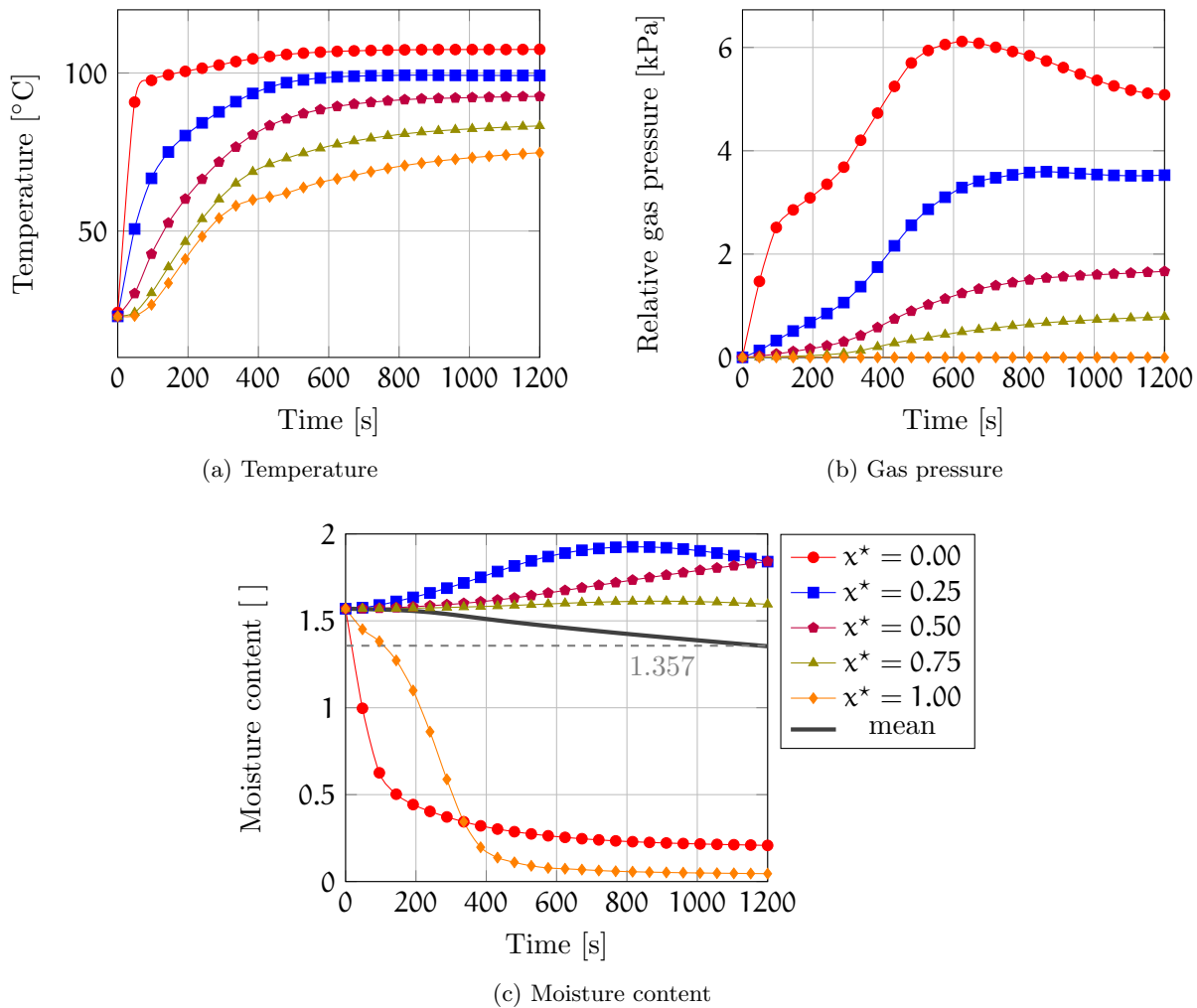


Figure 2.15: Simulated profiles of temperature (a), relative gas pressure (b) and moisture content (c) for multiphase model with equilibrium approach

Evaporation rate

This model has strong intermittent evaporation at free surface but a continuous positive evaporation rate at the bottom surface. Initially, evaporation is strong and as baking time increases, it decreases at the bottom of the product. Magnitude of evaporation is several times stronger than other two models presented before. The discontinuous trend of evaporation rate at free surface indicates presence of surface evaporation and condensation of water after some point of time. But in reality, there is no such condensation effect near free surface. Identical to earlier model, condensation effects are observed in the core region.

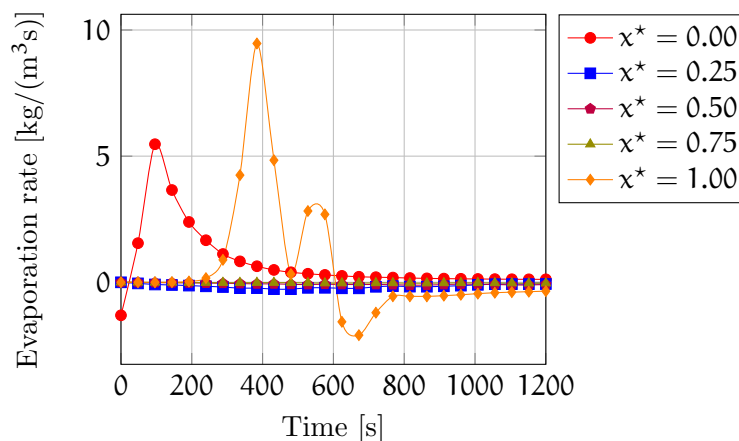


Figure 2.16: Evaporation rate for multiphase model with equilibrium approach

Overall comparison

Diffusive model has better temperature profile especially at bottom ($x^* = 0$) in comparison to the other two models as implied from the the trend of dough transformation into crust. TMPE model does not show any significant temperature rise after reaching 100°C while TMPN model has a small dip in temperature value which is scientifically incorrect. Core temperature of diffusive and TMPE models has not increased beyond 100°C as the moisture content in the core region did not evaporate. But in TMPN model, temperature raises beyond boiling point of water at $x^* = 0.25$, despite which the condensation is observed at this location. The major reason for this inappropriate physical result in TMPN model is the improper implementation of evaporation rate constant (H^*).

Inclusion of vapor phase has greater impact on local moisture content profile. TMPE model has higher drying rate than TMPN model while comparing against their mean values. Overall, the diffusive model has the highest drying rate as the mean moisture content at the end of baking is 1.284. But, TMPE model has a value close to the experimental value (which is approximately 1.31). Irrespective of the model, the trends of mean moisture content match with experimental profile. Unless local moisture measurement exists, it would be tedious to distinguish which model replicates the baking physics better.

Relative total gas pressure profiles in TMPE model are better than TMPN model and also profiles match with previous studies in literature [26]. In equilibrium approach, vapor pressure is greatly dependent on temperature and moisture content. Vapor pressure increases with increase in temperature which is reflected in increasing evaporation rate for this multiphase model. As

mentioned earlier, the magnitude of evaporation rate of TMPE model is several times greater than other two models. The maximum pressure reached in TMPN model is 65% more than TMPE model. But the rise of vapor pressure does not have a good impact on evaporation rate.

2.4 Conclusive remarks

This chapter briefly explained the experimental procedure carried out for measuring state variables like temperature and mean moisture content during contact baking. Some experimental considerations and reason behind measuring only the average moisture content have been described. A typical baking test setting the coil temperature to 200°C has been performed and reported. From the cast-iron floor temperature, heat transfer at the interface of the cast iron floor and dough was estimated using inverse algorithm as a function of baking time. Water activity or Sorption isotherm which is a significant function required for multiphase model simulation, has been measured as a function of moisture content and approximated using Ferro-Fontan model. Thermal properties of dough like thermal conductivity, diffusivity and specific heat capacity before and after baking process are also measured. Specific heat capacity is measured using micro-calorimeter and is found to lie in range of 2800 - 3400 [J/(kgK)]. Hot wire and hot plane methods have been employed for thermal conductivity measurements. Using Hot wire method, conductivity is estimated to be approximately 0.38 [W/(mK)], but the hot plane method resulted in higher values. Hot plane method gave thermal conductivity and volumetric heat capacity as 0.48 [W/(mK)] and 3.61 [MJ/(m³K)] respectively, which are lower than the average values for liquid water.

A mathematical model is required for accurate simulation of the baking process. Such a model is then used for estimating thermophysical properties either as constants or functions. With the basic understanding of physics involved in the baking process, three models are developed. They are tagged as Diffusive model, Multiphase model with Equilibrium approach (TMPE) and Non-equilibrium approach (TMPN) where T, M and P stand for Temperature, Moisture content and Pressure, respectively. Diffusive model is a phenomenal model in which explicit evaporation rate is computed using conditional functions. This model captures variations in temperature and moisture content only. Drawbacks of diffusive model like poor evaporation rate formulation are overcome by Multiphase model. There is always a debate about whether to assume equilibrium between vapor and liquid water inside the medium during baking or not. Hence, the two models, one with equilibrium approach and another with non-equilibrium approach have been formulated. The governing equations of all these models are transformed into non-dimensional form. Finally, the validation of each model with some derived key parameters has been performed.

List of symbols

Latin symbols

a_w	Water activity
U	Moisture content [kg/kg dm]

T1 - T7	Thermocouples
Q	Heat flux [W/m ²]
q	Heat source[W]
m	mass [kg]
C _p	Specific heat capacity [J/(kg.K)]
T	Temperature [K]
t	time [s]
I _v	Evaporation rate [kg/(m ³ s)]
S _i	Saturation of phase i
D _i	Mass diffusivity of element i [m ² /s]
n _i	Mass flux of element i [kg/(m ² s)]
k _g	Gas permeability [m ²]
μ _g	Dynamic viscosity of gas [Pa.s]
P _i	Pressure of element i [Pa]
H	Evaporation rate constant [1/s]
R _i	Specific gas constant of species i [J/(kgK)]
C _{1,2}	Step functions of temperature and moisture content respectively
k	Thermal conductivity [W/(mK)]
h _q	Convective heat transfer coefficient [W/(m ² K)]
h _m	Convective mass transfer coefficient [m/s]
L	Length of the domain [m]
Greek symbols	
α	Coefficient
γ	Coefficient
ρ	Density [kg/m ³]

λ	Latent heat of vaporization [J/kg]
ϵ	Phase conversion factor
π	porosity

Non-dimensional numbers

θ	Temperature
U	Moisture content
V	Vapor content
A	Air content
G	Total gas content
α_q^*	Thermal diffusivity
α_p^*	Capillary diffusivity
D_l^*	Liquid water diffusivity
D_v^*	Water vapor diffusivity
P_g^*	Gas pressure
R_v^*	Specific gas constant ratio
Bi_q	Biot number - heat
Bi_m	Biot number - mass
R_l	Latent heat of vaporization
I_v^*	Evaporation rate
t^*	time

Subscripts

eff	effective
l	liquid
g	total gas
v	vapor

a	air
s	solid
cr	critical value
sat	saturated
ref	reference
atm	atmospheric

Superscripts

r	Coefficient
a	apparent
*	elements in non-dimensional form
∞	Ambient condition
eq	equilibrium

Abbreviations

CT	Computer Tomography
MRI	Magnetic Resonance Imaging
NIR	Near Infrared Reflectance
PTFE	PolyTetraFluoroEthylene

Bibliography

- [1] Muriel J. Wagner, Lucas T., D. Le Ray, and G. Trystram. Water transport in bread during baking. *Journal of Food Engineering*, 78:1167 – 1173, 2007.
- [2] Urban Wählby and Christina Skjöldebrand. Nir-measurements of moisture changes in foods. *Journal of Food Engineering*, 47(4):303–312, 2001.
- [3] Karin Thorvaldsson and Christina Skjöldebrand. Method and instrument for measuring local water content inside food. *Journal of Food Engineering*, 29(1):1–11, 1996.
- [4] Muriel J. Wagner, Michel Loubat, Alain Sommier, Dominique Le Ray, Guylaine Collewet, Bertrand Broyart, Honoré Quintard, Armel Davenel, Gilles Trystram, and Tiphaine Lucas.

- Mri study of bread baking: Experimental device and mri signal analysis. *International Journal of Food Science and Technology*, 43(6):1129–1139, 2008.
- [5] J.R. Heil, Mustafa Özoligen, and Michael J. McCarthy. Magnetic resonance imaging analysis of water migration and void formation in baking biscuits. *AIChE Symposium series*, 89(297):39–45, 1993.
- [6] Jean-Pierre Bardon and Yvon Jarny. Process and device for transient measuring of surface temperatures and heat flux. US patent number: 5 772 329, June 1998.
- [7] S.S. Sablani, N. Marcotte, O.D. Baik, and F. Castaigne. Modeling of simultaneous heat and water transport in the baking process. *LWT - Food Science and Technology*, 31(3):201–209, 1998.
- [8] S.P. Venkateshan. *Mechanical Measurements*. John Wiley & Sons Ltd, 2015.
- [9] Zhang J. and Datta A.K. Mathematical modeling of bread baking process. *Journal of Food Engineering*, 75:78–89, 2006.
- [10] Nicolas V., Salagnac P., Glouannec P., Ploteau J.P., Jury V., and Boillereaux L. Modelling heat and mass transfer in deformable porous media : Application to bread baking, 2014.
- [11] S. Marc, J. P. Ploteau, P. Le Bideau, and P. Glouannec. Transient heat flux estimation during the baking of cereal batter by contact heating. *International Journal of Heat and Mass Transfer*, 155:119848, 2020.
- [12] Irene Lind and Christina Rask. Sorption isotherms of mixed minced meat, dough and bread crust. *Journal of Food Engineering*, 14:303–315, 1991.
- [13] Vincent Nicolas, Fernanda Vanin, David Grenier, Tiphaine Lucas, Christophe Doursat, and Denis Flick. Modeling bread baking with focus on overall deformation and local porosity evolution. *AIChE Journal*, 62(11):3847–3863, 2016.
- [14] A. Ousegui, C. Moresoli, M. Dostie, and B. Marcos. Optimal control and cfd modeling for heat flux estimation of a baking process. *Computers and Chemical Engineering*, 38:139–150, 2012.
- [15] Hadiyanto, A. Asselman, G. van Straten, R. M. Boom, D. C. Esveld, and A. J.B.van Boxtel. Quality prediction of bakery products in the initial phase of process design. *Innovative Food Science and Emerging Technologies*, 8(2):285–298, 2007.
- [16] Sylwester Furmaniak, Artur P. Terzyk, Roman Gołembiewski, Piotr A. Gauden, and Leszek Czepirski. Searching the most optimal model of water sorption on foodstuffs in the whole range of relative humidity. *Food Research International*, 42(8):1203–1214, 2009.
- [17] Santanu Basu, U. S. Shivhare, and A. S. Mujumdar. Models for sorption isotherms for foods: A review. *Drying Technology*, 24(8):917–930, 2006.
- [18] Emmanuel Purlis and Viviana O. Salvadori. A moving boundary problem in a food material undergoing volume change - simulation of bread baking. *Food Research International*, 43(4):949–958, 2010.

- [19] A.K. Luikov. Systems of differential equations of heat and mass transfer in capillary-porous bodies (review). 18:1–14, 1975.
- [20] Davide Papasidero, Flavio Manenti, and Sauro Pierucci. Bread baking modeling: Coupling heat transfer and weight loss by introduction of an explicit vaporization term. *Journal of Food Engineering*, 147:79–88, 2015.
- [21] Zhang J. and Datta A.K. Some considerations in modeling of moisture transport in heating of hygroscopic materials. *Drying Technology*, 22(8):1983–2008, 2004.
- [22] Jifeng Zhang. *Multiphase heat and mass transfer with large deformation in porous media*. PhD thesis, Cornell University, 2003.
- [23] Xiao Dong Chen and Putranto Aditya. *Modern Drying Processes, A Reaction Engineering approach*. Cambridge, 2013.
- [24] R.Byron Bird, Warren E. Stewart, and Edwin N. Lightfoot. *Transport Phenomena*. John Wiley & Sons, Inc., 2002.
- [25] A. Ousegui, C. Moresoli, M. Dostie, and B. Marcos. Porous multiphase approach for baking process - explicit formulation of evaporation rate. *Journal of Food Engineering*, 100:535–544, 2010.
- [26] D. Grenier, D. Le Ray, and T. Lucas. Combining local pressure and temperature measurements during bread baking: insights into crust properties and alveolar structure of crumb. *Journal of Cereal Science*, 52(1):1–8, 2010.

Chapter 3

Selection of the appropriate model for physical properties estimation

Abstract

Inverse procedure and other fundamental components required for the computation are elaborated in this chapter. Advantages and benefits of implementing complex step differentiation are discussed. The standard ordinary least square objective function will not be a suitable option for optimization due to presence of multiple components in objective function (temperature and moisture content) and the coupled equations (forward problem) are highly non linear. Hence, other kind of functions such as weighted and scaled least square objected functions are employed and their performance are compared to ordinary least square. Design of experiments are computed to select optimal sensor locations to conduct experiment that eases the optimization procedure. Finally, a numerical analysis with inverse solutions from the previously discussed models are studied before proceeding with experimental measurements. The numerical analysis shows that the retrieval of parameters is excellent for **TM** model but other two models has showed some difficulties.

3.1 Inverse procedure and considerations

A dynamic physical process can be modeled using mathematical tools likes ordinary or partial differential equations and rarely fractional differential equations. These equations contain dependent and independent variables and knowledge about them is mandatory to compete the model. Usually, the dependent variables are state variables that can be measured and are quantities of interest. Independent variables are the physical constants. For instance, consider a researcher who is trying to understand the thermal behavior of a metal rod that has been heated for a short time. Assuming unidirectional heat flow without any source or sink, the following partial differential equations can be used to solve the problem mathematically.

$$\rho c_p \frac{\partial T(x, t)}{\partial t} = \nabla(k \nabla T(x, t)) \quad (3.1a)$$

$$k \nabla T(0, t) = q(t) \quad (3.1b)$$

$$-k\nabla T(L, t) = h_q(T(L, t) - T^\infty) \quad (3.1c)$$

$$T(x, 0) = f(x) \quad (3.1d)$$

In the above problem, the independent or state variable is temperature (T , T^∞ & T_0) while other parameters or variables (which can be functions of state variables) such as density (ρ), specific heat capacity (c_p), thermal conductivity (k) and boundary conditions (q & h_q) are considered as dependent variables or constants. These dependent variables are physical properties of the metal and process parameters which are presumed to be known beforehand. The heating process can be simulated by solving the above equations (3.1) with aid of any numerical (like finite difference, finite volume, finite element methods, etc.) or analytical method. In such situations, the mysterious parameters are measured through either experimentation methods or inverse problem. The term ‘Parameter estimation’ has not been frequently used earlier rather it was termed as nonlinear least square or regression problems.

Carl Friedreich Gauss, one of the greatest mathematicians, is first to demonstrate parameter estimation using non-linear least square method for calculating orbital elements of the planets during late 1790s [1, 2]. Later in 1960s, due to great demand in space exploration program, attention towards inverse problem has been increased and extensively used for characterizing the thermal shield in space re-entry vehicle [3]. The inverse problem is diversified in the field of medicine/biology [4–7], applied mathematics [8], wave propagation/signal processing [9–11], optics [12, 13], heat transfer [14, 15] and many others. The essentials of inverse problems are a mathematical model and accurate measurements of state variable of focus. The unknown parameters are approximated with an optimization algorithm that minimizes the Euclidean distance between the measured and computed variables. Usually in heat transfer problem, the parameter and/or function focused to be estimated are unknown boundary conditions like surface heat flux, thermal properties like conductivity, source terms.

Several studies on inverse problems have been carried out in the field of baking process in order to estimate boundary conditions, thermophysical and rheological properties either as constants or functions of state variable like temperature. Many experimentation methodologies are available for evaluation of thermal and mass transfer properties like DSC, hot wire/disc method etc. Yet there is still a significant dependency on inverse procedure due to occurrence complex phenomena during baking process which has been already discussed in previous chapter. Rask in early nineties has reviewed and presented the available thermal properties for various stages (during baking) and formations of dough [16]. Even with this availability of detailed properties, the simulation were not found satisfactory in comparison with experimental measurements. Zaroni and his co-authors has estimated thermal diffusivity of bread during baking process as function of porosity [17]. Following them, authors like Jury has approximated thermal conductivity of frozen bread during thawing [18] and Omid has evaluated using ANN (artificial neural network) [19].

Apart from thermal conductivity estimation, there were several efforts made for evaluating liquid water mass diffusivity. Fabbri and his co-workers has speculated mass diffusivity of baked products as constant by considering only the mass transfer phenomenon [20]. Till that point of time, authors have been tried to approximate their required thermophysical properties as constant. Purlis and Salvadori were the first to demonstrate baking process as moving boundary problem (MBP or Stefan problem) and have obtained effective thermal conductivity and heat capacity as function of temperature for bread that accounts evaporation-condensation effect

[21, 22]. This effective thermal properties were extensively used by several other author to accurately simulate the baking process for different conditions [23–25]. As the focus were shifted to the physical attributes of bakery products, few researchers have dedicated their work only for examining the structural properties [26, 27]. Lostie et al. have worked to link the contribution of structural mechanics to heat and mass transfer phenomena in the baking of sponge cake and have estimated influential thermophysical and rheological parameters [28].

The estimation procedures that are stated above are termed as inverse problem. There is another kind of optimization problem which is known as inverse design problem. Inverse design problem helps to identify an optimal boundary and the geometry conditions for a process. Such kind of design problem helps in speculating an optimal boundary condition such as heat flux that is required to bake the product. Hadiyanto had been estimated an optimal process temperature comprising oven temperature, radiative and microwave power altogether that resulted in desired physical attributes on the bread like browning index, crispness, etc [29]. Authors like Ousegui and Reddy with their co-workers had been estimated the optimal surface heat flux with minimum energy requirement for baking of bread in a conventional oven using a coupled heat and mass transfer equations [30, 31]. There are many other inverse design problem dedicated to baking process. Herein, both inverse problem and inverse design problem are utilized. Inverse problem is performed to estimate the thermophysical properties as constant and function, and Inverse design problem is used to investigate optimal sensor locations. In the following chapter, the inverse design problem and other components that are required for computation of inverse problem are detailed in an elaborated manner.

3.1.1 Sensitivity or Jacobian matrix

Sensitivity of a parameter is defined as how much does the state or measured variable varies with respect to a small variation in the unknown parameter. Mathematically, sensitivity is expressed as the first derivative of the measured variable with respect to the unknown or estimable parameter. It is expressed as:

$$\chi_p = \frac{\partial T(x, t, p)}{\partial p} \quad (3.2)$$

where \mathbf{p} is set of unknown parameters. Objective function is the most important component in an optimization problem. In case of gradient based optimization, the basic requirement for the expected solution is that the derivative of the objective function must be as minimum as possible. This derivative is product of sensitivity that is stated above and difference between the measured and simulated variables.

$$S(\mathbf{p}) = [Y - T]^T [Y - T] \quad (3.3)$$

where $S(\mathbf{p})$ is the objective function

$$\nabla S(\mathbf{p}) = -2 \frac{\partial T}{\partial p} (Y - T) \quad (3.4)$$

where Y , T are measured and simulated quantities receptively.

There are several ways for computing the sensitivity coefficients and some of them are analytical solution (when they exist), finite difference method (FDM), complex step differentiation (CSD),

automatic differentiation (AD), equation based methods like direct differentiation, adjoint methods, etc. Among them, the most general and convenient method is the finite difference method (either forward or central difference scheme). These formulations are derived by truncating a Taylor series that is expanded about a point. With $\Delta\mathbf{p}$ being the step size which tends to zero, the sensitivity or Jacobian matrix by central difference scheme is given as follows,

$$\mathbf{X}_{\mathbf{p}} = \frac{T(\mathbf{p} + \Delta\mathbf{p}) - T(\mathbf{p} - \Delta\mathbf{p})}{2\Delta\mathbf{p}} + \mathcal{O}(\Delta\mathbf{p}^2) \quad (3.5)$$

Even though the above expressed formulation is second order accurate, it suffers from “step-size dilemma” due to the subtraction operation involved in this approximation. As the step-size h is reduced below a limit, subtraction cancellation error becomes significant and the resulting estimates become unreliable. When the step-size h is very small then there is no difference in the numerator of equation (A.5) that makes the central finite difference scheme to yield zero instead of the derivative. In a specialized literature, great effort had been made to overcome this deficiency by introducing an optimal selection of the step-size h by balancing the inherent shortcomings like truncation error and rounding-off error of the finite difference method.

If there are $n_{\mathbf{p}}$ parameters in the model, then $2n_{\mathbf{p}} + 1$ runs of the computational code will be required to compute the $n_{\mathbf{p}}$ first-order sensitivity coefficients with central difference FDM scheme. The simplicity of this method is paid by its high computational time. As stated before, the primary difficulty with this procedure is choosing an optimal perturbation size $\Delta\mathbf{p}$. Consequently, some numerical experimentation has recommended the right step size that are sufficiently small to overcome the truncation error.

Complex step differentiation (CSD) is a reliable and effective method for calculating n^{th} derivative of a function and it does not suffer from any kind of truncation or subtraction errors as seen in finite difference method. CSD is derived from the expansion of Taylor series for a function with an imaginary step interval $i \cdot h$ [32] as

$$f(x + ih) = f(x) + i \cdot h \cdot f'(x) - \frac{h^2}{2} f''(x) - i \cdot \frac{h^3}{3} f'''(x) + \dots \quad (3.6)$$

Where $i^2 = -1$. Taking imaginary part of the Taylor series and dividing it by perturbation size h yields the first derivative as

$$f'(x) = \frac{\text{Im}[f(x + ih)]}{h} + \frac{h^2}{3} f'''(x) + \dots \quad (3.7)$$

Im is a function which returns imaginary part of a complex variable. The above presented method can be also used for evaluating sensitivity or Jacobian matrix elements [33] as,

$$\mathbf{X}_{\mathbf{p}} = \frac{\text{Im}[T(\mathbf{P} + i\mathbf{h})]}{h} + \mathcal{O}(h^2) \quad (3.8)$$

On comparing the equations (A.5) and (3.8), it can be found that CSD does not suffer from any cancellation error and it is second order of approximation. Moreover, CSD requires only $n_{\mathbf{p}} + 1$ runs to compute the first order derivative for $n_{\mathbf{p}}$ number of parameters.

In order to understand the effectiveness of CSD over FDM, a standard and most commonly used heat transfer problem on the ARMCO iron is considered. A rod with homogeneous thermal properties is subjected to step heat flux at one end while the other end is insulated. The problem

statement is given mathematically by,

$$\rho c_p \frac{\partial T(x, t)}{\partial t} = k \frac{\partial^2 T(x, t)}{\partial x^2}, \quad \forall x \in [0, L], \quad t > 0 \quad (3.9a)$$

$$-k \frac{\partial T(0, t)}{\partial x} = \begin{cases} q_0 & \forall t \in [0, t_h] \\ 0 & \forall t \in [t_h, t_f] \end{cases} \quad (3.9b)$$

$$k \frac{\partial T(L, t)}{\partial x} = 0, \quad \forall t \in [0, t_f] \quad (3.9c)$$

$$T(x, 0) = f(x), \quad \forall x \in [0, L] \quad (3.9d)$$

To ease the problem, the governing equations are transformed into nondimensional form before obtaining the analytical solution. The sensitivities of parameters heat capacity and thermal conductivity with respect to temperature, are scaled down in dimensionless forms. The analytical solution are available from literature for temperature evolution, and its derivative with respect to physical properties like heat capacity, thermal conductivity. The analytical solutions are presented below.

$$T(x, t) = \begin{cases} t + \frac{x^2}{2} - x + \frac{1}{3} - 2 \sum_{m=1}^{\infty} \frac{\cos(\lambda_m x)}{\lambda_m^2} e^{-\lambda_m^2 t} & \forall t \in [0, t_h] \\ t_h + 2 \sum_{m=1}^{\infty} \frac{\cos(\lambda_m x)}{\lambda_m^2} [e^{-\lambda_m^2 (t-t_h)} - e^{-\lambda_m^2 t}] & \forall t \in [t_h, t_f] \end{cases} \quad (3.10)$$

The analytical solution for scaled sensitivity associated with heat capacity is expressed as:

$$X_c = \begin{cases} -t - 2 \sum_{m=1}^{\infty} \cos(\lambda_m x) e^{-\lambda_m^2 t} & \forall t \in [0, t_h] \\ -t_h - 2 \sum_{m=1}^{\infty} \cos(\lambda_m x) [e^{-\lambda_m^2 t} - e^{-\lambda_m^2 (t-t_h)}] & \forall t \in [t_h, t_f] \end{cases} \quad (3.11)$$

and with thermal conductivity is,

$$X_k = \begin{cases} x - \frac{x^2}{2} - \frac{1}{3} + 2 \sum_{m=1}^{\infty} \frac{\cos(\lambda_m x)}{\lambda_m^2} e^{-\lambda_m^2 t} (1 + \lambda_m^2 t) & \forall t \in [0, t_h] \\ 2 \sum_{m=1}^{\infty} \frac{\cos(\lambda_m x)}{\lambda_m^2} [e^{-\lambda_m^2 t} (1 + \lambda_m^2 t) - e^{-\lambda_m^2 (t-t_h)} (1 + \lambda_m^2 (t-t_h))] & \forall t \in [t_h, t_f] \end{cases} \quad (3.12)$$

The heat transfer governing equations (3.9) are solved using the analytical method given by equation (3.10). The analytical solutions of temperature variation (T) and its sensitivity with

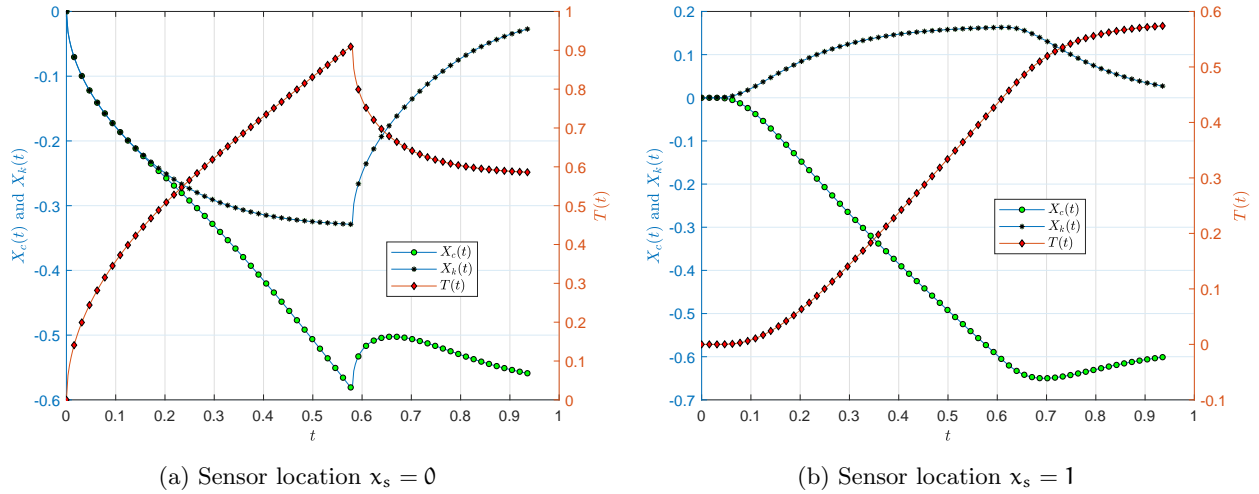


Figure 3.1: Sensitivity and temperature profiles as function of time computed analytically.

respect to heat capacity (X_c) and thermal conductivity (X_k) at boundaries are given in figure 3.1. The first derivative of temperature with respect to heat capacity and thermal conductivity are computed using CSD and FDM and its solutions are compared against analytical solutions given by equations (3.11, 3.12). The root mean square (rms , r_p^m) and relative errors (ϵ) are used for evaluating the difference in their computation with respect to analytical solution are given by

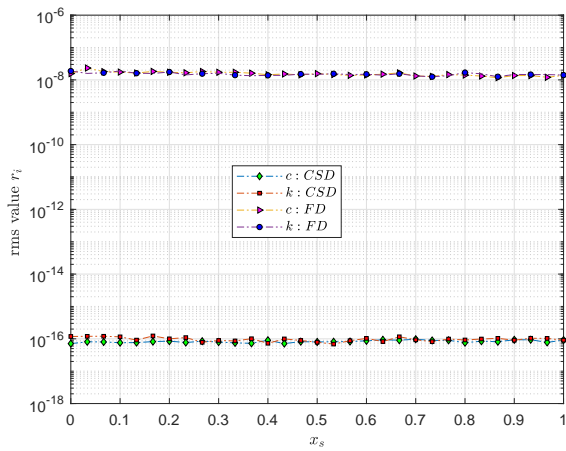
$$r_p^m = \sqrt{\frac{1}{n_t} \sum_{i=1}^{n_t} (X_{p,i}^a - X_{p,i}^m)^2} \quad (3.13)$$

$$\epsilon = 100 \times \max \left| \frac{\text{Numerical} - \text{Analytical}}{\text{Analytical}} \right| \text{ in } (\%) \quad (3.14)$$

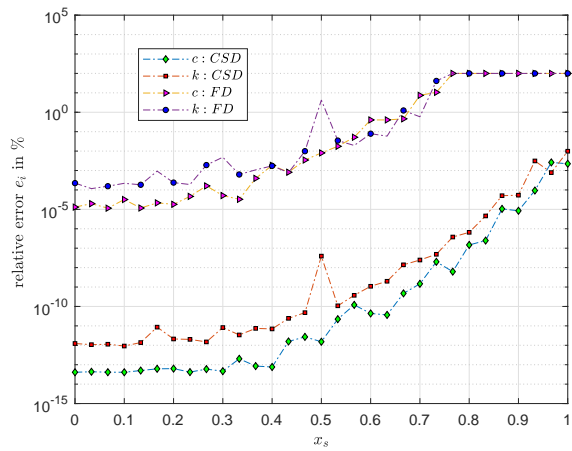
Where n_t is number of transient measurements, p is either c or k , m represents numerical method which is either FDM or CSD. The rms and relative errors computed for CSD and FDM with respect to analytical solutions along the length of the sample are given by figure 3.2.

The graphical representations show that CSD is superior to FDM in computing the sensitivity coefficients. CSD has least rms error in order of 10^{-16} for both the parameters irrespective of location whereas FDM has error in order of 10^{-8} for step size $h = 10^{-8}$. The additional error computation is aided by relative error ϵ and it also proves the same. The maximum relative error for both parameters in case of CSD is in order of 10^{-5} but for FDM is 100%. These maximum errors in both the methods are shown at insulated boundary.

FDM method fails for step size $h = 10^{-8}$ in the region near insulated boundary which is in range $x \in [0.8, 1]$. The choice of step size h is more important for FDM but this factor has very poor effect on the performance of CSD. This is evident from the figure 3.3. The optimal choice of step size for FDM is between $h = 10^{-5}$ and 10^{-8} . Though the step size does not influence CSD performance, least values for rms and relative errors are spotted beyond $h = 10^{-5}$. Conclusively from the above analysis, it is clear that CSD is more accurate and precise than FDM for computing the sensitivity coefficients.

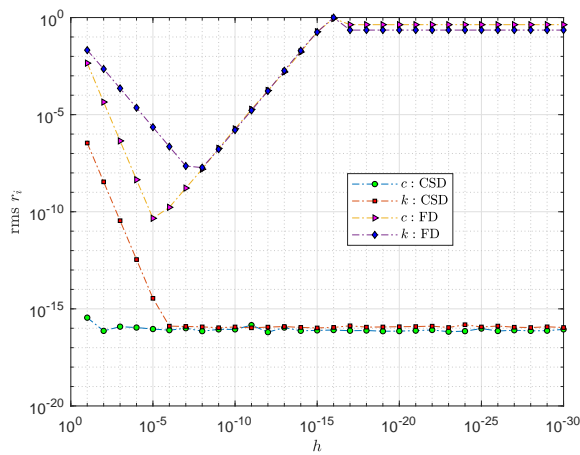


(a) rms

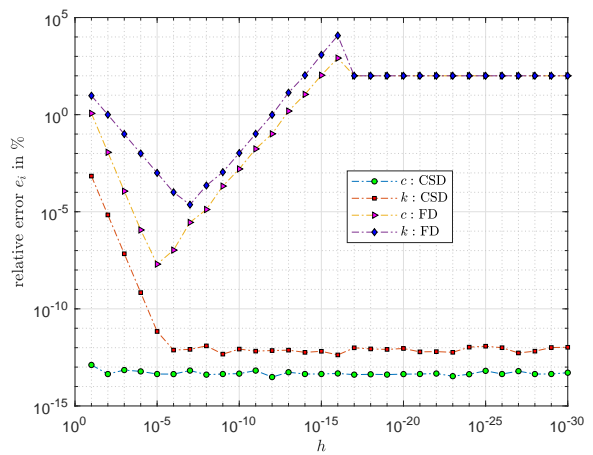


(b) Relative error ϵ_i in %

Figure 3.2: Variation of rms and relative error ϵ values for parameters c and k as a function of sensor position x_s with $h = 10^{-08}$



(a) rms



(b) Relative error ϵ_i in %

Figure 3.3: Variation of relative error ϵ and rms values for parameters c and k as a function step-size h in range between 10^{-01} and 10^{-30} at $x_s = 0$

3.1.2 Objective function

The main motive of an optimization or inverse problem is to extremize (either maximize or minimize) a desired function. Hence, this function is called as objective or cost function. In case of inverse problem, the objective function gives the closeness between simulated and measured state or desired variables. Any measurable variable can be taken as an element of objective function. For instance, measurable variables like temperature at several locations in the sample and heat flux at boundaries can be taken as elements of the objective function for a thermal related models. But in most of the cases, only temperatures were considered and it was also sufficient to solve the optimization problem efficiently. The improvement in the solution of inverse problem with inclusion of heat flux along with temperature in objective function is discussed in the following chapter.

With enough knowledge on experimentation of baking from the previous chapter 2, the elements that are considered in objective function for this case are temperature and mean moisture content. In literature, overall height of the sample in addition to temperature and moisture content measurements are taken as elements of objective function for determining the physical properties of sponge cake during conventional baking [28]. Measurement of pressure variation in the dough during baking will tremendously help the optimization problem for determining the capillarity and some other mechanical properties related to structural deformation. Grenier et al. measured the pressure variation in bread during baking process [34]. The measurement of pressure variation in this study was tedious and, measurements were inaccurate. It is due to presence of high moisture content and greater evaporation rate which leads to formation of pores at sensor nodes. Further, the sensitivities of parameters with respect to pressure were insignificant and shall be discussed in further section.

As stated before, in inverse problem the objective function is difference between the simulated and measured data. The components or elements of this function have different measuring units and non-dimensionalization will evades the mathematical difficulty in handling the problem. Gradient based optimization process demands the computations of first derivative of the function which must be non-zero. Thus, the objective functions are taken in quadratic form to satisfy this condition. From 18th century, ordinary least square (OLS) method is the most frequently utilized function in optimization problem. Least square norm between the two variables are given as follows,

$$S_{OLS} = [\mathbf{M} - \mathbf{E}(\Omega)]^T [\mathbf{M} - \mathbf{E}(\Omega)] \quad (3.15)$$

Where \mathbf{M} is measurement vector and \mathbf{E} is computed data vector which is function of parameter vector Ω . The measured variables are arranged in sequential manner of sensor locations and variables as,

$$\mathbf{M} = [\theta_1^1, \theta_2^1, \dots, \theta_{n_t}^1, \dots, \theta_1^{n_\theta}, \theta_2^{n_\theta}, \dots, \theta_{n_t}^{n_\theta}, \bar{U}_1, \bar{U}_2, \dots, \bar{U}_{n_t}] \quad (3.16)$$

The elements of simulated data \mathbf{E} are also arranged in similar fashion. Here θ corresponds to temperature, \bar{U} is mean moisture content, n_t is number of transient measurements, n_θ is number of temperature sensors. There are plenty of information available from temperature due to installation of multiple sensors at different locations whereas for moisture content only average measurement is feasible. Moreover, the magnitude of temperature and moisture content

in non-dimensional form is not in the same order of magnitude. In fact, the magnitude of temperature is approximately one tenth of the moisture content. With these discrepancies, the inverse solution from optimization of the objective function S_{OLS} may not result in a reliable comparison with measured values for either temperature or moisture content. To overcome this, utilization of weighted least square (WLS), scaled least square (SLS), etc are preferred as objective function [35]. Weighted least square is simple transformation of objective functions with some weights added to their elements as,

$$S_{WLS} = \phi [\mathbf{M}_\theta - \mathbf{E}_\theta]^\top [\mathbf{M}_\theta - \mathbf{E}_\theta] + (1 - \phi) [\mathbf{M}_U - \mathbf{E}_U]^\top [\mathbf{M}_U - \mathbf{E}_U] \quad (3.17)$$

Equation (3.17) is objective function using weighted least square method with weights ϕ varying from 0 to 1. $\phi = 1$ means only temperature measurements are used in the inverse procedure. Different values for ϕ specify the inverse problem to be focused more on certain element than another.

Another transformation of objective function is scaled form in which individual elements of function are normalized, so that all the elements are approximately in the same order of magnitude.

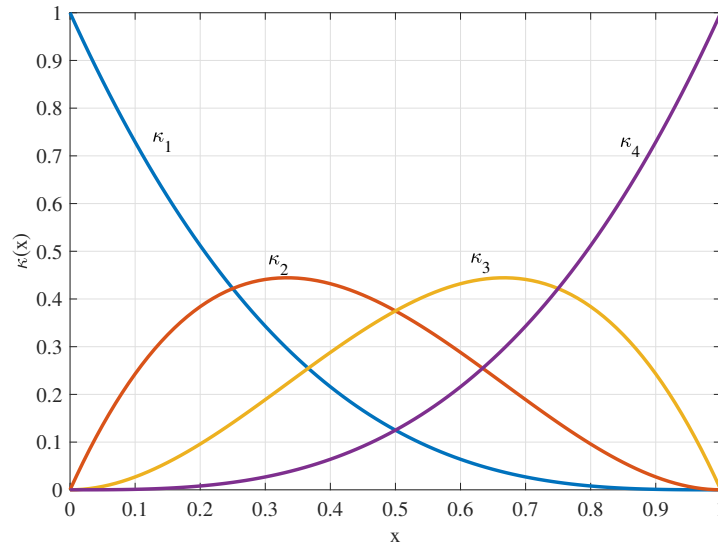
$$S_{SLS} = \left[\frac{\mathbf{M}_\theta - \mathbf{E}_\theta(\Omega)}{\max(\mathbf{M}_\theta)} \right]^\top \left[\frac{\mathbf{M}_\theta - \mathbf{E}_\theta(\Omega)}{\max(\mathbf{M}_\theta)} \right] + \left[\frac{\mathbf{M}_U - \mathbf{E}_U(\Omega)}{\max(\mathbf{M}_U)} \right]^\top \left[\frac{\mathbf{M}_U - \mathbf{E}_U(\Omega)}{\max(\mathbf{M}_U)} \right] \quad (3.18)$$

Since each elements are divided by its maximum value, all the components are scaled down and are in similar range in order of magnitude. This action reduces the difference in magnitude while solving the inverse problem. The elements E_θ, E_U, M_θ and M_U in S_{WLS}, S_{SLS} are not same as in the function S_{OLS} and E_θ, M_θ represent temperature measurements in sequential order of sensor location and E_U, M_U have mean moisture content. Since, the optimization procedure is gradient based method, any modification in objective function will also result in similar modification in Jacobian matrix before processing the problem in MATLAB.

3.1.3 Parameterization of a function

A function with prior information can be parameterization with aid of some mathematical expression. For instance, a function that varies exponentially can be formulated accurately by an exponent function. In many applications, activation energy with temperature dependency are formulated using Arrhenius equation. These formulated functions can be identified by estimating several unknown parameters that are controlling the behavior of the function. But for the function without prior information, it is a difficult task for parameterization. β -spline method aids to overcome this hurdle. Chapter 1 gave the glimpses of parameterization of a function using β -spline. In upcoming section, this procedure is elaborately explained with some examples.

The β -spline has several basis functions whose magnitude varies between 0 and 1. The behavior of these basis functions in a β -spline with unit coefficients for each basis functions ($\kappa_1, \kappa_2, \kappa_3, \kappa_4$) is given in figure 3.4. The order of spline is chosen as 4 and knots are taken as [00001111] for the above example. The flexibility of basis functions give β -spline a greater capability to approximate any kind of curve or surface. While incorporating the β -spline for solving the inverse problem, it is sufficient to manipulate the coefficients of basis functions that eases the function estimation. The feasibility of estimation lies in proper selection of spline order

Figure 3.4: Behavior of basis functions in β -splines for order 4

and knots. The functionality of β -spline is largely depended on these two parameters and behaves differently even with slight modifications in their parameters despite for same coefficients. The usability of β -spline in an inverse problem is studied with a following case study.

Consider the following dimensionless unidirectional nonlinear heat conduction problem with a source function of temperature, the domain $(x, \tau) \in [0, 1] \times [0, 1]$,

$$c^* \frac{\partial \theta(X, \tau)}{\partial \tau} = k^* \frac{\partial^2 \theta(X, \tau)}{\partial X^2} + g^*(\theta) \quad (3.19a)$$

$$k^* \frac{\partial \theta(0, \tau)}{\partial X} = 0 \quad (3.19b)$$

$$k^* \frac{\partial \theta(1, \tau)}{\partial X} = -1 \quad (3.19c)$$

$$\theta(X, 0) = 0 \quad (3.19d)$$

Thermophysical properties are assumed to be unity, i.e. heat capacity $c^* = 1$ and thermal conductivity $k^* = 1$. The source function is considered as unknown and to be estimated using adjoint method. The variational and adjoint equations for the same can be referred from literature [15]. In variational problem, the derivative of source term with respect to temperature ($\partial g^*/\partial \theta$) comes into the picture. With advantage of β -spline, the derivative of the function can be computed easily by a simple command in MATLAB environment. Simulated data with added noise are taken as measurements with source term that is formulated by three different mathematical functions like exponential, triangular and step functions. The performance of β -spline is visited for each case following.

For each test cases, temperature sensor is located only at boundary where heat flux is applied (i.e. at $X = 1$) with 100 transient measurements. It is assumed that there is no prior information is available for the function to be estimated. Hence, the knots are taken as vector between minimum and maximum of measurements with respect to order of spline. For example, if the order of spline is taken as 3, then the knots are chosen as $[\theta_{\min} \ \theta_{\min} \ \theta_{\min} \ \theta_{\max} \ \theta_{\max} \ \theta_{\max}]$.

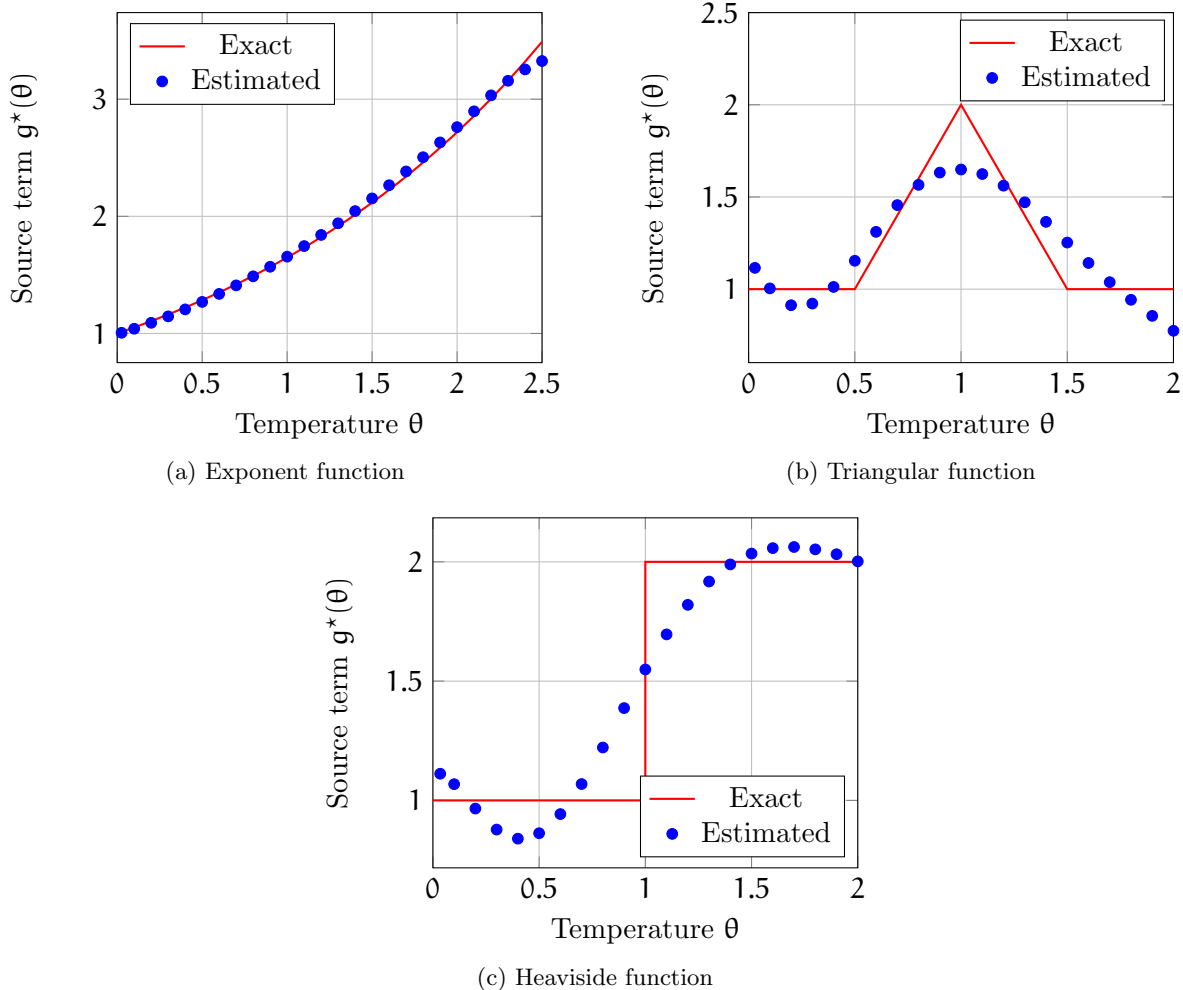
The table 3.1 gives an overall comparison of computation time, error between measurement and simulated and the order of spline used. For heat source of exponential form requires spline

Source function	Computation time (sec)	rms $\times 10^4$	order of spline
Exponent	08.34	9.7197	3
Triangular	41.15	4.2778	16
Heaviside	87.46	5.5950	12

Table 3.1: Comparison of test cases

of cubic order as the curve was smooth and simple. This case resulted in least computation time since the number of coefficients to be estimated are also least. With same order of spline, every test cases were converged in similar computation time but some of their results were not satisfactory unlike the exponent function which resulted in selection of higher orders. Excellent agreement between estimated and exact source term as function of temperature can be seen in figure 3.5a.

Both triangular and Heaviside functions have abrupt change in their magnitude which demands higher order of spline. The rms (root mean square) between simulated and measured temperature are least for triangular function among all. From figures 3.5b, 3.5c, it is visible that β -spline can easily handle any kind of function.

Figure 3.5: Performance of β -spline for different cases

The performance of β -spline in case of function with abrupt change can be improved by considering an additional knot point at temperature equals to 1. Since the interest is focused on estimating a function with no prior information, those studies are not elaborated here.

3.2 Sensitivity analysis

Sensitivity analysis is performed using efficient complex step differentiation method (CSD) for numerical models - **TM**, **TMPN** and **TMPE**, discussed in chapter 2. The magnitude of each sensitivity coefficients is normalized for comparison purpose. The sensitivities of parameters with respect to temperature are computed at non-dimensional space $X = [0, 0.25, 0.50, 0.75, 1]$ and for moisture content, the average values are computed. Sensitivity of parameter with respect to gas pressure can be computed only for **TMPN** and **TMPE** models.

TM Model : **TM** model has least number of parameters, $\Omega_1 = [\alpha_q^*, D_w^*, k^*, Bi_q, R_1]$, to be estimated. Their sensitivities with respect to temperature and mean moisture content are presented in figure 3.6. Irrespective of sensor location, temperature was least sensitive for the parameter D_w^* and highly sensitive for thermal related parameters α_q^* and k^* . Temperature at boundary with applied heat flux (i.e. $X = 0$) shows fluctuations for parameters α_q^* , k^* and R_1 . It might be due to implementation of step functions for explicit evaporation rate and evaporation is strong at this location. Such kind of fluctuations diminish when temperature sensor moved away from the boundary. Biot number Bi_q gives better temperature sensitivity near free surface boundary (i.e. $X = 1$) as the number appears inside the boundary condition.

The sensitivity of parameters with respect to moisture content will have been affected as its average value is only considered. Thermal properties like α_q^* , k^* and R_1 has better sensitivities than mass transport property D_w^* . The hypothesis of considering only liquid water with insulated boundary conditions had impacted the sensitivity of mass transfer property.

TMPN model : Key parameter vector $\Omega_2 = [\alpha_q^*, D_w^*, D_v^*, H^*, \alpha_p^*, k^*, Bi_q]$ governs the functionality of **TMPN** model. The temperature and moisture content variations with respect to a small change in the parameters are displayed in figure 3.7. The sensitivity variations of parameters with respect to temperature across the sensor locations are minimal. The evaporation rate constant H^* shows better temperature sensitivity near boundary with applied heat flux, as this region has greater evaporation rate. This model also shows weak sensitivity for mass transfer properties like D_w^* and D_v^* with respect to temperature at several sensor locations.

With respect to mean moisture content, the evaporation rate constant H^* , mass transfer properties D_w^* and D_v^* have better sensitivities along with thermal properties like α_q^* and k^* . But their sensitivities are non-zeros only after computational time $t^* = 0.4$. Capillary diffusivity α_p^* has least sensitivity with respect to both temperature and moisture content. It can be concluded that this parameters can not be identified with a gradient based optimization method.

TMPE model : With implementation of implicit evaporation rate in this model, the number of parameters to be analyzed are reduced from the previous model. It is enough to approximate the parameter vector $\Omega_3 = [\alpha_q^*, D_w^*, D_v^*, \alpha_p^*, Bi_q, k^*]$ in **TMPE** model. The figure 3.8 gives an overview of temperature and moisture content sensitivities for parameter vector Ω_3 . The

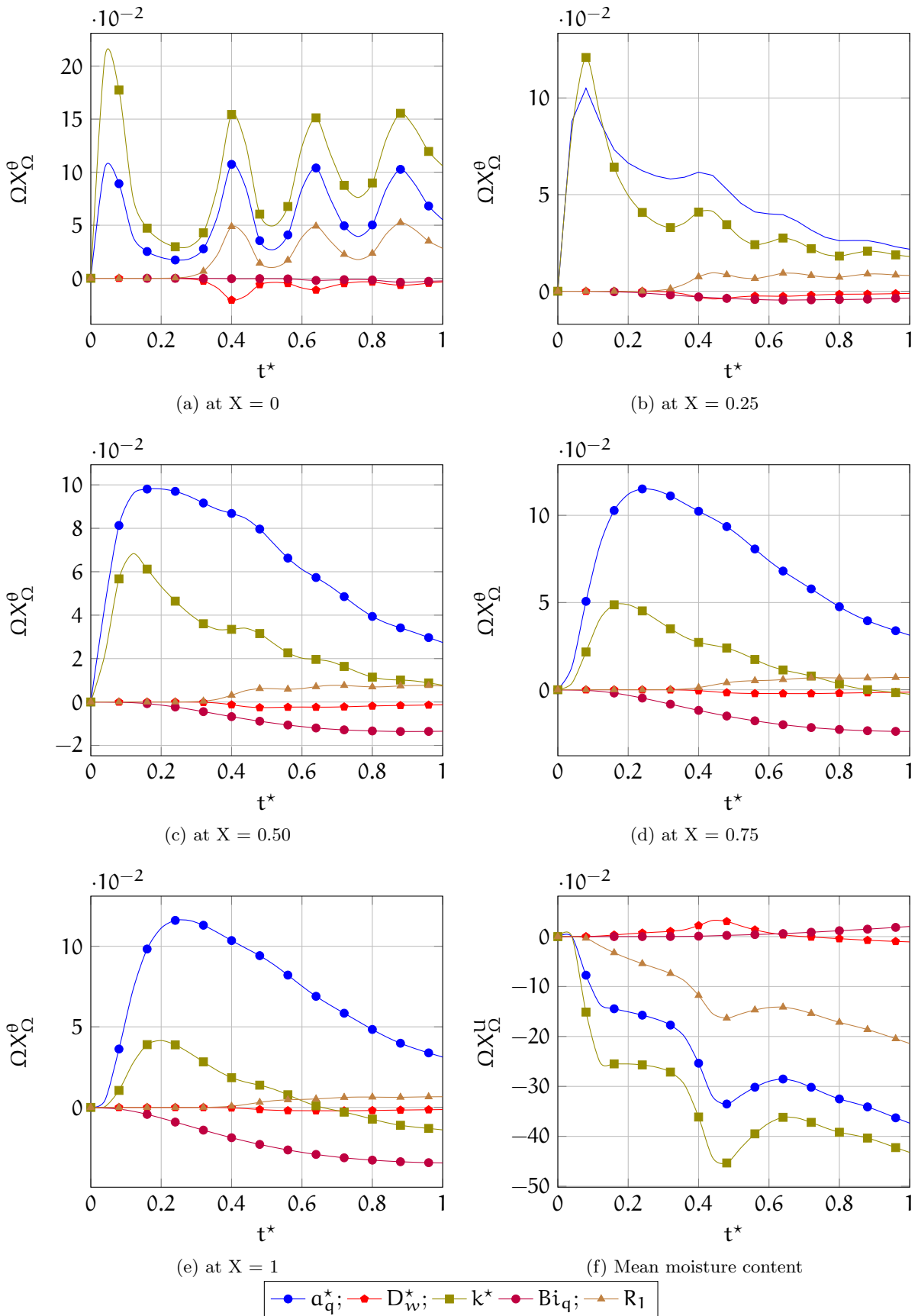


Figure 3.6: Scaled sensitivity profile for temperature at $X = 0$ (a), 0.25 (b), 0.50 (c), 0.75 (d), 1 (e) and mean moisture content (f) for TM model

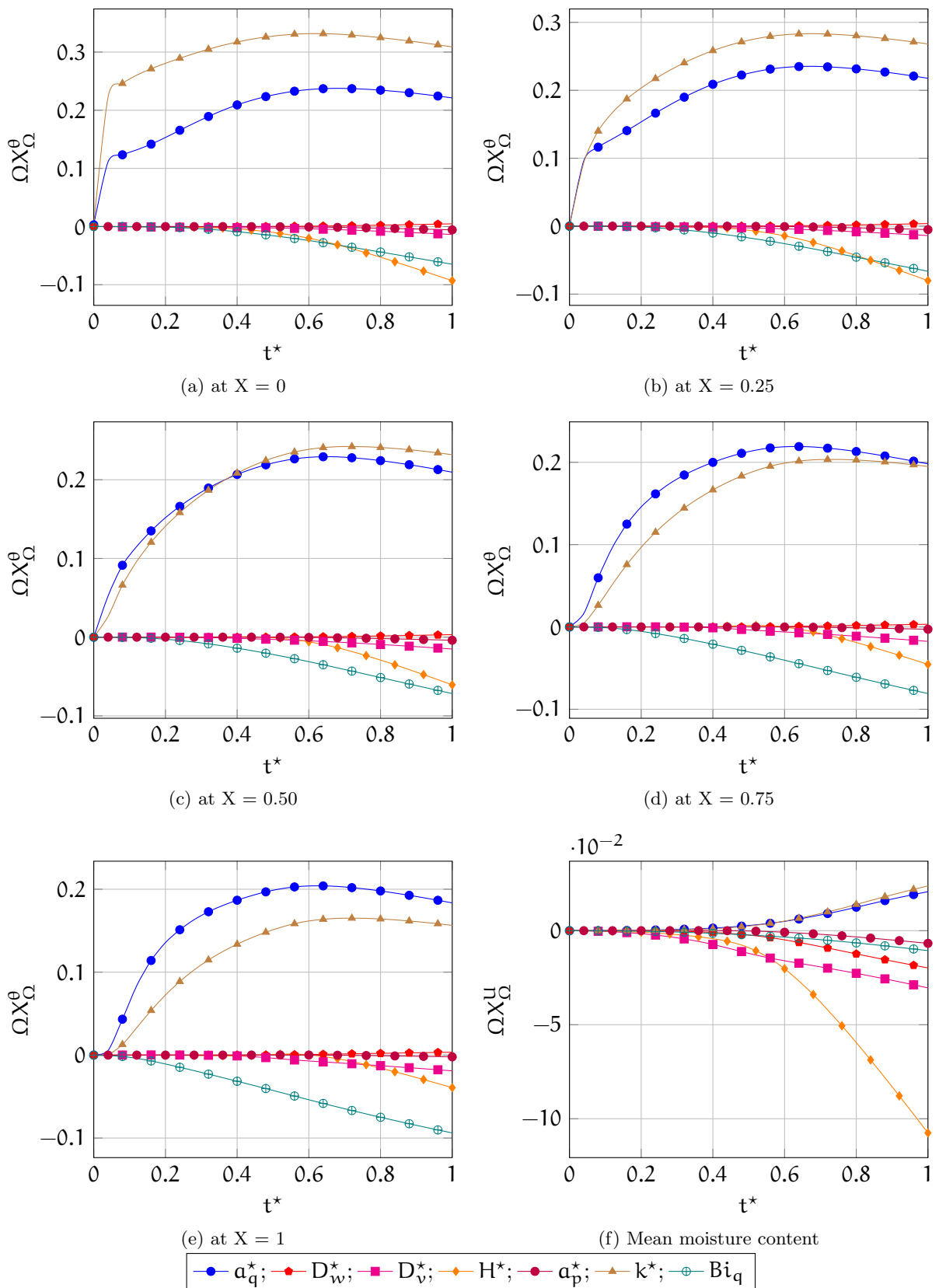


Figure 3.7: Scaled sensitivity profile for temperature at $X = 0$ (a), 0.25 (b), 0.50 (c), 0.75 (d), 1 (e) and mean moisture content (f) for TMPN model

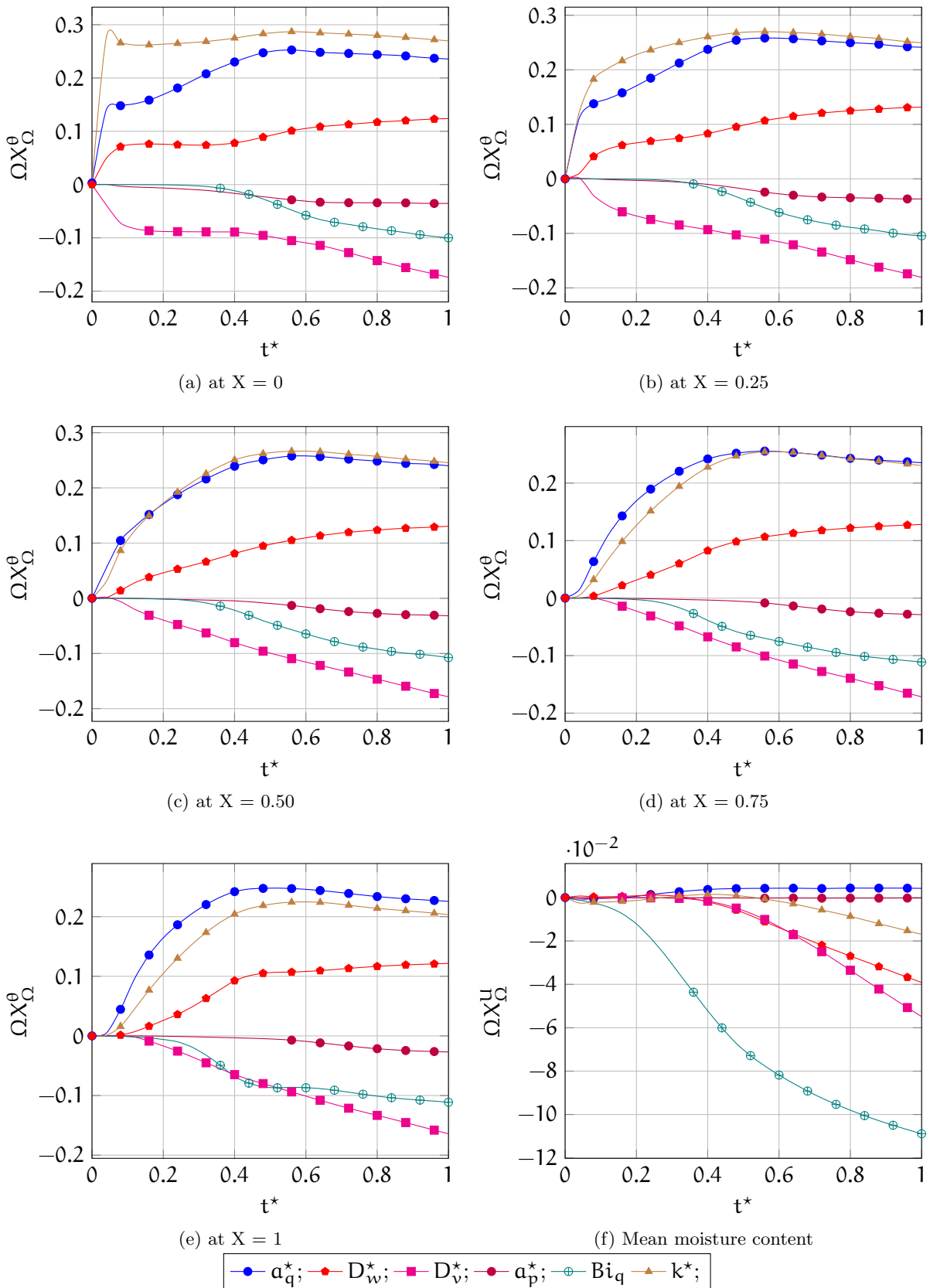


Figure 3.8: Scaled sensitivity profile for temperature at $X = 0$ (a), 0.25 (b), 0.50 (c), 0.75 (d), 1 (e) and mean moisture content (f) for TMPE model

sensitivity profiles of parameters with respect to temperature are quite different at the region near applied boundary (for $X = 0, 0.25$) from other locations. Unlike previous two models, mass transfer properties D_w^* and D_v^* have better sensitivities with respect to temperature. Formulation of implicit evaporation rate with equilibrium assumption is the main reason for the betterment in sensitivity for mass transfer properties. Temperature plateau near evaporation point of liquid water is predominant in region near $X = 0$ and this is the reason for existence of plateau in sensitivity profiles at sensor locations $X = 0$ and 0.25 .

Biot number Bi_q is the most sensitive parameter with respect to mean moisture content. Other mass transfer properties D_w^* and D_v^* also show better sensitivities. On contrast with previous two models, **TMPE** model shows least sensitivities to thermal properties with respect to moisture content.

On analyzing the sensitivity profiles of all the models, it can be concluded that information from both temperature and moisture content are mandatory since weak sensitivity of a parameter with respect to one state variable is compensated by another variable. For instance, thermal properties are highly sensitive with respect to temperature but have poor sensitivity with respect to moisture content. On contrast, mass transfer properties in TM model has poor sensitivity even with respect to mean moisture content.

Pressure sensitivity : The parameter sensitivities with respect to gas pressure for **TMPN** and **TMPE** models at $X = 0$ are presented in figure 3.9. Capillary diffusivity α_p^* has better sensitivity with respect to pressure for both the models as it is the key parameter that influences the pressure variation inside the domain. The evaporation rate content H^* is most sensitive parameter since this parameter appears in source term of pressure equation for **TMPN** model while other thermal and mass transfer properties are close to zero. In case of **TMPE** model, thermal and mass transfer properties show good sensitivities. Unfortunately, the magnitude of the parameter sensitivities with respect to pressure is 100 times smaller the magnitude of pressure in nondimensional form (the range of pressure in nondimensional form is between 1 and 3). Hence, these pressure sensitivities will not aid the optimization while compared to temperature and moisture content. This is one of the prime reasons for considering only temperature and moisture content in objective function.

3.3 Correlation analysis

Correlation analysis is an statistical tool to identify non-linearity between the parameters that is being estimated. For instance, it is mere possible for simultaneous estimation of heat capacity ρc_p and thermal conductivity k in a simple heat transfer problem with boundary conditions of first kind. It is due to their dependency on each other as they appear in ratio form as thermal diffusivity. To overcome this issue in estimation, it is preferred to have at least one of the boundary conditions as second or third kind. Hence, it is important to known dependency between the estimating parameters in the model.

Correlation can be computed for a matrix between its elements in MATLAB environment using a built-in function `corrcoef`. This function returns a square symmetric matrix of size $n_p \times n_p$ (where n_p is number of parameters) with unit diagonal elements. The magnitude of matrix elements will be in range between -1 and 1 . The off-diagonal elements represents the correlation between

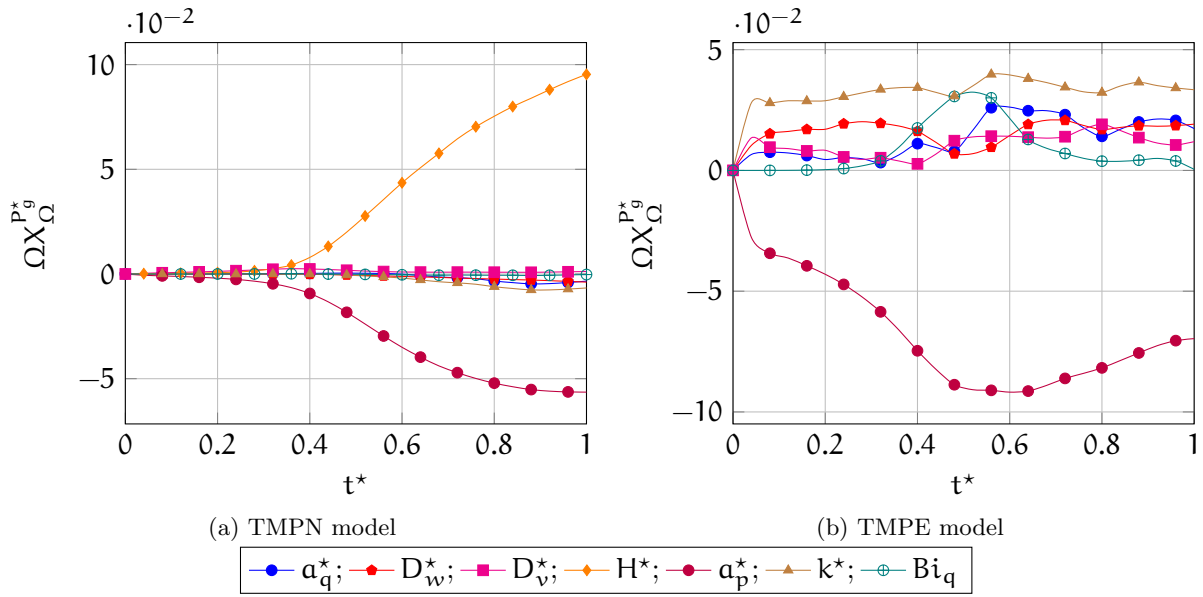


Figure 3.9: Sensitivities of parameters with respect to total gas pressure at $X = 0$ for TMPN model (a) and TMPE model (b)

the elements. When the absolute magnitude of an off-diagonal elements exceeds 0.9, then the elements are said to be dependent or correlated. The following statistical relations are used for correlation computation,

$$\text{Correlation } C_{lm} = \frac{\sum_{i=1}^{n_x} \left[\frac{X_l(i) - \mu_l(i)}{\eta_l(i)} \times \frac{X_m(i) - \mu_m(i)}{\eta_m(i)} \right]}{n_x - 1} \quad (3.20)$$

$$\text{Variance } \eta_l = \sum_{i=1}^{n_x} \sqrt{\frac{(X_l(i) - \mu_l(i))^2}{n_x + 1}} \quad (3.21)$$

Here n_x is total number of observations for each parameter in Jacobian or sensitivity matrix, μ_l is mean value of the parameter l . The above relation gives correlation between parameter l and m . Correlation analysis for each parameter vectors Ω_1 , Ω_2 , Ω_3 from **TM**, **TMPN** and **TMPN** models respectively are performed as below. Since, both temperature and moisture sensitivities are combined in similar fashion of objective function for computational purpose, the analysis is also performed over matrix that contains both sensitivities and called as combined form. In addition, correlation analysis are also performed individually for temperature and moisture content sensitivities.

TM model The correlation analysis in combined form is presented here,

From the above presented matrix, it can be seen that parameters α_q^* , k^* and R_1 are strongly correlated with each other. The mass transfer parameter D_w^* and Biot number Bi_q has least correlation with other parameters. The correlation between parameters based only on temperature sensitivities is

As per the above correlation matrix, every parameter is least dependent on each other. The reason behind the parameter dependency seen before can be understood after looking into correlation matrix based on moisture content sensitivity which is presented below

	a_q^*	D_w^*	k^*	Bi_q	R_1
a_q^*	1.0000	-0.4334	0.9662	-0.5065	0.9425
D_w^*		1.0000	-0.5197	0.0880	-0.4346
k^*			1.0000	-0.3687	0.9419
Bi_q				1.0000	-0.4947
R_1					1.0000

Table 3.2: Correlation matrix for **TM** model based on temperature and moisture content

	a_q^*	D_w^*	k^*	Bi_q	R_1
a_q^*	1.0000	-0.0598	0.4194	0.0276	0.0508
D_w^*		1.0000	-0.4671	-0.0883	-0.8565
k^*			1.0000	0.5771	0.5738
Bi_q				1.0000	0.1214
R_1					1.0000

Table 3.3: Correlation matrix for **TM** model based on temperature only

	a_q^*	D_w^*	k^*	Bi_q	R_1
a_q^*	1.0000	-0.0057	0.9676	-0.7278	0.9761
D_w^*		1.0000	-0.1707	-0.6268	0.0851
k^*			1.0000	-0.5652	0.8936
Bi_q				1.0000	-0.8078
R_1					1.0000

Table 3.4: Correlation matrix for **TM** model based on moisture only

It is clearly visible that correlation between thermal properties in the combined form is caused by moisture content. When the exact elements are in opposite signs for temperature and moisture matrix, then the absolute correlation value is reduced. For example, the correlation between k^* and Bi_q is 0.577 for temperature and -0.565 for moisture which resulted in correlation of -0.368 in combined form. Since, there is imbalance in number of sensors used for temperature and moisture content, the combined form is not exact average of temperature and moisture matrices. The graphical representation of dependency between thermal parameters are given in figure 3.10. Even the graphical representation shows that the moisture content only causes the maximum correlations.

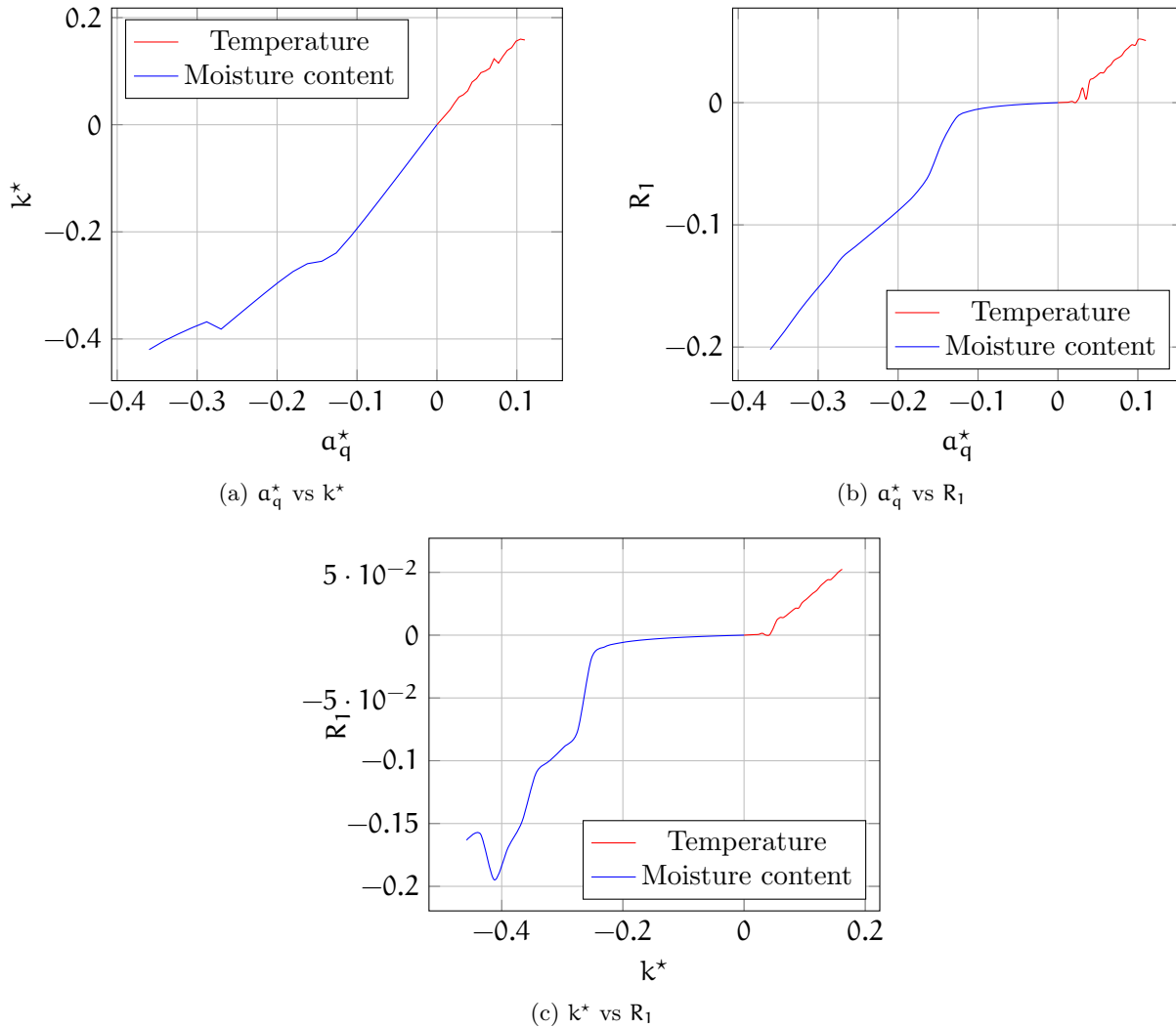


Figure 3.10: Correlation analysis for TM model

TMPN model The correlation between the parameters of vector Ω_2 for **TMPN** model is presented below for combined form.

Since the sensitivity of capillary diffusivity parameter a_p^* is least with respect to temperature and moisture content, this parameter is not considered for estimation in both **TMPN** and **TMPE** models. So, it is not included in the correlation analysis. Only thermal parameters a_q^* and k^* are linearly dependent while other parameters are independent. This is due to consideration of explicit evaporation rate based on non-equilibrium assumption which has curtailed the influence

	α_q^*	D_w^*	D_v^*	H^*	k^*	Bi_q
α_q^*	1.0000	0.5722	0.1149	-0.0705	0.8929	-0.6209
D_w^*		1.0000	0.4950	0.3110	0.4937	-0.4405
D_v^*			1.0000	0.8046	0.1133	0.4719
H^*				1.0000	-0.1695	0.4379
k^*					1.0000	-0.4306
Bi_q						1.0000

Table 3.5: Correlation matrix for **TMPN** model based on temperature and moisture content (combined form)

	α_q^*	D_w^*	D_v^*	H^*	k^*	Bi_q
α_q^*	1.0000	0.4388	-0.5096	-0.4443	0.7909	-0.5625
D_w^*		1.0000	-0.9317	-0.9189	0.3490	-0.8669
D_v^*			1.0000	0.7482	-0.3184	0.9630
H^*				1.0000	-0.4906	0.6556
k^*					1.0000	-0.2455
Bi_q						1.0000

Table 3.6: Correlation matrix for **TMPN** model based on temperature only

of parameters on each other. The linear dependency between parameters based on temperature sensitivities are,

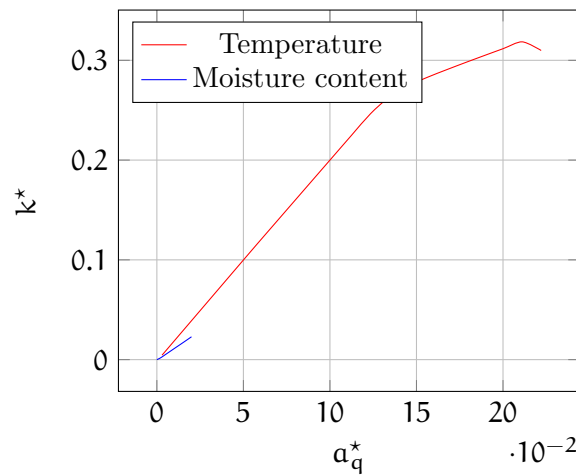


Figure 3.11: Correlation analysis for TMPN model

From the above table, the mass transfer parameter D_w^* has strong dependency with parameters D_v^* and H^* , vapor diffusivity parameter D_v^* with Biot number Bi_q . These parameter correlations are not visible in combined form as these dependencies are nullified by moisture content. The parameter correlations based on moisture content are,

Each and every parameters in the above matrix are dependent strongly each other. But these parameter connections are not extended in combined form as most of them are compensated by temperature sensitivities. The correlation between thermal properties α_q^* and k^* is graphically

	α_q^*	D_w^*	D_v^*	H^*	k^*	Bi_q
α_q^*	1.0000	-0.9992	-0.9508	-0.9981	0.9995	-0.9948
D_w^*		1.0000	0.9532	0.9965	-0.9987	0.9941
D_v^*			1.0000	0.9308	-0.9412	0.9759
H^*				1.0000	-0.9994	0.9876
k^*					1.0000	-0.9914
Bi_q						1.0000

Table 3.7: Correlation matrix for **TMPN** model based on moisture content only

	α_q^*	D_w^*	D_v^*	Bi_q	k^*
α_q^*	1.0000	0.9453	-0.7806	-0.1540	0.9422
D_w^*		1.0000	-0.8947	-0.2169	0.9172
D_v^*			1.0000	0.5599	-0.7722
Bi_q				1.0000	-0.0397
k^*					1.0000

Table 3.8: Correlation matrix for **TMPE** model based on temperature and moisture content

presented in figure 3.11. The magnitude of sensitivity with respect to moisture content is insignificant while compared to temperature and it is reflected in the plot.

TMPE model The influence between each parameters in the vector Ω_3 of **TMPE** model is analyzed using the below matrix presented in combined form

Unlike the previous two models, this model showed a strong linearity between mass transfer and thermal properties. The implicit evaporation rate formulation with equilibrium approach assumption has increased the non-linearity between thermal and mass transfer properties. The correlation matrix based on temperature sensitivity is given by

	α_q^*	D_w^*	D_v^*	Bi_q	k^*
α_q^*	1.0000	0.8979	-0.7719	-0.7012	0.8079
D_w^*		1.0000	-0.9488	-0.8454	0.7971
D_v^*			1.0000	0.8222	-0.7331
Bi_q				1.0000	-0.4104
k^*					1.0000

Table 3.9: Correlation matrix for **TMPE** model based on temperature only

A strong correlation of mass transfer parameter D_w^* with parameters α_q^* and D_v^* , is seen while other parameters are least dependent on each other. On contract, this model did not show a strong linearity between thermal properties α_q^* and k^* with respect to temperature sensitivities. The moisture sensitivities based correlation matrix is given below

Analyzing the above matrix, the thermal properties showed least dependencies among themselves. This is due to poor sensitivity of thermal properties with respect to moisture content

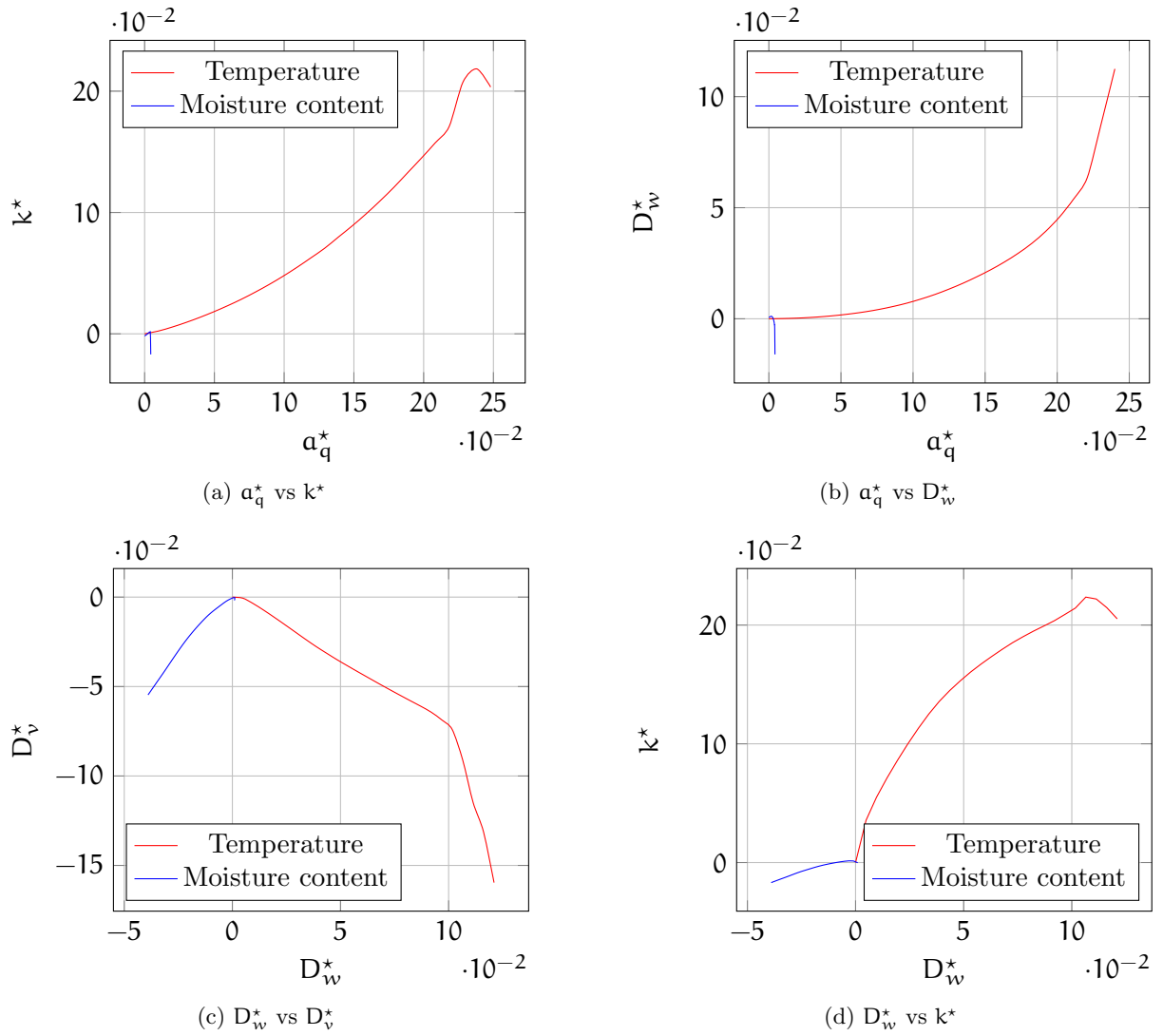


Figure 3.12: Correlation analysis for TMPE model

	a_q^*	D_w^*	D_v^*	Bi_q	k^*
a_q^*	1.0000	-0.0419	0.0999	-0.5228	0.2765
D_w^*		1.0000	0.9708	0.8703	0.9230
D_v^*			1.0000	0.7689	0.9824
Bi_q				1.0000	0.6422
k^*					1.0000

Table 3.10: Correlation matrix for **TMPE** model based on moisture content only

(see figure 3.8). But a strong correlation for parameter D_w^* with respect to k^* and D_v^* is noticed. The variation of the most correlated parameters are plotted in figure 3.12.

3.4 Design of experiments

An optimal design utilizes the observations made to the utmost that increases the accuracy and precision of parameter estimation by gradient-based optimization. Such kind of optimal design is evaluated by inverse design problem. Inverse design problem or design of experiment aids in determining the required duration for experimentation, number and location of sensors, profile of boundary conditions, etc. Authors have evaluated the boundary conditions like applied heat flux, that increases the sensitivities of desired parameters. Later, these modeled boundary conditions are utilized to result in an accurate estimation of parameters [36].

In this case study, the focus of inverse design problem will be on obtaining the maximum number and location of sensors required for temperature. Hitherto local measurement of moisture content is not feasible. So, inverse design problem regarding sensor location for moisture content and pressure are carried only as theoretical aspects. An important facet of experimental design is Fisher matrix, which is product of sensitivity matrix ($X^T \times X$). There are several kinds of optimum design criteria based on Fisher matrix and some are listed below

1. **D-Optimality** : design which maximizes the determinant of the Fisher matrix
2. **A-Optimality** : design that maximizes the trace of the Fisher matrix
3. **E-Optimality** : design which maximizes the minimum Eigenvalue of the Fisher matrix
4. **G-Optimality** : design that minimizes the maximum variance of the predicted value over experimental space

Out of these mentioned optimalities, conventional D-optimality is used to compute the determinants of Fisher matrix for all the models. E-optimality is computed for a particular model to verify the results obtained from D-optimality. Herein, a theoretical and experimental case studies are carried out and are categorized as individual and combined form respectively. In former case study, optimal location of sensors for temperature, moisture content and pressure are computed individually and hence it is termed as individual form. This study is carried out for theoretical purpose which may come in handy for future studies. Only most sensitive parameters with respect to corresponding state variables are taken into account for individual form.

For the current experimental setup, the possible locations of temperature sensors along with average moisture content measurements are examined by another **D**-optimality studies. Since the determinant is formulated from combined sensitivities of both temperature and moisture content, it is called as combined form. There are totally five different combinations of temperature sensor locations are possible as listed in table 3.11.

Mathematical expression: Determinant used for experimental studies in combined form is given by following equation,

$$\Delta = \frac{1}{t_f^*(n_\theta + 1)} \int_0^{t_f^*} \left[\det(\text{Sen}_\theta(t^*) \times \text{Sen}_\theta(t^*)^T) + \det(\text{Sen}_U(t^*) \times \text{Sen}_U(t^*)) \right] dt^* \quad (3.22)$$

Case	Temperature sensor at X^*
1	0, 1
2	0.5, 1
3	0.625, 1
4	0, 0.5, 1
5	0, 0.5, 0.625, 1

Table 3.11: Cases for determinant

Where the sensitivity matrices are fed as,

$$\text{Sen}_\theta(t) = \begin{bmatrix} \Omega(1) \frac{\partial \theta_t^1}{\partial \Omega(1)} & \Omega(2) \frac{\partial \theta_t^1}{\partial \Omega(2)} & \dots & \Omega(n_p) \frac{\partial \theta_t^1}{\partial \Omega(n_p)} \\ \Omega(1) \frac{\partial \theta_t^2}{\partial \Omega(1)} & \Omega(2) \frac{\partial \theta_t^2}{\partial \Omega(2)} & \dots & \Omega(n_p) \frac{\partial \theta_t^2}{\partial \Omega(n_p)} \\ \vdots & \vdots & \ddots & \vdots \\ \Omega(1) \frac{\partial \theta_t^{n_\theta}}{\partial \Omega(1)} & \Omega(2) \frac{\partial \theta_t^{n_\theta}}{\partial \Omega(2)} & \dots & \Omega(n_p) \frac{\partial \theta_t^{n_\theta}}{\partial \Omega(n_p)} \end{bmatrix}; \quad \text{Sen}_U(t) = \begin{bmatrix} \Omega(1) \frac{\partial \bar{U}_t}{\partial \Omega(1)} \\ \Omega(2) \frac{\partial \bar{U}_t}{\partial \Omega(2)} \\ \vdots \\ \Omega(n_p) \frac{\partial \bar{U}_t}{\partial \Omega(n_p)} \end{bmatrix}^\top$$

Here Ω is the parameter vector with n_p number of parameters, n_θ is number of temperature sensors. The determinant Δ is used without any modification for combined form but for individual form is used as scaled down version (i.e. the values are divided by its maximum value). The temperature scaled down determinant is,

$$\Delta^\theta = \frac{1}{t_f^*} \int_0^1 \int_0^{t_f^*} \det \left[\text{Sen}_\theta(x^*, t^*, \Omega_\theta) \times \text{Sen}_\theta(x^*, t^*, \Omega_\theta)^\top \right] dt^* dx^* \quad (3.23a)$$

$$\Delta_{\max}^\theta = \max(\Delta^\theta) \quad (3.23b)$$

Where Ω_θ is parameter vector contains only parameters that have significant sensitivities with respect to temperature and it is presented in upcoming sections for each model. The sensitivity matrix Sen_θ is arranged only at particular sensor location. Similar expression can be derived for moisture content and pressure. Solution of inverse design problem for different models are imparted in following sections.

3.4.1 D-Optimality

TM Model : The parameters to be used in individual form for determinant calculation are given by the following vectors $\Omega^\theta = [a_q^*, k^*, Bi_q, R_1]$ and $\Omega^U = [D_w^*]$ for temperature and moisture content respectively. As per **D-Optimum**, the most optimal locations for temperature sensors are at region near boundary in contact with ambient ($x^* = 1$). Due to fluctuations in the parameter sensitivities at applied heat flux boundary, the determinant calculated for temperature is affected. On contrast for moisture content, the most suitable location of sensor is region near boundary with applied heat flux ($x^* = 0$). Beyond this maximum point, the determinant for moisture content falls to zero. It is impacted due to assumption of zero fluxes at either boundaries and negligence of water vapor phase in the model. These observations can be inferred graphically from figure 3.13a.

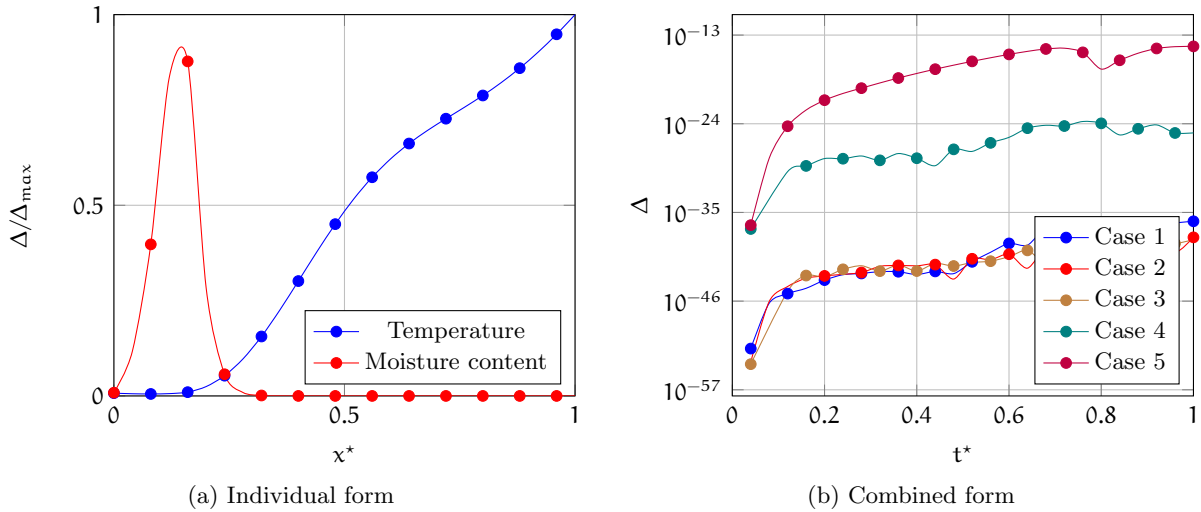


Figure 3.13: Determinant at various number of sensors in individual (a) and combined (b) form for TM model

For combined form, case 5 is resulted as the optimal design for current experimentation as seen in figure 3.13b. Case 4 is resulted second highest determinant while other cases gave almost identically lowest results. The analysis indicates that this model requires minimum of three sensors in order to achieve better accuracy in parameter estimation based on experimental measurements. The different combinations of sensors for first three cases have resulted similar determinants as there are huge similarities in their sensitivity profiles at these sensor locations. The graphical representation of determinants for both combined and individual forms is given in figure 3.13.

TMPN Model : The parameter vectors $\Omega^\theta = [a_q^*, k^*, Bi_q, H^*]$, $\Omega^U = [D_w^*, D_v^*]$ and $\Omega^P = [D_v^*, a_p^*]$ are taken for computing individually the determinant for temperature, moisture content and pressure respectively. Maximum determinant is observed at applied heat flux boundary ($x^* = 0$) for all variables i.e. temperature, moisture content and pressure. The second maxima are located approximately at $x^* = 0.75$ for temperature and $x^* = 0.9$ for moisture content. The determinant profile for pressure drops steeply from maximum at $x^* = 0$ to zero approximately at $x^* = 0.3$. These trends of determinants for individual forms are given in figure 3.14a.

From analysis on figure 3.14b, Case 5 is the optimal locations of sensors for this model. On contract, case 1, 2 and 4 have determinants that are close enough and case 3 resulted as least determinant. Sensor locations of case 4 are combinations of case 1 and 2 but surprisingly all these cases resulted in similar determinant trends. Moreover, the determinant for each case is kept increasing with respect to time but the previous model showed a plateau after $t^* = 0.65$.

TMPE Model : Individual form computed for temperature, moisture content and pressure from parameter vector $\Omega^\theta = [a_q^*, k^*, Bi_q]$, $\Omega^U = [D_w^*]$ and $\Omega^P = [a_p^*, D_v^*]$ respectively. The determinant trends for temperature and pressure were identical with TMPN model. It would be sufficient to have two temperature sensors at $x^* = 0$ and 0.80, two moisture content sensors at $x^* = 0.10$ and 1 and one pressure sensor at $x^* = 0$ for a better approximation by optimization. The determinants as function of location and time for individual form for **TMPE**

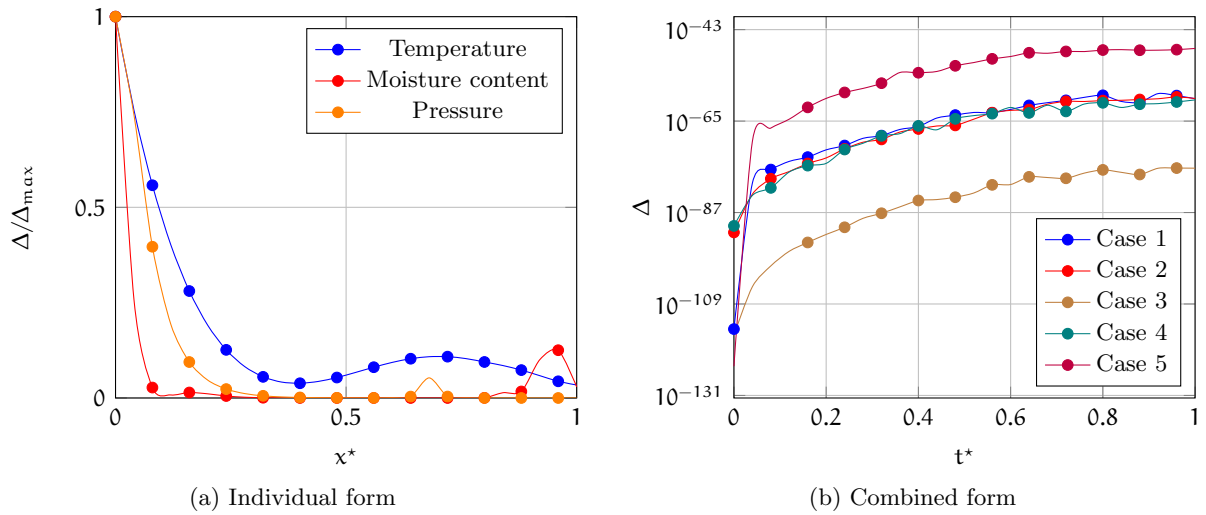


Figure 3.14: Determinant at various number of sensors in individual (a) and combined (b) form for TMPN model

model is given in figure 3.15a.

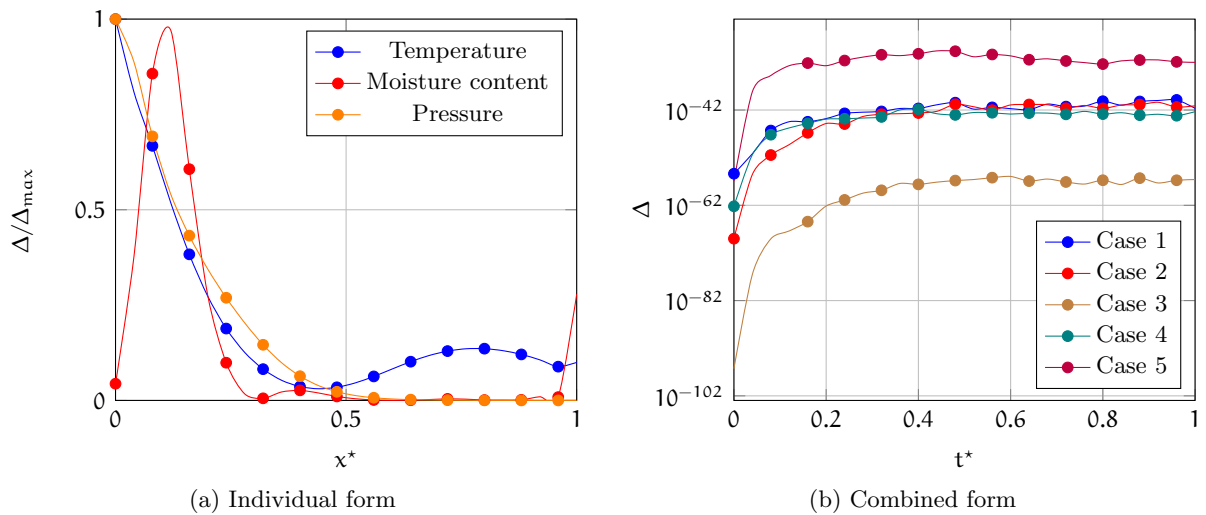


Figure 3.15: Determinant at various number of sensors in individual (a) and combined (b) form for TMPE model

As anticipated from the results given in figure 3.15b, Case 5 is resulted as maximum determinant even for this model. This determinant trends for combined form are quite similar to the previously presented **TMPN** model.

In all these three models, sensor locations for temperature as per case 5 is optimal choice for present experimentation setup that can result in accurate and precise parameter estimation. But case 4 is considered and proceeded for solving the inverse problem with measurements. The justification for selection of case 4 in place of 5 is given as follows. Case 3 is resulted as the lowest for all the models which has sensor locations at 0.65 and 1. Since the location at $x^* = 1$ is common for all the cases, the sensitivity at $x^* = 0.65$ may only have impacted that lowers determinant. Hence, there will not be any much improvement by considering sensor at $x^* = 0.65$. So, case 4 is chosen for solving the inverse problem.

3.4.2 E-Optimality

E-optimality results in a design that maximizes the minimum eigenvalues of the determinant or Fisher matrix. This is an extended version of **D**-optimality and computed for sake of verifying the results which were obtained previously. The eigenvalues for different cases for **TMPE** model are presented below

Case	Eigenvalue				
1	0.398	14.636	6.410×10^5	2.361×10^7	6.116×10^{13}
2	0.357	12.870	6.124×10^5	5.330×10^7	5.299×10^{13}
3	0.341	12.314	4.162×10^5	3.099×10^7	5.381×10^{13}
4	0.479	18.487	8.670×10^5	6.732×10^7	6.726×10^{13}
5	0.534	22.593	9.969×10^5	9.137×10^7	7.419×10^{13}

Table 3.12: Eigenvalues of determinant for **TMPE** model

The results of **E**-optimality agree with **D**-optimality of **TMPE** model. As the number of sensors increases, the lowest eigenvalue is also increased. For first three cases, the difference between the lowest eigenvalues are minimal but there is significant improvement for case 4. As prescribed earlier, the sensitivity at location $x^* = 0.65$ is insignificant to improve the determinant that is reflected here. Case 5 has managed to maximize the eigenvalue by 0.055 but case 4 were able to maximize around 0.1 from the previous greatest, which is case 1.

3.5 Numerical Analysis

Before proceeding to inverse solution with actual measurements, a numerical study with synthetic data, i.e. the measurements are obtained from simulation with presumed parameters, is carried out for sake of surety. This analysis provides the feasibility of retrieving the parameters by inverse problem. The sensor locations are taken as per the solution of inverse design problem presented in previous section. The measurements of temperatures that are taken at $x^* = [0, 0.5, 1]$ along with average moisture content are used for optimization. The frequency of sensor response is taken as 1 Hz with total of 1200 transient observations for both temperatures and moisture content.

In order to represent the simulated data close to reality, a random noise is added to the exact simulated profiles of temperature θ_x and moisture content U_x as following

$$\theta(x^*, t^*) = \theta_x(x^*, t^*) + \omega \sigma_\theta \quad (3.24a)$$

$$U(t^*) = U_x(t^*) + \omega \sigma_u \quad (3.24b)$$

Here θ and U are simulated measurements with random errors, σ_θ and σ_u are standard deviation of errors and ω is random variable with normal distribution, zero mean and unitary standard deviation. The standard deviations of temperature and moisture content are chosen as some percentage to its maximum and given by $\sigma_\theta = 1.0\% \times \max(\theta)$ and $\sigma_u = 1.0\% \times \max(U)$ respectively.

The performance of the inverse solution is evaluated by error estimation ε between the exact and estimated parameters. The error estimation for parameters is given by

$$\varepsilon = \frac{|\text{Actual} - \text{Estimated}|}{\text{Actual}} \times 100\% \quad (3.25)$$

The forward problem is solved by finite difference method for TM model and by finite element method by implementing in a commercial solver COMSOL for **TMPN** and **TMPE** models. The optimization portion is carried out in **Matlab** environment with aid of *lqsnonlin* command that fits the nonlinear least square problems.

3.5.1 TM Model

The inverse solution using S_{OLS} objective function with information of temperature from sensor locations at $x^* = [0, 1]$ are presented in table 3.13. Whether synthetic data is used with or without noise, the inverse problem was able to retrieve the parameters exactly without any hindrance. The inverse problem is started with initial guess approximately as $1/10^{\text{th}}$ of their exact values. The inverse solution without noise returned exactly the same parameters with zero errors while the solution with noise have error less than 1%. The maximum error spotted is for the mass transfer parameter D_w^* with 0.8%. The deviations between measured and simulated profiles based on inverse solution are graphically presented for temperature and moisture content in figure 3.16.

Parameters			Estimation without noise		Estimation with noise	
	Actual parameter	Initial guess	Estimated	Error percent	Estimated	Error percent
α_q^*	1.40	0.200	1.40	0.0	1.398	0.12
D_w^*	0.0093	0.00093	0.0093	0.0	0.0092	0.79
k^*	3.20	0.500	3.20	0.0	3.204	0.12
Bi_q	0.08	0.007	0.08	0.0	0.080	0.02
R_1	0.85	0.080	0.85	0.0	0.849	0.08

Table 3.13: Inverse solution with synthetic measurements for **TM** Model

The root mean square (rms) difference between simulated and measured data with added noise for temperature and moisture content is presented in table 3.14. There is a good agreement between simulations and measurements which has resulted in slight deviations up to 3×10^{-3} for both temperature and moisture content. Conclusively, it can be said that for **TM** model, objective function with ordinary least square (S_{OLS}) is adequate for solving the inverse problem unlike other two models which are presented in upcoming sections.

rms values		
Temperature sensors		Moisture
T4 [°C]	T7 [°C]	content $\times 10^3$
0.86	0.83	3.10

Table 3.14: The rms values between simulated and measured data for **TM** model

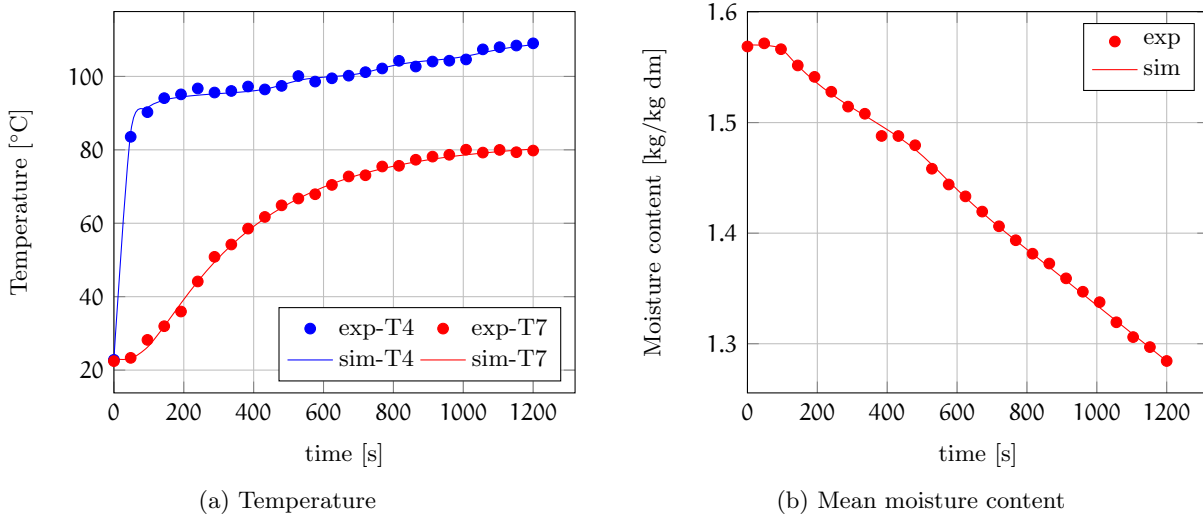


Figure 3.16: Comparison of synthetic data with noise with simulated data of temperature (a) and mean moisture content (b) for TM model

3.5.2 TMPN Model

Unlike the previous model, this and upcoming models shall take into account of information from temperature at $x^* = [0, 0.5, 1]$ and mean moisture content. Moreover, inverse problem is extended for other objective functions like S_{WLS} and S_{SLS} . The inverse solutions for synthetic data are displayed in table 3.15. There is no inverse solution for noiseless measurements with error less than 1% for each parameter. The inverse solution obtained using weighted least square with weighting factor of 0.6 for temperature has overall least error among others for both noiseless and noised measurements. Parameters related to thermal properties like α_q^* , k^* and Bi_q , including evaporation rate constant H^* have better retrieval while mass transfer parameters D_w^* and D_v^* have significant errors. This might be due to poor sensitivities of mass transfer parameters with respect to temperature and, as more weight is given for temperature than moisture content.

Parameter	Actual Parameter	Initial guess	Percentage error %									
			Estimation without noise						Estimation with noise			
			S_{OLS}	S_{WLS}, ϕ			S_{SLS}	S_{OLS}	S_{WLS}, ϕ		S_{SLS}	
			0.4	0.5	0.6	0.90	1.33	9.21	12.47	9.61	2.20	0.94
α_q^*	1.5173	0.08278	2.03	14.79	10.67	0.90	1.33	9.21	12.47	9.61	2.20	0.94
D_w^*	0.0028	0.00093	32.49	66.64	61.22	15.59	25.28	66.67	66.67	66.67	40.38	41.98
D_v^*	28.125	9.375	28.57	66.18	34.34	7.83	19.57	58.15	65.39	58.15	36.25	32.04
H^*	11496	120.00	5.16	200.02	108.67	1.31	3.10	59.54	137.16	56.55	12.49	23.33
k^*	3.228	0.584	1.17	8.16	9.24	0.59	0.76	12.23	14.61	12.72	4.72	3.40
Bi_q	0.096	0.032	14.68	63.91	33.74	6.36	9.98	28.16	37.84	27.86	3.28	0.13

Table 3.15: Inverse solution with synthetic measurements for **TMPN** Model for various objective functions

The rms values between measured and simulated data from each objective functions at different

sensor locations are presented in table 3.16. The temperature trend at location $x^* = 0$ has not been able to approximate closely to measurement for objective functions S_{OLS} and S_{WLS} for $\phi = 0.4, 0.5$. As per rms comparison, S_{SLS} has resulted better approximation of profiles for temperature and mean moisture content. Figure 3.17 gives graphical similarity of measured and simulated data for weighted least square with weight $\phi = 0.6$.

Objective functions	Temperature sensor			Mean moisture content $\times 10^3$
	T4 [$^{\circ}\text{C}$]	T5 [$^{\circ}\text{C}$]	T7 [$^{\circ}\text{C}$]	
S_{OLS}	3.29	1.18	2.51	8.10
$\phi = 0.4$	4.06	1.28	3.17	8.17
$S_{WLS}, \phi = 0.5$	3.35	1.17	2.47	8.30
$\phi = 0.6$	1.25	0.86	0.88	6.46
S_{SLS}	1.11	0.82	0.69	6.41

Table 3.16: The rms values of measured and simulated data at sensor locations for different objective functions for **TMPN** model

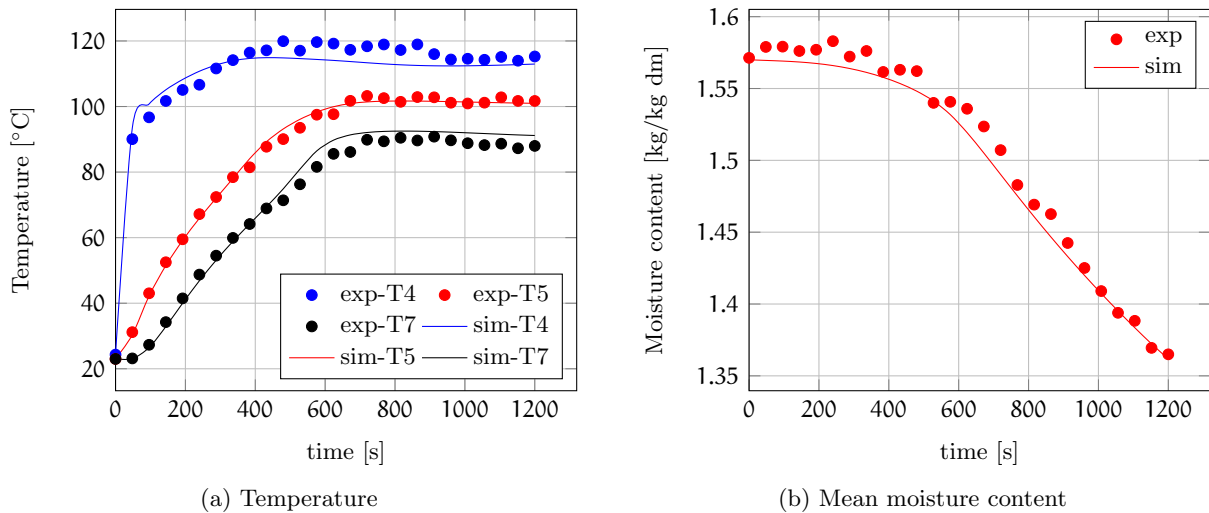


Figure 3.17: Comparison of synthetic data with noise with simulated data for S_{WLS} with weight $\phi = 0.5$, of temperature (a) and mean moisture content (b) for **TMPN** model

3.5.3 TMPE Model

In **TMPE** model, the inverse problem with noiseless synthetic measurements was able to recover almost every parameter except mass transfer parameter D_v^* . The objective functions S_{OLS} , S_{SLS} and S_{WLS} , specifically for weight $\phi = 0.5$, have resulted inverse solutions with error less than 2%. When the weighing factor for temperature increases in the case of S_{SLS} , the relative error for parameters are also increased. On contrast, the scaled least square objective function S_{SLS} is preferable for measurement with added noise since the overall error in parameters is least. Table 3.17 elaborates the above discussed results of inverse solutions.

Table 3.18 presents the rms difference between the measured with added noise and simulated data. Though S_{SLS} has relatively lower parameter errors, as per rms difference between the

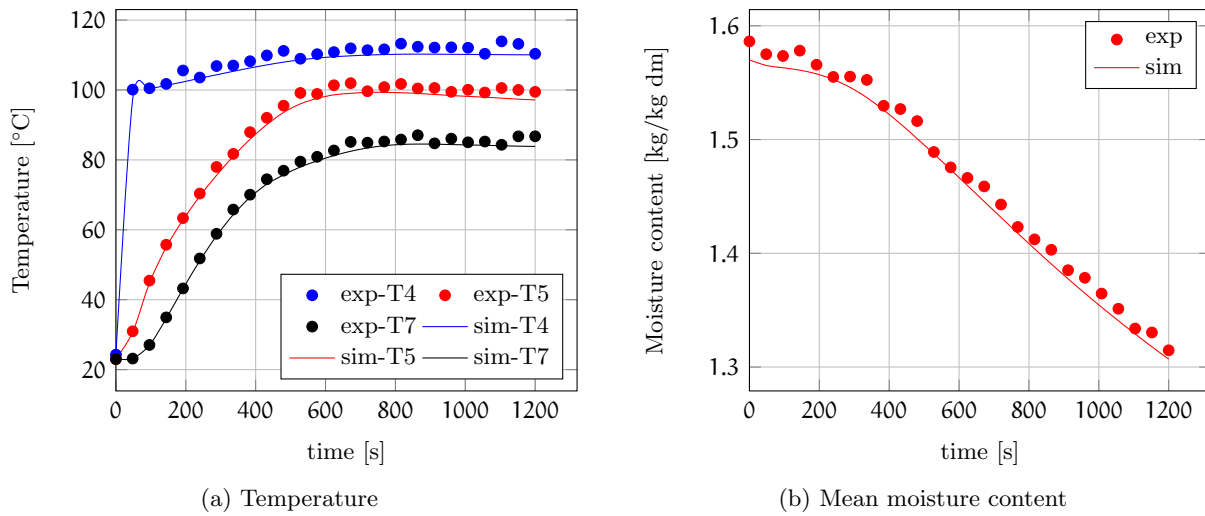


Figure 3.18: Comparison of synthetic data with noise with simulated data for S_{SLS} of temperature (a) and mean moisture content (b) for TMPE model

Parameters	Actual Parameter	Initial guess	Percentage error %										
			Estimation without noise						Estimation with noise				
			S_{OLS}	S_{WLS}, ϕ		S_{SLS}		S_{OLS}	S_{WLS}, ϕ		S_{SLS}		
α_q^*	1.3554	0.08278	0.17	0.4	0.5	0.08	0.88	0.25	33.94	4.49	3.34	1.87	1.99
D_w^*	0.0187	0.00093	0.11	0.11	0.61	0.78	7.82	0.77	38.79	11.64	15.42	16.19	14.78
D_v^*	28.125	9.375	1.10	1.10	3.71	1.25	1.33	1.75	15.10	7.96	13.03	18.01	22.69
Bi_q	0.048	0.032	0.12	0.12	0.06	0.64	7.29	0.22	79.59	12.89	12.39	7.36	2.16
k^*	3.125	0.584	0.05	0.05	0.01	0.10	4.03	0.25	98.22	11.31	10.49	8.55	8.01

Table 3.17: Inverse solution with synthetic measurements for **TMPE** Model for various objective functions

data, S_{OLS} has the least differences among all. But the difference in their values among other objective functions was insignificant. Compared to previous model, **TMPE** model has better approximation of temperature at sensor location $x^* = 0$. The similarities of temperature and moisture content profiles between simulation and measurements are given in figure 3.18.

Objective functions	Temperature sensor			Mean moisture content $\times 10^3$
	T4 [$^{\circ}$ C]	T5 [$^{\circ}$ C]	T7 [$^{\circ}$ C]	
S_{OLS}	2.05	1.63	1.15	8.26
$S_{WLS}, \phi =$	0.4	2.08	1.65	8.65
	0.5	2.11	1.64	8.31
	0.6	2.12	1.66	8.57
S_{SLS}	2.10	1.63	1.19	8.54

Table 3.18: The rms values of measured and simulated data at sensor locations for different objective functions for **TMPE** model

3.6 Conclusive remarks

This chapter gave an elaborate explanation about implementation of the inverse problem with the presented models. Some of the prime components like sensitivity, objective function, of inverse methodology were deeply discussed. The effectiveness of sensitivity coefficients can be improved with utilization of complex step differentiation (CSD). An example of heat transfer problem was presented to show the performance of CSD in comparison to conventional FDM (Finite Difference Method). It was shown that step size h does not affect the computational capability of CSD. The relative errors of computed sensitivities by CSD were minimal against the analytical solutions in comparison with FDM.

The sensitivity analyses for each models were performed and examined at various sensor locations. Due to averaging effect, the magnitude of parameter sensitivities are reduced with respect to moisture content. In TM model, parameters corresponding to thermal properties are quite sensitivity for both temperature and moisture content. The capillary diffusivity appearing in **TMPN** and **TMPE** models is insensitive irrespective of location. The magnitude of parameter sensitivities with respect to pressure are negligible hence inclusion of pressure as a component in objective function will not help in minimizing the objective function. The mass transfer properties D_w^* and D_v^* are sensitive with respect to temperature for **TMPE** model but not for **TMPN** model.

The steps of parameterization of a unknown function by β -spline method were presented with an example. The inverse problem equipped with β -spline was able to identify any kind of function even with abrupt changes. The performance is influenced by important facets like order of the spline, knots, etc. Hence, a proper knowledge of these parameter is necessary while handling inverse problem with β -spline.

Correlation between estimating parameters was investigated for models using variance-covariance of sensitivity matrices. Out of these models, **TMPE** model has most number of parameters correlated. Inverse design problem was solved by commonly used D-optimality as individual and

combined forms. Individual form was computed for theoretical aspect while combined form was solved for current experimental set-up. As per the solution, case 4 i.e. temperature sensors are located at $x^* = 0, 0.5$ and 1 , along with mean moisture content is the most optimal design.

Generally, ordinary least square (OLS) form of function is used as cost/objective function which to be extremized by an inverse problem. But with presence of several components with different scale of magnitude and dimensional units, other kinds of objective functions like weighted least square (WLS), scaled least square (SLS), etc shall perform one step ahead of OLS. The accomplishment of different objective functions were compared with numerical measurements for three models. Different objective functions were preferred for three models based on error analysis. TM model was able to retrieve the parameters with S_{OLS} but for **TMPN** and **TMPE** models, S_{OLS} with $\phi = 0.6$ and S_{SLS} gave better outcomes respectively.

List of symbols

Latin symbols

T1 - T7	Thermocouples
q	Heat flux[W/m ²]
c _p	Specific heat capacity [J/(kg.K)]
T	Temperature [K]
t	time [s]
k	Thermal conductivity [W/(mK)]
h _q	Convective heat transfer coefficient [W/(m ² K)]
L	Length of the domain [m]
X _p	Sensitivity of parameter p
S(p)	Objective function dependent of parameter p
Im	Function returning imaginary part of a complex variable
h	step size
Y	Measurement
n _p	number of parameters
n _t	number of transient measurement

n_θ	number of temperature sensors
\max	Function returning maximum value of an vector
\det	Function returning determinant of a matrix
Sen_i	Matrix containing sensitivity coefficients with respect to variable i
$C_{l,m}$	Correlation between parameters l and m

Greek symbols

ρ	Density [kg/m ³]
Δ	Small perturbation or Determinant
ε	Relative error in %
η_l	Variance of parameter l

Dimensionless numbers

θ	Temperature
U	Moisture content
α_q^*	Thermal diffusivity
α_p^*	Capillary diffusivity
D_l^*	Liquid water diffusivity
D_v^*	Water vapor diffusivity
P_g^*	Gas pressure
H^*	Evaporation rate constant
Bi_q	Biot number - heat
R_l	Latent heat of vaporization
t^*	time
Ω_i	Parameter vector of model i
M_i	Measured vector of component i
E_i	Estimated vector of component i

g^*	Source term
k^*	Thermal conductivity
C^*	Heat capacity

Subscripts

q	heat
l	liquid
v	vapor
θ	temperature
U	moisture content

Superscripts

a	analytical
m	numerical method
$*$	elements in non-dimensional form
T	Transpose of a matrix

Abbreviations

FDM	Finite Difference Method
CSD	Complex Step Differentiation
OLS	Ordinary Least Square
WLS	Weighted Least Square
SLS	Scaled Least Square

Bibliography

- [1] James V. Beck and Kenneth J. Arnold. *Parameter Estimation in Engineering and Science*. John Wiley and sons, 1977.
- [2] Arthur E. Bryson. *Applied Linear Optimal Control*. Cambridge University Press, 2002.

- [3] James V. Beck. *The optimum analytical design of transient experiments for simultaneous determinations of thermal conductivity and specific heat*. PhD thesis, Michigan State University, 1930.
- [4] C. Guiot, E. Madon, D. Allegro, P. G. Piantà, B. Baiotto, and P. Gabriele. Perfusion and thermal field during hyperthermia. experimental measurements and modelling in recurrent breast cancer. *Physics in Medicine and Biology*, 43(10):2831–2843, 1998.
- [5] Tahar Loulou and Elaine P. Scott. Thermal dose optimization in hyperthermia treatments by using the conjugate gradient method. *Numerical Heat Transfer; Part A: Applications*, 42(7):661–683, 2002.
- [6] Xingui Tang, Weizhong Dai, Raja Nassar, and Adrian Bejan. Optimal temperature distribution in a three-dimensional triple-layered skin structure embedded with artery and vein vasculature. *Numerical Heat Transfer, Part A: Applications*, 50(9):809–834, 2006.
- [7] E. P. Scott, P. S. Robinson, and T. E. Diller. Development of methodologies for the estimation of blood perfusion using a minimally invasive thermal probe. *Measurement Science and Technology*, 9(6):888–897, 1998.
- [8] Yu. E. Anikonov. *Multidimensional Inverse and Ill-Posed Problems for Differential Equations*. De Gruyter, 1995.
- [9] M. Cheney and J.H. Rose. Three-dimensional inverse scattering for the wave equation: weak scattering approximations with error estimates. *Inverse Problems*, 4(2):435–447, 1988.
- [10] A. Zinn. On an optimisation method for the full- and the limited-aperture problem in inverse acoustic scattering for a sound-soft obstacle. *Inverse Problems*, 5(2):239–253, 1989.
- [11] A. E. Yagle. One-dimensional inverse scattering problems: an asymmetric two-component wave system framework. *Inverse Problems*, 5(4):641–646, 1989.
- [12] Gang Bao. A uniqueness theorem for an inverse problem in periodic diffractive optics. *Inverse Problems*, 10(2):335–340, 1994.
- [13] V. I. Oliker. On reconstructing a reflecting surface from the scattering data in the geometric optics approximation. *Inverse Problems*, 5(1):51–65, 1989.
- [14] M. Necati Özisik. *Heat Conduction*. John Wiley & sons Inc., 1993.
- [15] M. Necati Özisik and Helico R.B. Orlande. *Inverse Heat Transfer, Fundamentals and Applications*. Taylor and Francis, 2000.
- [16] Christina Rask. Thermal properties of dough and bakery products: A review of published data. *Journal of Food Engineering*, 9(3):167 – 193, 1989.
- [17] B. Zanoni, C. Peri, and R. Gianotti. Determination of the thermal diffusivity of bread as a function of porosity. *Journal of Food Engineering*, 26(4):491–510, 1995.
- [18] V. Jury, J. Monteau, J. Comiti, and A. Le-Bail. Determination and prediction of thermal conductivity of frozen part baked bread during thawing and baking. *Food Research International*, 40(7):874–882, 2007.

- [19] M Omid, A Akram, and A Golmohammadi. Modeling thermal conductivity of iranian flat bread using artificial neural networks. *International Journal of Food Properties*, 14(4):708–720, 2011.
- [20] Angelo Fabbri, Chiara Cevoli, and Rodrigo Troncoso. Moisture diffusivity coefficient estimation in solid food by inversion of a numerical model. *Food Research International*, 56:63–7, 2014.
- [21] Emmanuel Purlis and Viviana O. Salvadori. Bread baking as a moving boundary problem. part 2: Model validation and numerical simulation. *Journal of Food Engineering*, 91:434 – 442, 2009.
- [22] Emmanuel Purlis and Viviana O. Salvadori. A moving boundary problem in a food material undergoing volume change – simulation of bread baking. *Food Research International*, 43(4):949–958, 2010.
- [23] A. Ousegui, C. Moresoli, M. Dostie, and B. Marcos. Porous multiphase approach for baking process - explicit formulation of evaporation rate. *Journal of Food Engineering*, 100:535–544, 2010.
- [24] Farzad Sadeghi, Nasser Hamdami, Mohammad Shahedi, and Ali Rafe. Numerical modeling of heat and mass transfer during contact baking of flat bread. *Journal of Food Process Engineering*, 39(4):345–356, 2016.
- [25] Maria Micaela Ureta, Daniela F. Olivera, and Viviana O. Salvadori. Baking of sponge cake : Experimental characterization and mathematical modelling. *Food and Bioprocess Technology*, 9(4), 2016.
- [26] J. Fan, J.R. Mitchell, and J.M.V. Blanshard. A model for the oven rise of dough during baking. *Journal of Food Engineering*, 41(2):69–77, 1999.
- [27] B.D. De Cindio and S. Correr. Mathematical modeling of leavened cereal goods. *Journal of Food Engineering*, 24(3):379–403, 1995.
- [28] Mathieu Lostie, Roman Peczalski, Julien Andrieu, and Michel Laurent. Study of sponge cake batter baking process. ii. modeling and parameter estimation. *Journal of Food Engineering*, 55(4):349 – 357, 2002.
- [29] Hadiyanto, D. C. Esveld, R. M. Boom, G. van Straten, and A. J.B. van Boxtel. Product quality driven design of bakery operations using dynamic optimization. *Journal of Food Engineering*, 86(3):399–413, 2008.
- [30] A. Ousegui, C. Moresoli, M. Dostie, and B. Marcos. Optimal control and cfd modeling for heat flux estimation of a baking process. *Computers and Chemical Engineering*, 38:139–150, 2012.
- [31] Ravula Sudharshan Reddy, Divyasree Arepally, and Ashis K. Datta. Estimation of heat flux in bread baking by inverse problem. *Journal of Food Engineering*, 271, 2020.
- [32] Lyness J. N. and Moler C. B. Numerical differentiation of analytic functions. *SIAM J. Numer. Anal.*, 4(2):202–210, 1967.

- [33] Puvikkarasan Jayapragasam, Pascal Le Bideau, and Tahar Loulou. Computing sensitivity coefficients by using complex differentiation: Application to heat conduction problem. *Numerical Heat Transfer, Part B: Fundamentals*, 74(5):729–745, 2018.
- [34] D. Grenier, D. Le Ray, and T. Lucas. Combining local pressure and temperature measurements during bread baking: insights into crust properties and alveolar structure of crumb. *Journal of Cereal Science*, 52(1):1–8, 2010.
- [35] Lei Xiujuan and Shi Zhongke. Overview of multi-objective optimization methods. *Journal of Systems Engineering and Electronics*, 15(2):142–146, 2004.
- [36] Abdelmalek Bensefia, Mohammed Boussaid, and Tahar Loulou. Optimal heat input for estimating luikov’s parameters in a heat and mass transfer problem. *Numerical Heat Transfer, Part B: Fundamentals*, 60(5):399–423, 2011.

Chapter 4

Estimation of physical properties from experimentation

Abstract

Simultaneous estimation of key parameters in the **TM**, **TMPN** and **TMPE** models are performed with aid of experimental measurements. Ordinary, weighted and scaled least square functions are employed as objective functions in inverse problem. Out of these, weighted least square with significant weight given to temperature is resulted better for all the models. In order to implement the phenomenon of crust-crumbs transformation in the model, the properties are to be considered as functions of state variables. These functions to be estimated are simplified through process of parameterization using β -spline method. The most influential thermophysical properties that are estimated by this approach are thermal conductivity, heat capacity and mass diffusivity of liquid water. The inclusion of heat flux in objective function has really helped the inverse problem for more accurate and precise estimation. Further analysis of inverse solutions for different cases shows that properties are greatly influenced by moisture content.

4.1 Introduction

In literature, hardly few authors have performed simultaneous estimation of required key parameters in food engineering and especially in baking process. Lostie and his co-authors have estimated simultaneously the thermophysical properties as functions of state variables through parameterization [1], i.e., the functions are approximated thorough estimation of several parameters present in it. In this chapter, the unknown properties of a moist dough during contact baking are approximated by optimization techniques from experimental data. This chapter is divided into two parts: one with parameter estimation which is an extension to the numerical analysis presented in the previous chapter and second as function estimation of influential properties that governs the baking process.

With advancement in technology that gives the ability to measure heat flux entering or leaving the surface, a new dimension in solving inverse heat conduction problem (IHCP) is found. Thus for function estimation, heat flux measurement is included along with temperature and mean moisture content measurements in the objective function. In this case, heat flux is not measured

but is obtained through another inverse problem that estimates heat flux leaving the cast-iron floor. The procedure for heat flux estimation is elaborated in appendix A. If a heat flux sensor is placed at the interface, it would have definitely affected the baking process. Moreover, the inverse solution of heat flux is independent from the below explained estimation process. Therefore, considering the estimated heat flux as measured data will have no interconnection with the current optimization process.

4.2 Parameter estimation

The parameter vectors Ω_1 , Ω_2 and Ω_3 are estimated from the models TM, TMPN, and TMPE respectively. The effectiveness of inverse problems with objective function formulated by ordinary least square (OLS), weighted least square (WLS), and scaled least square (SLS) are compared and a better choice for each model is selected. The contrasts of the inverse solutions from the previously discussed results are studied in this chapter.

In order to ensure the confidence of the estimated parameters, confidence interval is calculated for estimated parameters. The expression for confidence interval P_e is given by [?]

$$P_e \pm Z\sigma_{P_e} \quad \text{where} \quad \sigma_{P_e} = \text{diag} \left[\sqrt{(X^T X)^{-1} \frac{S^T S}{n}} \right] \quad (4.1)$$

Where P_e is estimated parameter vector, $Z = 1.968$ for 95 % of confidence level, diag is a function which returns diagonal elements of a square matrix, S is residual between measurements and simulated data with n number of components, X is sensitivity or Jacobian matrix. If a parameter returns a wider confidence interval means the estimated value is not precise and it might be due to several factors like lack of enough information (i.e. measurements), improper experimental design, poor or weak sensitivity of the desired state variable with respect to the parameter, etc. With a inbuilt MATLAB command *nlparci* returns confidence intervals for the estimated parameters.

Another fundamental method for evaluating the performance of inverse solution is rms (root mean square) which was utilized also in previous cases with synthetic data. When rms between the simulated results based on estimated parameters and measurements is minimal then the inverse algorithm is capable of reproducing similar estimated profiles with precise and accurate estimations. The necessary properties that are required for completing the models, are listed in table4.1.

4.2.1 TM Model

This is a simplest model among other presented ones, which consists of unknown parameter vector $\Omega_1 = [\alpha_q^*, D_1^*, k^*, Bi, R_1]$. Table 4.2 gives the rms between measured and simulated results from estimated parameters for each objective functions. On observation, the major difference is noted for temperature at T4, the region with incoming heat flux. The temperature sensor that is in contact with the ambient surface, is resulted the least rms among the temperatures. S_{SLS} is returned a better approximation for temperatures but failed for mean moisture content profile to a larger extent. The results for S_{OLS} and S_{WLS} for $\phi = 0.5$ are very similar. For weighted least square, as the weighting factor increases, the rms for temperature is decreased

Parameters	Expression/Values	Units	Descriptions
Bi_m	$\frac{Bi}{\rho C_p^{air} L e^{2/3} (L^2 / k_{ref} t_f)}$	–	From boundary layer theory [?].
R_1	$\frac{\lambda}{\rho C_p} \frac{\rho_s^a}{T_{int}}$	–	Calculated from known variables
ρC_p	$\frac{k_{ref}}{k^* a_q^*} \frac{t_f}{L^2}$	J/(m ³ K)	Calculated from known variables
a_w	$\frac{0.99}{\exp(0.042U^{-1.11})}$	–	Water activity
P_{sat}	$\exp \left[23.5771 - \left(\frac{4042.9}{(T + 273.15) - 37.58} \right) \right], T \text{ in } ^\circ\text{C}$	Pa	Saturated vapor pressure
λ	2.5×10^6	J/kg	Latent heat of vaporization
μ_g	1.8×10^{-5}	Pa.s	Dynamic viscosity for gas
k_g	1.2×10^{-14}	m ²	Calculated as average from function $k_g^i \times k_g^r$
a_p^*	1284	–	Capillarity diffusivity
π	0.76	–	Porosity (calculated)
S_{int}	0.9	–	Liquid Saturation initial (calculated)
U_{int}	1.6	–	Moisture content initial
T^{inf}	294	K	Ambient temperature
k_{ref}	1	W(mK)	reference thermal conductivity
L	0.008	m	Overall length
t_f	1200	s	end time
ρ_s^a	436	kg/m ³	Apparent solid density (calculated)

Table 4.1: Imposed parameters

but the error for moisture content is increased. Among all these objective functions, S_{WLS} with $\phi = 0.4$ is chosen as recommended result for **TM**.

Objective functions	Temperature sensor			Mean moisture content $\times 10^2$
	T ₄ [°C]	T ₅ [°C]	T ₇ [°C]	
S_{OLS}	14.13	7.08	3.14	1.88
S_{WLS} $\phi =$	0.4	14.75	7.11	1.40
	0.5	14.12	7.07	1.88
	0.6	12.79	6.90	2.98
S_{SLS}	9.92	6.46	2.84	8.94

Table 4.2: The rms values between simulated and measured data for **TM** model

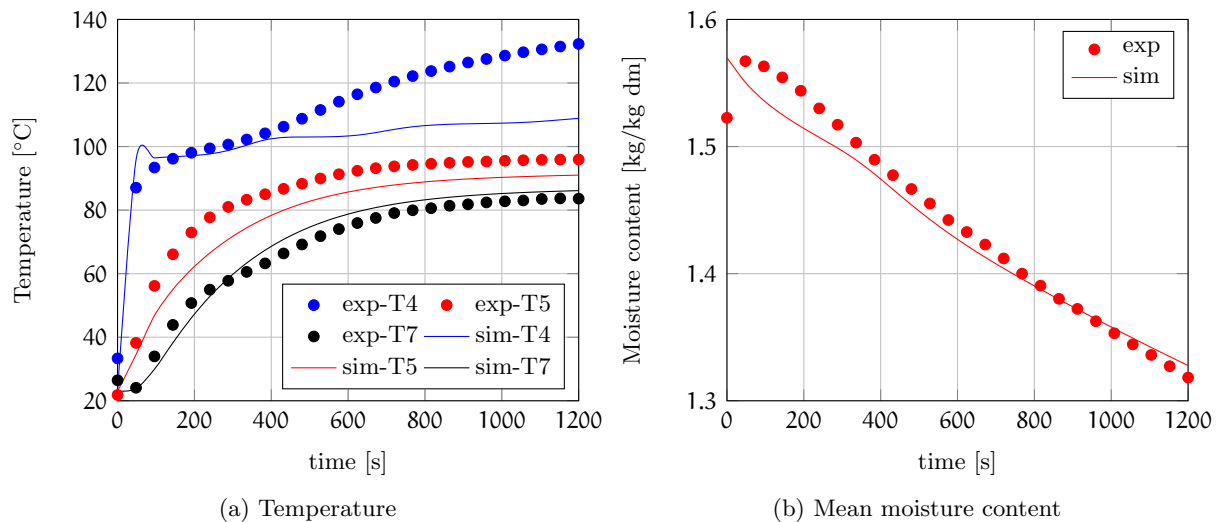


Figure 4.1: Comparison of measurements and simulations of temperature (a) and mean moisture content (b) for **TM** model

The inverse results for the objective function S_{WLS} with $\phi = 0.4$ are presented in table 4.3. The inverse solution with synthetic data had been resulted better for ordinary least square objective function with relative error less than 1 %. But the current inverse solution did not result the same and has some difficulties in the approximation. The estimated parameters are presented with their confidence intervals. Thermal properties like thermal conductivity and thermal diffusivity have variation of intervals of about 2.5 %. Mass diffusivity of liquid water has larger confidence interval with variation about 32 %. The graphical representation of simulated and measured profiles of temperature and moisture content are plotted in figure 4.1.

4.2.2 TMPN Model

In this model, the parameter vector $\Omega_2 = [\alpha_q^*, D_l^*, D_v^*, H^*, k^*, Bi_q]$ is estimated. The rms values for temperature and moisture content between simulation and measurement are displayed in table 4.4. Inclusion gaseous phases in the model has refined the inverse solution which had reflected as better results for temperatures especially at sensor locations T₄ and T₅. On contrast

Parameter	Initial guess	Estimated	
α_q^*	0.2000	1.65	± 0.037
D_t^*	0.0009	0.0045	± 0.0014
k^*	0.5000	4.20	± 0.117
Bi_q	0.0070	0.036	± 0.0077
R_1	0.0800	0.316	± 0.062

Table 4.3: Inverse solution for **TM** model with experimental measurements using S_{WLS} of $\phi = 0.4$

to results of **TM** model, the objective functions with more weighting factor for temperature has evolved better profiles here. From analysis, the inverse solution by weighted least square S_{WLS} with $\phi = 0.6$ is preferred due to their least rms values. This shows that **TMPN** model has properties which are largely dependent on temperature. In earlier case study with synthetic data, the same model had been resulted accurately for S_{SLS} . This is indication of incompleteness of the model to represent the baking phenomenon.

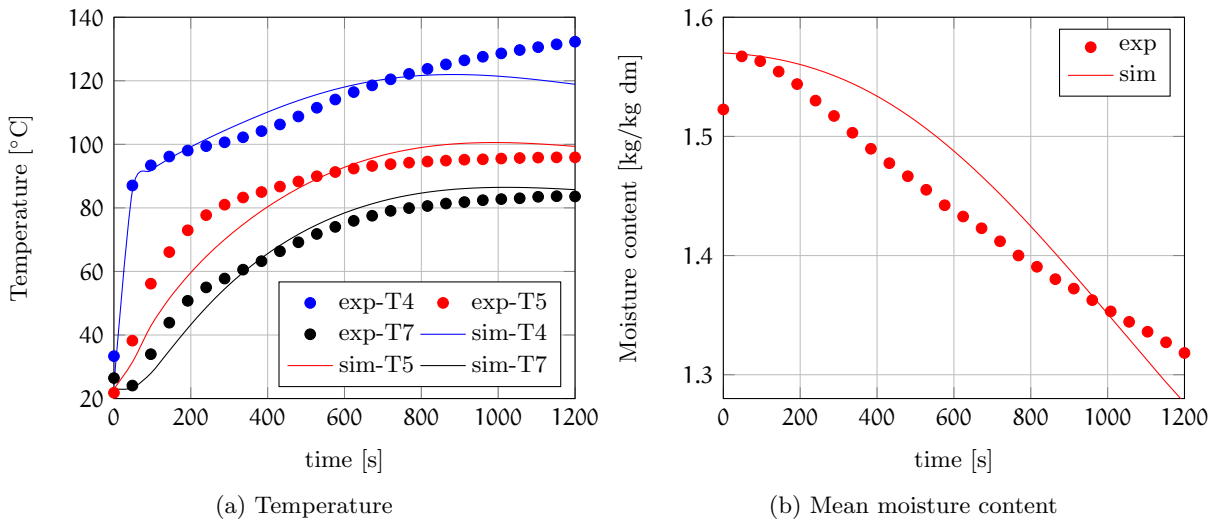


Figure 4.2: Comparison of measurements and simulations of temperature (a) and mean moisture content (b) for TMPN model

Objective functions	Temperature sensor			Mean moisture content $\times 10^2$
	T_4 [°C]	T_5 [°C]	T_7 [°C]	
S_{OLS}	8.23	4.91	4.27	2.95
S_{WLS} $\phi = 0.40$	8.22	4.90	4.26	2.88
S_{WLS} $\phi = 0.50$	9.77	6.28	7.20	3.12
S_{WLS} $\phi = 0.60$	4.38	5.82	3.68	2.88
S_{SLS}	8.96	5.91	6.18	3.79

Table 4.4: The rms values between simulated and measured data for **TMPN** model

The estimated properties in non-dimensional form are showcased in table 4.5 along with their confidence intervals. The thermal properties (thermal conductivity, k^* and diffusivity, α_q^*), and mass diffusivity of water vapor, D_v^* have variation of confidence interval in range of 3.5% of the estimated values. This ensures the reliability of these estimated properties. But mass diffusivity of liquid water has variation up to 57% of the estimation. This and previous model were able to estimate mass diffusivity of liquid water with ease but their confidence region are wider as the sensitivity of this parameter was weak. The evolution of temperature and moisture content profiles with respect to baking time is plotted in figure 4.2.

Parameter	Initial guess	Estimated	
α_q^*	0.0827	1.633	± 0.0624
D_l^*	0.0093	0.148	± 0.0845
D_v^*	9.3750	28.114	± 6.7147
H^*	120.00	2328.90	± 264.919
k^*	0.5844	2.956	± 0.0814
Bi_q	0.0320	0.096	± 0.0126

Table 4.5: Inverse solution for **TMPN** model with experimental measurements using S_{WLS} of $\phi = 0.6$

4.2.3 TMPE Model

Due to assumption of equilibrium approach for evaporation rate computation, the number of parameters to be estimated are reduced by one while compared to the previous **TMPE** model. The unknown parameter vector $\Omega_3 = [\alpha_q^*, D_l^*, D_v^*, Bi, k^*]$ is needed to be estimated using an optimization techniques. The rms values of temperature and moisture content between simulation and measurement are presented in table 4.6. On comparison with previous two models, the rms for mean moisture content is least in the model irrespective of objective function. Temperature at sensor locations T_5 and T_7 have comparatively lower rms values. But the temperature at incoming heat flux boundary has the maximum rms value but way better than **TM** model. Similar to **TMPN** model, as the weighting factor increases, the rms value for temperature is decreased. Even the rms value for mean moisture content is reduced with increasing weighting factor. The main reason behind this behavior is due to better sensitivities for mass transfer properties with respect to temperature which were not found in other two models.

The approximated parameter vector Ω_3 from the inverse solution using objective function S_{WLS} with $\phi = 0.6$ is presented below in the table 4.7. The estimated parameters have smaller confidence interval with maximum variation of 5.50% for parameter D_v^* . Figure 4.3 gives the agreement of simulated results with measurements for temperature and moisture content.

Out of these models, **TMPE** model has better results for temperature at sensor locations T_5 and T_7 , and mean moisture content. But this model has terribly failed for the temperature at T_4 . The main reason for this failure is due to selection of properties as constant parameters and these constants were unable to address the crust-crumbs transformation. **TMPN** model was able to result more desirable trends for temperature at T_4 but it does not represent a plateau near

Objective	Temperature sensor			Mean moisture
Functions	T_4 [°C]	T_5 [°C]	T_7 [°C]	content $\times 10^2$
S_{OLS}	10.92	4.59	3.82	0.61
$S_{WLS} \phi =$	0.4	11.25	3.67	0.84
	0.5	10.93	4.59	0.61
	0.6	10.89	4.92	0.57
S_{SLS}	10.87	4.41	4.29	1.15

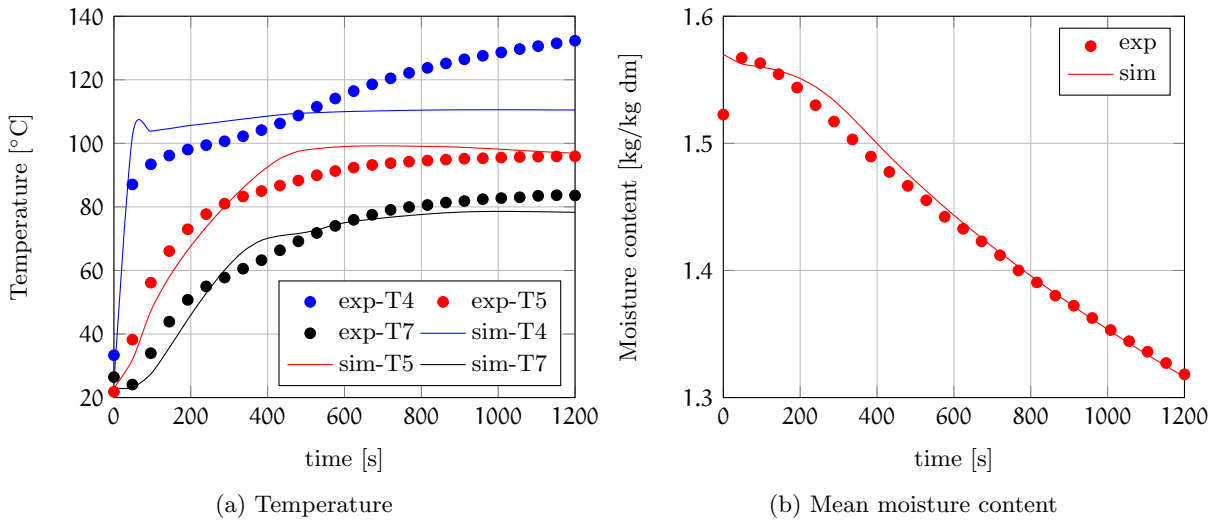
Table 4.6: rms value between simulated and measured data for **TMPE** model

Figure 4.3: Comparison of measurements and simulations of temperature (a) and mean moisture content (b) for TMPE model

Parameter	Initial guess	Estimated	
α_q^*	0.0827	1.364	± 0.0355
D_t^*	0.0093	0.012	± 0.0005
D_v^*	9.3750	19.414	± 1.0801
Bi_q	0.0320	0.0680	± 0.0008
k^*	0.5844	3.3890	± 0.0740

Table 4.7: Inverse solution for **TMPE** model with experimental measurements using S_{WLS} of $\phi = 0.6$

100 °C. Moreover, there is a large deviation for mean moisture content in **TMPN** model. For all three models, weighted least square objective function with $\phi = 0.4$ for **TM** and $\phi = 0.6$ for **TMPN** and **TMPE** models have better approximations which is in contrast to the previous synthetic data case studies. Based on these observations, ordinary least square method was found to be insufficient in solving the inverse problem with several components that to be minimized. Moreover, the variation of confidence intervals from the estimated parameters were least for only **TMPE** model. The mass transfer properties like D_l^* and D_v^* have wider confidence interval and this is due to their weak sensitivities. Due to averaging effect on moisture content, it has even worsened the sensitivities of these parameters.

4.2.4 Extension of inverse solution

The experimental measurements for all the above cases were performed for a regulator temperature 200 °C. For the purpose of evaluating the accuracy of the inverse solutions, the problem is extended for other baking condition. In the current case study, the regulator temperature is set at 170 °C which had decreased the intensity of the incoming heat flux at the interface of dough and cast iron floor but all other process parameters were remained exactly same as previous case. The reduced heat intensity had also lowered the mass loss due to evaporation from 15 to 12.1 gms.

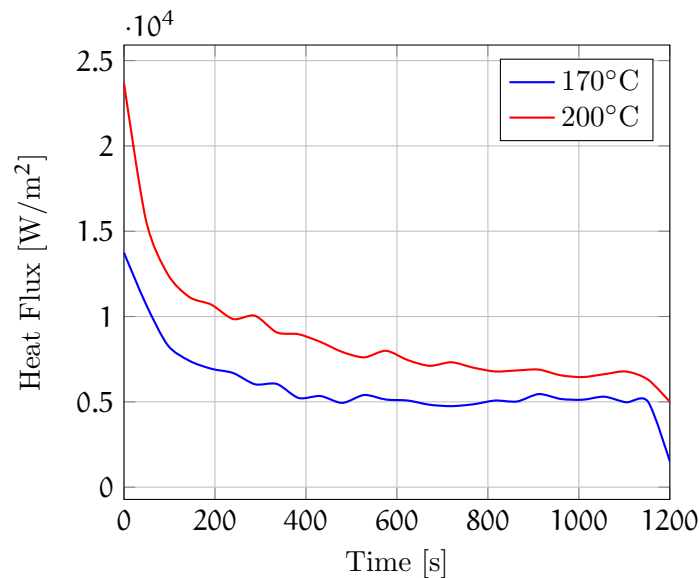


Figure 4.4: Evolution of heat flux for temperature 170°C (a) and 200°C (b)

The estimated heat flux for regulator temperature 170°C obtained with the procedure as explained in appendix A, is given in figure 4.4. The temperature and moisture content profiles are simulated for **TMPN** and **TMPE** models with presented heat flux and inverse solutions from previous sections. These simulated results are plotted and collated in figure 4.5 against the measurements to identify whether the estimated properties are able extend for other conditions.

Analyzing the measurement trends, the temperature sensor at T_3 has a plateau at 125 °C which is not the boiling point of water and this is unacceptable. This is due to the fact that the thermocouple came in contact with the cast iron floor while pouring the dough into the PFTE mold. The measurement of T_3 corresponds to the variation on the cast iron floor surface.

Hence, in upcoming analysis of simulated results with measurements, temperature value at sensor location T_3 is ignored. Though the mean moisture content profile is linear alike previous case, it has lesser value than for the higher regulator temperature as stated earlier.

Concerning the simulated results from **TMPN** model, the temperature profiles are close enough to the measurement trends. The profile of moisture content do not match with measured values but towards the end of baking time, both experimental and simulated values are near by. In the intermediate time of baking, the simulated moisture content trend show an underestimation of mass loss. While in inverse solution, it had showed underestimation for certain baking time but towards the end of baking, it had ended up in overestimation of mass loss. This behavioral difference can be caused by inappropriate estimation of parameters like D_t^* , D_v^* , H^* and Bi_m , that are influencing the mass transfer. The convective mass transfer coefficient is derived from heat transfer coefficient with a simple relation established between them. The temperature variation at sensor location T_7 do not show any major conflict with the measurements. It depicts that the estimated convective transfer coefficients were accurate enough for the model. Considering a small variation in the mass diffusivity parameters D_t^* and D_v^* , it will have some effects on the local moisture content but not on the spatial average value since these diffusivities does not contribute to evaporation-condensation to a greater extent. Conclusively, it eliminates all the parameters that can caused such deviation except evaporation rate constant H^* . Since it is an empirical constant, it should be approximated individually for each experimental setup and is not successful in accurate simulation of mass loss for other baking conditions.

The agreement between simulated and measured variables for **TMPE** model implies that the estimated properties are accurate enough to simulate different baking conditions for the batter considered here. Unlike **TMPN** model, this model do not show any behavioral change in the simulated profiles from previous inverse solutions. Temperature at sensor location T_3 has the maximum deviation and a raise in temperature after a plateau at 100°C is not observed. At the same time, the mean moisture content almost coincides with the measured profiles representing that the approximated properties of the model are capable of accurate prediction of mass loss for other baking conditions.

Model	Temperature [$^\circ\text{C}$]			Mean moisture content [] $\times 10^2$
	T_4	T_5	T_7	
TMPN	19.74	5.31	4.58	3.34
TMPE	22.72	5.41	6.33	0.75

Table 4.8: The rms values between simulated and measured profiles for regulator temperature 170°C

The rms values between the simulated and measured profiles for both the models are presented in table 4.8. On analyzing the above presented results, the model with implicit evaporation rate is more suitable for solving the inverse problem and its solution can be extended for other conditions.

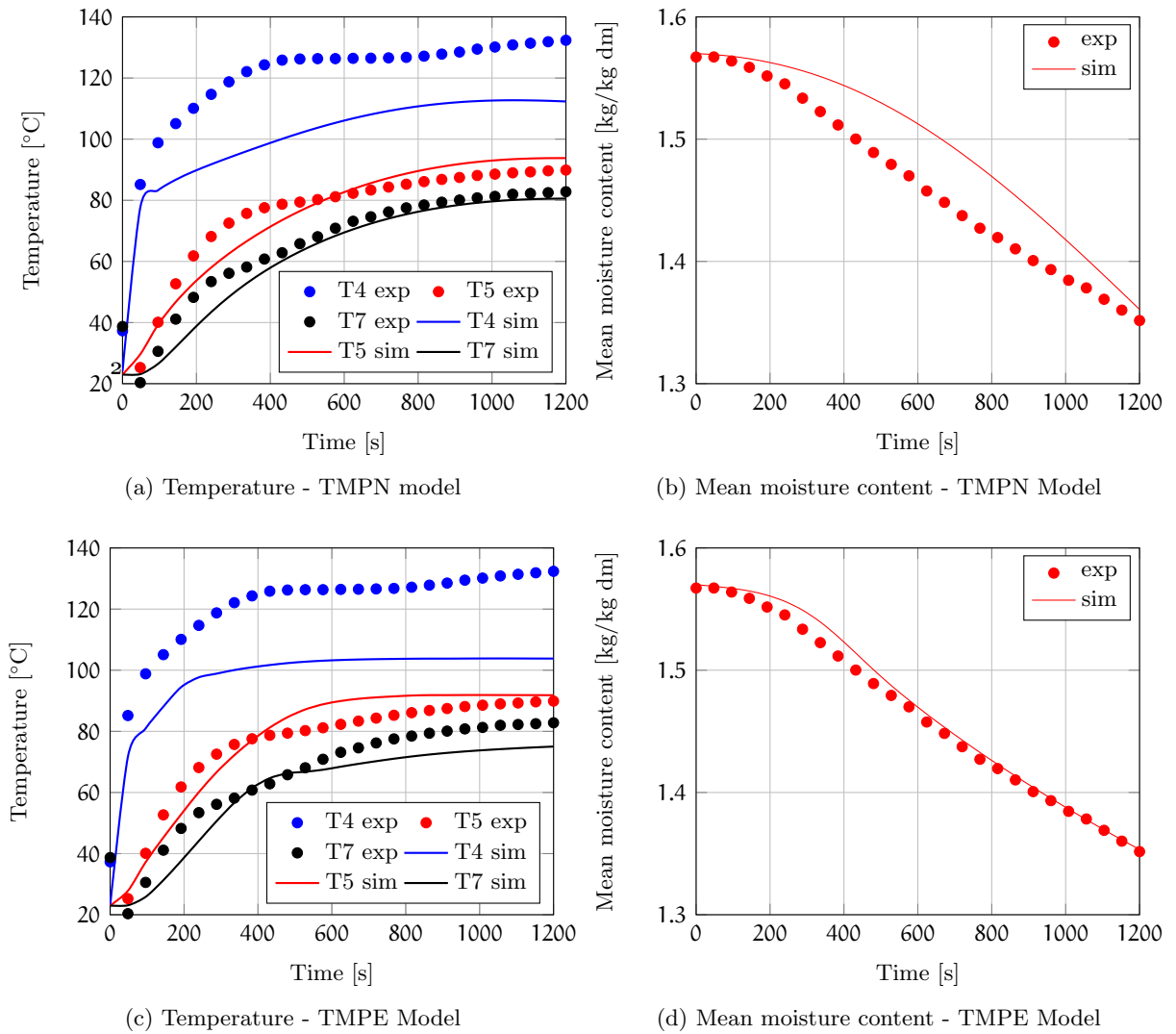


Figure 4.5: Experimental measurements and simulated results of TMPN and TMPE models for regulator temperature 170°C (where exp is experimental data and sim is simulated results)

4.2.5 Literature

The estimated parameters in dimensional form for all the models are presented in table 4.9 and compared with the range given in literature. In all the models, thermal conductivity k_{eff} is within the range given in the literature but the volumetric heat capacity for **TM** model is smaller than the range presented.

	Parameter	Description	unit	TM model	TMPN model	TMPE model	Range
Thermal properties	k_{eff}	thermal conductivity	W/mK	0.238	0.338	0.295	0.21 - 0.44 [1]
	ρc_p	volumetric heat capacity	$\text{kJ}/(\text{m}^3\text{K})$	2704.54	3881.61	4052.09	3400 - 4100 [1]
Mass properties	D_w	mass diffusivity of liquid water	$\text{m}^2/\text{s} \times 10^9$	0.24	7.91	0.67	0.7 - 1.3 [2]
	D_v	mass diffusivity of water vapor	$\text{m}^2/\text{s} \times 10^6$	–	1.49	1.04	0.70 - 0.92 [2]
Closure term	h_q	convective heat transfer	$\text{W}/\text{m}^2\text{K}$	4.51	11.97	8.48	2 - 25 [3]
	H	evaporation rate constant	1/s	–	1.95	–	1 [4]

Table 4.9: Estimated parameters in dimensional form

Regarding the mass transfer properties, only **TMPE** model has the estimation close enough to the literature range while the other two models gave a value that is either smaller or greater than the nominal mean. But, there is some consistency in estimation of D_v^* for models **TMPE** and **TMPN**, and are also near the nominal value.

The boundary condition, convective heat transfer coefficient h_q , also have least consistency and **TMPN** model required higher coefficient value while **TM** model required least value. The estimated evaporation rate constant for **TMPN** model is twice larger than the nominal mean. The only model whose estimated values are in range stated in literature and having smaller confidence regions is **TMPE** model and this model shall be carried forward for function estimation. The above analysis of inverse solutions with available data from literature is performed only for a comparison purpose and it is obvious that the batter and the baking process presented in literature are not identical to the presented one.

4.3 Function estimation

The significant thermophysical properties governing the baking process are thermal conductivity, heat capacity and mass diffusivity of liquid water and these are functions of state variable like temperature, moisture content. From the previous inverse solutions, it was understood that constant properties were unable to represent some critical phenomenon like crust-crumble transformations from dough. Thus in upcoming part of this chapter, properties are estimated as functions of temperature, moisture content or both.

Function estimation is carried out through parameterization of the functions and estimating those parameters that are appearing in it. Usually, the parameterization of a function is performed either by a mathematical expression of a function with prior information, for example Arrhenius type equations for diffusivities, or with help of power series represented by $f(x) = \sum_{n=0}^{\infty} a_n^n(x)$. Author had estimated simultaneously several thermophysical properties through parameterization by a well-defined expression for oven baking of a sponge cake [1]. But these expression are mathematically constrained (only exponential behavior for the stated example) or the magnitude of coefficients a_n in the power series are unequal making the function to be less flexible. Thus, the properties and process parameters like thermal conductivity, heat capacity, mass diffusivity and incoming heat flux at cast-iron/dough interface are parameterized by means of β -spline which has explained in previous chapter 3 through different examples.

The key factors influencing and controlling the curves of β -spline are order of spline and choice of knots. As the order of spline increases, the number of parameters to be estimated are also increased. Hence, the order is chosen either 3 or 4 which makes the curves to be cubic or quadratic respectively. Since the point of discontinuity or abrupt change in curves are mysterious, the knots are taken only at extreme points. For example, if the property is considered as function of moisture content and with order of spline as 3, the knots are chosen as $[0, 0, 0, 2.5, 2.5, 2.5]$ with guess of moisture content extremes as 0 and 2.5. The study of other spline order is also performed but there is no major improvement in estimation. Henceforth the order of the spline is considered as 3 in the upcoming sections.

Out of the three models presented earlier, **TMPE** modeling approach is considered for function estimation of certain properties. Even during the estimation of constant parameters, only

TMPE model has least rms for both temperatures and mean moisture content except at bottom temperature at T_3 . Thus, by considering the volumetric heat capacity and thermal conductivity as function of temperature or moisture content, the approximation of temperature profile at T_3 will be improved. In the following section, the steps carried for transforming the **TMPE** model from dimensional form to non-dimensional is explained in detail.

4.3.1 Mathematical Modeling

The **TMPE** model with some modifications is extended for function estimation of thermophysical properties like thermal conductivity, heat capacity and mass diffusivity of liquid water with means of β -spline.

Hypothesis: The following assumptions are considered while building the mathematical model,

1. Except the incoming heat flux, thermal conductivity, heat capacity and mass diffusivity of liquid, all the other properties are assumed as constants and taken from previous estimation
2. The gaseous components like vapor and air, obey ideal gas law and Dalton's law of partial pressure
3. The evaporation of liquid water is formulated by equilibrium approach
4. The effect of deformation is ignored

Temperature:

$$\rho c_p(U, T) \frac{\partial T}{\partial t} = \frac{\partial}{\partial x} \left(k_{\text{eff}}(U, T) \frac{\partial T}{\partial x} \right) - \lambda I_v \quad (4.2)$$

Moisture content:

$$\begin{aligned} \frac{\partial U}{\partial t} &= \nabla \left\{ \underbrace{D_l(U) \nabla U + \rho_v \frac{k_g}{\mu_g} \frac{\partial P_g}{\partial x} + \rho_g D_v \frac{\partial}{\partial x} \left(\frac{\rho_v}{\rho_g} \right)}_{\Gamma} \right\} \\ &= \pi \rho_v \frac{\partial S}{\partial t} + \pi (1 - S) \frac{P_v}{T^2} \frac{\partial T}{\partial t} - \pi (1 - S) \frac{1}{T} \frac{\partial P_v}{\partial t} \end{aligned} \quad (4.3)$$

Gas pressure:

$$\begin{aligned} \frac{\pi (1 - S)}{R_v T} \frac{\partial P_g}{\partial t} &= \nabla \left\{ \underbrace{(\rho_g - \rho_v) \frac{k_g}{\mu_g} \nabla P_g - (\rho_g - \rho_v) D_v \nabla \left(\frac{\rho_v}{\rho_g} \right)}_{\Phi} \right\} \\ &= \pi (1 - S) \frac{R_v}{T} \frac{\partial P_v}{\partial t} + \pi \rho_g \frac{\partial S}{\partial t} \end{aligned} \quad (4.4)$$

Boundary conditions : The heat entering the dough from cast-iron floor at $x = 0$ is computed either as heat flux or convective heat transfer. There is no change in the boundary conditions for other components. The summary of applied boundary conditions are,

	$x = 0$	$x = L$
$-k_{\text{eff}} \frac{\partial T}{\partial x}$	$q(t)$ or $h_q(t)(T_{\text{surface}} - T(0, t))$	$h_q(T(L, t) - T^\infty)$
Γ	0	$h_m(\rho_v - \rho_v^\infty)$
Φ	0	-
P_g	-	P_{atm}

Dimensionless form

The main differences from previously stated **TMPE** model is in the way of implementing the parameters in non-dimensional form since some of them are functions. It would have noted that the parameter α_q^* is transformed as α_{ref} and its value is known prior to estimation. The governing equations in non-dimensional form are given below,

Temperature :

$$C^*(U, T) \frac{\partial \theta}{\partial t^*} = \alpha_{\text{ref}}^* \frac{\partial}{\partial x^*} \left(k^*(U, T) \frac{\partial \theta}{\partial x^*} \right) - R_1 I_v^* \quad (4.5)$$

Moisture content :

$$\begin{aligned} \frac{\partial U}{\partial t^*} &= \pi \frac{\rho_{\text{ref}} P_v^*}{R_v^* (\theta + 1)} \frac{\partial S}{\partial t^*} - \pi(1 - S) \rho_{\text{ref}} \frac{P_v^*}{(\theta + 1)^2} \frac{\partial \theta}{\partial t^*} + \pi(1 - S) \frac{\rho_{\text{ref}}}{\theta + 1} \frac{\partial P_v^*}{\partial t^*} \\ &= \nabla^* \left(\underbrace{D_{\text{ref}} D^*(U) \nabla^* U + \alpha_p^* V \nabla^* P_g^* + \rho_{\text{ref}} \frac{(P_g^* - P_v^* (R_v^* - 1))}{(\theta + 1)} D_v^* \nabla^* \left\{ \frac{1}{1 + (P_g^* - P_v^*) R_v^* / P_v^*} \right\}}_{\Gamma^*} \right) \end{aligned} \quad (4.6)$$

Gas pressure :

$$\begin{aligned} \pi(1 - S) \rho_{\text{ref}} \frac{R_v^*}{\theta + 1} \frac{\partial (P_g^* - P_v^*)}{\partial t^*} + \pi(1 - S) \rho_{\text{ref}} \frac{(P_g^* - P_v^*) R_v^*}{(\theta + 1)^2} \frac{\partial \theta}{\partial t^*} + (P_g^* - P_v^*) \pi \rho_{\text{ref}} \frac{R_v^*}{\theta + 1} \frac{\partial S}{\partial t^*} &= \\ &= \nabla^* \left\{ \underbrace{\rho_{\text{ref}} \alpha_p^* \frac{(P_g^* - P_v^*) R_v^*}{\theta + 1} \nabla^* P_g^* - \rho_{\text{ref}} \frac{(P_v^* + (P_g^* - P_v^*) R_v^*)}{\theta + 1} D_v^* \nabla^* \left(\frac{1}{1 + (P_g^* - P_v^*) R_v^* / P_v^*} \right)}_{\Phi^*} \right\} \end{aligned} \quad (4.7)$$

Boundary conditions : The boundary conditions that complete the equations are:

The steps of non-dimensionalization are detailed in appendix B.

The non-dimensional parameters appearing in the governing equations are presented in table 4.10. The parameters that are not mentioned in the table are same as presented for the previous models given in chapter 2.

	$x^* = 0$	$x^* = 1$
$-k_{\text{eff}} \nabla^* \theta$	$Q^*(t^*)$ or $\text{Bi}_q^0(t^*)(\theta_{\text{surface}} - \theta(0, t^*))$	$\text{Bi}_q^L(\theta(1, t^*) - \theta^\infty)$
Γ^*	0	$\text{Bi}_m(V - V^\infty)$
Φ^*	0	–
P_g^*	–	1

4.3.2 Sensitivity analysis

The sensitivity analysis of the coefficients that govern the profiles of β -splines are executed. Since, some of the coefficients represent a particular property, they are strongly correlated. As said earlier, the order of the spline and knots are chosen in such a way that each property are represented by a β -spline with 3 coefficients. Thus with four unknown properties, totally 12 parameters are needed to be estimated. Figure 4.6 shows how temperature, mean moisture content and Biot number reflect for a small variation in those coefficients. The Biot number represented here corresponds to the heat transfer number at interface between cast-iron and dough. For case of representation, thermal conductivity, heat capacity and mass diffusivity are considered as function of moisture content and the Biot number as function of baking time.

The temperature sensitivity is presented only at sensor location $x = 0$ since the major variation of temperature is observed here. The scaled sensitivities of $C_{1,2,3}$ and $\text{Bi}_{1,2,3}$ have order of magnitude ten times bigger than $k_{1,2,3}$ and $D_{1,2,3}$. From the profiles, it can be said easily that these parameters are strongly correlated among them. During first half of baking time, a maximum variations for all the coefficients are observed while in remaining period almost constant profiles are noted. Out of these coefficients, temperature at this location showed least sensitivities for mass diffusivity coefficients.

All the coefficients are in similar order of magnitude for the scaled sensitivities with respect to moisture content. Thermal conductivity showed minute variations for mean moisture content which depicts that the thermal conductivity has least influence on mass transfer. During initial time of baking, as the most of heat observed are stored as latent heat of vaporization, the mass loss is lower at this point. This is reflected as undisturbed sensitivity profiles which are almost zero during initial time of heating. one of the coefficients (Bi_3) in Biot number, which is an integral part of heat flux and another coefficient (k_1) of thermal conductivity have least sensitivities among all coefficients. The coefficient k_1 controls the conductivity at lower moisture content range approximately between 0 and 0.5. It illustrates that the heat transfer for the region with lower moisture content either has no major impact or the region is smaller than wetter regions which has damped their effect due to averaging. Similarly Bi_3 , corresponding to Biot number towards the end of baking time, is insensitivity for baking time up to first 12 minutes. Heat flux as a component of objective function was not considered in previous cases of inverse solutions. But in following section, it is showed how the inclusion of heat flux in objective function has improved the inverse solution. For this reason only, additional Biot number for heat transfer at the interface comes into the picture. Temperature and mean moisture content have showed that they are sensitive to a small variation in the coefficients of Biot number. In addition, the conductivity and heat capacity are also sensitive to heat flux measurements. Thus, it can be understood that the heat flux measurement will provide more support for the optimization

Parameter	Expression	Value	Description
k_{ref}	-	0.5 [W/(mK)]	Reference thermal conductivity
Cp_{ref}	-	1000 [J/(kgK)]	Reference heat capacity
$\rho_{\text{ref}}^{\theta}$	-	1000 [kg/m ³]	Reference thermal density
ρ_{ref}^g	$\frac{P_{\text{int}}}{R_a T_{\text{int}}}$	1.2041 [kg/m ³]	Reference gas density
a_{ref}	$\frac{k_{\text{ref}}}{\rho_{\text{ref}} Cp_{\text{ref}}}$	5×10^{-7} [m ² /s]	Reference diffusivity
a_{ref}^*	$a_{\text{ref}} \times \frac{t_f}{L^2}$	9.375	Reference diffusivity in non-dimensional form
R_1	$\frac{\rho_s^a}{\rho_{\text{ref}}} \times \frac{\lambda}{Cp_{\text{ref}} T_{\text{int}}}$	3.68065	Latent heat of vaporization
I_v^*	$\frac{I_v \times t_f}{\rho_s^a}$	-	Evaporation rate
C^*	$\frac{\rho Cp}{\rho_{\text{ref}}^{\theta} Cp_{\text{ref}}}$	-	Volumetric heat capacity
k^*	$\frac{k_{\text{eff}}}{k_{\text{ref}}}$	-	Thermal conductivity
ρ_{ref}^*	$\frac{\rho_{\text{ref}}^g}{\rho_s^a}$	-	Reference density-gas
D_{ref}	-	10^{-8} m ² /s	Reference mass diffusivity
D_{ref}^*	$\frac{D_{\text{ref}} \times t_f}{L^2}$	0.1875	Reference mass diffusivity
R_v^*	R_v/R_a	1.6078	Ratio of specific gas constants
D^*	$D_l(U)/D_{\text{ref}}$	-	Mass diffusivity of moisture content - liquid
a_p^*	$\frac{k_g P_{\text{int}}}{\mu_g} \times \frac{t_f}{L^2}$	1284.25	Darcy term
D_v^*	$\frac{D_v t_f}{L^2}$	19.414	Mass diffusivity of water vapor
Bi	$\frac{h_q L}{k_{\text{ref}}}$	0.13568	Biot number for heat transfer
Bi_m	$\frac{h_m t_f}{L}$	1080.85	Biot number for mass transfer
π	-	0.76	Porosity

Table 4.10: Dimensionless variables and constants

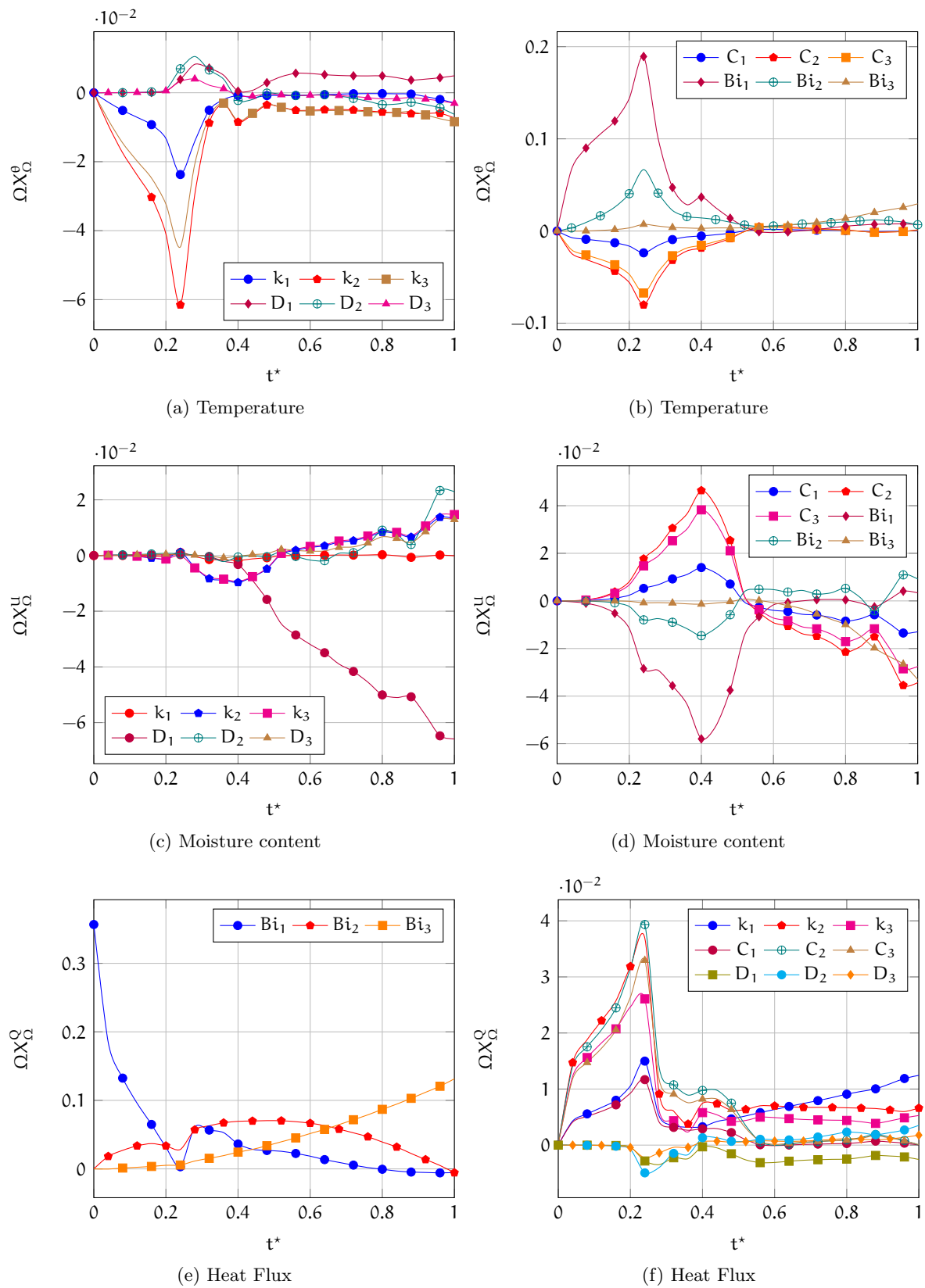


Figure 4.6: Sensitivity coefficient

to search accurately thermal properties like heat capacity and conductivity. Moreover, the Biot number at interface indirectly represents thermal contact resistance that gives the measure of heat loss due to surface irregularities and improper contact.

While estimating the essential properties as constant parameter, mass transfer parameters were very sensitive with respect to both temperature and moisture content in **TMPE** model. While moving forward with function estimation, mass transfer coefficients are least sensitive for temperature and heat flux. Since the scaled sensitivity of D_1 is significant with respect to mean moisture content, the mass diffusivity becomes crucial for lower moisture content. Eventually, the trends of the sensitivities of all coefficients that are plotted in figure 4.6 show that there will be no struggle in simultaneously estimation of the functions.

4.3.3 Analysis on inverse solution

Until now, the objective function used for the inverse solution were based on temperature and mean moisture content alike most of the cases in literature. But authors have showed the possibilities and advantages of considering the heat flux measurements either alone or along with temperature for solving inverse heat conduction problems [5–7]. Thus, the function estimation is performed with two kind of objective functions, one with heat flux and another without heat flux as one of their components.

After identifying which kind of objective function is more effective in solving the inverse problem, analysis is further extended to point out which state variable (either temperature or moisture content) is associated strongly with those properties.

In the remaining part of this chapter, it shall also introduce heat flux as one of the elements of objective functions. Even though there is no direct measurement of heat flux entering the dough, heat flux data were available before solving the principle inverse problem for estimating the dough properties during baking.

Objective function

Ordinary least square (OLS) is used for the both the cases as objective function. Since the functions to be estimated are in non-dimensional form, the coefficients that are to be estimated are almost in similar range of order of magnitude. The objective function for the case ignoring heat flux as its components is given as OLS

$$\text{OLS} = \left[X(x, t) - \theta(x, t) \right]^T \left[X(x, t) - \theta(x, t) \right] + \left[Y(t) - \bar{U}(t) \right]^T \left[Y(t) - \bar{U}(t) \right] \quad (4.8)$$

And for the case with heat flux as one of the components is tagged as OLS_q by the following equation

$$\begin{aligned} \text{OLS}_q &= \left[X(x, t) - \theta(x, t) \right]^T \left[X(x, t) - \theta(x, t) \right] \\ &+ \left[Y(t) - \bar{U}(t) \right]^T \left[Y(t) - \bar{U}(t) \right] + \left[Z(t) - q(t) \right]^T \left[Z(t) - q(t) \right] \end{aligned} \quad (4.9)$$

As of now for the purpose of analysis, the properties like conductivity, heat capacity, mass diffusivity are considered as function of moisture content and Biot number as function of baking

time. In following section, a detailed study is executed for identifying which state variable should be considered.

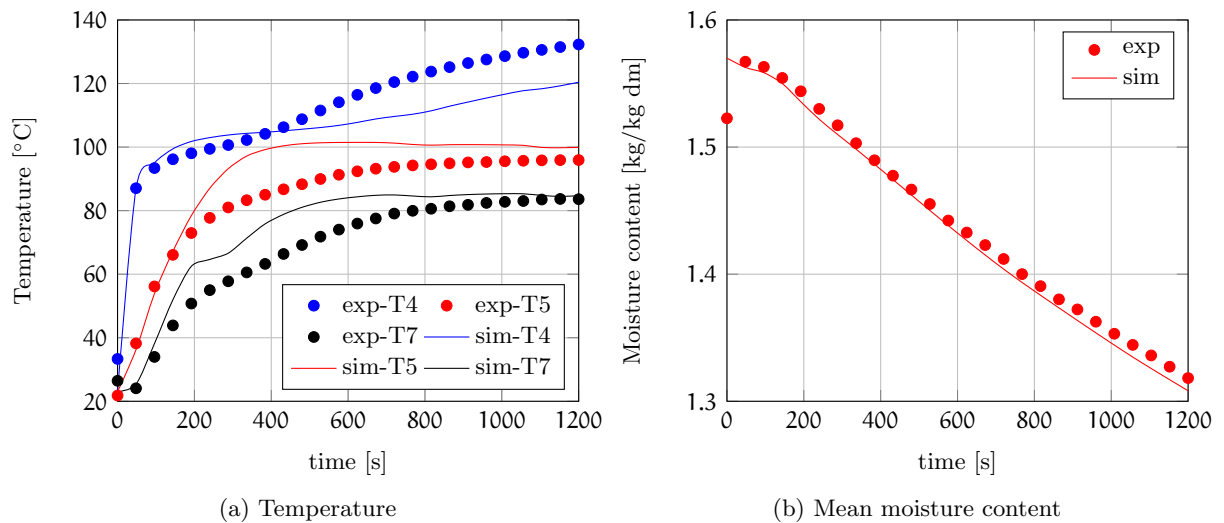


Figure 4.7: Comparison of measurements and simulations of temperature (a) and mean moisture content (b) for model without heat flux in objective function OLS

In the former case OLS, the properties that are to be estimated are thermal conductivity k^* , volumetric heat capacity C^* and mass diffusivity D^* but in latter case OLS_q , an additional Biot number appears. The approximation of temperature and moisture content profiles against experimental data for case OLS is displayed in figure 4.7. Looking closely at the trends, there is some improvement in the temperature approximation while comparing with the temperature profiles from parameter estimation given in last chapter. The most important features in temperature profile are a plateau at boiling point of water and then a linear increase in temperature when there is no more free water available for evaporation. The same is seen in the temperature at T4, but they did not follow exactly the same path as the measured data. From this analysis, it can be said that certain thermal and mass transfer properties are functions of state variables. Concerning the moisture content profile, the deviation between the measured and simulated profiles are minimal.

Figure 4.8 gives the result of inverse solution for the case with heat flux in objective function. The variation between measured and simulated results for temperature, moisture content and heat flux are insignificant. The temperature especially at sensor location T_4 is much more closer to the measured profile. The simulated moisture content and heat flux profiles follows almost exactly the path of measurements. It depicts that inclusion of heat flux measurement will definitely help in improving the accuracy of inverse problem.

The absolute difference between the measured and simulated profiles for moisture content and temperature, of both the cases are showcased in figure 4.9. At any given sensor location and time, for both the state variables, the profile simulated from OLS_q (represented by square symbols) are lower than the other case OLS (represented by circle symbols). For these cases, the maximum deviations for temperature are spotted at sensor T_5 around baking time 400 seconds. As there is increase in moisture content due to condensation and migration of water, thermal properties are greater than expected and it caused an inevitable increase in core temperature than expected. The temperature difference at T_4 were minuscule initially and in later stage it becomes larger in

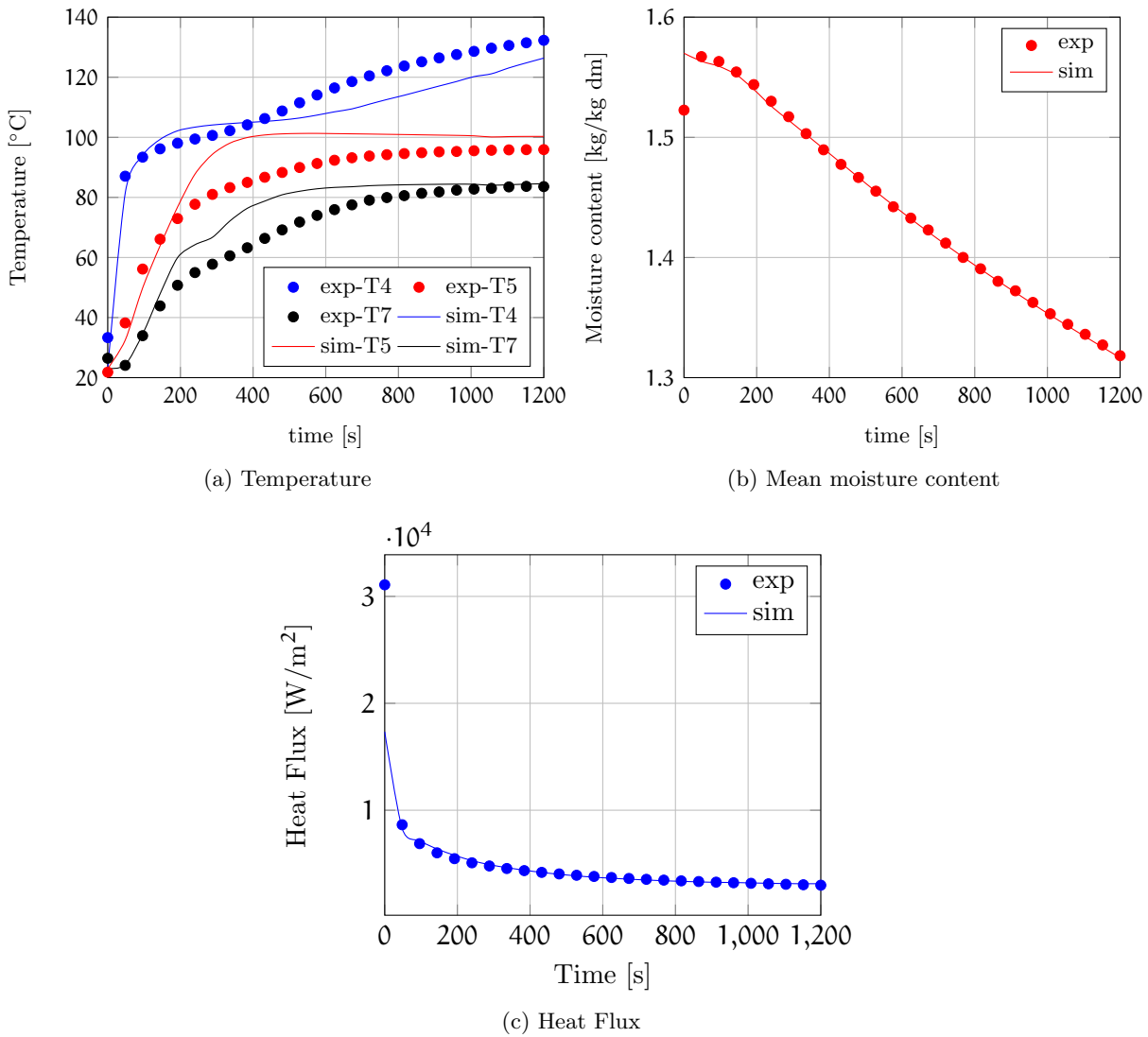


Figure 4.8: Comparison of measurements and simulations of temperature (a), mean moisture content (b) and heat flux(c) for model with heat flux in objective function OLS_q

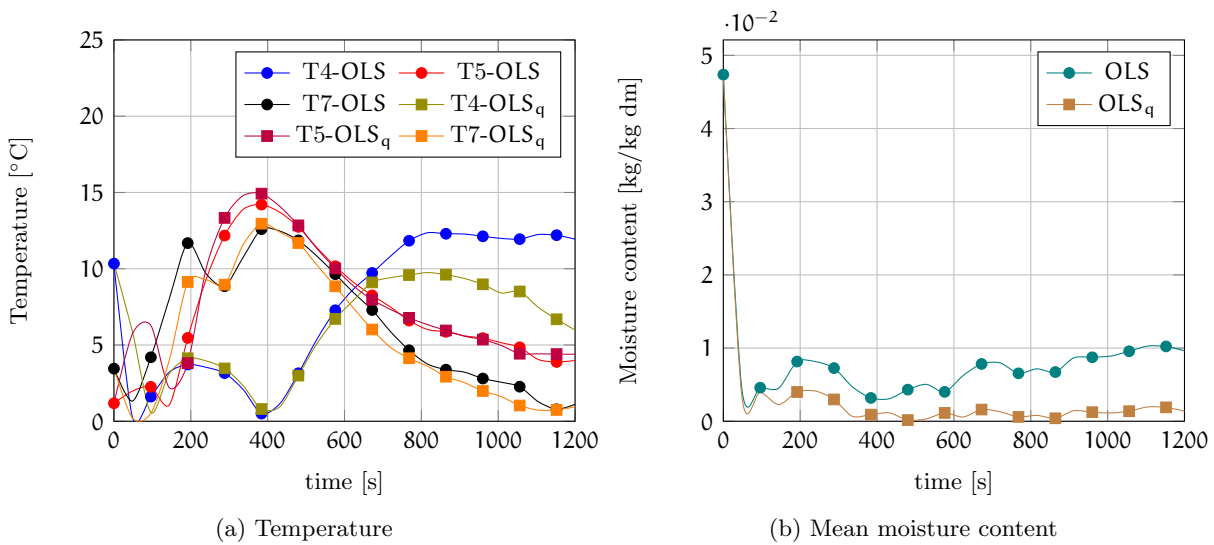


Figure 4.9: Absolute difference between measurements and simulations of temperature (a) and mean moisture content (b) for model without heat flux (OLS) and with flux (OLS_q) in objective function

its value. As per moisture content differences, the case OLS_q almost approaches to zero while compared to OLS.

The estimated properties as functions are given in figure 4.10 for both the cases. The thermal properties are almost similar for both cases but major difference is seen in mass diffusivity estimations. From the trends, it can be said that this model requires thermal properties that vary linearly with increase in moisture content. As the moisture content reaches the maximum value of 2.5, the thermal conductivity goes close to value of liquid water i.e. 0.6 W/mK . Similarly for heat capacity, the estimation reaches the value corresponding to heat capacity of liquid water. The mass diffusivity of liquid water, for OLS case have an exponent increase in their value as increase in moisture content but for OLS_q case, the trend is quite different and is lower than the other case. The heat transfer coefficient decreases almost linearly until first half of baking time and showed an increase there after. The reason behind this curvature is due to transformation of liquid to solid phase that has decreased the value of convective heat transfer. Due to formation of a stiff solid which can not enforce a perfect contact, it has introduced thermal contact resistance that increases along the baking time.

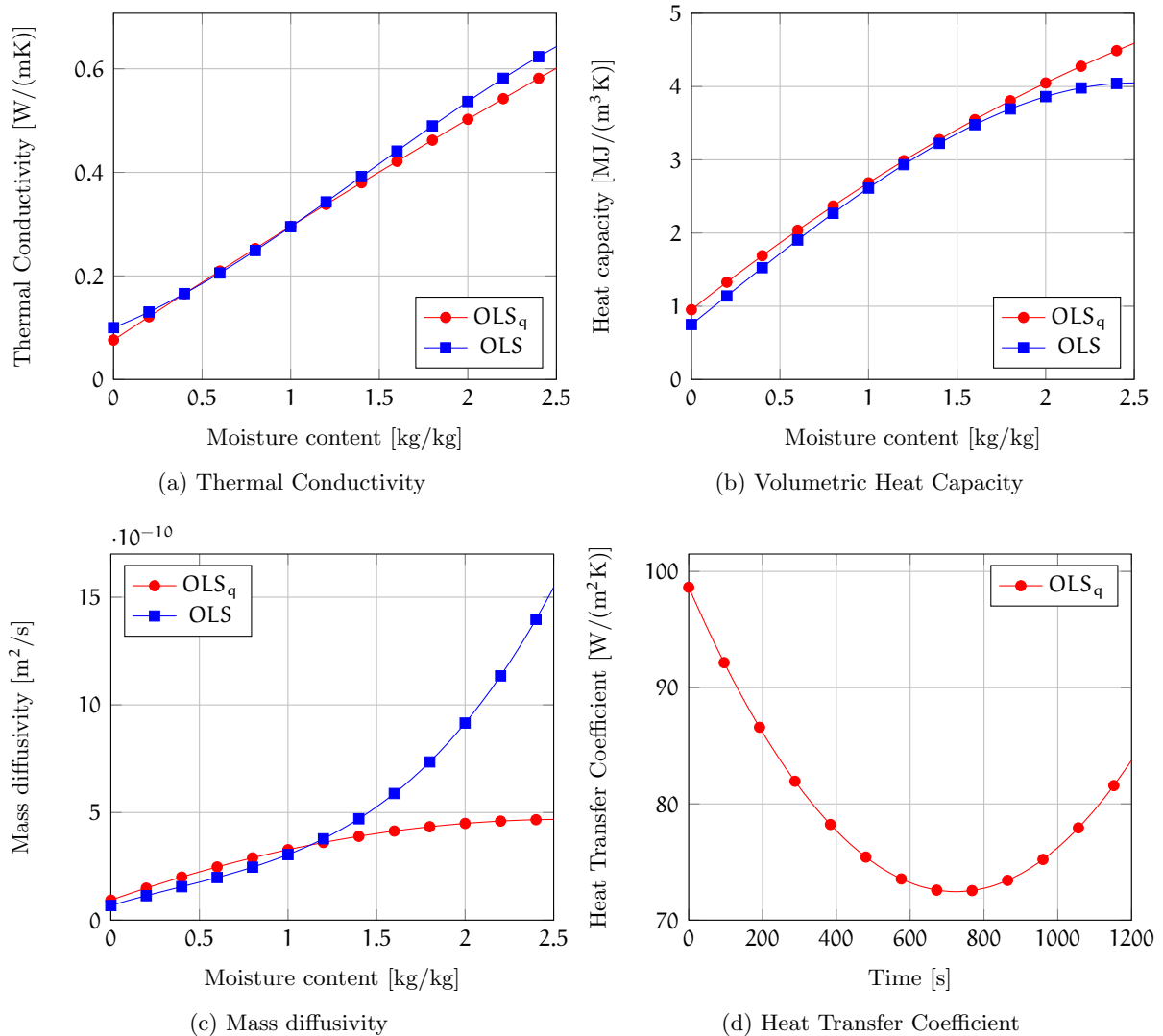


Figure 4.10: Comparison of thermophysical properties for model with (OLS_q) and without (OLS) heat flux in objective function

4.3.4 Functionality

Until now, the influential properties are considered as functions of moisture content in this chapter. But it is uncertain whether these properties are functions of temperature or moisture content or sometimes both. Thus, an elaborate study with different cases listed in table 4.11 are demonstrated with their inverse solution. The order of spline is chosen as 3 and knots with respect to moisture content is same and for temperature is $[0, 0, 0, 0.5, 0.5, 0.5]$, since 0.34 is the maximum temperature reached inside the dough in dimensionless form during experimentation. The objective function with heat flux measurements OLS_q is considered for the following cases. Since the governing equations are in non-dimensional form, changing their functionalities do not require any modification in the equations or in their implementation.

Case	Properties function of		
	k	ρc_p	D_t
I	U	U	U
II	T	T	U
III	T	U	U
IV	T, U	U	U

Table 4.11: Cases with T - temperature and U - moisture content

Case I

The considered case is exactly same as the one presented in previous section with heat flux. Since enough examination of this case is already done, the study is proceeded to next case.

Case II

In this case study, the thermal properties are taken as function of temperature and mass diffusivity as function of moisture content. Figure 4.11 gives the approximated results using inverse problem for the case. The temperature profile which is focused at sensor location T4 did not resemble a preferred profile. The results are not satisfactory and are much closer to parameter estimation performed earlier.

Case III

Volumetric heat capacity is generally formulated as summation of their values as per their composition ratio. Thus, it is completely fair to consider heat capacity as function of moisture content. But as for thermal conductivity, it is taken as function of temperature which might solve the undesired temperature raise at sensor location T5 as seen in last case.

The agreement between measured and simulated profiles for the case can be understood from figure 4.12. This case has resulted the maximum deviation for moisture content and temperatures. There is no linear rise of temperature after a plateau observed at T4. Considering thermal conductivity as function of temperature does not play an vital role in improving the approximation process and in fact, it has degraded the result.

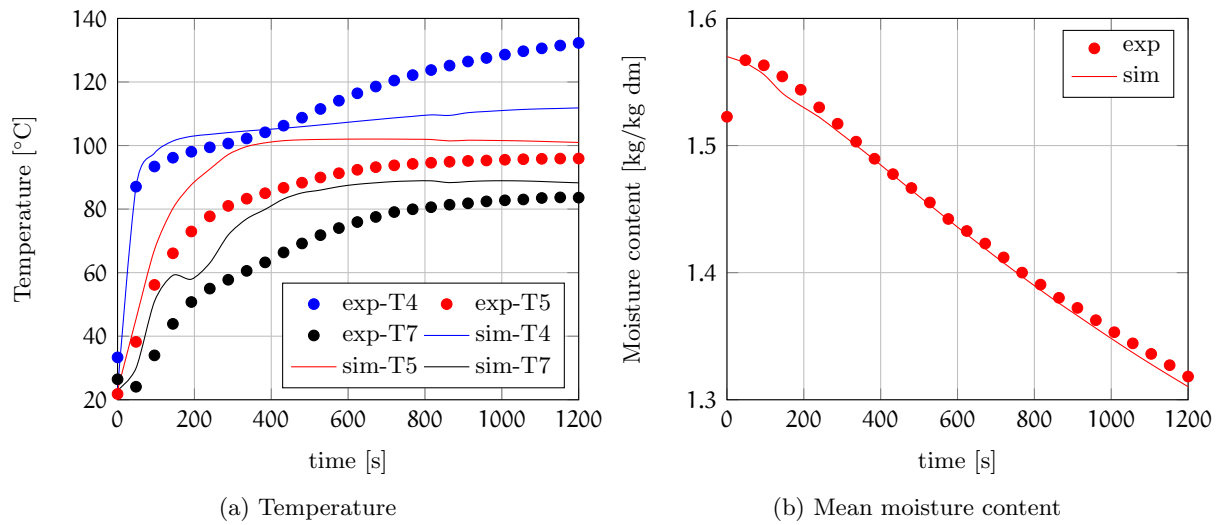


Figure 4.11: Comparison of measurements and simulations of temperature (a) and mean moisture content (b) for test case II

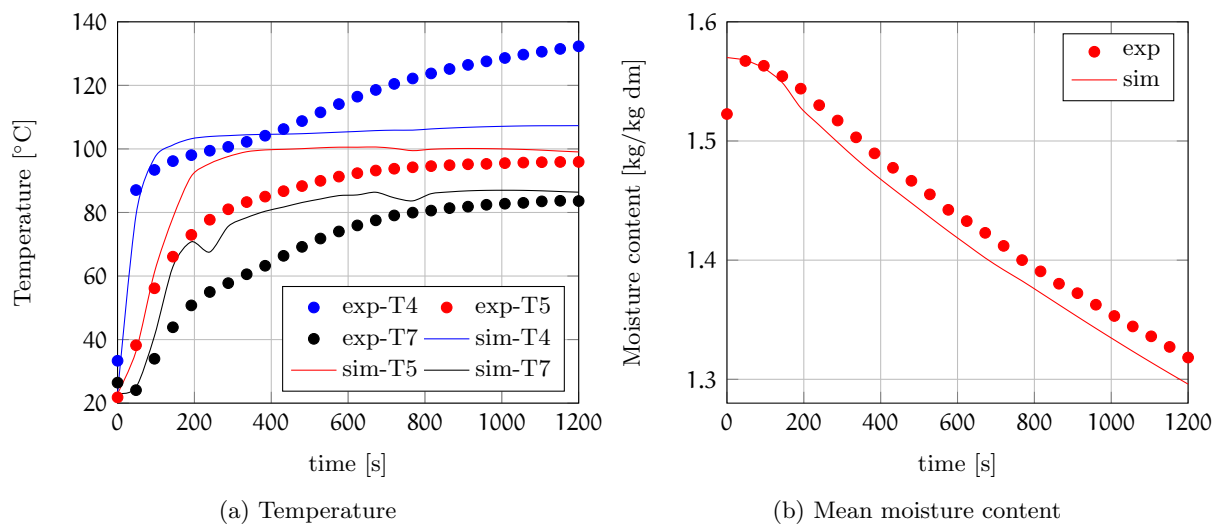


Figure 4.12: Comparison of measurements and simulations of temperature (a) and mean moisture content (b) for test case III

Case IV

Considering thermal conductivity as function of temperature did not have a desirable results but by considering as function of moisture content is much better. Hence, thermal conductivity is taken as function of temperature and moisture content in this case. Though β -spline can be extended for surface estimation, implementation or interpolation of a surface imported in COMSOLTM had created some hindrance during estimation process. Thus, the thermal conductivity $k(T,U)$ is formulated by exponential Arrhenius function and expressed by [8]

$$k(T,U) = \underbrace{\frac{k_1}{1+U} \exp\left(-\frac{E_1}{R} \times \left(\frac{1}{T} - \frac{1}{T_r}\right)\right)}_I + \underbrace{\frac{k_2 U}{1+U} \exp\left(-\frac{E_2}{R} \times \left(\frac{1}{T} - \frac{1}{T_r}\right)\right)}_{II} \quad (4.10)$$

There are four key parameters k_1 , k_2 , E_1 and E_2 that tune the behavior of this mathematical function. In the equation, term I corresponds to thermal conductivity for dry state or when moisture content approaches zero while II term represents conductivity for wet state or when moisture content tends to ∞ . The thermal conductivity for each state, i.e. either dry or wet, is governed by Arrhenius energy equations. With suitable transformations, this thermal conductivity is converted into non-dimensional form

$$k^*(\theta, U) = \frac{k_1^*}{1+U} \exp\left(-k_2^* \times \left(\frac{1}{\theta+1} - \frac{1}{\theta_r+1}\right)\right) + \frac{k_3^* U}{1+U} \left(-k_4^* \left(\frac{1}{\theta+1} - \frac{1}{\theta_r+1}\right)\right) \quad (4.11)$$

Other properties such as heat capacity, mass diffusivity of liquid water and convective heat transfer are considered in similar fashion as in case I. Figure 4.13 shows how well the inverse solution admit with measurements of temperature and moisture content. The temperature profile especially at bottom sensor T4 is much more accurate than case I but it also resulted in unexpected rise at T5 for first half of baking period. The simulated mean moisture content obeys the trend of measured values.

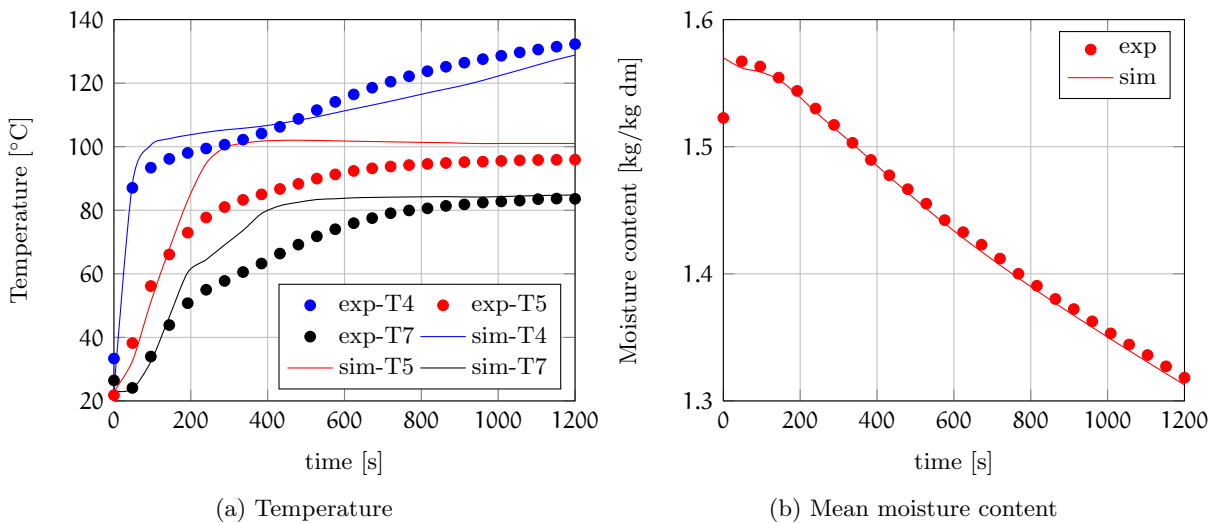


Figure 4.13: Comparison of measurements and simulations of temperature (a), mean moisture content (b) and heat flux(c) for case IV

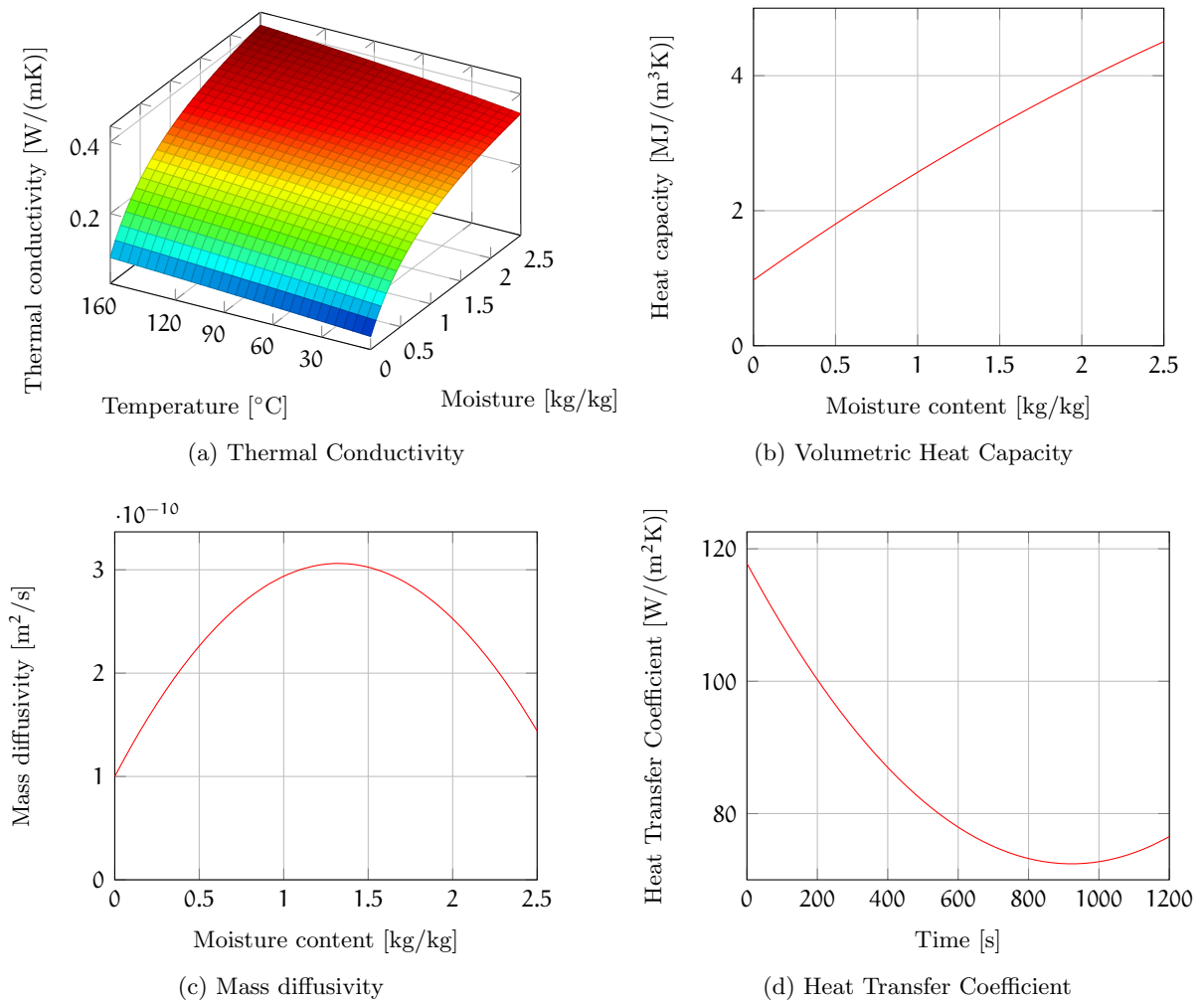


Figure 4.14: Estimated thermophysical properties for case IV

Since the deviation of simulated and measured profiles for temperature and moisture content are minimal for the case, their estimated properties are given in figure 4.14. Volumetric heat capacity that is estimated in this case is quiet similar to the estimation of case I. The thermal conductivity reaches a maximum value of 0.4 W/mK when the medium is moist whereas in the former discussed case I, the value was near to liquid water conductivity 0.6 W/mK. Thermal conductivity has a linear and minor increase in its value as there is increase in temperature.

The approximated convective heat transfer of this case can be related to the estimated profile as in case I. Though its magnitude is slighter higher in the current case, the trends are similar. On contrast, the mass diffusivity has complete mismatch with the last presented profile. A decreasing diffusivity trend is noted for higher moisture content values. This kind curvature does not follow the physics of mass transfer and, in general it should increases as moisture content increases to facilitate mass transfer.

Summary

Table 4.12 gives the rms between the measured and simulated data of temperature, mean moisture content and heat flux for various cases used. Overall, case I and IV gives better solutions than other two cases. The cases II and III have either any of their thermal properties as function of temperature. Despite employing the information of heat flux, these cases have terribly failed to give desired results. Heat flux, moisture content and temperature at T_4 have smallest rms values for case IV. Even temperature at free surface was comparable to the lowest value of temperature rms from case I. Yet the inverse solution for case IV, especially the mass diffusivity was not satisfactory and does not resemble the physics behind mass diffusion. For this reason only, case I whose rms values are close to case IV and this case have estimated physical properties that are similar to the one used in literature for other baking process like bread.

rms		Case I	Case II	Case III	Case IV
Temperature [$^{\circ}$ C]	T_4	9.11	12.84	15.65	6.73
	T_5	9.14	12.35	10.37	10.52
	T_7	6.93	11.19	10.89	7.55
Mean Moisture content $\times 10^2$		1.29	1.97	5.40	1.17
Heat flux [W/m^2] $\times 10^{-2}$		7.57	16.86	12.80	6.32

Table 4.12: rms comparison

The main summaries of the inverse solutions with different formulations are:

- Utilization of heat flux measurement has enhanced the accuracy in estimation procedure.
- Thermal and mass transfer properties were strongly influenced by moisture content.
- Considering the properties dependent on temperature, they did not provide enough information on crust-crumbs transformation.
- There was no major improvement in the inverse solution of the case considering thermal conductivity as function of both temperature and moisture content while compared to solution with conductivity taken as function of moisture content only.

- None of the cases succeed in reducing the distance between measured and simulated temperature profiles at location T5 during first 600 seconds of baking. If the local variations of moisture content were available, it would have helped in finding more accurate mass diffusivity and other properties. In practical, there is increase in moisture content at center due to condensation of water vapor and migration of liquid water towards the core. Since, the value of thermal properties increases with increase in moisture content, it was resulted in undesirable rise in temperature at core.
- With available of local moisture content, more accurate and precise estimation of properties will be feasible.
- There is no significant difference was spotted in estimation and inverse solutions for models with spline order between cubic and quadratic.

4.3.5 Literature

The profile of estimated properties are compared with the predefined functions from literature for bread baking. Even though this properties discussed here does not represent the exact material or the process, the comparison is carried out to know whether these properties are in the similar league. Thermal conductivity is expressed by Maxwell's formulation for a porous media with constant porosity $\pi = 0.76$ [9, 10]

$$k = k_d \frac{2k_d + k_g - 2\pi(1 - S)(k_d - k_g)}{2k_d + k_g - \pi(1 - S)(k_d - k_g)} \quad \text{where } k_d = \frac{\pi k_s + \pi S k_l}{\pi + \pi S} \quad [W/mK] \quad (4.12)$$

where k_s , k_l and k_g are conductivity of solid, liquid and gases whose value are chosen as 0.2, 0.6, 0.025 W/mK respectively and S is liquid saturation inside the medium. The volumetric heat capacity with different phases is generally governed in series as

$$\rho c_p = \rho_s^a c_{p_s} + \rho_l^a c_{p_l} + \rho_g^a c_{p_g} \quad [J/m^3K] \quad (4.13)$$

With c_{p_s} , c_{p_l} and c_{p_g} are specific heat capacity of solid, liquid water and gas respectively. The solid heat capacity is given as 1600 kg/m³. Finally, the mass diffusivity of liquid water for bread baking process is provided by exponential function [10]

$$D_l = 2 \times 10^{-9} \exp(\pi(-2.8 + 2U)) \quad [m^2/s] \quad (4.14)$$

Since the deformation effect was not considered in the model, the porosity remained constant here. These properties from literature expression are also vary linearly. Figure 4.15 gives the graphical comparison of the estimated and reference properties as function of moisture content.

The reference thermal conductivity is taken from Maxwell's expression which is a general form for any porous media with multiphase system. Thus, the evolution of conductivity with respect to moisture content align closely with the reference. Similarly for heat capacity, the most suitable expression for any kind of multiphase system is chosen and it gave a good comparison. Thermal conductivity and heat capacity are quite close to each other but there is huge difference for mass diffusivity. Since the literature expression is constrained mathematical, these profiles did not match but they have similar order of magnitude.

The inverse of convective heat transfer coefficient represents the thermal contact resistance that arose due to improper contact between the surfaces. In previous work of similar study, it was found that the thermal contact resistance is approximately $15.6 \text{ m}^2\text{K}/\text{kW}$ [11, 12]. The present study also resulted an average thermal contact resistance of value $15 \text{ m}^2\text{K}/\text{kW}$. From this comparison study, it can be conclusively understood that the estimated properties are in similar range to those presented in literature for other baking process.

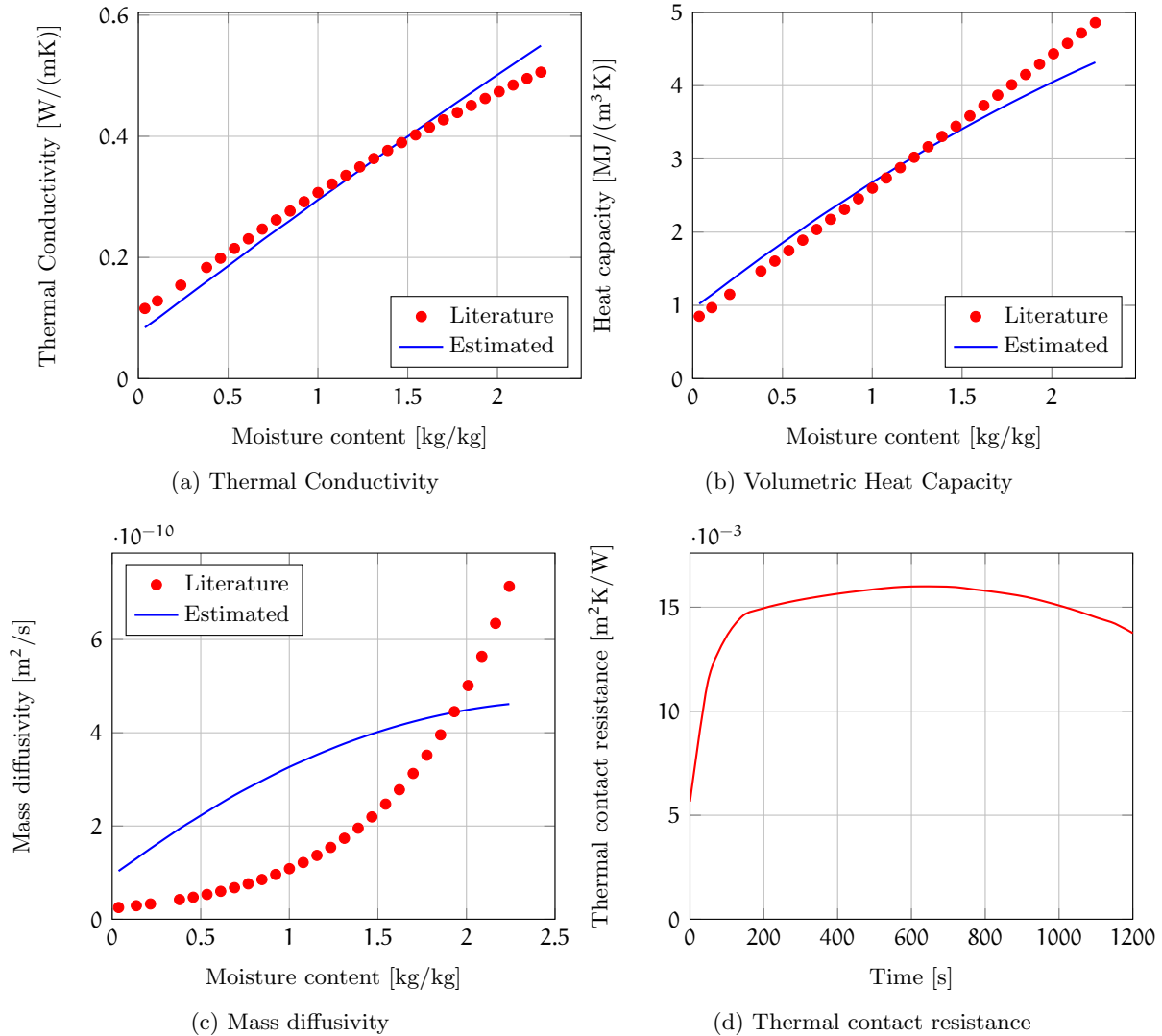


Figure 4.15: Overview of estimated thermophysical properties for model with heat flux in objective function compared against literature data

4.4 Note about one way coupling

Some authors have been using one-way coupling to link deformation effect in their mathematical models. In one way coupling, the author prescribes the deformation of geometry measured during experimentation directly in the model with aid of moving mesh algorithm. In this case, the deformation will have no influence or impact on any of the state variables as they are uncoupled. This study is carried out to know whether this kind of formulation is capable of describing precisely the deformation effect along with heat and mass transfers or not. The mathematical

model and the thermophysical properties shall remain same and only thing that vary from the previous presented model is implementation of ALE (Arbitrary Lagrangian Euler - moving mesh) along with other PDF solvers for the model in COMSOLTM. From the experimental measurement of overall volumetric variation, the final height of the dough is formulated as function of baking time. This formulated helps in determining mesh velocity that is required to employ the change in geometric dimensions. The deformation of dough in % can be visualized from figure 4.16(d).

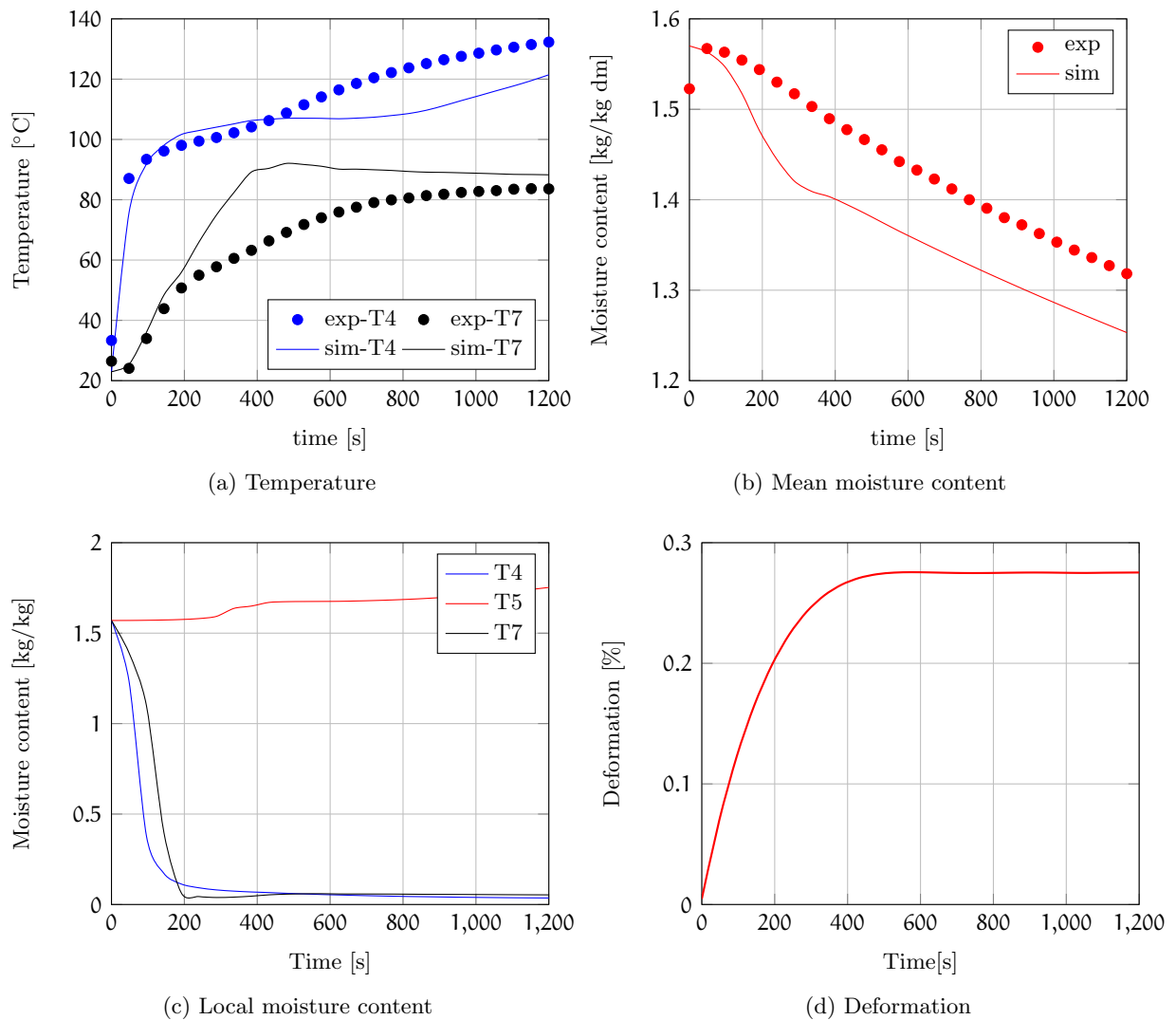


Figure 4.16: Comparison of measurements and simulations of temperature (a), mean moisture content (b), local moisture content (c) and deformation in % (d) for model with one-way coupling

On comparing the simulated and experimental results, they are quite different from the previous discussed results. It should be noted that the thermophysical properties were not estimated as per the current modeling approach. Hence, it is common to expect certain variations in the results. Both temperature and mean moisture content trends have much deviations from measurements. The mean moisture content has faced such a worst agreement due to elongation and averaging effects. The deformation by this form is simple elongation of the domain length and rearranging the mesh elements instantaneously. In such cases, the moisture content at the elongated region does not correspond to real physical values.

To validate the point whether one-way coupling is best suited for inverse problem or not, following analysis is performed. The variation in node position along the time is plotted in figure 4.17(a)

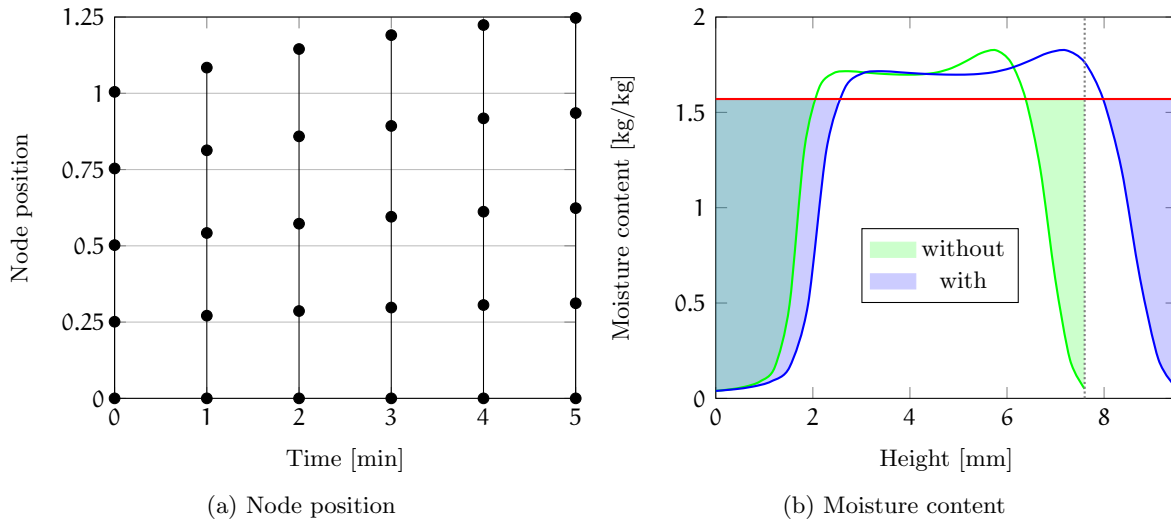


Figure 4.17: Evolution of nodes during deformation with respect to time (a) and comparison of moisture content for model with and without deformation (b)

for first five minutes as upto this point only maximum deformation is noted. It can be seen that gap between the nodes are equivalent as per variation in overall length. The gap between nodes is increasing linearly as there is increase in overall length. In FEM solver, the governing equations are solved over discretized element domain. These governing equations are transformed into weak formulations and then solved for each elements. The solution of each individual elements are then approximated through weighted interpolations. Thus in most of the complicated cases, the solutions are mesh dependent. In the case of one-way coupling, the nodes are stretched and elongated to match to deformation that is imposed in the model. Due to elongation of nodes, the solutions of individual elements as well as the interpolation steps are altered which causes to lower or increase the values of certain state variables. In such cases, the calculated variables wont be able to follow the similar trends with the same model with out any deformation. Such difference in computation of moisture content for either models are given in figure 4.17(b). It is clearly visible that the area covered for moisture loss of the case without deformation is almost doubled for the case with deformation. These factors have affected the temperature profiles also at free surface.

Conclusively, the local moisture content seems to follow the phenomenon observed during baking but the overall mass loss is literally doubled due to lack of interconnection between transport phenomenon and solid mechanics during baking. Hence, the model with one way coupling does not support approximation of thermophysical properties by inverse problem.

4.5 Conclusive remarks

In the beginning of this chapter, simultaneous estimation of parameters for the three models, **TM**, **TMPN** and **TMPE** with the experimental measurements were preformed for various objective functions. The weighted least square objective function with significant weight given to temperature, provided better and desirable results for all the models. Out of these models, **TMPE** model has given better approximation for moisture content and temperature except at sensor location near interface of cast-iron and dough.

These constant parameters has failed to capture the crust-crumbs transformation by the models. Such phenomenon can be taken into account by employing thermophysical properties as functions of state variables. Thus, **TMPE** model was extended for function estimation of most influential properties like thermal conductivity, heat capacity and mass diffusivity of liquid water. The one of main reasons for opting specially **TMPE** model is due to better sensitivity for the parameters with respect to temperature and moisture content that helps in accurate estimations.

Usually, inverse heat conduction problem (IHCP) is solved based on temperature information from several locations. But some authors have provided an insight of using heat flux measurement of solving such problems. In this chapter, a study was performed to identify whether inclusion of heat flux data in objective function will have any improvement on inverse problem or not. Though such action has introduced additional parameter to be identified, the inverse solutions of this case were much superior than the case without heat flux measurement. At any sensor location and time, the difference between the simulated and measured profile were minimal for case with heat flux data.

Until now, it is unclear in formulating dependency of the heat and mass transfer properties. Authors have generally used thermal properties as function of temperature and mass transfer dependent on moisture content. In order understand the dependency of these functions with respect to state variables, four case studies were employed. The cases with any thermal properties that is function of temperature had inverse solution that were quiet similar to results of parameter estimation. But for cases with properties reliant on moisture content had desirable outputs. While utilizing thermal conductivity as function of both temperature and moisture content and other properties relying on moisture content, the objective function was lowest. But this case had the estimated mass diffusivity that did not imply the reality behind mass transfer. By overview of these results, it is concluded that thermophysical properties invoked in a baking process of a highly moist dough are largely reliant on moisture content than temperature.

List of symbols

Latin symbols

a_w	Water activity
T1 - T7	Thermocouples
q	Heat flux [W/m ²]
C_p	Specific heat capacity [J/(kg.K)]
T	Temperature [K]
t	time [s]
H	Evaporation rate constant [s]

D_i	Mass diffusivity of component i [m^2/s]
k	Thermal conductivity [$W/(mK)$]
h_q	Convective heat transfer coefficient [$W/(m^2K)$]
h_m	Convective mass transfer coefficient [m/s]
L	Length of the domain [m]
X_p	Sensitivity of coefficient p
exp	Experimental measurements
sim	Simulated data

Greek symbols

ρ	Density [kg/m^3]
λ	Latent heat of vaporization [J/kg]
μ_g	Dynamic viscosity of gas [$Pa.s$]
k_g	Gas permeability [m^2]
Δ	Small perturbation or Determinant
ε	Relative error in %
η_l	Variance of parameter l

Dimensionless numbers

θ	Temperature
U	Moisture content
α_q^*	Thermal diffusivity
α_p^*	Capillary diffusivity
D_l^*	Liquid water diffusivity
D_v^*	Water vapor diffusivity
P_g^*	Gas pressure
H^*	Evaporation rate constant

Bi_i	Biot number with $i = q$ or m
R_1	Latent heat of vaporization
t^*	time
Ω_i	Parameter vector of model i
M_i	Measured vector of component i
E_i	Estimated vector of component i
g^*	Source term
k^*	Thermal conductivity
C^*	Heat capacity
X	Measured temperature when without index
Y	Measured mean moisture content
Z	Measured heat flux

Subscripts

q	heat
m	mass
l	liquid
v	vapor
sat	saturated
int	initial
ref	reference
f	final
eff	effective
surface	location at interface between dough and cast-iron

Superscripts

$*$	elements in non-dimensional form
-----	----------------------------------

0	location at $x^* = 0$
L	location at $x^* = L$
θ	heat
U	moisture content
g	gas

Abbreviations

OLS	Ordinary Least Square
OLS _q	Ordinary Least Square with heat flux
WLS	Weighted Least Square
SLS	Scaled Least Square

Bibliography

- [1] Mathieu Lostie, Peczalski, Julien Andrieu, and Michel Laurent. Study of sponge cake batter baking process. ii. modeling and parameter estimation. *Journal of Food Engineering*, 55, 2002.
- [2] Aberham Hailu Feyissa, Krist V. Gernaey, and Jens Adler-Nissen. Uncertainty and sensitivity analysis: Mathematical model of coupled heat and mass transfer for a contact baking process. *Journal of Food Engineering*, 109:281 – 290, 2012.
- [3] Philip Kosky, Robert Balmer, William Keat, and George Wise. Chapter 12 - mechanical engineering. In Philip Kosky, Robert Balmer, William Keat, and George Wise, editors, *Exploring Engineering (Third Edition)*, pages 259 – 281. Academic Press, Boston, third edition edition, 2013.
- [4] A. Ousegui, C. Moresoli, M. Dostie, and B. Marcos. Porous multiphase approach for baking process - explicit formulation of evaporation rate. *Journal of Food Engineering*, 100:535–544, 2010.
- [5] Mustapha Samaï and Tahar Loulou. A comparative study of heat flux and temperature based objective functional to solve inverse heat conduction problems. *Numerical Heat Transfer, Part B: Fundamentals*, 56(1):75–104, 2009.
- [6] Tahar Loulou and Elaine P. Scott. An inverse heat conduction problem with heat flux measurements. *International Journal for Numerical Methods in Engineering*, 67(11):1587–1616, 2006.

- [7] Jianhua Zhou, Yuwen Zhang, J. K. Chen, and Z. C. Feng. Inverse heat conduction using measured back surface temperature and heat flux. *Journal of Thermophysics and Heat Transfer*, 24(1):95–103, 2010.
- [8] Z.B. Maroulis, G.D. Saravacos, M.K. Krokida, and N.M. Panagiotou. Thermal conductivity prediction for foodstuffs : Effects of moisture content and temperature. *International Journal of Food Properties*, 5(1):231–245, 2007.
- [9] James K. Carson, Simon J. Lovatt, David J. Tanner, and Andrew C. Cleland. Thermal conductivity bounds for isotropic, porous materials. *International Journal of Heat and Mass Transfer*, 48(11):2150–2158, 2005.
- [10] J. Zhang and A. K. Datta. Mathematical modeling of bread baking process. *Journal of Food Engineering*, 75(1):78–89, 2006.
- [11] S. Marc, J. P. Ploteau, P. Le Bideau, and P. Glouannec. Transient heat flux estimation during the baking of cereal batter by contact heating. *International Journal of Heat and Mass Transfer*, 155:119848, 2020.
- [12] Sylvain Marc. *Experimental and numerical study of a direct contact heating process*. PhD thesis, Université Bretagne Sud, 2017.

Conclusion

This work focuses on estimation of thermophysical properties of an one sided baking process as constants and functions. The major aspects covered by the chapters are:

1. The experimental observations made during baking process are governed by mathematical models with different approaches. These models are transformed into dimensionless form to ease the estimation of parameters. These models are then validated with available data from literature. Form the validation steps, all the three models were good enough to result the phenomenons seen in experiments except deformation.
2. The identifiable parameters are found out using the sensitivity analysis evaluated by complex step differentiation. It was discovered that the capillary diffusivity arose from Darcy law of permeability is difficult to estimate along with other parameters. In **TM** and **TMPN** models, the mass transfer properties are mostly sensitive to moisture content and show weak sensitive with respect to temperature. But **TMPE** model has mass transfer properties responsive to both moisture content and temperature. It is due to equilibrium approach that interconnects heat and mass transfer phenomena to a greater extent. The optimal number and location of thermocouples are spotted by means of Design of experiments. D-optimality has showed that it is enough to have three sensors located at either ends and center of the medium. Correlation study between the parameters pointed out that the **TMPE** model has most of the parameters are linearly dependent on each other. A numerical study with synthetic data has recognized that the best objective function is weighted least square with significant weight given to temperature measurements.
3. The estimation of parameter vectors from **TM**, **TMPN** and **TMPE** models are performed. The temperature profiles that were less than 100 °C and mean moisture content profiles were accurately approximated in all the three models. Out of these models, **TMPE** model has least rms error between simulated and measured data. The outcomes of inverse solutions clearly indicate the point that none of the models has successfully represented the crust-crumbs transformation from dough which will reflect in temperature profile. To overcome this, the thermophysical properties are considered as functions of state variables. For function estimation, an objective function with heat flux measurements along with temperature and moisture content, has superior inverse solution than the objective function without heat flux. Moreover, it is also identified that the physical properties are largely dependent on moisture content than temperature. The estimated properties are close enough to the functions given in literature.

Future work

The present work gave attention to the models that have ignored the deformation of volume during baking. In future, a mechanistic model with equilibrium approach for evaporation rate coupled with structural mechanics can be used to simulate the temperature, moisture content variations along with volume change. This model than can be used to estimate the properties like viscosity, relaxation time, capillary diffusivity, etc that play a significant role in governing equation of solid mechanics while other properties can be used from this study. With availability of all the required parameters, optimal heat source required for baking process that results desirable physical attributes can be evaluated eventually.

Appendix A

Heat-flux estimation

Incoming heat flux is estimated in two stages: first estimation of initial temperature distribution to increase accuracy in upcoming inverse problem and second estimation of heat flux as function of time. Before seeing the inverse procedure, the governing equations and required physical properties are looked.

A.1 Governing equations

The heat flow in cast iron disk is formulated by Fourier law of conduction in metals. The problem is transformed from two-dimensional to one-dimensional as the circumference are insulated. The total height of the cast iron is 2 cm but for the convenience it is considered upto location of bottom sensor which becomes 1.5 cm. The reason for curtailing the bottom part which is exposed to induction coil is to minimize the error and directly taking the measurement temperature as boundary condition.

$$\mathcal{O}(T) = \rho(T)C_p(T)\frac{\partial T}{\partial t} - \nabla(k(T)\nabla T) = 0 \quad (\text{A.1})$$

With applied negative heat flux (since heat is removed) at top surface and Dirichlet boundary condition at bottom surface.

$$-k(T)\nabla T(L, t) = q(t) \quad (\text{A.2})$$

$$T(0, t) = T_1(t) \quad (\text{A.3})$$

The thermophysical properties of cast iron used is presented in figure A.1.

A.1.1 Variational problem

For a functional $f(T)$, Taylor series expansion is given as [1],

$$f_\epsilon(T_\epsilon) = f(T) + \epsilon \frac{\partial f}{\partial T} \Delta T + \epsilon \Delta f(T) \quad (\text{A.4})$$

The final term on right hand side is not considered, if $f(T)$ is assumed to be known. Since here the heat flux is to be estimated as function of time, the remaining thermophysical properties such as k , ρ and C_p which are function of temperature are known beforehand. The variational

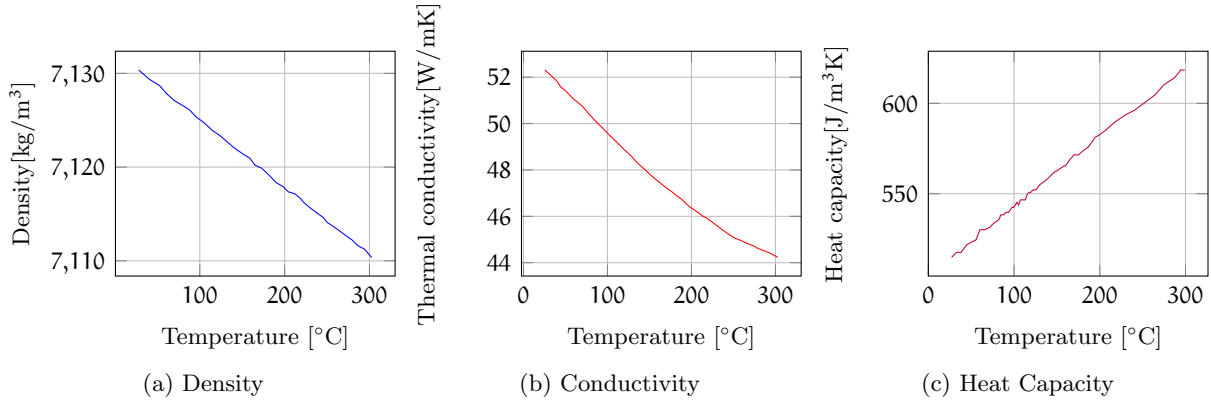


Figure A.1: Thermophysical properties of cast iron

problem is formulated by perturbing the function and subtracting from its original state as

$$\Delta f(T) = \frac{f_\epsilon(T_\epsilon) - f(T)}{\epsilon} \quad (\text{A.5})$$

Thus the governing equation is perturbed as,

$$\rho_\epsilon C_{p_\epsilon} \frac{\partial T_\epsilon}{\partial t} = \frac{\partial}{\partial x} \left\{ k_\epsilon(T_\epsilon) \frac{\partial T_\epsilon}{\partial x} \right\} \quad (\text{A.6})$$

On expanding the above equation as per Taylor series,

$$\begin{aligned} & \left\{ \rho(T) + \epsilon \frac{\partial \rho}{\partial T} \Delta T \right\} \left\{ C_{p_\epsilon}(T) + \epsilon \frac{\partial C_p}{\partial T} \Delta T \right\} \left\{ \frac{\partial T}{\partial t} + \epsilon \frac{\partial \Delta T}{\partial t} \right\} = \\ & \frac{\partial}{\partial x} \left\{ \left(k(T) + \epsilon \frac{\partial k}{\partial T} \Delta T \right) \left(\frac{\partial T}{\partial x} + \epsilon \frac{\partial \Delta T}{\partial x} \right) \right\} \\ & \rho C_p \frac{\partial T}{\partial t} + \epsilon \rho C_p \frac{\partial \Delta T}{\partial t} + \epsilon \rho(T) \frac{\partial C_p}{\partial T} \Delta T \frac{\partial T}{\partial t} + \epsilon \frac{\partial \rho}{\partial T} C_p(T) \Delta T \frac{\partial T}{\partial t} + \\ & + \epsilon^2 \left(\rho(T) \frac{\partial C_p}{\partial T} \frac{\partial \Delta T}{\partial t} \Delta T + C_p(T) \frac{\partial \rho}{\partial T} \frac{\partial \Delta T}{\partial t} \Delta T + \frac{\partial \rho}{\partial T} \Delta T \frac{\partial C_p}{\partial T} \Delta T \frac{\partial T}{\partial t} + \epsilon \frac{\partial \rho}{\partial T} \frac{\partial C_p}{\partial T} \frac{\partial \Delta T}{\partial t} \Delta T^2 \right) = \\ & \frac{\partial}{\partial x} \left\{ k(T) \frac{\partial T}{\partial x} + \epsilon k(T) \frac{\partial \Delta T}{\partial x} + \epsilon \frac{\partial k}{\partial T} \frac{\partial T}{\partial x} \Delta T + \epsilon^2 \frac{\partial k}{\partial T} \frac{\partial \Delta T}{\partial x} \Delta T \right\} \quad (\text{A.7}) \end{aligned}$$

On eliminating higher power of ϵ and subtracting equation (A.1) from equation (A.7) leads to,

$$\frac{\partial(\rho C_p \Delta T)}{\partial t} = \frac{\partial^2(k \Delta T)}{\partial x^2} \quad (\text{A.8})$$

and boundary conditions are obtained as,

$$-\frac{k \Delta T(L, t)}{\partial x} = \Delta q \quad (\text{A.9})$$

$$\Delta T(0, t) = 0 \quad (\text{A.10})$$

A.1.2 Adjoint problem

Usually for computation of gradient of objective function, sensitivity or Jacobian matrix is calculated using some numerical methods. In case of unknown parameters as constant, it is feasible to solve the sensitivity problem using any numerical methods like finite difference scheme. But for objective functional, solving sensitivity or variational problem requires variation of unknown function that is to be estimated which is not known prior. The adjoint problem is solved to get expression for gradient of objective function which is substituted as variation of the unknown function for solving variational problem. This procedure is achieved by help of Lagrangian multiplier [2]. Consider a auxiliary function $G(x,y,z)$ such that,

$$G(x, y, z) \equiv F(x, y, z) + \lambda\phi(x, y, z) \quad (\text{A.11})$$

subjected to constrain like $\nabla \cdot G = 0$ and λ is called Lagrangian multiplier and independent of x, y, z .

$$\Rightarrow 0 = \nabla \cdot F + \lambda \nabla \cdot \phi \quad (\text{A.12})$$

Mathematically, ∇F and $\nabla \phi$ are parallel which indicates that for a relative extrema of the function $F(x,y,z)$ occurring at a set of points, $\nabla F = 0$ and $\nabla \phi = 0$. Thus the necessary condition when the function $F(x, y, z)$ passes through set of points which leads to its extrema is $\nabla G = 0$. Similar approach is taken in case for computing gradient of objective function. Here G is objective function, F is equivalent to Euclidean distance between measurement and simulated results, ϕ is mathematical constrains (governing PDE equations used). Thus solving the Lagrangian multiplier after some integral transformations will give gradient of the objective function.

$$S(q(t)) = (Y - T)^2 + \lambda(x, t)\mathcal{O}(T) \quad (\text{A.13})$$

Where S is objective functional, Y is measurement at desired locations, T is simulated temperature profiles, λ is Lagrangian multiplier. Performing a minute perturbation for objective function similar to variational problem and integrating over entire time and space domain as

$$\iint S_\epsilon(T_\epsilon) dx dt = \iint (Y - T_\epsilon)^2 dx dt + \iint \lambda(x, t)\mathcal{O}(T_\epsilon) dx dt \quad (\text{A.14})$$

On expanding the above equation using Taylor series and using equation (A.5), variation of objective function is given as,

$$\Delta S(q(t)) = - \iint 2(Y - T)\Delta T dx dt - \underbrace{\iint \lambda(x, t) \frac{\partial}{\partial t} (\rho C_p \Delta T) dx dt}_I + \underbrace{\iint \lambda(x, t) \frac{\partial^2 (k \Delta T)}{\partial x^2} dx dt}_{II} \quad (\text{A.15})$$

The equation is further developed segment by segment by integration by parts for part I and II and utilizing the boundary and initial conditions of variational problem.

$$I \rightarrow - \iint \lambda(x, t) \frac{\partial (\rho C_p \Delta T)}{\partial t} = - [\rho C_p \Delta T(x, t) \lambda(x, t)]_0^{t_f} + \iint \rho C_p \frac{\partial \lambda}{\partial t} \Delta T dx dt$$

$$II \rightarrow \iint \lambda \frac{\partial^2 (k \Delta T)}{\partial x^2} = \left[\frac{\partial (k \Delta T)}{\partial x} \lambda(x, t) \right]_0^L - \left[k \Delta T \frac{\partial \lambda}{\partial x} \right]_0^L + \iint k \frac{\partial^2 \lambda}{\partial x^2} \Delta T dx dt$$

Finally, the variational problem is written as,

$$\Delta S(q) = \mathcal{O}(\lambda)\Delta T + \int \Delta q(t)\lambda(0, t)dt \quad (\text{A.16})$$

With properties of Lagrangian multiplier defined earlier (i.e. $\mathcal{O}(\lambda) = 0$) and taking the inner product of objective function,

$$\nabla S(q) = \frac{\Delta S(q)}{\Delta q} \Rightarrow \nabla S(q) = \lambda(0, t) \quad (\text{A.17})$$

The mathematical constrain of Lagrangian multiplier λ is called adjoint problem which is solved in addition to sensitivity problem is given as,

$$\rho C_p \frac{\partial \lambda}{\partial t} + k \frac{\partial^2 \lambda}{\partial x^2} - 2(Y - T) = 0 \quad (\text{A.18})$$

and boundary and final conditions are

$$-k\nabla\lambda(L, t) = 0 \quad (\text{A.19})$$

$$\lambda(0, t) = 0 \quad (\text{A.20})$$

$$\lambda(x, t_f) = 0 \quad (\text{A.21})$$

It should be noted that the adjoint problem is solved backward in time as its condition at end time is only known. On looking carefully the adjoint problem, it could be noted that when residual between measurement and simulated data are minimized the adjoint problem tends to zero.

A.2 Inverse problem procedure

Conjugate gradient method (CGM) is used for solving the inverse problem. Slight modification of the presented algorithm (Chapter 1, algorithm 1) is required since the before showcased is for parameter estimation.

1. Solve governing equation ($\mathcal{O}(T)$) and adjoint problem (λ) to get gradient of objective function
2. Substitute direction of descent (d^k) with gradient and equate it to Δq
3. Compute sensitivity problem to evaluate step size (β^k)
4. Update the function (q)
5. Solve governing equation ($\mathcal{O}(T)$) and adjoint problem (λ)
6. Compute conjugation coefficient (γ), direction of descent (d^k)
7. Continue step 3 - 6 until convergence criteria (ε) is met

A.3 Conjugate gradient algorithm

Conjugate gradient method is generally utilized gradient based optimization scheme for either parameter or function estimation [?]. The flowchart for the CGM is presented in figure 1.7 and detailed procedure for computation is given in algorithm 1. \mathcal{O} is mathematical constrains which is formulated as partial differential equations.

Algorithm 1 Conjugate gradient method

```

1: Input:  $Y, \epsilon, \mathcal{O}, P \triangleright Y$  : measurement,  $\epsilon$  - stopping criteria,  $\mathcal{O}$  - mathematical constrain,  $P$ 
   - parameter vector
2:  $T \leftarrow \mathcal{O}(P)$   $\triangleright T$  -state variable,  $\mathcal{O}$  solution of governing equation
3:  $k \leftarrow 0$   $\triangleright$  iteration number
4:  $S(P^k) \leftarrow \|Y - T\|$   $\triangleright S(P)$  - objective function
5: if  $S(P^k) > \epsilon$  then
6:    $J^k \leftarrow \frac{\partial T}{\partial P}$   $\triangleright$  computation of Jacobian matrix
7:    $\nabla S(P^k) \leftarrow -2(J^k)^T [Y - T(P^k)]$   $\triangleright T$  - transpose of the matrix
8:   if  $k > 0$  then
9:      $\gamma^k \leftarrow \frac{\nabla S(P^k)^2}{\nabla S(P^{k-1})^2}$   $\triangleright \gamma$  - conjugation coefficient
10:     $d^k \leftarrow \nabla S(P^k) + \gamma^k d^{k-1}$   $\triangleright d$  - direction of descent
11:   else
12:      $\gamma^k \leftarrow 0$ 
13:      $d^k \leftarrow \nabla S(P^k)$ 
14:   end if
15:    $\beta^k \leftarrow \frac{[J^k d^k]^T \times [T(P^k) - Y]}{[J^k d^k]^T [J^k d^k]}$ 
16:    $p^{k+1} \leftarrow p^k - \beta^k d^k$   $\triangleright$  Update the parameter values
17:    $k \leftarrow k + 1$   $\triangleright$  increase iteration
18: end if
19: Output:  $P$   $\triangleright$  Optimized parameters

```

A.4 Inverse solutions

The partial differential equations are solved by implicit finite difference scheme with 31 spatial nodes and 1201 temporal nodes. For estimating the initial temperature distribution, transient problem is converted into steady state problem by setting the time derivative as zero. At $t = 0$, the heat flux is found as - 9.69 (kW/m²) with temperature distribution shown in figure A.2a. Using the calculated initial condition, the heat flux is estimated as function of time with rms at $T_3 = 0.021^\circ\text{C}$ and $T_2 = 0.37^\circ\text{C}$. It took totally 158.66 seconds for solving the inverse problem. The solution of inverse problems is presented graphically in figure A.2.

Bibliography

- [1] M.Necati Özisik and Helcio R. B. Orlande. *Inverse Heat Transfer, Fundamentals and Applications*. Taylor and Francis, 2000.
- [2] Robert Wrede and Murray R. Spiegel. *Advanced Calculus*. Number 3. McGraw-Hill Educations, 2010.

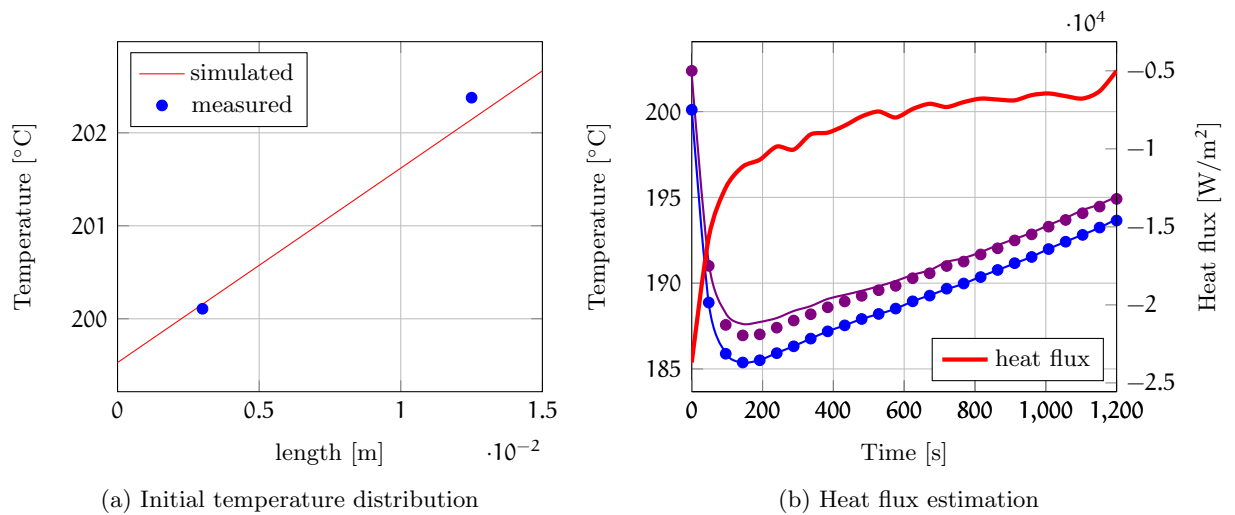


Figure A.2: Inverse solutions for estimation of initial condition (a) and heat flux evolution (b)[— T3 simulated, — T2 simulated, • T3 measured, • T2 measured]

Appendix B

Steps of Non-dimensionalization

B.1 Diffusive model

The governing equations are non-dimensionalized as, Energy balance:

$$\begin{aligned} \rho C_{p_{eff}} \frac{\partial T}{\partial t} &= \frac{\partial}{\partial x} \left(k_{eff} \frac{\partial T}{\partial x} \right) - \lambda I_v \\ \frac{\partial((T - T_o)/T_o)}{\partial(t/t_f)} &= \frac{\partial}{\partial(x/L)} \left(\frac{k_{eff}}{\rho C_{p_{eff}}} \times \frac{t_f}{L^2} \frac{\partial((T - T_o)/T_o)}{\partial(x/L)} \right) - \\ &\quad - \frac{\lambda C_1 C_2}{\lambda} \frac{\partial}{\partial(x/L)} \left(\frac{k_{eff}}{\rho C_{p_{eff}}} \times \frac{t_f}{L^2} \frac{\partial((T - T_o)/T_o)}{\partial(x/L)} \right) \\ \Rightarrow \frac{\partial \theta}{\partial t^*} &= (1 - C_1 C_2) (\nabla^* \alpha_q^* \nabla^* \theta) \end{aligned} \quad (B.1)$$

Mass balance:

$$\begin{aligned} \rho_s^a \frac{\partial U}{\partial t} &= \rho_s^a \frac{\partial}{\partial x} \left(D_w \frac{\partial U}{\partial x} \right) - I_v \\ \frac{\partial U}{\partial(t/t_f)} &= \frac{\partial}{\partial(x/L)} \left(D_w \times \frac{t_f}{L^2} \frac{\partial U}{\partial(x/L)} \right) - \frac{C_1 C_2 \nabla k \nabla T}{\lambda \rho_s^a} \\ \frac{\partial U}{\partial(t/t_f)} &= \frac{\partial}{\partial(x/L)} \left(D_w \times \frac{t_f}{L^2} \frac{\partial U}{\partial(x/L)} \right) - C_1 C_2 \frac{\rho C_{p_{eff}} T_o}{\rho_s^a \lambda} \frac{\partial}{\partial(x/L)} \left(\frac{k_{eff}}{\rho C_{p_{eff}}} \times \frac{t_f}{L^2} \frac{\partial((T - T_o)/T_o)}{\partial(x/L)} \right) \\ \frac{\partial U}{\partial t^*} &= \nabla^* D_w^* \nabla^* U - R_1 C_1 C_2 \nabla^* \alpha_q^* \nabla^* \theta \\ \Rightarrow \frac{\partial U}{\partial t^*} &= \nabla^* D_w^* \nabla^* U - R_1 I_v^* \end{aligned} \quad (B.2)$$

Boundary conditions: Energy balance:

at $x^* = 0$:

$$k_{eff} \nabla T = q(t)$$

$$\frac{\partial((T - T_o)/T_o)}{\partial(x/L)} = \frac{q(t)L}{k_{ref}T_o} \times \frac{k_{ref}}{k_{eff}}$$

$$\Rightarrow \nabla^* \theta = k^* Q(t^*) \quad (B.3)$$

at $x^* = 1$:

$$k_{eff} \nabla T = h_q (T - T^\infty)$$

$$\frac{\partial((T - T_o)/T_o)}{\partial(x/L)} = \frac{h_q L}{k_{ref}} \times \frac{k_{ref}}{k_{eff}} \left(\frac{(T - T_o) - (T^\infty - T_o)}{T_o} \right)$$

$$\Rightarrow \nabla^* \theta = k^* Bi_q (\theta - \theta^\infty) \quad (B.4)$$

Mass balance:

$$D_w \frac{\partial U}{\partial x} = 0$$

$$\frac{D_w \times t_f}{L \times L} \frac{\partial U}{\partial(x/L)} = 0$$

$$\Rightarrow D_w^* \nabla^* U = 0 \quad \text{at } x^* = 0,1 \quad (B.5)$$

B.2 TMPN model

The steps of non-dimensionalization are started with moisture content,

$$\rho_s^a \frac{\partial U}{\partial t} = \frac{\partial}{\partial x} \left(D_w \rho_s^a \frac{\partial U}{\partial x} \right) - I_v$$

$$\frac{\partial U}{\partial(t/t_f)} = \frac{\partial}{\partial(x/L)} \left(D_w \times \frac{t_f}{L^2} \times \frac{\partial U}{\partial(x/L)} \right) - I_v \times \frac{t_f}{\rho_s^a}$$

$$\Rightarrow \frac{\partial U}{\partial t^*} = \nabla^* (D_w^* \nabla^* U) - I_v^* \quad (B.6)$$

For water vapor,

$$\frac{\partial \rho_v S_g \pi}{\partial t} = \frac{\partial}{\partial x} \left(\frac{\rho_v k_g}{\mu_g} \frac{\partial P_g}{\partial x} + D_v \rho_g \frac{\partial}{\partial x} \left(\frac{\rho_v}{\rho_g} \right) \right) + I_v$$

$$\begin{aligned} \frac{\partial(\rho_v^a/\rho_s^a)}{\partial(t/t_f)} &= \frac{\partial}{\partial(x/L)} \left(\frac{\pi S_g \rho_v}{\rho_s^a} \times \frac{1}{\pi S_g} \times \frac{k_g}{\mu_g P_o} \times \frac{t_f}{L^2} \frac{\partial(P_g/P_o)}{\partial(x/L)} + \right. \\ &\quad \left. + D_v \times \frac{t_f}{L^2} \frac{\rho_g}{\rho_s^a} \frac{\partial}{\partial(x/L)} \left(\frac{\rho_v^a/\rho_s^a}{\rho_g^a/\rho_s^a} \right) \right) + I_v \times \frac{t_f}{\rho_s^a} \end{aligned}$$

$$\Rightarrow \frac{\partial V}{\partial t^*} = \nabla^* \left(\frac{V}{\pi S_g} a_p^* \nabla^* P_g^* + D_v^* G \nabla \left(\frac{V}{G} \right) \right) + I_v^* \quad (B.7)$$

For remaining air conservation,

$$\begin{aligned}\frac{\partial \rho_a S_g \pi}{\partial t} &= \frac{\partial}{\partial x} \left(\frac{\rho_a k_g}{\mu_g} \frac{\partial P_g}{\partial x} + D_v \rho_g \frac{\partial}{\partial x} \left(\frac{\rho_a}{\rho_g} \right) \right) \\ \frac{\partial (\rho_a^a / \rho_s^a)}{\partial (t/t_f)} &= \frac{\partial}{\partial (x/L)} \left(\frac{\pi S_g \rho_a}{\rho_s^a} \times \frac{1}{\pi S_g} \times \frac{k_g}{\mu_g P_o} \times \frac{t_f}{L^2} \frac{\partial (P_g/P_o)}{\partial (x/L)} + \right. \\ &\quad \left. + D_v \times \frac{t_f}{L^2} \frac{\rho_g}{\rho_s^a} \frac{\partial}{\partial (x/L)} \left(\frac{\rho_a^a / \rho_s^a}{\rho_g^a / \rho_s^a} \right) \right) \\ \Rightarrow \frac{\partial A}{\partial t^*} &= \nabla^* \left(\frac{A}{\pi S_g} a_p^* \nabla^* P_g^* + D_v^* G \nabla \left(\frac{A}{G} \right) \right)\end{aligned}\quad (B.8)$$

Energy conservation

$$\begin{aligned}\rho C_{p\text{eff}} \frac{\partial T}{\partial t} &= \frac{\partial}{\partial x} \left(k_{\text{eff}} \frac{\partial T}{\partial x} \right) - \lambda I_v \\ \frac{\partial ((T - T_o)/T_o)}{\partial (t/t_f)} &= \frac{\partial}{\partial (x/L)} \left(\frac{k_{\text{eff}}}{\rho C_{p\text{eff}}} \times \frac{t_f}{L^2} \frac{\partial ((T - T_o)/T_o)}{\partial (x/L)} \right) - \frac{\lambda}{C_{p\text{eff}} T_o} \times \frac{\rho_s^a}{\rho} \frac{I_v t_f}{\rho_s^a} \\ \Rightarrow \frac{\partial \theta}{\partial t^*} &= \nabla^* (a_q^* \nabla^* \theta) - R_1 I_v^*\end{aligned}\quad (B.9)$$

Boundary condition Beginning with moisture content condition at free surface (i.e. at $x = 0$),

$$\begin{aligned}n_l &= -D_w \rho_s^a \frac{\partial U}{\partial x} = h_m \pi S_l (\rho_v - \rho_v^\infty) \\ -D_w \times \frac{t_f}{L \times L} \frac{\partial U}{\partial (x/L)} &= \frac{h_m t_f}{L} \times \frac{\pi S_l}{\pi S_g} \left(\frac{\rho_v \pi S_g}{\rho_s^a} - \frac{\rho_v^\infty \pi S_g}{\rho_s^a} \right) \\ \Rightarrow -D_w^* \nabla^* U &= \text{Bi}_m S_l / S_g (V - V^\infty)\end{aligned}$$

In nutshell

$$n_l^* = \begin{cases} 0 & : x^* = 0 \\ \text{Bi}_m S_l / S_g (V - V^\infty) & : x^* = 1 \end{cases}$$

For water vapor,

$$\begin{aligned}n_v &= -D_v \rho_g \nabla \left(\frac{\rho_v}{\rho_g} \right) - \rho_g \frac{k_g}{\mu_g} \nabla P_g = h_m \pi S_l (\rho_v - \rho_v^\infty) \\ -D_v \times \frac{t_f}{L \times L} \frac{\rho_g}{\rho_s^a} \frac{\partial}{\partial (x/L)} \left(\frac{\rho_v^a / \rho_s^a}{\rho_g^a / \rho_s^a} \right) - \frac{\rho_v \pi S_g}{\rho_s^a} \times \frac{1}{\pi S_g} \frac{k_g}{\mu_g P_o} \times \frac{t_f}{L \times L} \frac{\partial (P_g/P_o)}{\partial (x/L)} &= \\ &= \frac{h_m t_f}{L} \frac{\pi S_g}{\pi S_g} \left(\frac{\rho_v \pi S_g}{\rho_s^a} - \frac{\rho_v^\infty \pi S_g}{\rho_s^a} \right)\end{aligned}$$

$$\Rightarrow -D_v^* G \nabla^* \left(\frac{V}{G} \right) - \frac{V a_p^*}{\pi S_g} \nabla^* P_g^* = \text{Bi}_m (V - V^\infty)$$

In nutshell

$$n_v^* = \begin{cases} 0 & : x^* = 0 \\ \text{Bi}_m (V - V^\infty) & : x^* = 1 \end{cases}$$

For air conservation,

$$\rho_a = \frac{P_o - P_v}{R_a T} \Rightarrow \frac{\rho_a \pi S_g}{\rho_s^a} = \pi S_g \frac{P_o}{R_a T_o \rho_s^a} \frac{(P_o/P_o - P_v/P_o)}{(T + T_o - T_o)/T_o}$$

$$\Rightarrow A = \pi S_g \rho_{ref}^* \frac{1 - P_v^*}{\theta + 1}$$

In nutshell

$$n_a^* = 0 \quad : x^* = 0$$

$$A = \pi S_g \rho_{ref}^* \frac{1 - P_v^*}{\theta + 1} \quad : x^* = 1$$

B.3 TMPE model

For the moisture content equation,

$$\rho_s^a \frac{\partial U}{\partial t} + \frac{\pi P_v}{R_v T} \frac{\partial S_g}{\partial t} - \frac{P_v \pi S_g}{R_v T^2} \frac{\partial T}{\partial t} + \frac{\pi S_g}{R_v T} \frac{\partial P_v}{\partial t} = \nabla \left(\rho_s^a D_w \nabla U + \rho_v \frac{k_g}{\mu_g} \nabla P_g + \rho_g D_v \nabla \left(\frac{\rho_v}{\rho_g} \right) \right)$$

$$\frac{\partial U}{\partial(t/t_f)} + \pi \frac{P_o}{R_a T_o \rho_s^a} \frac{R_a}{R_v} \frac{P_v T_o}{(T + T_o - T_o)} \frac{\partial S_g}{\partial(t/t_f)} - \pi S_g \frac{P_o}{R_a T_o \rho_s^a} \frac{P_v R_a}{R_v} \frac{T_o^2}{(T - T_o + T_o)^2} \times$$

$$\times \frac{\partial((T - T_o)/T_o)}{\partial(t/t_f)} + \pi S_g \frac{P_o}{\rho_s^a R_a T_o} \frac{R_a}{R_v} \frac{T_o}{(T - T_o + T_o)} \frac{\partial(P_v/P_o)}{\partial(t/t_f)} = \frac{\partial}{\partial(x/L)} (D_w \times$$

$$+ \times \frac{t_f}{L^2} \frac{\partial U}{\partial(x/L)} + \frac{\pi S_g \rho_v}{\pi S_g \rho_s^a} \frac{k_g}{\mu_g P_o} \times \frac{t_f}{L^2} \frac{\partial(P_g/P_o)}{\partial(x/L)} + \frac{\rho_g}{\rho_s^a} D_v \times \frac{t_f}{L^2} \frac{\partial}{\partial(x/L)} \left(\frac{(\rho_v/\rho_s^a)}{(\rho_g/\rho_s^a)} \right))$$

$$\Rightarrow \frac{\partial U}{\partial t^*} + \pi \frac{\rho_{ref} P_v^*}{R_v^* (\theta + 1)} \frac{\partial S_g}{\partial t^*} - \pi S_g \frac{\rho_{ref} P_v^*}{R_v^* (\theta + 1)^2} \frac{\partial \theta}{\partial t^*} + \pi S_g \frac{P_v^* \rho_{ref}}{R_v^* (\theta + 1)} \frac{\partial P_v^*}{\partial t^*} =$$

$$= \nabla^* \left(\underbrace{D_w^* \nabla^* U + \frac{V}{\pi S_g} a_p^* \nabla^* P_g^* + G D_v^* \nabla^* \left(\frac{V}{G} \right)}_{\Gamma^*} \right) \quad (\text{B.10})$$

For total gas pressure,

$$\frac{\partial}{\partial t} \left(\frac{\pi S_g P_g}{R_a T} \right) - \frac{\partial}{\partial t} \left(\frac{\pi S_g P_v}{R_a T} \right) - \frac{\pi S_g (P_g - P_v)}{R_a T^2} \frac{\partial T}{\partial t} + \frac{\pi (P_g - P_v)}{R_a T} \frac{\partial S_g}{\partial t} =$$

$$\begin{aligned}
&= \nabla \left(\frac{(P_g - P_v) k_g}{R_a T} \nabla P_g - \left(\frac{(P_g - P_v)}{R_a T} + \frac{P_v}{R_v T} \right) D_v \nabla \left(\frac{1}{((P_g - P_v) R_v) / (P_v R_a) + 1} \right) \right) \\
&\frac{\partial}{\partial(t/t_f)} \left(\pi S_g \frac{P_o}{\rho_s^a R_a T_o} \frac{T_o}{T - T_o + T_o} \frac{P_g}{P_o} \right) - \frac{\partial}{\partial(t/t_f)} \left(\pi S_g \frac{P_v}{P_o} \frac{P_o}{R_a T_o \rho_s^a} \frac{T_o}{T - T_o + T_o} \right) - \\
&- \pi S_g \frac{P_o}{R_a T_o \rho_s^a} \frac{(P_g - P_v)}{P_o} \frac{T_o^2}{(T - T_o + T_o)^2} \frac{\partial((T - T_o)/T_o)}{\partial(t/t_f)} + \pi \frac{(P_g - P_v)}{P_o} \frac{P_o}{R_a T_o \rho_s^a} \times \\
&\times \frac{T_o}{T - T_o + T_o} \frac{\partial S_g}{\partial(t/t_f)} = \frac{\partial}{\partial(x/L)} \left(\frac{P_o}{R_a T_o \rho_s^a} \left(\frac{P_g}{P_o} - \frac{P_v}{P_o} \right) \frac{k_g}{\mu_g P_o} \frac{t_f}{L^2} \frac{\partial(P_g/P_o)}{\partial(x/L)} - \right. \\
&\frac{P_o}{R_a T_o} \frac{T_o}{T - T_o + T_o} \left(\frac{P_g}{P_o} - \frac{P_v}{P_o} + \frac{P_v R_a}{P_o R_v} \right) D_v \frac{t_f}{L^2} \times \\
&\left. \times \frac{\partial}{\partial(x/L)} \left(\frac{1}{1 + ((P_g/P_o - P_v/P_o) / (P_v/P_o) \times R_v/R_a)} \right) \right) \\
\Rightarrow \frac{\partial}{\partial t^*} \left(\frac{\pi S_g \rho_{ref} P_g^*}{\theta + 1} \right) - \frac{\partial}{\partial t^*} \left(\frac{\pi S_g \rho_{ref} P_v^*}{\theta + 1} \right) - \pi S_g \rho_{ref} \frac{(P_g^* - P_v^*)}{(\theta + 1)^2} \frac{\partial \theta}{\partial t^*} + \pi \rho_{ref} \frac{(P_g^* - P_v^*)}{\theta + 1} \frac{\partial S_g}{\partial t^*} = \\
&= \nabla^* \left(\underbrace{\rho_{ref} (P_g^* - P_v^*) \alpha_p^* \nabla^* P_g^* - \frac{\rho_{ref}}{\theta + 1} \left(P_g^* - P_v^* + \frac{P_v^*}{R_v^*} \right) D_v^* \nabla^* \left(\frac{1}{1 + R_v^* ((P_g^* - P_v^*) / P_v^*)} \right)}_{\Phi^*} \right) \tag{B.11}
\end{aligned}$$

The evaporation rate in non-dimensional form is presented as,

$$\begin{aligned}
I_v \times \frac{t_f}{\rho_s^a} &= \frac{\partial}{\partial(t/t_f)} \left(\pi S_g \frac{P_o}{R_a T_o \rho_s^a} \frac{P_v}{P_o} \frac{R_a}{R_v} \frac{T_o}{T - T_o + T_o} \right) - \frac{\partial}{\partial(x/L)} \left(\frac{\pi S_g \rho_v}{\pi S_g \rho_s^a} \frac{k_g P_o}{\mu_g} \frac{t_f}{L^2} \frac{\partial(P_g/P_o)}{\partial(x/L)} + \right. \\
&\left. + \frac{\rho_g}{\rho_s^a} D_v \frac{t_f}{L^2} \frac{\partial}{\partial(x/L)} \left(\frac{(\rho_v/\rho_s^a)}{(\rho_g/\rho_s^a)} \right) \right) \\
\Rightarrow I_v^* &= \frac{\partial}{\partial t^*} \left(\frac{\pi S_g \rho_{ref} P_v^*}{\theta + 1} \right) - \nabla^* \left(\frac{V}{\pi S_g} \alpha_p^* \nabla^* P_g^* + G D_v^* \nabla^* \left(\frac{V}{G} \right) \right) \tag{B.12}
\end{aligned}$$

The boundary conditions are simplified as,

$$\begin{aligned}
\Gamma \times \frac{t_f}{\rho_s^a L} &= h_m \times \frac{t_f}{L} \left(\frac{\rho_v}{\rho_s^a} - \frac{\rho_v^\infty}{\rho_s^a} \right) \\
\Rightarrow \Gamma^* &= \begin{cases} 0 & : x^* = 0 \\ \text{Bi}_m (V - V^\infty) & : x^* = 1 \end{cases}
\end{aligned}$$

and for mass transfer of gases:

$$\Phi^* = \begin{cases} 0 & : x^* = 0 \\ P_g^* = 1 & : x^* = 1 \end{cases}$$

B.4 TMPE model for function estimation

The total gas pressure equation is same as presented previous section. The only difference arises in energy balance and moisture content equations. The energy conservation are transformed as,

$$\begin{aligned}
\rho C_{p_{eff}} \frac{\partial T}{\partial t} &= \frac{\partial}{\partial x} \left(k_{eff} \frac{\partial T}{\partial x} \right) - \lambda I_v \\
\frac{\rho C_{p_{eff}}}{\rho_{ref} C_{p_{ref}}} \frac{\partial((T - T_o)/T_o)}{\partial(t/t_f)} &= \frac{k_{ref}}{\rho_{ref} C_{p_{ref}}} \times \frac{t_f}{L^2} \frac{\partial}{\partial(x/L)} \left(\frac{k_{eff}}{k_{ref}} \frac{\partial((T - T_o)/T_o)}{\partial(x/L)} \right) - \\
&- \frac{\lambda}{C_{p_{ref}} T_o} \times \frac{\rho_s^\alpha I_v t_f}{\rho_{ref} \rho_s^\alpha} \\
\Rightarrow C^* \frac{\partial \theta}{\partial t^*} &= a_{ref}^* \nabla^* (k^* \nabla^* \theta) - R_1 I_v^* \tag{B.13}
\end{aligned}$$

The moisture content equation becomes,

$$\begin{aligned}
\rho_s^\alpha \frac{\partial U}{\partial t} + \frac{\pi P_v}{R_v T} \frac{\partial S_g}{\partial t} - \frac{P_v \pi S_g}{R_v T^2} \frac{\partial T}{\partial t} + \frac{\pi S_g}{R_v T} \frac{\partial P_v}{\partial t} &= \nabla \left(\rho_s^\alpha D_w \nabla U + \rho_v \frac{k_g}{\mu_g} \nabla P_g + \rho_g D_v \nabla \left(\frac{\rho_v}{\rho_g} \right) \right) \\
\frac{\partial U}{\partial(t/t_f)} + \pi \frac{P_o}{R_a T_o \rho_s^\alpha} \frac{R_a}{R_v} \frac{P_v T_o}{(T + T_o - T_o)} \frac{\partial S_g}{\partial(t/t_f)} - \pi S_g \frac{P_o}{R_a T_o \rho_s^\alpha} \frac{P_v R_a}{R_v} \frac{T_o^2}{(T - T_o + T_o)^2} \times \\
\times \frac{\partial((T - T_o)/T_o)}{\partial(t/t_f)} + \pi S_g \frac{P_o}{\rho_s^\alpha R_a T_o} \frac{R_a}{R_v} \frac{T_o}{(T - T_o + T_o)} \frac{\partial(P_v/P_o)}{\partial(t/t_f)} &= \frac{\partial}{\partial(x/L)} \left(\frac{D_w}{D_{ref}} \times \right. \\
+ \times \frac{D_{ref} t_f}{L^2} \frac{\partial U}{\partial(x/L)} + \frac{\pi S_g \rho_v}{\pi S_g \rho_s^\alpha} \frac{k_g}{\mu_g P_o} \times \frac{t_f}{L^2} \frac{\partial(P_g/P_o)}{\partial(x/L)} + \frac{\rho_g}{\rho_s^\alpha} D_v \times \frac{t_f}{L^2} \frac{\partial}{\partial(x/L)} \left(\frac{(\rho_v/\rho_s^\alpha)}{(\rho_g/\rho_s^\alpha)} \right) \Big) \\
\Rightarrow \frac{\partial U}{\partial t^*} + \pi \frac{\rho_{ref} P_v^*}{R_v^*(\theta + 1)} \frac{\partial S_g}{\partial t^*} - \pi S_g \frac{\rho_{ref} P_v^*}{R_v^*(\theta + 1)^2} \frac{\partial \theta}{\partial t^*} + \pi S_g \frac{P_v^* \rho_{ref}}{R_v^*(\theta + 1)} \frac{\partial P_v^*}{\partial t^*} &= \\
= \nabla^* \left(\underbrace{D_{ref}^* D^* \nabla^* U + \frac{V}{\pi S_g} a_p^* \nabla^* P_g^* + G D_v^* \nabla^* \left(\frac{V}{G} \right)}_{\Gamma^*} \right) \tag{B.14}
\end{aligned}$$

The boundary conditions has no major change from last model except for heat transfer at bottom where the applied heat flux is replaced by convective heat transfer with coefficient $Bi_q^0 = h_q^0 \times L/k_{ref}$.



Puvikkarasan Jayapragasam received bachelor's degree in Mechanical Engineering from College of Engineering, Anna University, Chennai, India in 2014 and master's degree in Computational Fluid Dynamics from University of Petroleum and Energy Studies, Dehradun, India and in Thermal Science and Energies from Polytech Nantes, Université de Nantes, France in 2017. He is currently pursuing the Ph.D. degree in Mechanical engineering with the Université Bretagne Sud, Lorient, France. He served as Graduate Engineer Trainee with RaneTRW, Chennai, India from 2014 to 2015.

His main research interests are inverse problem, drying, heat and mass transfer, porous media, mathematical modelling, parameter and/or function estimation and optimal design.

The following are some of the recent research activities,

International Journals

[1] [Puvikkarasan J.](#), Le Bideau P. and Loulou T., Computing sensitivity coefficients using complex differentiation: Application to heat conduction problem. Numerical Heat Transfer, Part B: Fundamentals, 74(5): 729-745, 2018.

[2] [Puvikkarasan J.](#), Le Bideau, P. and Loulou, T. Luikov's Analytical Solution with Complex Eigenvalues in Intensive Drying. Transport Porous Media, 130, 923–946 (2019).

[3] [Puvikkarasan J.](#), Le Bideau P. and Loulou T., Approximation of heat and mass transport properties for one sided cake baking, Journal of Food Engineering, 290, 110211 (2021).

[4] [Puvikkarasan J.](#), Le Bideau P. and Loulou T., Selection of better mathematical model describing cake baking for inverse analysis, Food and Bio-products Processing, 126, 265-281 (2021).

International Conference

[1] [Puvikkarasan J.](#), Le Bideau P. and Loulou T., Parameter estimation for bread baking process in non-dimensional form, EuroDrying 2019, Turin, Italy.

Titre : Conception d'une expérience optimale pour l'estimation des propriétés hydro-thermiques des milieux poreux. Application dans le processus de cuisson

Mots clés : Cuisson par contact, Problème inverse, Conception d'expériences, Paramétrage, Estimation des propriétés thermo-physiques, diffusion de masse et de chaleur

Résumé : Ce travail se concentre sur l'estimation par techniques inverses des propriétés thermo-physiques et hydriques significatives qui régissent le processus de cuisson par contact unilatéral. Trois modèles mathématiques avec des approches différentes ont été utilisés comme TM (approche phénoménologique), TMPN (modèle mécanistique sans équilibre hydrique) et modèle TMPE (modèle mécanistique avec équilibre hydrique). Avant de procéder à l'estimation des propriétés considérées constante dans un premier temps, une étude portant sur l'emplacement optimal et le nombre de capteurs est menée en suivant une approche de conception optimale d'expériences. D'après l'analyse, il a été constaté que trois thermocouples, deux extrémités et un au centre, sont suffisants. Des mesures expérimentales sont menées dans les conditions prédéfinies et sont ensuite exploitées dans le problème inverse. Plusieurs formes de fonctions d'objectif

sont testées et analysées : moindres carrés ordinaires, mises à l'échelle et pondérées. Pour l'estimation des paramètres, l'étude montre que l'usage d'une fonction objectif basée sur les moindres carrés pondérés associée au modèle direct TMPE permet une meilleure estimation des propriétés en limitant l'erreur entre les réponses mesurées et simulés. On conclut également que le modèle mécanistique avec équilibre hydrique est plus adapté à représenter la cuisson d'une pâte céréalière. Dans un second temps, la procédure mise en place est exploitée pour estimer des propriétés thermo-physiques et hydriques dépendantes de la teneur en eau du produit qui varie fortement temporellement et spatialement au cours de la cuisson. Dans cette partie, les propriétés thermiques telles que la conductivité et la capacité thermique, et la diffusivité massique de l'eau liquide sont alors estimées en fonction de variables d'état.

Title : Design of optimal experiment for estimation of Hydro-thermal properties of porous media. Application in the baking process

Keywords: Contact baking, Inverse problem, Design of experiments, Parameterization, Thermo-physical properties estimation, heat and mass transfer.

Abstract: This work focuses on estimation of significant thermophysical properties that governs the one-sided contact baking process. Three mathematical model with different approaches has been used as TM (phenomenological approach), TMPN (mechanic model with non-equilibrium approach) and TMPE model (mechanic model with non-equilibrium approach). Before proceeding to estimation of the properties, optimal location and number of sensors are identified using Design of experiments. From the analysis, it was found that three thermocouples at either ends and at centre are sufficient. The experimental measurements from the desired sensor locations are attained and used in inverse problem. Ordinary, Scaled and Weighted Least Square objective functions are employed in the

optimization segment as the measurements of temperature and moisture content are not in same league. For parameter estimation, weighted least square with significant weight given to temperature has preferable results and TMPE model has least error between measured and simulated profiles. It can be concluded that mechanistic model with equilibrium approach for evaporation rate is much suited for solving the inverse problem. The estimated properties failed to account the crust-crumbs transformation from dough. Hence, thermal properties like conductivity and heat capacity, and mass diffusivity of liquid water are estimated as functions of state variables. From the observation of case studies, it is understood that the hydro-thermal properties are greatly dependent on moisture content.